RELIABILITY AND LIFE-TIME IMPROVEMENT OF HIGH-POWER LASER DIODES

A Thesis Submitted to

The Maharaja Sayajirao University of Baroda

For the Degree of

Doctor of Philosophy

In

Applied Physics

By

Mr. Gopal Gautambhai Bhatt

Under the Supervision of

Dr. C. J. Panchal

Applied Physics Department
Faculty of Technology and Engineering
The M. S. University of Baroda
Vadodara-390001

May 2014

APPLIED PHYSICS DEPARTMENT

Telephone No.: (0265) 2434188
Fax No.: (0265) 2423898

Phy No.: 299

Faculty of Technology & Engineering
M S University of Baroda,
Kalabhavan, Vadodara – 390 001
Gujarat, India

14 MAY 2014

CERTIFICATE

This is to certify that the thesis entitled "**Reliability and Life-Time Improvement of High-Power Laser Diodes**" submitted by **Gopal Gautambhai Bhatt** to **The Maharaja Sayajirao University of Baroda, Vadodara**, for the award of degree of **Ph.D.** in **Applied Physics** is bona fide and the work has been carried out by him in this department.

14-05-2014

Dr. C. J. Panchal
Research Guide
Applied Physics Department

Date: 14th May, 2014

Head
Applied Physics Department

Dean
Faculty of Technology and Engineering

DEAN
Faculty of Tech. & Engg.
M. S. University of Baroda.
VADODARA.

Dedicated to

My Family…

❖ Acknowledgement

वसुदेव सुतं देवं कंस चाणूर मर्दनम् ।
देवकी परमानन्दं कृष्णं वन्दे जगद्गुरुम् ॥

The six years of doctoral research will end with this thesis submission. It is a beautiful opportunity for me that I can express my appreciations and thankfulness to many people including my well wishers, my teachers and guides, my friends, colleagues, and various institutions. At this moment of accomplishment, first I would like to thank my guide, *Dr. C. J. Panchal*, for giving me an opportunity to join the research under his guidance. I am indebted to him not only for introducing me the objective of this work but also for his support, encouragement and faith in me, which enabled me to solve the problems encountered during the various stages of my research work.

I express my sincere and warmest thanks to *Dr. S. M. Oak*, Head, Solid-State Laser Division, Raja Ramanna Center for Advance Technology (RRCAT), Indore (M.P), *Dr. T. K. Sharma*, and *Dr. V. K. Dixit*, Scientific Officer, Semiconductor Laser Section, RRCAT, Indore, for giving me an opportunity to carry out a part of my Ph.D. work at RRCAT. Especially, I would like to thank *Dr. V. K. Dixit* for his continuous support and guidance. I am not only thankful to him for the discussion on various topics viz. fundamental theories, various experiments and laser characterizations, but also for providing me a moral support to be a quality researcher. I have benefited a lot from his experience and expertise in the field as well as from his suggestions on general research methods. Here, I also thank *Prof. B. M. Arora*, and *Dr. Sandip Ghosh*, of Tata Institute of Fundamental Research (TIFR), Mumbai, too, for inspiration and encouragement to carry out various experiments.

In addition, I must express, here, my personal and particular gratitude to *Dr. Mukesh Desai*, of our department, for his profound interest, care, advices and motivation. I have also benefited enormously and learned a lot from his writing skills and I am very grateful to him for revising my manuscripts and thesis.

I in fact believe that my work would have been not come to an end without the suggestions, help and co-operation of my buddies of the journey– my lab-mates. Thanks to my colleagues and best friends, *Dr. Vipul Kheraj*, *Dr. Nitinbhai Shah, Dr. Keyur Patel*,

and *Dr. Jaymin Ray*, who have made the lab a friendly environment for working and made it unforgettable by their grace. I learnt the ABCs of thin-film deposition and its characterizations, and a LabVIEW programming from them. They supported me by all means, as brother, teacher and philosopher.

It has been a privilege and a pleasing experience to be at Semiconductor Laser Section (SCLS), RRCAT, Indore, for accomplishment of my dissertation work. I am greatly thankful to *Dr. S. Pal*, *Mr. Sailesh Khamari*, *Mr. Ravikumar Jain*, *Mr. Abhishek Chatterjee*, *Mr. Sanjay Porwal*, *Mr. Alexander Khakha*, *Mr. U. K. Ghosh*, *Mr. A. K. Jaiswal*, *Mr. Vishal Agnihotri*, *Mr. Ravindra Jangir* and all SCLS team members for their invaluable help and co-operation. I am also thankful to *Dr. C. Mukharjee*, and *Mr. Rajiv Kamparath,* RRCAT, for useful discussion and tips regarding thin film deposition and characterizations. I also thank *Ms. Monika Shrivastava*, and *Ms. Archana Marathe*, M. Tech. project trainees and *Mr. Dipankar Jana*, Ph.D. scholar at SCLS, RRCAT for their invaluable support and fruitful discussion.

I am thankful to *Dr. Arvindbhai L. Patel*, Director, Sahjanand Laser Technology Ltd. Ghandhinagar (Gujarat) for providing a Nd:YAG laser facility to measure the damage threshold of thin films. I also thank to *Mr. Ashwin Patel* and *Mr. Hitesh Moghariya*, Employee, Sahjanand Laser Technology Ltd., for providing a technical support.

I thank *Prof. A. N. Mishra*, the Dean of the Faculty of Technology and Engineering, and *Prof. Arun Pratap*, the Head of the Applied Physics Department, for providing me the infrastructural facilities. I also thank all teaching and non-teaching staff of Applied Physics Department for their support during this work.

I would like to acknowledge financial, academic, technical and medical support of the various institutions. First, I thank to The Maharaja Sayajirao University of Baroda and RRCAT for providing library facilities and computer/internet facilities to access number of books and on-line international articles, which is indispensable to carry out literature survey for the research. I thank them for providing me a necessary infrastructure and technical support. Beside this, I am also thankful to them for providing a health care center which is indeed beneficial for me in a crucial time. I would like to acknowledge

here, *Dr. Sonalben Mishra*, and *Dr. S. Bhavani*, of University Health Center, The M. S. University of Baroda, and Health Center, RRCAT, respectively, for their kind treatment and curing me in time. I want to thank, for providing financial assistance, to the Board of Research in Nuclear Science (BRNS), Department of Atomic Energy (DAE), BARC, Mumbai, and to University Grants Commission (UGC) under the UGC-BSR RFSMS scheme.

I wish to convey my gratitude to some of the teachers – '*Gurus'*, who have always been an inspiring force in my life, starting form primary to post-graduation: *Dilipbhai Patel*, *Jasuben*, *Kantibhai*, *Rakshitaben*, *Pareshbhai Trivedi*, *Jasuben Pandya*, *Sanjivbhai Bhatt*, *Bharatbhai Raval*, *Umeshbhai Dodia*, *Dr. G. M. Sutariya*, *Prof. S. P. Bhatnagar*, and *Prof. R. V. Upadhyay*.

I would like to thank all project trainees, *Sandip*, *Hemali*, *Ashwini*, *Ashish*, *Nirav*, *Ankit*, *Hina*, *Hiren*, and *Priya*, M. Sc. students and *Dr. Usha Parihar* and *Dr. Ramesh Sachdeva*, a M.Phil/Ph.D. scholar, at the department, who were eventually joined and involved in this project and helped in running the experiments at our lab.

During the various stages of my life I have come across some people who have become a precious wealth of my life– my friends, *Dr. Abbasi*, *Maulik*, *Rajsinh*, *Jehan*, *Vishal*, *Paresh*, *Rajvir*, *Gaurav*, *Dr. Kanti*, *Raju*, *Pratik*, *Virabhadra*, *Mehul*, *Naveen*, *Shyam*, *Kinjal*, *Palakbhabhi*, *Dr. Narinder*, *Vikas*, *Shyamsunder*, *Krishnakant*, *Dipankar*, *Monika*, *Priyanka*, *Archana*, *Kavita*, *Harshal* and many more. I would like to thank them all for being with me and directly or indirectly contributed in my research. My warmest thanks to all my hostel buddies, *Narayan*, *Dr. Mayur*, *Dr. Parimal*, *Dr. Vinod*, *Dr. Mahesh*, *Dr. Rajesh SV*, *Dr. Anup*, *Rahul*, *Jigar*, *Balchand*, *Naveen Agrawal*, *Hemant*, *Dr. Harishbhai*, *Dr. Murlibhai*, and *Dr. Subbuanna*.

My sincere gratitude goes to my family. Especially, my deepest and graceful thanks to my mother, *Smt. Nayanaben*, my father, *Shri Gautmabhai*, my sister, *Komal*, and my beloved wife, *Swati*, for always believing in me, for their endless love and support in my decisions, without whom I could never make it through this research voyage.

Last, but not the least, I thank gracefully to a divine family of *Lord Yogeshwar*, *Swadhyay Parivar* and its founder *Rev. Pandurang Shastri Athavale* for giving me a selfless love, and optimistic view towards life. Only due to them I could sustain throughout this voyage of research and never had an idea of giving up my task. They have given me a special relation, a precious jewel in my life– *a divine friendship* and also a deep understanding of indwelling *GOD,* that made me believe "*Life is Beautiful"*. So, finally great thanks to *GOD* for always being with me as an active partner and thereby increasing my potential and self-confidence during the research.

With the blessing of *GOD* I put my word to the end…

Gopal Bhatt

* * *

Contents

* * *

❖ Abstract

The present thesis covers the optimization of post-growth processing and various fabrication techniques for high-power laser diodes (HPLDs). This process includes laser diode processing, facet coating and packaging. Each of these processes play a significant role in determining the overall performance of the laser diode and need to be optimized very carefully, as various laser diode characteristic parameters viz. electrical, optical, spectral, and device life-time, depends on it. Present thesis includes the development and optimization of these processes for HPLDs to improve its performance and hence its reliability. The thesis also consists of optimization of various laser diode characterization techniques to characterize laser diode at different stages of optimization. The fabrication and automation of these characterization facilities are also discussed in the thesis.

The double quantum well (DQW) InGaAs/GaAs laser diode epitaxially grown at SCLS, RRCAT, Indore (M.P.), was processed to develop mesa-stripe geometry structure. Processing steps viz. photolithography, lift-off processes, mechanical lapping and polishing, insulation and metal contact layer deposition, has been optimized to fabricate edge-emitting laser diode bars and are very important to achieve high-power operation.

Design, simulation and optimization of anti-reflection and high-reflection coating of dielectric thin films on front and rear facets of laser diode, respectively are discussed here. The facet coating is designed for 808 nm and 980 nm HPLDs and the effects of facet-coating on the device characteristics have been studied. The optimized facet coating has also been tested for laser-induced-damage threshold (LIDT) measurements and proved to be a suitable facet coating for HPLDs. Various experimental setups have been developed and automated to characterize various laser diodes.

Finally, the packaging processes for high-power laser diode, consisting of die-bonding and wire-bonding, were optimized using different solder materials viz. indium and gold-tin preform, and the process is further carried out on a 650 nm and 980 nm HPLDs using indigenously developed setup. A complete package has been successfully tested under pulse and continuous wave (CW) operation. The improved device performance has been demonstrated successfully after applying various optimized post-

growth process to HPLDs, and the device life-time has been estimated under accelerated aging conditions, 80 °C, as well as at room temperature.

Subsequently, the developed semi-package, non hermetic, 980 nm laser diode was used for the characterization of electronic transitions of InAsP/InP quantum well in photoluminescence (PL) spectroscopy.

* * *

Chapter 1

Introduction

1. Introduction

Since the invention of the GaAs based homojunction semiconductor laser, it has been continuously revolutionized in terms of material system, structure, growth mechanism, efficiency and off course its reliability. This chapter gives a brief introduction about the semiconductor laser and its applications. The contemporary research leading to the device lifetime improvement and the challenges to achieve such reliable operation of the laser diode are also discussed in this chapter. The overview of thesis and its organization are given at the end of the chapter.

1.1 Laser Fundamentals

It is almost difficult to cover a complete study of laser diode physics within the chapter. Hence this part of the chapter includes only the most basic concepts of laser action and an overview of the theory of laser diodes here for convenience and completeness. There are several classical literatures available covering various types of laser diodes, the physics of their operation, and applications [1,2,3].

1.1.1 General Laser Theory

Light Amplification by the Stimulated Emission of Radiation, also known as LASER, is special kind of electromagnetic radiation emitted when atoms make a transition from one quantum state to a lower one. As the name suggest the radiation takes place by stimulation, unlike an ordinary light source. Basically, there are three different processes by which interaction between electromagnetic radiation, i.e. light, and matter takes place namely absorption, spontaneous emission and stimulated emission, shown in Fig. 1.1.

- **Absorption**

As shown in Fig. 1.1 (a), let us consider an atom in its ground state (E_0) and having only one high energy state, excited state (E_1). If an atom is exposed to the electromagnetic radiation having energy $h\nu$ ($h\nu \geq E_1 - E_0$), where h is Plank's constant and ν is the radiation frequency, the atom can absorb an amount of energy and get excited to the higher energy level, E_1, shown in Fig. 1.1 (b). The process is known as absorption.

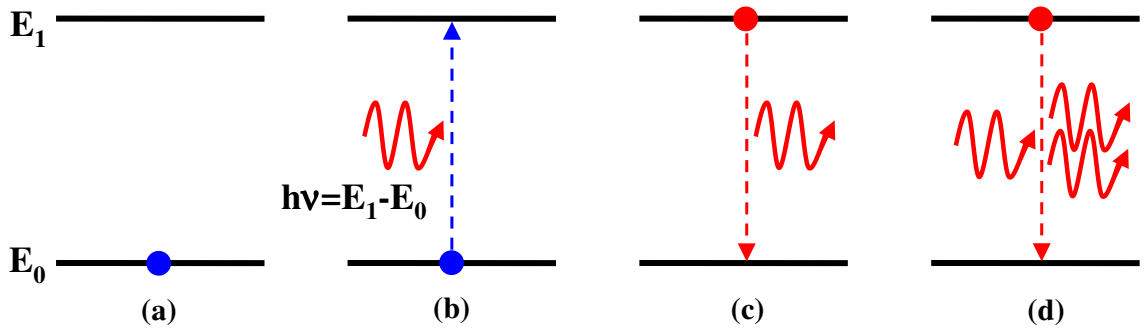

Figure 1.1: Light-matter interactions in simple two energy level system. (a) atom at ground state, (b) absorption of photon having energy $h\nu$, (c) spontaneous emission of photon and (d) stimulated emission of photon.

➢ Spontaneous Emission

After being excited to the higher energy level, the atom returns to the ground state within time interval of the order of 10^{-8} - 10^{-9} s by emitting a photon of energy $h\nu$. The process is known to as spontaneous emission because it is not triggered by any external influence. Fig. 1.1 (c) shows spontaneous emission from the system. In spontaneous emission the atom simply falls to the ground state while emitting randomly directed photons

➢ Stimulated Emission

In 1917, Albert Einstein proposed a theory that emission from excited atom can occur in two ways: spontaneous emission that we have discussed earlier and another one is stimulated emission. Unlike spontaneous emission, the excited atom returns to its ground state by externally triggered or spontaneously emitted photons having energy $h\nu$ and emits the photon, whose energy is also $h\nu$. Hence, in general the phenomenon of photon assisted light emission is known as stimulated emission, shown in Fig. 1.1 (d). The emitted photon is identical to the stimulating photon in all aspects. The light waves associated with these photons have the same direction, energy, phase, and polarization. Thus, in the case of stimulated emission, the wave representing the stimulated photon adds to the incident wave on a constructive basis, thereby increasing its amplitude.

So far we have discussed a system of only one atom to understand absorption and emission process in matter. Now considering the system/material in thermal equilibrium and having large number of atoms at temperature T. Before excitation, number of atoms, say N_0, in its ground state with energy (E_0) and N_1 is in a higher energy state (E_1). Ludwig Boltzmann showed that the number of atoms or molecules in higher energy state, E_1, i.e.

N_1, is represented in terms of the number of atoms in ground state energy, E_0, i.e. N_0, in thermodynamic equilibrium

$$N_1 = N_0 \, e^{\frac{-(E_1 - E_0)}{kT}} \tag{1.1}$$

where *k* is Boltzmann's constant and *kT* is the kinetic energy of an atom at temperature T. Hence at the higher temperature atoms will get excited thermally to its higher energy state E_1. In thermodynamic equilibrium, most of the atoms are in the ground state, the net effect will be the absorption of photons, and probability of the stimulated emission is rare. To produce laser light we must have a situation in which stimulated emission dominates. It is only possible if more atoms are in excited state than in the lower or ground state. Such a situation, in which the majority of atoms are excited, is referred to as a *population inversion*; this is a non-equilibrium situation under ordinary conditions.

In order to obtain a population inversion, the material must be excited by an external energy source having energy greater than or equal to the energy level of the atoms or molecules. This excitation of the laser medium is called *pumping*, which can be done optically, electrically, or by other excitation methods. Normally atoms in excited states have a short lifetime (~10^{-9} s) and release their energy by spontaneous emission. Therefore to produce population inversion, longer lived excited states are required, and such states, called meta-stable states, do exist. Meta-stable levels are stable on an atomic time scale and survive for microseconds or even for milliseconds.

1.1.2 Elements of Laser

To achieve lasing, a basic requirement is to realize population inversion by means of *external pumping* in *gain medium*. Once the population inversion is achieved and stimulated emission starts, it must be maintained in the gain medium by means of the *positive optical feedback*. By placing reflective surfaces at the ends of the gain medium parallel to each other, photons will be reflected back and forth along the cavity, forcing the excited atoms to decay via stimulated emission, making the laser beam highly directional. This positive feedback causes wave amplification along the cavity-length. A portion of this propagating wave transmits as a laser from partially reflective mirror.

Thus, any laser system consists of three basics components; gain medium, pumping source and resonator cavity. A simple laser diode configuration is illustrated in Fig. 1.2.

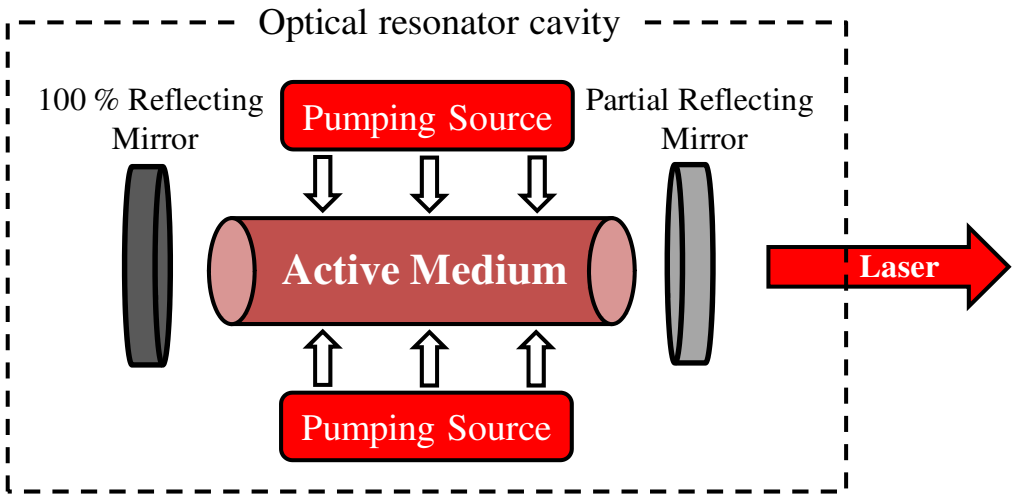

Figure 1.2: Illustration of basic structure of laser system.

Laser gain medium is the essential part of the laser system and used to realize gain and subsequent laser generation. It can be a solid, gas, crystal or semiconductor which can be pumped to the higher energy level. The material should have the suitable energy state, i.e. metastable state, to achieve population inversion. Also the gain medium should be of controlled purity, size and shape. Table 1.1 illustrates various types of material system currently used for lasers and the corresponding wavelengths. The wavelength of light being emitted from the system depends on the type of lasing material being used.

In order to achieve stimulated emission and to excite the atoms, electrons, molecules or ions a suitable **pumping mechanism** is necessary. Otherwise absorption will dominate at the cost of stimulated emission. There are several types of pumping mechanisms available viz. optical, electrical, thermal or chemical techniques, which depends on the type of the laser gain medium utilized.

Finally, **optical resonator** plays a vital role in the generation of the laser, which not only provides gain to the wave generated in the medium but also provides directionality to the out coming laser beam. The optical gain is achieved to overcome

losses like absorption, scattering or diffraction, by means of two mirrors, one is 100 % reflective and second one is partially reflective

Table 1.1: Common lasers and their wavelengths.

Laser	Wavelength (nm)
Argon Fluoride	193
Xenon Chloride Excimer	308 and 459
Xenon Fluoride	353 and 459
Helium Cadmium	325 - 442
Rhodamine 6G	450 - 650
Copper Vapor	511 and 578
Argon	457 - 528 (514.5 and 488 most used)
Krypton	337.5 - 99.3 (647.1-676.4 most used)
Ruby	694.3
Semiconductor Laser	UV to far-IR
Ti:Sapphire	690 - 960
Alexandrite	720 - 780
Hydrogen Fluoride	2600 - 3000
Erbium:Glass	1540
Carbon Dioxide	10600
Krypton-Fluoride Excimer	296
Nitrogen	337
Organic dye	300-1000 (tunable)
Helium-Neon	543, 632.8, 1150
Neodymium:YAG	1064

1.1.3 Lasing in Semiconductor

Unlike gas and solid materials, having electronic energy levels which are nearly as sharp as of isolated atoms, in semiconductors the energy levels are broadened into energy bands, consists of a very large number of closely packed energy levels, due to the

overlapping of atomic orbitals. In an undoped semiconductor with no external excitation at a temperature of T = 0 K, the uppermost energy band, called the *conduction band*, is completely empty and the energy band below the conduction band, called the *valence band*, is completely filled with electrons. The conduction band and the valance band are separated by a region of forbidden energy, called the *bandgap*. The semiconductor is characterized by its bandgap energy $E_g = E_C - E_V$, which corresponds to the energy difference between the bottom of the conduction band, E_C, and top of the valence band, E_V.

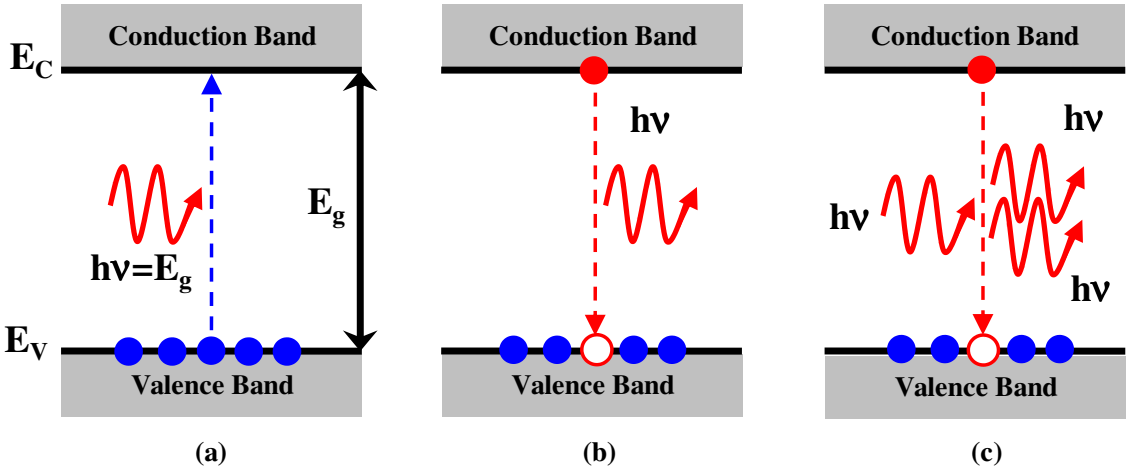

Figure 1.3: Radiative band-to-band transition in semiconductor. (a) Absorption, (b) spontaneous emission and (c) stimulated emission.

Energy transitions between bands are similar to changes of energy state in an atom, shown in Fig. 1.3. Basically, there are two types of carriers contribute to electronic transaction i.e. electrons in the conduction band and holes in the valence band. Initially, most of the electrons may occupy the lower energy and the conduction band is almost empty. If photon having energy $\geq E_g$ interact with semiconductor, it will excite the electron from valance band to the conduction band, leaving behind a hole in a valance band, as shown in Fig. 1.3 (a). However, this excited state is not stable and this excited electron will recombine with hole into the valance band radiatively by emitting a photon, either spontaneously or by stimulation (shown in Fig. 1.3 (b) & (c)), of the energy E_g. All three basic elements of a laser, i.e. gain medium, pumping, and resonator cavity apply special mechanism in case of laser diodes.

1.2 Elements of Semiconductor Laser

The basic elements necessary to realize a semiconductor laser are:

- A gain medium that provides optical gain by stimulated emission,
- Fabry-Perot resonator cavity creating optical feedback,
- An optical waveguide confining the photons in the active region of the device, and
- A lateral confinement of current, carriers, and photons

1.2.1 Gain Medium

The gain in laser diodes involves a whole crystal structure rather than excited single atoms, ions, or molecules. Semiconductor lasers can be excited by optical pumping with sufficient energy or by electron beams like gas or solid-state lasers. However, pumping the laser diode by applying an electrical current is the most efficient process compared to the other conventional technologies. Laser diode utilizes the conductivity of doped semiconductor material. The doping, either p-type or n-type, is achieved by introducing respective impurity atoms, acceptor or donor, to the intrinsic semiconductor material. Hence, the gain medium used in semiconductor laser is typically a p-n junction or a direct bandgap semiconductor material viz. gallium arsenide (GaAs).

Figure 1.4 shows energy band structure E(k) for electrons in direct and indirect semiconductor material. In indirect semiconductor like silicon or germanium, minima and maxima of conduction and valance band have different k-values as shown in Fig. 1.4 (a). Therefore, band-to-band recombination can occur not only with photons but also with the contribution of phonons or traps. Furthermore, these transitions are mostly nonradiative and are not suitable for laser activity as the light emission is not very efficient because the spatial density of phonons and traps is very low [3]. The mostly used material in laser diode is direct semiconductor where the maximum of valance band and the minimum of conduction band are at Γ-point (k = 0, shown in Fig. 1.4 (b)), i.e. at the center of the Brillouin zone. Direct bandgap structures maximize the tendency of electrons and holes to recombine radiatively and are more efficient for laser diodes and other light emitting devices.

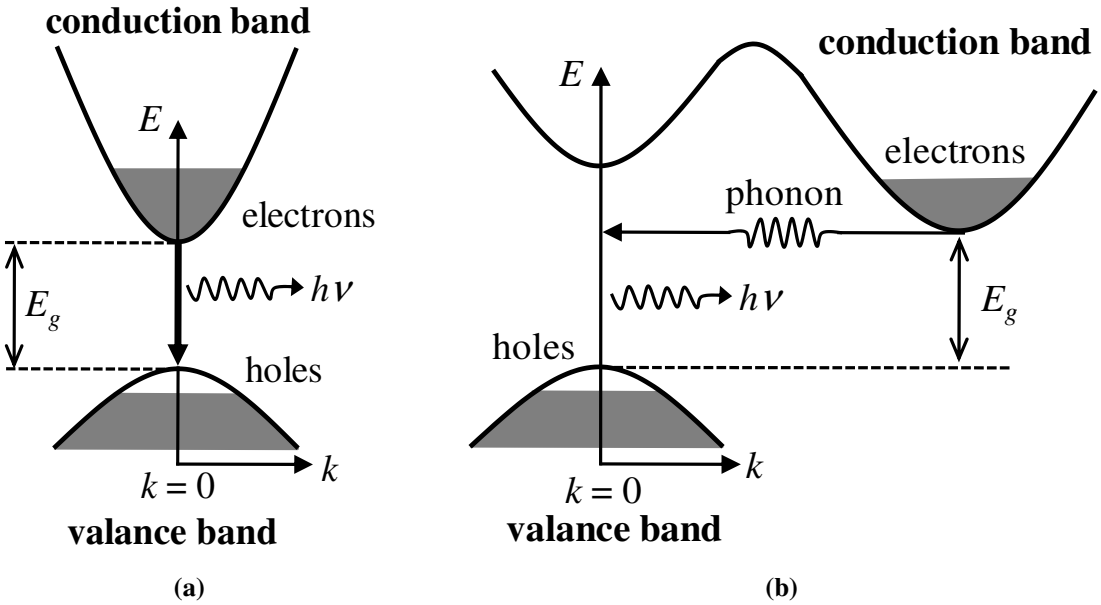

Figure 1.4: (a) Indirect and (b) direct bandgap in semiconductors.

Most direct bandgap semiconductors used for laser diodes are III-V binary or ternary compound material, i.e. combination of elements from the III and V group of periodic table. The attractive feature of these materials is that the binary compounds like GaAs and InAs can be alloyed to form ternary or quaternary compounds. By choosing appropriate compositions, it is possible to tailor the bandgap of the active layer and consequently tune the lasing wavelength. This is one of the key features that make it possible to fabricate laser diodes over a wide range of wavelengths. Gallium arsenide (GaAs), indium phosphide (InP), aluminum gallium arsenide (AlGaAs), indium gallium arsenide (InGaAs), indium gallium phosphide (InGaP) are commonly used direct semiconductor materials according to the desired lasing wavelength. Recently III-V nitride and III-nitride compound such as gallium nitride (GaN) and aluminum gallium nitride (AlGaN) have been used to achieve lasing in ultraviolet and blue regions [4].

1.2.2 Population Inversion

We have already discussed that, laser diodes utilizes the electrical conductivity of semiconductor materials by doping of impurity atoms. The doping, either p-type or n-type, is achieved by introducing respective impurity atoms, i.e. acceptor or donor, to the intrinsic semiconductor material. These atoms create new quantum mechanical states, donor level and accepter level, within the bandgap. Similar to the conventional

semiconductor diode, the laser diode consists of both p-doped and n-doped materials. When a forward electrical bias is applied to the device optical gain is generated at the active region viz. p-n junction or undoped direct bandgap semiconductor material. At the active region carriers i.e. electron and hole, will recombine radiatively and generates a photon, shown in Fig. 1.5.

Laser operation requires a process called pumping, which is achieved by means of nonequilibrium carrier distribution in to the semiconductor material. This carrier distribution has to be large enough to enable a population inversion to generate optical gain and is realised using forward biased laser diode. Considering a simple p-n junction laser diode consists of heavily doped, and hence degenerate, p- and n-type material where the Fermi levels are pushed in to the valance band and conduction band, respectively. At the p-n junction, a depletion region exists which prevents majority carrier flow, through diffusion, by forming diffusion potential. Hence, with no forward voltage bias, the quasi-Fermi levels are identical throughout the p-n junction at thermal equilibrium, as shown in Fig. 1.6 (a).

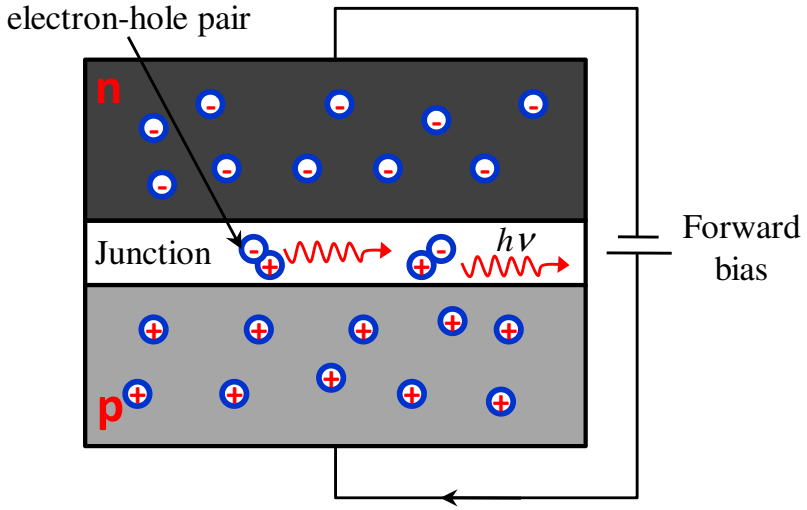

Figure 1.5: p-n junction under forward bias condition.

When the p-n junction is forward biased with a voltage (≈ E_g voltage), the diffusion potential is reduced, and free carriers can flow into p- and n-regions through the junction. Figure 1.6 (b) shows that, under forward bias, sufficient number of electrons and hole are injected into the conduction and valance band, respectively, and can create a population inversion in an active region where carries can recombine radiatively. Thus,

while population inversion, photon generated in radiative recombination process either can be reabsorbed or can induce stimulated emission. For stimulated emission to occur, the externally applied field must results in separation of the quasi-Fermi levels such that $(E_{Fc} - E_{Fv}) > h\nu > E_g$ [1].

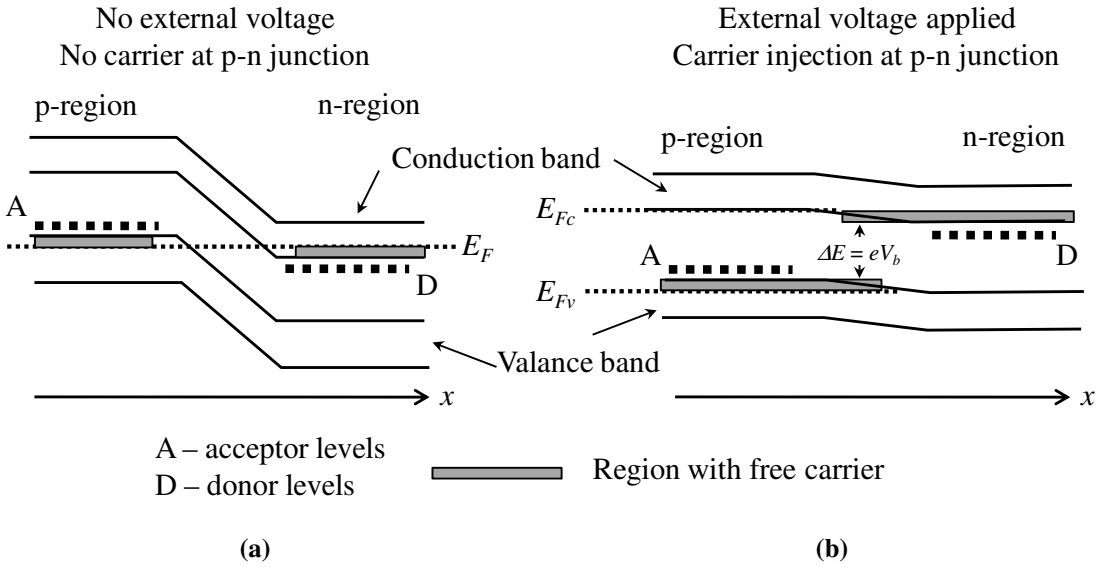

Figure 1.6: Band diagram of p-n junction under (a) zero bias and (b) forward bias conditions.

1.2.3 Resonator Cavity

The resonator cavity is used to provide a positive feedback loop for laser action. Usually, this can be realized by means of Fabry-Perot resonator consists of two parallel plane mirrors. In case of laser diode, usually edge-emitting laser diode, Fabry-Perot resonator cavity is achieved by cleaving the semiconductor crystal perpendicular to the cavity along well define crystal plane, shown in Fig. 1.7.

For GaAs the facets are cleaved at (110) plane and the growth of the active layer is in direction of (100) plane. Since the refractive index of the semiconductor material is very high (e.g. 3.6 for GaAs) in comparison with air, the reflectivity of the cleaved facets is sufficiently high to provide feedback for the laser oscillations. The reflectivity of the cleaved facets depends on the refractive index of the semiconductor. Equation 1.2 gives the reflectivity value for the case of normal incidence by Fresnel reflection [5],

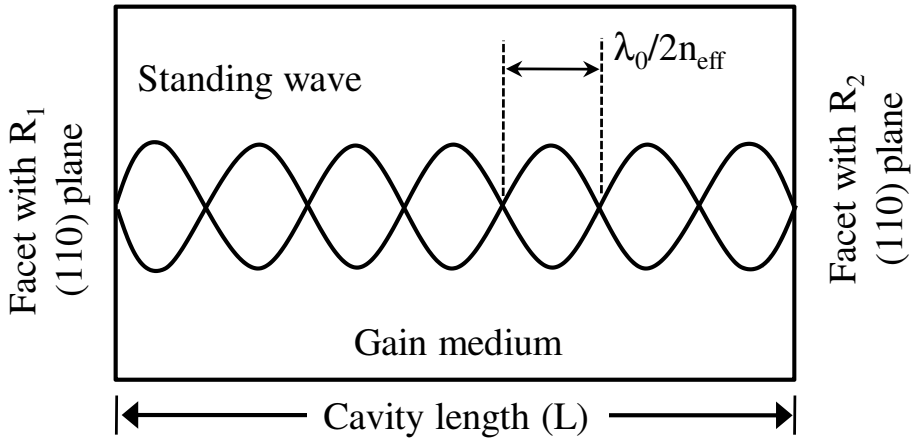

Figure 1.7: Illustration of standing wave in a Fabry-Perot resonator.

$$R = \frac{\left(n_s - n_a\right)^2}{\left(n_s + n_a\right)^2} \tag{1.2}$$

where, n_s and n_a is refractive index of semiconductor and air, respectively. For GaAs the reflectivity at normal incident is about 32 % at the GaAs/Air interface, which is sufficient to sustain laser oscillations in the medium. Before emission, photons emitted in parallel direction to the cavity length will be reflected severally at the facets. Each time they pass through the cavity, the light is amplified by stimulated emission. Hence, if there is more amplification than loss, the diode begins to lase. Also to enhance the lasing from the device, optical coatings of dielectric with appropriate refractive index can be applied to the facets to modify their reflectivities. Further the lateral confinement of photon is accomplished by gain or index guiding.

1.2.4 Vertical and Lateral Confinement

An epitaxial growth structure of a laser diode determines an optical waveguide and hence vertical optical confinement. An optical waveguide in a laser diode consists of a core film (e.g. quantum well) with high refractive index surrounded by a cladding material, i.e. n- and p-doped shield, with lower refractive index. Figure 1.8 illustrates the basic structure of laser diode consists of a three layer optical waveguide. The number of possible vertical modes and their distributions depends on the core film thickness and the refractive index difference between core and classing layers.

In addition, from the Fig. 1.9 we can say that this vertical growth structure also provides the carrier and optical confinement. To obtain single-mode operation in both transversal directions, an additional lateral confinement is required. There are three types of lateral-confinement mechanisms are possible: current confinement, optical confinement, and carrier confinement. Further details regarding lateral confinement are discussed in Chapter-3.

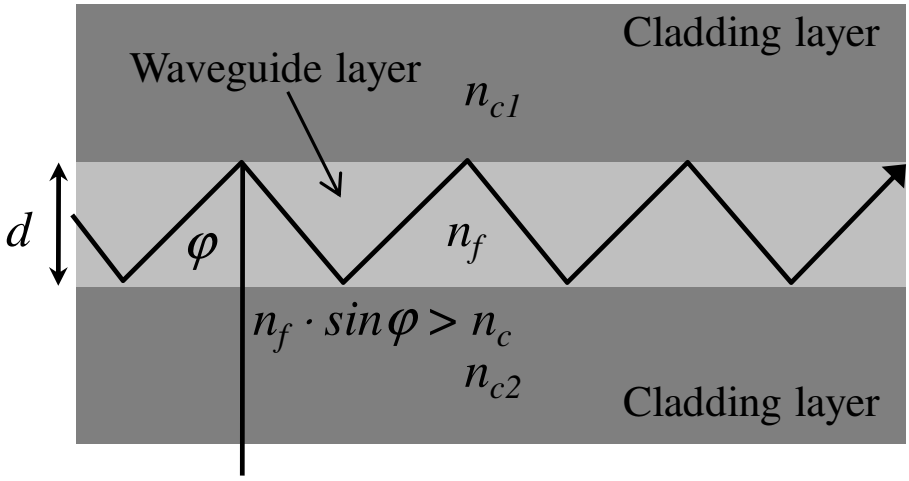

Figure 1.8: Schematic of an optical waveguide for double-heterostructure laser.

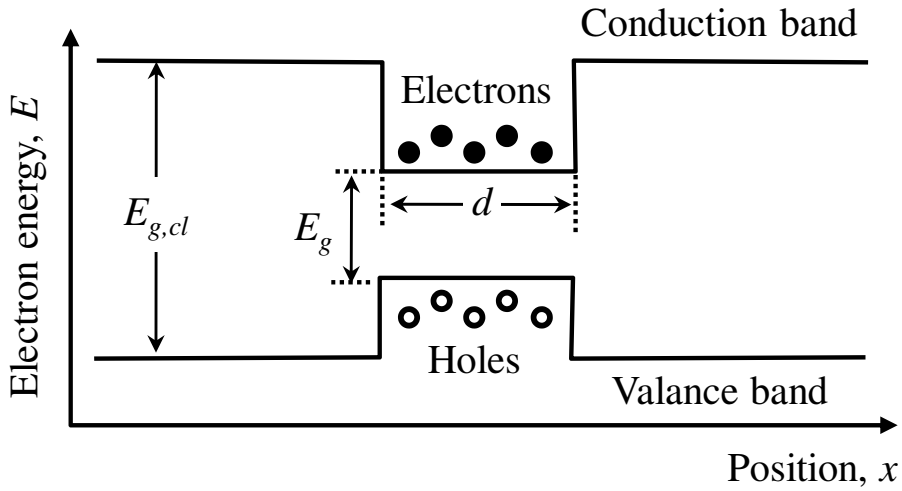

Figure 1.9: Energy band diagram shows vertical confinement of the carrier (electrons and holes) and photon in a double-heterostructure laser.

1.2.5 Condition for Lasing

A mathematical description of the lasing process in the laser diode can be obtained by calculating the optical field density inside the laser diode cavity [6]. As shown in Fig. 1.10, a Fabry-Perot resonator of cavity length, *L*, and a gain medium between two partial reflecting mirrors, with reflectivity R_1 and R_2.

The intensity, *I*, of a planar optical wave exponentially decreases while passing through an absorbing material in the z-direction, i.e.

$$I(z) = I_0 e^{(-\alpha_i z)} \tag{1.3}$$

here, I_0 is the initial intensity and α_i is the absorption coefficient, also know to as internal loss.

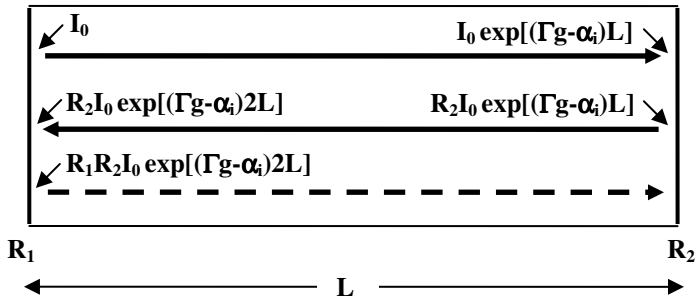

Figure 1.10: Intensity of an optical wave during a roundtrip in a Fabry–Perot resonator with cavity length L and mirror reflectivities R_1 and R_2.

Nevertheless, in laser diode the optical wave gets amplified and hence the optical gain is referred to as $g = (-\alpha)$. In an optical waveguide, the optical gain is classified in to two part because only a part of the intensity of the optical mode overlaps with active region, which is located in the center of the waveguide; one is material gain, *g*, i.e. the gain of active material itself and second one is the modal gain, g_{modal}, i.e. significantly lower gain of the optical mode. Thus intensity of a planar optical wave in an amplifying medium is given as

$$I(z) = I_0 e^{(g_{\text{modal}} z)} e^{(-\alpha_i z)} \tag{1.4}$$

The relation between modal gain and material gain is expressed by defining a confinement factor, Γ, which depends on the overlap of the optical-mode pattern with the gain region of the laser.

$$g_{\text{modal}} = \Gamma g \tag{1.5}$$

so, we can write Eq. 1.4 as,

$$I(z) = I_0 e^{(\Gamma g - \alpha_i) z} \tag{1.6}$$

The intrinsic modal absorption is caused by scattering of the optical mode at defects or rough interfaces and by free-carrier absorption. Although scattering is extremely low for semiconductor lasers with good crystalline quality, free-carrier absorption is inevitable since part of the optical-mode pattern overlaps with the p- and n-doped cladding regions. When the modal gain, g_{modal}, is larger than the modal loss, α_i, the propagating optical mode is amplified.

Moreover, some optical intensity leaves the cavity at these mirrors since the mirrors are partially reflective. As illustrated in Fig. 1.10, the intensity, I_{rt}, of the optical mode after a roundtrip in the cavity is given by

$$I_{rt} = I_0 R_1 R_2 e^{2(\Gamma g - \alpha_i) L} \tag{1.7}$$

Lasing occurs when the gain provided to the optical mode compensates the intrinsic absorption and the mirror losses for a roundtrip. The minimum gain, g, where the device starts lasing operation is called the threshold gain, g_{th}. In this case, the intensity, I_{rt}, after a roundtrip in the cavity again has its initial value, I_0.

$$I_{rt} = I_0 \tag{1.8}$$

This implies that

$$R_1 R_2 e^{2(\Gamma g_{th} - \alpha_i) L} = 1 \tag{1.9}$$

this gives,

$$\Gamma g_{th} = \alpha_i + \frac{1}{2L} \ln\left(\frac{1}{R_1 R_2}\right) \tag{1.10}$$

Equation 1.10 illustrates that the gain must compensate for the losses due to internal absorption, α_i, on the one hand, and the light leaving the cavity, also referred to as mirror loss on the other hand.

1.3 Laser Diode Structures

Laser diode has been evolved from a simple p-n junction diode structure to very complex structures like vertical external cavity surface emitting laser (VECSEL) due to the inventions of various growth technologies. The brief description of the various laser diode structures with their merits and demerits are discussed below.

- **Homojunction Laser**
  - ***Structure:*** a simple p-n junction of heavily doped same p- and n-type semiconductor material.
  - Carrier recombination and population inversion takes place in an active region, i.e. a depletion layer formed by p-n junction.
  - Optical feedback is realized by means of resonator cavity formed by cleaved mirror facets.
  - Since, there is no cladding layer, photon generated inside active region getting absorbed in p- and n- regions.
  - Also, the depletion region itself acts as an active layer having relatively higher thickness increases the threshold current density, at which laser begin to lase.
  - They can only be operated at cryogenic temperature with very high input current density of the order of 10^3 A/cm^2.

- **Heterostructure Laser**
  - ***Structure:*** a heterojunction of two unlike semiconductor materials.
  - Classified into two: (a) single heterostructure (SH) (b) double heterostructure (DH)
  - ***Single heterostructure:*** consists of only one side cladding layer
    - Confines only photon
    - Threshold current is high in comparison with double heterostructure laser.
  - ***Double heterostructure:*** consists of two side cladding layer, usually a p-i-n structure i.e. undoped semiconductor (low bandgap, high refractive index) sandwiched between two cladding layers (p- and n-type layer with high bandgap, low refractive index).
    - Confines both photon and carriers

- Carrier confinement can enhance stimulated emission and eventually reduce the threshold current.

➢ **Quantum Well Laser**

- ***Structure:*** similar to DH, quantum well laser consists of an active layer having thickness comparable to the de-Broglie wavelength of the electrons or holes (typically 5 – 10 nm), the motion of the carriers is quantized in two dimensions and the structure is known to as quantum well (QW) structure [2].
- Good carrier confinement due to potential well structure however, reduced active layer thickness exhibits poor optical confinement.
- Low threshold current compared to DH.
- Separate optical confinement is required.
- Wavelength tenability by means of strained QW structure.

➢ **Quantum Dot Laser**

- ***Structure:*** Dimensions of the QW is further reduced in such a way that carriers are confined in all three dimensions.
- Low threshold current
- High temperature stability
- High wavelength tunability

1.4 Brief History of Laser Diode

The word laser is an acronym for Light Amplification by the Stimulated Emission of Radiation. Basically the laser diode has a history as long as that of the laser itself. In 1917 Albert Einstein first suggested the existence of stimulated emission. However, it takes about 43 years to support the theory empirically when Theodore Maiman built the first laser using a synthetic ruby, two mirrors, and a flash lamp [7] in 1960. This first ruby laser, operated at 694 nm, opened the gateway for a variety of lasers, with various materials and operating wavelengths. Few year back in 1962, Robert N. Hall and his team has demonstrated first laser diode at General Electric Research Center, United States [8].

The laser diode has a history essentially as long as that of the laser itself, being first demonstrated in November 1962 by Robert N. Hall and his team at General Electric Research and Development Laboratories in Schenectady, United States [8]. In the same year, three more groups, at IBM T. J. Watson Research Center [9], at MIT Lincoln Laboratory, Texas Instruments, and RCA Laboratories, succeeded in making laser diodes at their respective laboratories [10,11]. Since then, the design of laser diode has undergone an almost continuous evolution. These first generation laser diodes were simple GaAs homojunction p-n diodes with polished sides of the crystal itself forming resonator cavity [8]. These laser diodes are operated with threshold current densities of 1000 A/cm^2 at 77 K temperature in pulse mode. The CW operation at room temperature was made possible only after the demonstration of double-heterostructure (DH) laser diode in which the active layer is sandwiched between two layers of higher bandgap materials. This was demonstrated almost simultaneously by Zhores Alferov of the Soviet Union [12], and Morton Panish and Izuo Hayashi working in the United States [13]. The concept of DH laser diode was proposed earlier by Kroemer [14] and Alferov [15] in 1963, whose importance was recognized by the 2000 Nobel Prize in Physics. The further need and search of better efficiency, reliability and higher power led the laser diode to the design of quantum-well (QW), strained QW, and multiple QW laser diodes.

In 1975, J. P. van der Ziel et al. [16] made the first observation of QW laser operation. However, they were operated at 15 K. The first room-temperature operation of QW injection laser was demonstrated by Dupius et. al. in 1977 [17]. It had a single QW and a threshold current of about 3 kA/cm^2 at 300 K when pulse-operated. Very next year, they demonstrated the first CW operation of single-QW and multiple-QW lasers [18,19]. This started a steady growth in the popularity of QW lasers, which is still continuing. Further improvements in the laser efficiency have also been demonstrated by confining the carrier in two dimensions or three dimensions. This can be realize by reducing the QW layer to a ‘layer’ of quantum-wires (QWRs) [20,21] or quantum-dots (QDs) [22].

1.5 Application of Laser Diode

Semiconductor lasers, laser diode, due to their small size, robust, high efficiency, and low cost, cover extremely wide range of lasing wavelengths and hence applications from

military to medicine and material science to meteorology. They are present in almost all field of our day-to-day life like, data storage, printing, lighting, laser marking, measuring, etc. Laser diodes find wide use in fiber optics communication as a signal source. It is a key component for laser printers, barcode readers, CD, DVD and Blu-ray disc drive. Moreover, the innovative improvement in laser diode fabrication technology and semiconductor material systems has revolutionize the two major systems of the information technology in last decay i.e. optical data transfer and optical data storage. Laser diodes are also used as optical pumping source or an optical amplifier in diode pumped, solid-state laser and fiber laser [23]. On basis of wavelength emitted from the laser diode, they have different application in various fields, as shown in Table 1.2.

Table 1.2: Various laser diodes applications depending on their emission wavelength [24].

Laser wavelength (nm)	Applications
405	Blu-ray disc and HD DVD disc drive
375 - 485	GaN based ultra-violate laser used in biomedical/medical applications
532	Laser pointer,
650	Laser pointer, CD-DVD disc drive
670	Bar code reader, printer
780	Raman spectroscopy
785	CD disc drive
808	Thermal printing
810	Nd:YAG diode pumped solid state laser (DPSSL)
980	Erbium doped fiber amplifier, Yb:YAG DPSSL
1310, 1550	Fiber optic communications
1650 - 3300	Gas sensing (mostly in meteorology)

Besides this, medical diagnosis and surgery, sensing, illuminators, weaponry, and industrial applications such as welding, cutting, heat-treating, cladding, and industrial machining are some of the other significant high-power applications of laser diode. Due to their high-power, small size, high efficiency and advancement in packaging

technology, laser diodes are becoming an alternative to flash-lamp pump solid-state laser and carbon dioxide (CO_2) gas lasers.

These applications require reliable and efficient high-power continuous-wave (CW) or pulse mode operation of laser diodes. This application outline gives an impulse for the improvement of high-power laser diode (HPLD) reliability.

Despite their extensive usage, laser diodes are still a subject of dedicated research in a view of technological development, especially in India, because the technology of semiconductor processing is in its infancy in India. The optimization of various processes for the fabrication of high-power laser diode is of principal importance and five national laboratories in India are presently pursuing research in this direction: (1) Raja Ramanna Centre for Advanced Technology (RRCAT), Indore; (2) Tata Institute of Fundamental Research (TIFR), Mumbai; (3) Solid State Physics Laboratory (SSPL), New Delhi; (4) Central Electronics Engineering Research Institute (CEERI)-Pilani, Rajasthan and (5) Society for Applied Microwave Electronics Engineering and Research (SAMEER), Mumbai. Facet coating of laser diodes is being carried out at SSPL and CEERI only, whereas for bonding purposes some efforts have been put by TIFR and SSPL. Packaging of laser diode is being carried out at SAMEER, Mumbai. Fabrication and processing of laser diode is also being carried out at RRCAT. They have also started optimising facet coating and packaging of the laser diode. Recently, the unbounded diode laser of 450 mW/facet continuous wave (CW) power from single diode element of 980 nm wavelength with slope efficiency 0.82 W/A has already been reported at Semiconductor Laser Section (SCLS), RRCAT [25]. However, the high-power laser diode is still at a laboratory level and so far no industrial or manufacturing unit has entered this field of technology in India as per the best of our knowledge.

1.6 Motivation

Laser diodes are basically consists of a gain section between two mirror facets of a semiconductor crystal. Due to their high output power, small size and high efficiency laser diodes have potential to replace other laser viz. gas laser or solid-state laser, in various scientific and industrial applications. However, the reliability and lifetime of the

laser diodes are still the crucial matter of concern and require significant development in laser diode fabrication technology. The major issue concerning with high-power laser diode is the device degradation. Basically, there are three main degradation modes namely rapid, gradual and sudden failure [26], affecting reliable performance of the laser diode. In case of high-power laser the most common degradation mode is sudden failure, also known to as catastrophic optical damage (COD) or catastrophic optical mirror damage (COMD).

In last decade, several studied have been performed to improve COMD level in various laser diode structures and its material systems such as AlGaAs, InGaAs, InGaP and InGaAsP. The increasing demand and importance of extracting more output power from the high-power laser diode has not only promoted the need to improve laser diode characteristics, but also encouraged the study to understand the causes behind the various failure modes. It has been revealed that during COMD dark line defects (DLDs) develop from the output facet into the lasers as dislocations and dislocation networks [27,28].This characterizes COD as a general mechanism related to high-power densities. Recent developments to overcome COMD include facet passivation [29] to reduce surface recombination velocity and hence facet degradation, variations in laser diode structures viz. quantum well intermixing [30] and low optical confinement structures [31] are introduced to decrease absorption at the facet, and non-injecting mirror [32,33] and non-absorbing mirror approach [34,35] to reduce current density and optical density in the vicinity of the laser facets.

Today's laser diodes are most efficient devices that convert electrical power into the optical. However, while operating in high-power mode part of the electrical power remains in the device and converted into the heat causes poor device performance. Therefore, to achieve high-power operation packaging of the device is the most vital part to attain. The present thesis deals with the optimization of various processes for the fabrication of high-power laser diodes to improve its lifetime and reliability. These processes include the epitaxial growth of laser diode structure, post-growth device-processing, facet coating, packaging and characterizations.

1.7 Thesis Overview

The present thesis deals with the post-growth processing and various fabrication processes for HPLD. These processes include laser diode processing, facet coating, and packaging. Each of these processes plays a vital role in determining the overall performance of the laser diode and need to be optimized very carefully, as various laser diodes characteristic parameters viz. electrical, optical, spectral, and device life-time, depend on it. The thesis includes the development and optimization of these processes for HPLDs to improve its performance and hence it reliability. The thesis also consists of various laser diode characterization techniques to characterize laser diode at different stages of optimization. The fabrication and automation of these characterization facilities are also discussed in the thesis.

The post growth processing has been optimized for InGaAs/GaAs double QW HPLD, fabricated at semiconductor laser section (SCLS), Raja Ramanna Center for Advance Technology (RRCAT), Indore (M.P), using metal organic vapor phase epitaxy (MOVPE) technique. The epitaxially grown wafer was processed to make laser diode bars using mesa-stripe geometry. Photolithography and lift-off processes are employed to form top metal contact stripe on the wafer. The contact stripe geometry of the laser diode defines the threshold current and external efficiency of the device and hence the optimization if this process is very crucial for HPLD. Moreover, mechanical lapping and polishing has been done to thin down the substrate up to 150 μm thickness, which reduces the device's electrical and thermal resistance and hence increase the efficiency. The metal contact deposition is also a very important process as it contributes to the series resistance of the devices. This process is optimized to minimize the series resistance.

The next step after optimizing the device processing is to passivate facets of cleaved laser bars by means of coating the facets with dielectric materials such as aluminum oxide (Al_2O_3), silicon dioxide (SiO_2), zirconium oxide (ZrO_2), titanium dioxide (TiO_2), or magnesium fluoride (MgF_2). The face-passivation to the laser diode reduces the surface recombination velocity and hence the degradation of the facets. Eventually, it increases the optical output power level at COMD (P_{COMD}). The cleaved bare facet, without facet coating, laser gives optical output from both the facets. In most of the

applications optical power from only one of the two facets is useful. So we have designed and optimized single layer anti-reflection (AR) and quarter-wave optical thick (QWOT) multilayer high-reflection (HR) coatings on the front-and on the back-facets of the laser diode, respectively. The AR-HR films are deposited using electron beam evaporation technique. A special jig is designed and fabricated to hold the laser diode bar in the vacuum chamber during the facet coating. The AR-HR coatings are optimized for various laser diode structures such as,

- 808 nm multimode commercial laser diode [36];
- 980 nm, InGaAs/GaAs double QW laser diode grown by MOVPE [25,37,38];

We have also designed and installed in-situ reflectivity measurement system for precise control and monitoring of thin film reflectivity of AR and HR film during facet coating. To verify the empirical reflectivity data, measured in-situ, we have developed a numerical simulation based on the characteristic matrix solution [39]. The optical output power is enhanced from the front facet by a significant amount [36, 38] as a result of AR-HR facet coating. The optimized facet coating have also been tested for laser-induced-damage thresholds (LIDT) measurements and proved to be a suitable facet coating for HPLD [40].

The HPLDs characterization facility viz. L-I-V characteristics, spectral response, junction temperature measurement [41], life-time [42], and thin film characterization viz. transmission and reflection spectral measurements have been automated using Laboratory Virtual Instrument Engineering Workbench (LabVIEW).

Finally, the laser diode packaging has been optimized to mount the device on proper packages, according to its utilization. The packaging of the HPLDs is the most essential process for device production. It provides not only the mechanical support but also the electrical and thermal conduction to the device that makes it suitable for all applications. The leading factor in the laser diode packaging is die-and wire-bonding. The process to solder the laser chip or bar to the appropriate substrate by means of the any solder material viz. indium (*In*), gold tin (*AuSn*), known as die-bonding; while the further electrical interconnections of the laser chip/bar to the contact lead of the package by

means of gold wire or ribbon is known as wire-bonding. Laser diode die-bonding is an essential part of the packaging which makes the device handy for further application. We have optimized the HPLD die-bonding process with two different types of solder material/s, namely, *In* preform (soft solder) and eutectic *AuSn* (hard solder) preform, using an indigenously developed setup [43].

Thermal management is an important factor for HPLDs packaging because the spectral response and lifetime are very sensitive to the device operating temperature. The chip material, the bonding medium and mount may have different coefficient of thermal expansion (CTE). As a result, significant stresses are produced on the bonded laser diode structure. These stresses may induce chip cracking and joint fracture thereby causing the device failure. Hence, the packaging substrate material selected for the laser diode should have high thermal conductivity and the coefficient of thermal expansion (CTE) should be matched with the device's substrate material i.e. GaAs, in our case. We have used gold plated Copper (*Cu*) and KOVAR (Ni:Co:Fe::29:17:54 wt%), as packaged substrate to optimize the bonding process. Once the laser diode chip is attached on the package, the next step in the packaging is assembly interconnection. The most common method for electrical interconnections is wire bonding. Thin metal wire, usually gold, was used to connect device and contact lead. Wire bonded laser diode assemblies are then tested and characterized for high-power CW operation and life-time measurements.

The improved device performance has successfully been demonstrated after applying various optimized post growth process to the HPLDs. Single laser diode element with effective packaging gave an output power of ~ 670 mW/facet at ~ 2 A under CW operation with the dynamic series resistance of ~ 200 mΩ. Subsequently, the developed semi-packaged, non hermetic, laser diode was used for the characterization of electronic transitions of InAsP/InP quantum well in photoluminescence (PL) spectroscopy.

1.8 Thesis Organization

The thesis entitled "Reliability and Life-Time Improvement of High-Power Laser Diodes" has been organized in total six chapters, as follow:

Chapter 2: Following to the introductory chapter-1, the chapter includes primary characteristics of the laser diode, i.e. L-I and I-V characteristic, spectral response, lifetime measurement, and the optimization of its characterization processes. The development and upgradation of these characterization facilities and online data acquisition by means of LabVIEW (ver. 8.2) is also discussed in this chapter. The successful extraction of various laser parameters [Threshold current (I_{th}), Optical power (P_{out}), Turn-on voltage (V_0), Dynamic series resistance (R_s), Slope efficiency (η_{slope}), Differential efficiency (η_d), Junction temperature (T_j), and device Life-time (τ)] using an automated data acquisition system is described in this chapter.

Chapter 3: The chapter describes the study of growth and processing of HPLDs. It discusses laser structure design and growth techniques used for the fabrication of quantum well (QW) laser, in brief. The optimization of post-growth processes to fabricate the laser diode out of grown wafers is discussed in detail in this chapter. The laser diode processing to develop desired laser geometry (i.e. mesa-stripe in our case), comprise of: photolithography and lift-off process to make stripes, metal-semiconductor contact layer deposition, rapid thermal annealing (RTA), mechanical lapping and polishing, chemical etching, and scribing.

Chapter 4: This chapter deals with AR and HR coating of the front and back facets of the HPLD, respectively. Various dielectric oxide materials like aluminum oxide (Al_2O_3), titanium dioxide (TiO_2), silicon dioxide (SiO_2), zirconium oxide (ZrO_2), and magnesium fluoride (MgF_2), and their combinations are used to achieve the desired reflectivity, on respective facets, to optimize the facet coating process. Thin film deposition and its optical characterization, i.e. reflectivity measurement, are also discussed in brief, including in-situ reflectivity measurement, i.e. online reflectivity measurement and optimization while material is being deposited for the desired laser wavelength. The numerical simulation was done to calculate thin film reflectivity for particular wavelength using LabVIEW (ver. 8.2). The thickness of the film was estimated by means of matching the empirical reflectivity data to the simulated one. The effect of facet coating on laser diode performance is studied by measuring various laser parameters like, threshold current, optical power, and device-efficiency.

Chapter 5: This chapter describes optimization of bonding and packaging process for the HPLD. After being fabricated, the laser diode has to be bonded on some packages, to get properly utilized, by means of solder materials. Laser diode packaging process consists of die-bonding and of wire-bonding of the device. The laser diode chip/bar, generally known as die in technical terminology, is attached to the package by means of any solder material, the process is known as die-bonding. Parameters like bonding-temperature and curing-time are optimized for indium preform and gold-tin eutectic solder preform. Consecutively, the wire-bonding parameters viz. bonding-time, temperature, ultrasonic power, bonding-force, etc., have been optimized to provide external connection to the laser diode with package. The effect of bonding on various characteristic parameters of the laser diode is studied in this chapter, in detail.

Chapter 6: This final chapter contains miscellaneous topics related to the studies on damage testing of facet coated materials, device life-time measurement, and application of the packaged device. In case of HPLD, the main factor which limits the high-power operation is facet-degradation. To overcome this limitation, we have already optimized the facet coating; however, to improve the quality of the facet coating further, we have measured the damage threshold of these optical coatings using high-power solid state Nd:YAG laser operated under pulse mode and continuous wave (CW) operation. The effect of packaging on the reliability and performance of laser diode by measuring the device life-time is also discussed in this chapter. Finally, we have demonstrated the device application in photoluminescence spectroscopy of InAsP/InP quantum well samples.

* * *

Chapter 2

Development of Characterization Facilities for the High-Power Laser Diode

2. Development of Characterization Facilities for the High-Power Laser Diode

The consistent measurement of the laser diode performance characteristics is an essential tool during development and qualification of the laser diode. It is also necessary to test the laser diode performance frequently over the different stages of its production viz. from the structure-growth to packaging. The characterization measurement mainly includes the performance test namely optical, electrical, spectral, thermal parameters and the reliability test such as lifetime measurement of the device. In order to preserve the uniformity of measurement conditions with higher precision, we have developed and established an automated laser diode characterization facility using LabVIEW. This chapter discusses the characterization setup along with interfacing and programming technology used for the automation.

2.1 Laser Diode Characteristics

The laser diodes have a variety of applications including communications systems and solid-state laser pumping. When using a laser diode it is essential to know its performance characteristics. This can be done by carrying out series of experiments and obtaining certain significant parameters from which we can determine how well the laser diode is performing. There are number of laser diode characteristics that are essential to the overall device performance. The following is a brief description of the most common parameters that can be experimentally determined and the techniques involved in the analysis of the data.

2.1.1 Light–Current (L–I) Characteristics

One of the most commonly used and important laser diode characteristics is the Light – Current (L–I) characteristic curve, referred to as L–I curve (shown in Fig. 2.1). It is a plot of light output power as a function of drive/operating current for a specific laser diode at a certain temperature.

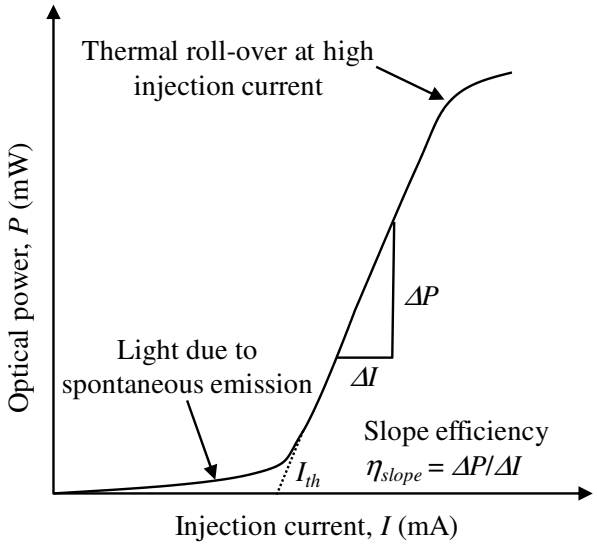

Figure 2.1: A typical Light vs. Current (L–I) characteristic curve of a high-power laser diode. I_{th} represents the threshold current at which the device begins to lase. The efficiency of the laser in converting electrical power to light power is determined by the slope of the L–I curve, denoted by the change in output power over the change in current (ΔP/ΔI).

As shown in Fig. 2.1, as the operating current is increased, initially the laser shows spontaneous emission which increases gradually until net gain through the cavity overcome the losses and stimulated emission dominates. From this characteristic, it can be seen that there is a threshold current (I_{th}) below which the laser action does not take place. Analyzing the L-I curve can yield some important information about the laser diode. The evidence of undesirable "kinks" or non-linearity's in the L–I curve indicate the intrinsic problems that lead to rejection of the device. For example a kink can be indicative of filamentary emission due to defects in laser structure or mode-hopping in the optical spectrum [44], which is very undesirable, particularly in applications like optical pumping and optical communication [45]. The L–I curve analysis provides us three fundamental laser characteristic of the laser – light output power, threshold current, and device efficiency. Furthermore, by varying the measurement conditions for L–I characteristics, more important parameters like characteristic temperature T_0 and thermal impedance R_{th} of laser diode can be extracted.

❖ Threshold Current

The first parameter of interest is the exact operating current value at which laser diode begins to lase. In other words, the current must supply enough carriers to overcome other internal losses, such as leakage current – The current going around the active region, not contributing any carriers for useful recombination and nonradiative recombination process, so that it can provide the necessary threshold gain [46]. At a low current level, spontaneous recombination dominates and the L–I curve (output power) remains low [47]. Once the current level passes threshold current, the stimulated emission causes sudden increase in curve and hence change in the slope of the curve [3].

It is generally desirable that the threshold current (I_{th}) be as low as possible, resulting in a more efficient device. A high threshold current can significantly heat up the device and cause its degradation. Also, a low threshold current minimizes the input power requirement of a laser and hence reduces the operating expenses of the laser based systems. As a result, threshold current is one measure used to quantify the performance of a laser diode.

Threshold current depends upon the laser diode structure design and the quality of the semiconductor material from which the device is fabricated. Nevertheless, the threshold current is more influenced by the physical dimensions of laser diode stripe, i.e., stripe width and cavity length. Hence, the threshold current is higher for a laser diode with larger stripe-area. In consequence to that it is better to evaluate the laser diode structures by means of threshold current density rather than by the threshold current. The threshold current density is the ratio of threshold current to stripe-area of the laser diode and is denoted by the symbol J_{th}. It is always desirable for a laser diode to have as low threshold current density as possible.

Since the lasing process is a steady-state phenomenon, gain should clamp at the threshold gain even as current is increased [47]. Therefore, ideally, the graph should exhibit linear behavior after lasing has begun. Using this fact one can plot a straight line on a linear part of the graph that extended down to the current axis, i.e. abscissa in L–I curve (as shown in Fig. 2.1). The intercept on the abscissa of this straight line is taken as

threshold current, I_{th}. There are four different algorithms available to calculate the threshold current of a laser diode viz. linear fit, two segment fit, 1st derivative of L–I, and 2nd derivative of L–I [48]. We have combined the Linear Fit method with the Second derivative method to find the threshold current programmatically from experimental L–I curve.

❖ Device Efficiency

➢ Slope Efficiency (η_{slope})

Since it is necessary to get lasing at low threshold current, I_{th}, it is also desirable to get more and more extraction of the light from the laser diode with the expense of as little current as possible. In other words, with very little increase in operating current we want to have rapid increase in the output light emission. A laser diode, which has good electrical to optical conversion efficiency, is obviously a device that performs well. Hence, the laser diode efficiency is another essential parameter that is deduced from slope of the L–I characteristic curve above the I_{th} of the laser. It is very useful and practical parameter let us to know that how much more output power can be estimated from the laser at given ascertain amount of increasing in current above I_{th}. The laser diode slope efficiency is generally defined as the slope of the straight line, i.e. *dP/dI*, used to estimate I_{th} and measured in terms of watt/ampere (W/A), as shown in Fig. 2.1.

$$\eta_{slope} = \frac{dp}{dI} \tag{2.1}$$

➢ External Quantum Efficiency (η_d)

This is a figure of merit which indicates the efficiency of a laser device in converting the injected current carriers (electron–hole pairs) to photons emitted from the device (output light). It can be determined by measuring the slope efficiency of the device. In an ideal laser diode, the recombination of each electron–hole pair results in the generation of one photon, which is emitted from the device as well. Whereas in case of real laser diode, not all injected electron–hole pairs are results in the generation of the photons, some often recombine non-radiatively and cause device heating. In addition to that, some photons generated inside the laser cavity do not contribute to the light emission as they are getting absorbed into the laser material [3].

Thus, on increasing the operating current *I* by an amount *dI*, i.e. by injecting *dI/q* numbers of charge carriers in time *dt*, where *q* is the fundamental electronic charge, if the optical power increases by an amount *dP*, then we get *dP/(hc/λ)* number of photons emitted out, where *(hc/λ)* is the energy of single photon with wavelength *λ*. Thus, according to the definition of external differential quantum efficiency (as per Eq. 2.2),

$$\eta_D = \frac{dP/(hc/\lambda)}{dI/q} = \frac{q\lambda}{hc}\frac{dP}{dI} \tag{2.2}$$

where, *h* is the Planck's constant, *c* is the velocity of light in vacuum and *dP/dI* is the slope efficiency of the laser diode.

- **Internal Quantum Efficiency (η_i)**

This is one of the main laser diode parameter that should be used to evaluate the quality of the semiconductor material from which the laser diode is manufactured. This parameter is a measure of the efficiency of a laser in converting injected current carriers (electron–hole pairs) into photons (light) within the laser diode structure. The net internal optical loss, on the other hand, is a coefficient that relates the number of existing photons to the number of photons that will remain inside the cavity after having traveled a certain distance. Hence, the internal quantum efficiency (Eq. 2.3) (η_i) is defined as the radiative recombination rate divided by the total (radiative + nonradiative) recombination rate [3]:

$$\eta_i = \frac{R_{rr}}{R_{rr} + R_{nr}} \tag{2.3}$$

The laser diode having longer cavities have a lower facet loss as the photons tends to remain inside the cavity for a longer period of time, rather than being emitted from the laser. This does not mean that laser with shorter cavities are preferred; lasers of longer cavities can reach a higher power although they have lower efficiencies [49]. Unlike the external differential quantum efficiency, the internal quantum efficiency is independent of the geometrical properties of the laser device, such as the cavity length or the stripe width. Consequently, it is the proper parameter for comparison of the material quality of various lasers made from various semiconductor wafers. Thus, the internal quantum efficiency can be derived by experimentally measuring external differential quantum efficiency of the devices having different cavity lengths and fitting the measured data into the following Eq. 2.4.

$$\frac{1}{\eta_d} = \frac{1}{\eta_i}\left[\frac{\alpha}{ln\left(1/R\right)}L + 1\right] \tag{2.4}$$

where, η_d is the device external quantum efficiency, α is the net internal optical loss, η_i is the internal quantum efficiency, R is the mean mirror reflectivity, and L is the cavity length.

As the equation suggests, a straight line can be obtained by plotting the reciprocal of the measured external efficiency versus cavity length. The intercept on the ordinate, i.e. Y axis, of the straight line gives the inverse of the internal quantum efficiency and that can be used in the Eq. 2.4 to obtain the net optical loss [47].

Note that there is a difference between internal quantum efficiency, η_i and external differential quantum efficiency, η_d. The internal quantum efficiency is a direct indication of the efficiency of a laser in converting electron-hole pairs (injected current) into photons (light) within the laser diode structure. But not all of the photons that are generated find their way out of the device; some of them are reabsorbed due to various internal loss mechanisms. As a result, the external differential quantum efficiency is an indication of the efficiency of a laser in converting electron-hole pairs (injected current) into photons emitted from the laser device (output light). The value of the external differential quantum efficiency is always smaller than the internal quantum efficiency. $(\eta_d) / (\eta_i)$ is the ratio of number of photons emitted from the laser to number of photons generated within the laser.

2.1.2 Voltage–Current (V–I) Characteristics

The Voltage – Current (V–I) characteristic is also an important measure of the laser diode like any other electronic or optoelectronic components. The laser diode specification for the forward voltage across the diode is essential in number of areas of its application. The forward voltage specification will vary according to the materials used in the diode, current, etc. Although the forward voltage does vary with temperature, this is not normally a major consideration. The typical laser diode V–I characteristic curve is shown in the Fig. 2.2.

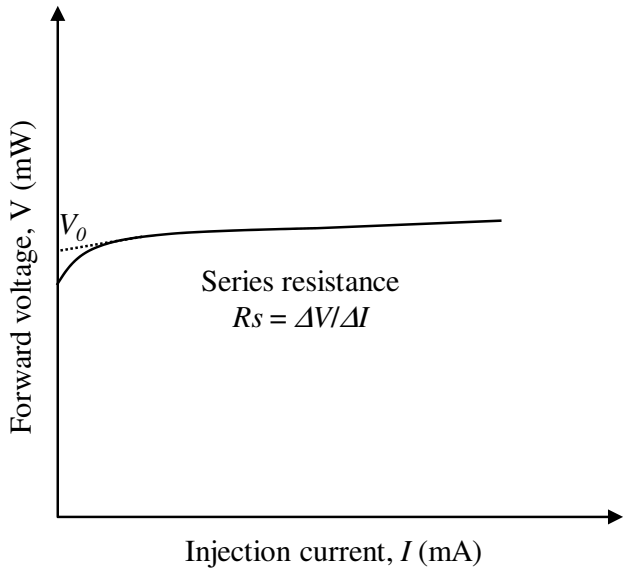

Figure 2.2: The typical laser diode V–I characteristic curve. The intercept on the Y-axis gives the value of the turn-on voltage, V_0, and the series resistance, R_S, can be determined from the slope of the linear part above the turn-on voltage of the V–I curve.

From the laser diode V–I characteristic curve we can extract two parameter viz. turn-on voltage, V_0, and series resistance, R_S. The intercept on the ordinate i.e. Y-axis of the V–I curve gives the value of the V_0. The turn-on voltage, V_0, indicates the lasing wavelength of the laser diode, which is ideally almost equal to the bandgap voltage i.e. $h\nu/q$ [1] of the device. The series resistance, R_S, of the laser diode is determined through calculating the derivative of the V–I characteristic curve above the turn-on voltage of the device [50]. From the values of the V_0 and R_S the total voltage, $V = V_0 + R_S I$, can be determined. The high series resistance values could be the result of low quality metal ohmic contacts of the device, leading to the degradation of laser diode. Thus, measurement of the series resistance value can be a means of assessing the quality of the metallic contacts deposited on the laser.

2.1.3 Spectral Response Measurement

The laser diode specification for wavelength will determine many of the applications for which it can be utilized. The capability of the laser diode to support number of spectral lines is a function of the cavity structure and the operating current as well. The laser diode may be specified as being either single or multimode following to their geometry. The photon generated into the laser diode structure is confined in a very thin waveguide layer

viz. quantum well; such structure allows only a single mode operation in the direction perpendicular to the layers. However, the laser structure with wide waveguide compared to the wavelength of the light in the lateral direction can support multiple lateral optical modes, and the laser is known as a "multimode" laser diode. The number of spectral lines supported by a laser diode depends upon the cavity structure [51].

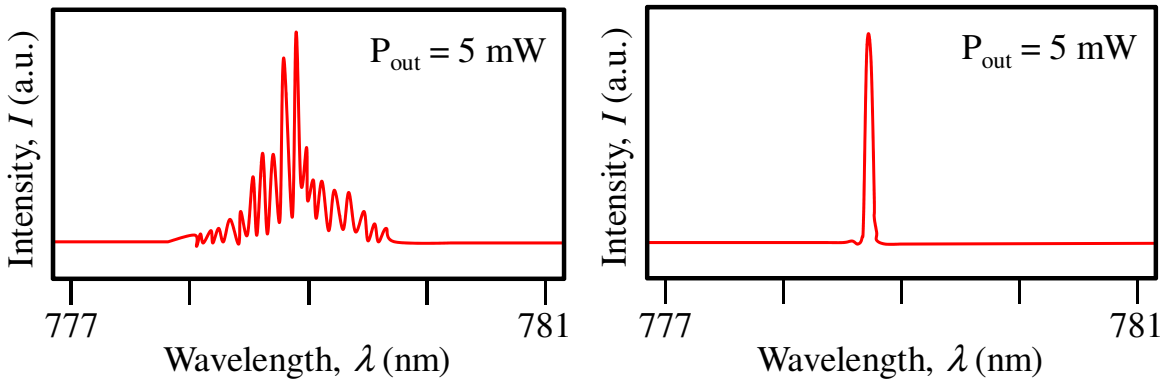

(a) **(b)**

Figure 2.3: Typical spectral response of (a) multimode laser diode exhibits spectral output having many peaks around their center wavelength and (b) single mode laser diode shows a well defined spectral peak.

The optical wave propagating through the laser cavity forms a standing wave between the two mirror facets of the laser diode. The period of oscillation of this curve is determined by the distance L between the two mirrors. This standing optical wave resonates only when the cavity length L is an integer number m of half wavelengths existing between the two mirrors, i.e., for $L = m\lambda/2$, where λ is the wavelength of light in the semiconductor material and is related to the wavelength of light in free space λ_0 through the index of refraction n by the relationship $\lambda = \lambda_0/n$. As a result of this situation, there can exist many longitudinal modes in the cavity of the laser diode each resonating at its distinct wavelength of $\lambda_m = 2L/m$. Thus, a multimode laser diode exhibits spectral output having many peaks around their center wavelength. The two adjacent longitudinal laser modes are separated by a wavelength of $\Delta\lambda = (\lambda_0)^2/2nL$. Unlike the multi-mode laser diodes, single frequency laser diodes such as Distributed Feed-Back (DFB) and Distributed Bragg Reflector (DBR) type of devices display a single well defined spectral peak [52,53]. Figure 2.3 shows these two spectral behaviors.

One of the measures of the spectral response quality is the linewidth. It is defined as the full width at half maxima (FWHM) of the main laser mode. The spectral linewidh is a measure of the phase noise under continuous wave (CW) operation. For distributed feed-back (DFB) lasers linewidths should be less than 5 nm. The spectrum of the main lasing mode can be approximated by a Lorentzian with a FWHM given by [54]:

$$\Delta v = \frac{R_{SP}}{4\pi} \frac{(1+\alpha^2)}{P_0} \tag{2.5}$$

where, R_{SP} is the spontaneous emission rate. One interesting fact about Eq. 2.5 is that the linewidth decreases as the output power increases. This is only true for low power levels as it has been shown experimentally that the linewidth saturates above 10 mW for 1.55 μm DFB lasers [55]. The linewidth enhancement factor is a material parameter influenced by the doping and geometry of the active region. From (11), it is clear that smaller enhancement factors are more desirable. Strained MQWs offer the smallest linewidth because such lasers have enhancement factors near unity [56].

Unlike other laser devices the laser diodes are unfavorably poor to provide a stable output in terms of the wavelength. They are affected by both the operating current and the temperature. Changes in temperature affect the bandgap, and hence the gain frequency profile of the junction. The lasing wavelength strongly depends on the operating temperature of laser diode [57]. As the temperature increases, the center wavelength shows the red-shift. This property of laser diode is useful in optical communication [58,59], spectroscopic applications [60,61], and pumping of solid state lasers [62] where the emission-wavelength of the laser diode can be accurately temperature-tuned.

2.1.4 Lifetime Measurement

Reliability and lifetime are concern in every laser diode application. In general, laser diode reliability may be defined as the ability to operate the device satisfactorily in a defined environment for a specified period of time, also known as *lifetime*. The laser diode life testing is used for part qualification during product development as well as for lot testing during the production life of the laser. Life tests generally consist of monitoring the operation of a sample group of lasers under carefully controlled

conditions. Degradation is observed and recorded throughout the test by precise measurement of changes in the laser's operating characteristics.

There are several methods of extrapolating laser diode lifetime. Depending on the type and application of the laser diode, life test studies involve the periodic measurement of a variety of device parameters including operating current, optical output power, threshold current, and forward voltage. Aging studies are conducted in one of the following modes of operation:

❖ Constant Current Aging

Constant current aging mode is often referred to as ACC (automatic current control) mode [63]. In this mode laser current is held constant for the duration of the test and the optical output power is monitored continuously. The optical power shows exponential decay with time at constant current, following Eq. 2.6, due to the device degradation [64].

$$P_{out}(t) = P_0 \, exp\left(-\frac{t}{\tau}\right) \tag{2.6}$$

Here, P_0 is the initial power output of the device at time $t = 0$ and τ is the lifetime. The lifetime of the device can be determined by plotting the optical power data as function of time t and fitting the curve with exponential decay curve. We have estimated the device lifetime using ACC mode. The detail description of experimental and results are discussed in Ch. 6.

❖ Constant Power Aging

Constant power aging mode is also referred to as APC (automatic power control) mode [63]. In this mode, laser output power is held constant by continuously adjusting the current. The operating current has to be increased to maintain the constant optical power from the laser diode due to the device degradation. Conventionally, the laser diode lifetime is defined at the 50 % increase of operating current (*Iop*) [65]. Thus, by plotting operating current as a function of time, we can extrapolate the time necessary to increase the current by 50 % of initial current for constant optical power and can determine the life

time of the device. Constant power aging is used most frequently in life- test studies because it closely resembles the typical mode of operation of laser diodes in use.

To reduce the testing time, the accelerated aging test could be performed to measure the device lifetime at precisely controlled high temperature. Aging is empirically related to temperature through the Arrhenius equation [66]:

$$t = c\ exp\left(\frac{E_a}{kT}\right) \tag{2.7}$$

where, c is a device constant in units of time, E_a is the activation energy, and k and T are Boltzmann's constant and absolute temperature respectively. Depending on the type of laser, typical activation energies range from 0.2 eV to 0.7 eV [63]. Thus, to measure the life time τ_1 of the laser diode at room temperature T_1, the experiment is performed at high temperature T_2 and the life time at that temperature τ_2 is obtained. Then by using Eq. 2.7, one can get the life time at room temperature as,

$$\tau_1 = \tau_2\ exp\left[\frac{E_a}{kT}\left(\frac{1}{T_1} - \frac{1}{T_2}\right)\right] \tag{2.8}$$

2.2 Why Automation?

In recent technological advancement there is a huge demand of the laser diodes in many applications. Hence, it is necessary to fabricate most reliable devices having good operation lifetime. The laser diode characterization is the most crucial part of the device manufacturing process. One has to check and assort a device/s for its different characteristics performance either good or bad. It is very time consuming and impractical practice to characterize each and every device manually. The handling of the instruments manually lead to the operator dependent output, and also one cannot fulfill the demands of good devices in time. Above all the manual testing can't assure the repeatability of the acquired data with quite accuracy. Hence an economic fabrication of the laser diode in volume has in turn necessitated development of automated production test.

2.2.1 Virtual Instrumentation

An instrument is a device designed to collect data from any system under the test and to display the information to a user based on the collected data. Such instrument consists of a transducer for data acquisition, a physical or software device that performs analysis on acquired data and finally gives an output via a display device or in form of memory/record. Now the question arises that from where the word *Virtual Instrumentation* (VI) comes from? So, when a large variety of data collection instruments were developed and designed specifically for computerized control operation, a new field has been created called VI. In general VI is the use of customizable software and standard measurement hardware to create user defined measurement systems, called VIs [67]. Conventional instrumentation systems are made up of pre-defined hardware components, such as digital multimeters and oscilloscopes that are completely specific to their measurement or analysis function. Because of their hard-coded functionalities, these systems are more limited in their versatility than virtual instrumentation systems.

The primary difference between conventional instrumentation and virtual instrumentation is the software component of a VI. The software enables complex and expensive equipment to be replaced by simpler and less expensive hardware and by means of simulation, of course. Thus, a VI is a user defined instrument that brings all the essential equipments for an experiment on a single workbench. The VI provides great functional flexibility to the user. Moreover, since VI is a PC based instrument, the data acquisition, analysis, and presentation of results are all done together on a single platform. The VI involves three technologies and, in general, allows the user to use the PC as a flexible instrument for measurements and characterization. These are: (1) Data Acquisition System, (2) Communication protocols, i.e. hardware interfacing, and (3) Programming.

2.2.2 Instruments for Laser Diode Characterization

The laser diode characterization requires various sophisticated equipments viz. current driver, photodetector, integrating sphere, spectrometer etc. The sophisticated laser current driver drives the laser diode in either pulse mode or continuous wave (CW) mode. The

optical power is measured using a photodetector, accompanied by an integrated sphere and a lock-in amplifier. The spectral response measurement of the laser is carried out by means of a monochromator. And, finally, the laser diode mount attached with thermo electric cooler (TEC) heat sink arrangement. The technical specification and particulars of all the instruments used are discussed below.

❖ Current Driver

A precise laser diode current source is critical for L-I and I-V characteristics measurements. Any good laser diode current source must both drive and protect the laser diode under test. Protection means that external current and voltage spikes must not reach the laser diode. The ability to pulse a laser diode at low-duty-cycles is very useful in diode evaluation since a laser diode will not generate significant heat in a pulse mode and the characterization can be accomplished with minimal thermal effects.

(a) **(b)**

Figure 2.4: Front panel of (a) ILX Lightwave's LDP–3840 laser diode precision pulse current source and (b) Newport – 5600 high-power laser diode driver.

We have used ILX Lightwave's LDP-3840 Precision Pulse Current Source, shown in Fig. 2.4 (a) for low power pulse measurements of laser diodes. LDP-3840 is a microprocessor controlled instrument ideal for providing clean, reliable current pulses to laser diodes. The driver provides 0 to 3 A maximum peak pulse current, with pulse widths adjustment from 100 ns to 10 μs. The advanced pulse network of the LDP-3840 provides fast rise times while maintaining overshoots less than 5 %, and offers selectable polarity pulse modes.

For high-power and CW operation, we have used Newport-5600 high-power laser diode driver, shown in Fig. 2.4 (b). The driver is capable to source current up to 65 A CW current with high precision. It can also be operated in quasi-CW (QCW) mode with 0.25 % to 20 % duty cycle variation. The pulse width can be varied from 100 µs to 1 s. The driver also has the facility to measure the forward voltage across the diode as well as the optical power through photodetectors or thermopile detectors directly.

Beside these current drivers we have also used the voltage–current source meter (Keithley 2420C, Keithley Instruments Inc.) to source the laser diode with constant CW current. The source meter provides measurement of voltage from ±5 µV (source) and ±1 µV (measure) to ±60 V and current from ±100 pA to ±3 A with 0.012 % basic measure accuracy with 5½-digit resolution. Also the source meter features Standard SCPI GPIB, RS-232, and Keithley Trigger Link interfaces useful for device interfacing with PC.

❖ Photodetectors

The photodetector senses the optical power of the light falling upon it and converts the variation of this optical power into a correspondingly varying photo-current. A good photodetector must fulfill these requirements i.e. high sensitivity to the specific wavelength, minimum noise and a fast response such that it can handle the desired data rate. The photodetector should also be insensitive to the temperature variations and have a long operation life. Figure 2.5 shows the photograph of two photodetectors used for the experiments.

(a) **(b)**

Figure 2.5: Photograph of photodetectors, (a) silicon detector (818-SL) and (b) germanium detector (818-IR), used for the experiment.

The choice of the detector depends on the wavelength of emission of the laser diode. A variety of semiconductor detectors are available to cover the spectral range from 200 – 1800 nm. The spectral response of a photodetector is principally determined by the construction of the detector and the type of material used. We have used the 818 Series low power semiconductor detectors for laser diode characterization setups. For wavelength range from 400 nm to 1100 nm, Model 818-SL silicon detector is used while for 1100 nm to 1800 nm wavelength range; 818-IR germanium detector is used for the experiments in combination with the integrated sphere. For high-power laser diodes, optical attenuators are used in front of photodetectors.

❖ Integrating Sphere

Integrating spheres are designed to collect the power of highly divergent laser beams from laser diode or other light sources, since these beams can overfill the input of a photodetector and cause considerable measurement error. The hollow spherical cavity has a diffusive internal wall and two or more ports. The photodetector placed on one port measures the light intensity and depending on the integrating sphere's attenuation and calibration data, the optical power can be measured. The optical power measurement with integrated sphere is insensitive to errors caused by the detector positioning or problems associated with overfilling or saturation of the active area of detector.

Typically the laser diode is positioned very close to the internal port of the sphere as shown in the Fig 2.6 (a) and light emitted from the front facet of the device is collected by the internal cavity of the integrating sphere which is coated with a highly reflective material. A baffle positioned between the input port and the detector port prevents the detector from directly viewing the emitting aperture of the laser. What the detector sees is a uniformly illuminated environment within the cavity of the sphere.

In an integrating sphere, the detected radiation flux is always a small fraction of the incident flux. This attenuation is caused by light reflecting many times before reaching the detector, which makes the integrating sphere an ideal tool for measurement of optical output power of high-power laser diodes. We have used Newport's 819-IS-2 inch integrating sphere which is suitable for laser diode measurements because of their

relatively thin walls, only a few millimeters thick, making it possible to position the laser diode very close to the internal cavity of the sphere. Figure 2.6 (b) shows the actual photograph of the integrating sphere used for the experiments with a photodetector fixed on one of its ports. The assembly consists of a Model 819-IS integrating sphere with one of the 818 Series low-power semiconductor detectors, and is calibrated to NIST traceable standards.

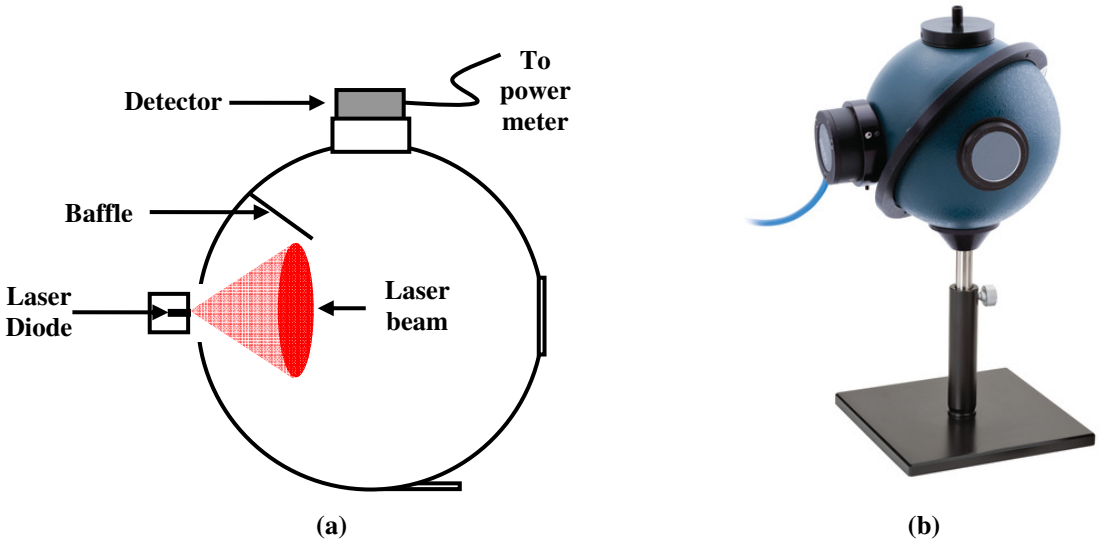

Figure 2.6: (a) Schematic representation and (b) photograph of integrating sphere.

❖ Lock-in Amplifier

Operation and significance of a lock-in amplifier can be visualized in a number of ways. The lock-in amplifier relies on the concept of phase sensitive detection [68]. The phase sensitive detection refers to the demodulation or rectification of an ac signal by a circuit which is controlled by a reference waveform. The phase sensitive detector effectively responds to signals which are coherent (same frequency and phase) with the reference waveform and rejects all others. In a light measurement system the device which causes the signal to be modulated is usually a chopper or pulse current driver. The reference waveform is an output coherent with the chopping action provided by the chopper or trigger pulses from current driver and the ac signal is the signal from the photo detector.

An approach to visualizing the phase sensitive detector is to consider the switch as a multiplier as shown in Fig 2.7. The output of a multiplier switch includes component at

two frequencies, $f_s + f_r$ and $f_s - f_r$, where, f_s – signal frequency, f_r – reference frequency. If $f_s = f_r$, as is the case where the reference waveform is derived from the device which is modulating the signal, then there will be an output at 0 Hz i.e. dc. Any other component in the signal e.g. a noise component at a frequency of f_n will give rise to an ac output at frequencies of $f_n + f_r$ and $f_n - f_r$ which will be smoothed or averaged to the mean value of noise, i.e. zero, by the filter.

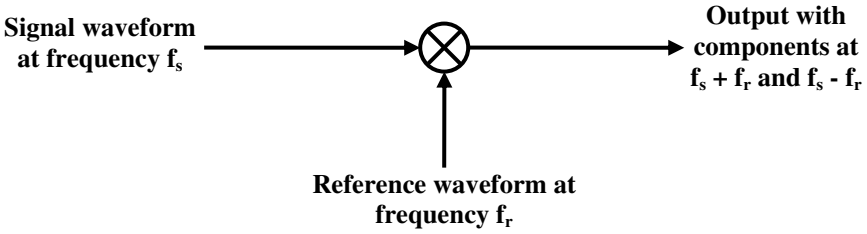

Figure 2.7: Simplified view of lock-in operation.

Lock-in amplifiers are used to detect and measure very small AC signals – all the way down to a few nano-volts. Accurate measurements may be made even when the small signal is obscured by noise sources thousands of times larger. The device behaves as a band pass filter and performs the same function as a tuned amplifier followed by a rectifier but with some advantages like a very precise bandwidth and very high noise rejecting capability. We have used SR-530 analog lock-in amplifier supplied by Stanford Research Systems, Inc.

❖ Monochromator

The monochromator is a very useful instrument in spectroscopic characterizations. It passes only a certain desired wavelength of light with a small band-pass window from a polychromatic input light. It is based on diffraction of light by a grating. One or more diffraction gratings are mounted on a stepper motor and can be rotated to get desired wavelength diffracted at the output slit. The band pass is determined by the slit width. We have used CVI's CM-110 1/8 m monochromator for spectral response measurement of laser diodes. The monochromator contains two gratings, one with 600 groves/mm and the other with 1200 groves/mm. The two gratings cover a wide spectral range from 0 to 3000 nm with the resolution of 0.2 nm.

❖ Spectrometer

Measurement of the spectral response of the laser diode by a monochromator provides quite appreciable data. However, the minimum scanning step for spectral response is limited by the resolution of monochromator i.e. 0.2 nm only. Due to this limitation we have used the spectrometer HR2000 (High-resolution Miniature Fiber Optic Spectrometer, Ocean Optics), shown in Fig. 2.8. It is a small-footprint, modular spectrometer that provides wavelength scanning starting from 200 nm to 1100 nm with optical resolution to 0.035 nm (FWHM). However the specific range and resolution depends on the grating and entrance slit selections. The HR2000 is especially suited for applications such as wavelength characterization of lasers and LEDs. A simplistic interfacing approach to PC via USB makes this instrument handy and versatile, as it doesn't required any external power supply - it draws its power from the computer.

Figure 2.8: Ocean Optics HR2000 High-Resolution Fiber Optic Spectrometer.

❖ Data Acquisition Systems

The data acquisition (DAQ) system consists of the computer (PC i.e. personal computer) and other hardware/s to make the physical component of the VI. The elements of the DAQ system include the PC, transducers, signal conditioning, DAQ hardware and software as shown in Fig. 2.9. The detail of the complete DAQ system is discussed below.

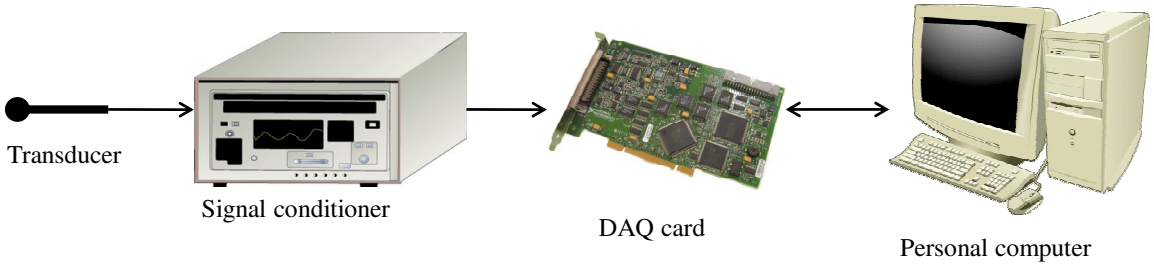

Figure 2.9: A typical data acquisition system comprise a transducer, signal conditioner, a data acquisition card, and a computer of course having specific software to acquire, store and analyzed the data.

A transducer senses changes in a physical parameter, such as temperature, and converts into an electrical signals, such as voltage variations. The electrical signals generated by the transducer must be optimized for the input range of the DAQ card. Signal conditioning accessories can amplify low-level signals, and then isolate and filter them for more accurate measurements. In addition, some transducers require voltage or current excitation to generate a voltage output which can be provided by the signal conditioning circuit. Following to the signal conditioning the DAQ system consist of DAQ hardware, which converts the analog signal into the digital data format. In other words we can say that it enables the user to communicate with computer in a simple way. We have used National Instrument's PCI-6024E DAQ card (Fig. 2.10) for our data acquisition purpose, discussed in detail below.

DAQ hardware (PCI-6024 DAQ Card): The DAQ hardwares, which are usually special kind of circuit boards, are generally installed in the PC. We have used PCI-6024E DAQ card from National Instruments, shown in Fig. 2.10.

The National Instruments PCI-6024E is a low-cost data acquisition board that delivers high-performance, reliable data-acquisition capabilities in a wide range of

applications. It provides 12-bit resolution on 16 single-ended analog inputs with sampling rate up to 200 kS/s and two 12-bit analog outputs with sampling rate of 10 kS/s. It also contains 8 digital I/O lines and two 24-bit counters. The input and output voltage range is from -10 V to +10 V.

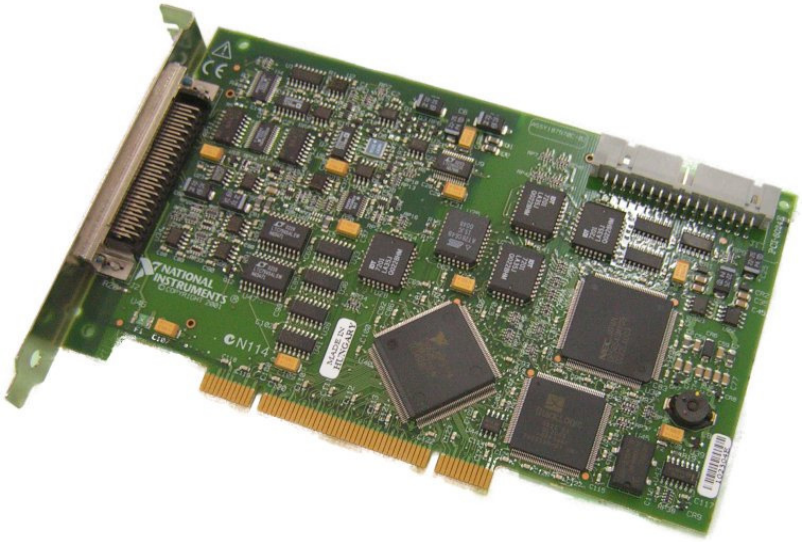

Figure 2.10: PCI-6024E data acquisition card from National Instruments having analog input and output sampling rate 200kS/s and 10 kS/s, respectively. It also contains 8 digital I/O lines and two 24-bit counters.

Finally, the signals in the form of digital data are processed in the PC with the help of appropriate software and are analyzed to give meaningful information about the device under test (DUT). The PC used for the data acquisition system decides the maximum speeds at which one can continuously acquire the data. We have used LabVIEW (ver. 8.2) as a software tool to build our VIs. Details about the LabVIEW software are given in section 2.2.4

2.2.3 Hardware Interfacing

A typical automated measurement setup will use multiple instruments to conduct an experiment. For a virtual instrumentation, any of these aforementioned instruments need to be connected to the PC. There are various communication protocols to connect different hardware/s and instruments with PC. These protocols include serial communication, parallel communication, general purpose interface bus (GPIB) etc.

❖ Serial Communication

Serial communication is a popular means of transmitting data between a computer and a peripheral device such as a programmable instrument or even another computer. The data transfer takes place one bit at a time over a single communication line in serial communication. It can be utilized when data transfer rate is low or over a long distance communication.

For serial communication, four parameters have to be specified: (1) baud rate of the transmission, (2) number of data bits encoding a character, (3) parity-bit (optional), and (4) number of stop-bits. Each transmitted character is packaged in a character frame, which consists of a single start bit followed by the data bits, the optional parity bit, and the stop bit or bits. The Fig. 2.11 shows a typical character frame encoding of the data.

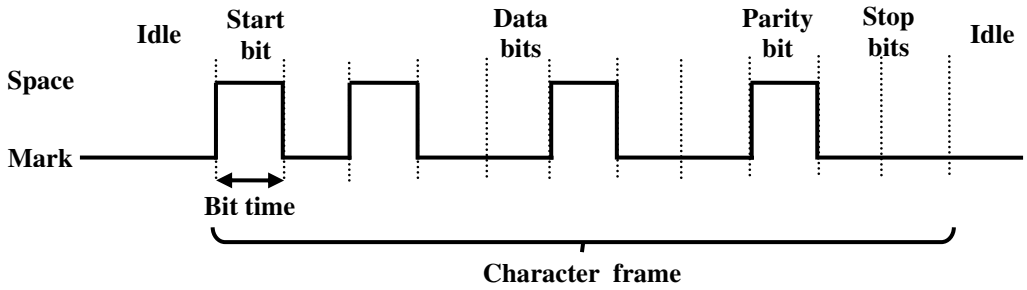

Figure 2.11: A package of a single byte containing data and framing bits i.e. start bit and stop bit comprise with one parity bit.

Serial Ports can be of two types, D-Type 25 pin connector and D-Type 9 pin connector. There are different standards of serial port communication, including RS-232, RS-449, RS-422, and RS-423. RS-232 is the most widely used serial communication standard.

❖ Universal Serial Bus (USB)

Universal serial bus (USB) is a high-speed serial bus which allows a user to connect electronic device and computer peripherals to a computer. The USB interface is not only providing communication but also an electric power supply to the device connected to the computer. It has effectively replaced a standard interfaces viz. serial and parallel ports,

and separate power chargers for portable devices, as well. It also supports plug-and-play installation of the devices and hot plugging, where device can be connected or disconnected while power is on. The computer does not need to restart every time to use the device having USB interface. USB can transfer data starting from 1.5 MBit/s to 5GBit/s depending on its standard, i.e. USB 2.0, USB 3.0 etc.

❖ Parallel Port Communication

The Parallel Port allows the input of up to 9 bits or the output of 12 bits at any given time, thus requiring minimal external circuitry to implement many simpler tasks. The port is composed of 4 control lines, 5 status lines and 8 data lines. It uses mostly a D-Type 25 Pin female connector. Newer Parallel Port's are standardized under the IEEE 1284 standard first released in 1992.

❖ General Purpose Interface Bus (GPIB)

The GPIB, also referred to as IEEE 488 or HPIB (Hewlett-Packard Interface Bus), was invented by Hewlett-Packard Corporation in 1974 to simplify the interconnection of test instruments with computers [69]. It is a digital, 8-bit parallel communications interface with data transfer rates of 1 Mbyte/s and higher, using a three-wire handshake. A standard GPIB setup has one controller, one or more instruments and GPIB cables.

The controller usually refers to a PCI-GPIB card connected to a PC. The picture of GPIB board used for the experiment is shown in Fig. 2.12. This controller allows the user to interact with the instruments. The instrument can be anything that has a GPIB connection such as current driver, lock-in amplifier, etc. The GPIB cable simply connects the instrument and the controller. These instruments can either be arranged in a star or in a linear configuration as shown in Figs. 2.13 (a) and (b), respectively.

The GPIB uses a 24-conductor parallel bus that consists of eight data lines, five bus management lines (ATN, EOI, IFC, REN, and SRQ), three handshake lines, and eight ground lines. GPIB uses a byte-serial, asynchronous data transfer scheme. This means that whole bytes are sequentially handshake across the bus at a speed that the slowest

participant in the transfer determines. Because the unit of data on the GPIB is a byte (eight bits), the messages transferred are frequently encoded as ASCII character strings. All GPIB devices and interfaces must have a unique GPIB address between 0 and 30. Address 0 is normally assigned to the GPIB interface. The instruments on the GPIB can use addresses 1 to 30.

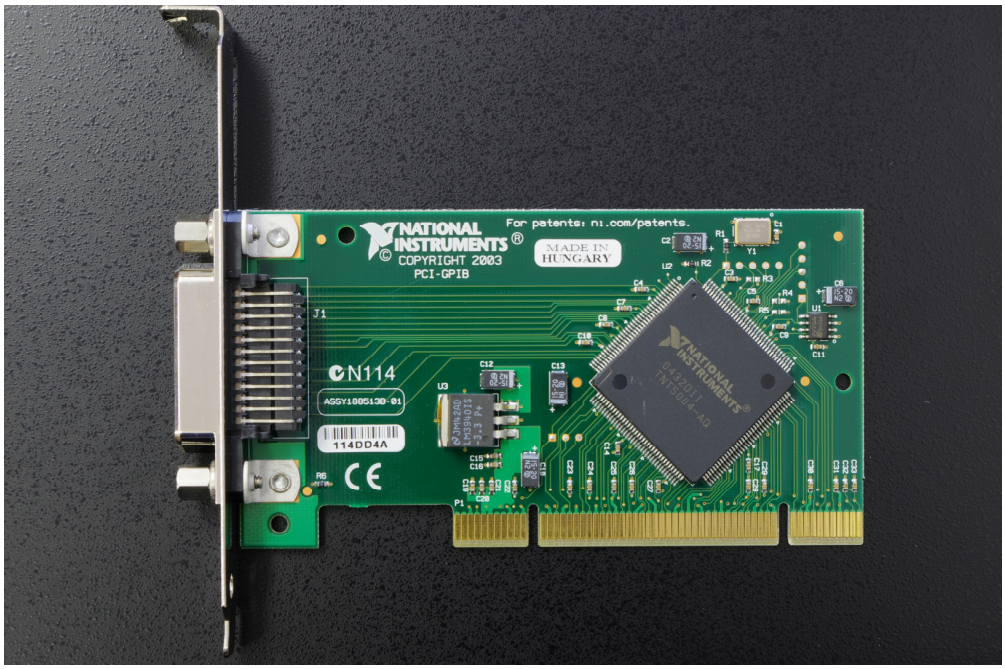

Figure 2.12: National Instruments' PCI-GPIB card with GPIB cable.

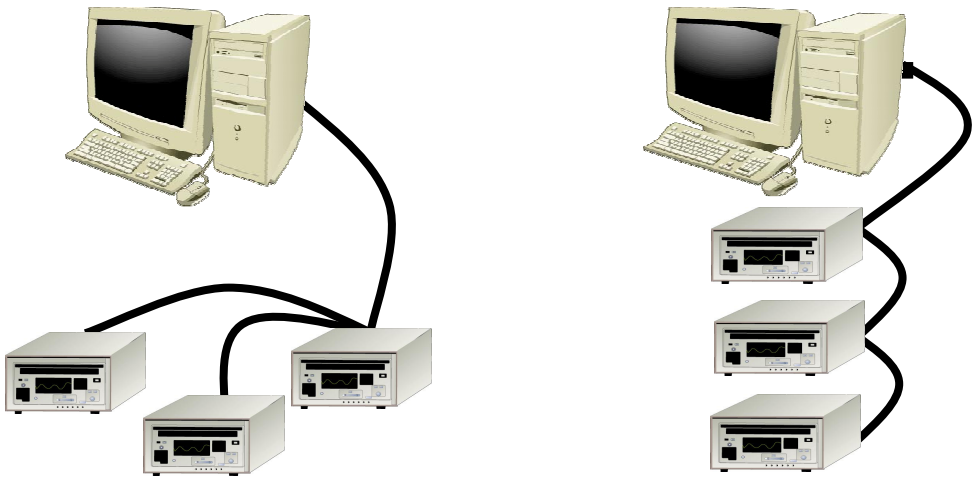

(a) **(b)**

Figure 2.13: Interfacing of the PC with instruments via GPIB in (a) Star configuration and (b) linear configuration.

The GPIB exists due to the need for a standard to control and communicate with multiple bench-top instruments. It also provides fast data transfer rates. GPIB is also relatively easy to program, enabling the communication to be readily established.

2.2.4 LabVIEW Programming

We have used LabVIEW developed by National Instruments as a programming tool to build VIs for laser diode characterization. A term LabVIEW stands for '***Lab***oratory ***V***irtual ***I***nstrument ***E***ngineering ***W***orkbench'. Instead of using text-based programming code the LabVIEW is a graphical programming language utilizes the icon to create an application. The main difference between LabVIEW and the other text based programming language is the program execution. In text based programming language the instruction determines the program execution where as in case of LabVIEW the flow of the data determines the program execution. The LabVIEW is a powerful software tool for designing test, measurement and control systems as it provides complete integrated environment to interface with real-world signals and analyze data for meaningful information and display results in flexible manner. LabVIEW programs are called virtual-instruments (VIs), because their appearance and operation reproduce the physical instruments. A VI in another LabVIEW program is called a sub-VI which corresponds to a subroutine in text-based programming languages. A VI consists of three components: (1) Front panel, (2) Block diagram and (3) Icon and connector pane.

The front panel is a set of controls and displays for the user to operate the system while it is running. As their name suggests, controls are the inputs and indicators are the outputs to the system. Furthermore, graphical displays, lights, analog meter displays, switches, and other controls and indicators like in oscilloscope, can be utilized on the front panel of the VI and make the system interactive and easy to use. One can easily customize the front panel to operate the system in a convenient manner.

The block diagram is a collection of actions bound together like a flowchart and can be manipulated to clearly show the flow of data. The block diagram is where the user can link all the controls and indicators together with various logics and operations. To build a VI for any system application user has to select significant icons from the ***icon and connector pane*** corresponding to the particular action and place it on the block

diagram. Later the icons placed on the block diagram need to be *wired* together by means of connectors in an order to produce a coherent path through the system. LabVIEW follows a dataflow model for running VIs. A block diagram node executes when all its inputs are available. When a node completes execution, it supplies data to its output terminals and passes the output data to the next node in the dataflow path.

Although the original use of LabVIEW was graphical measurement and data acquisition, it can also be used for general purpose programming. All of the basic functions of a traditional text-based language such as file input and output, data structures, and program flow are available in LabVIEW.

2.3 Automation of the Experimental Setup

In order to carry out laser diode characterization in less amount of time with better accuracy and uniformity, we have automated the whole laser diode characterization facility. The automated characterization facility allows very fast data acquisition with more precision and reliability. Since the test and measurements are done in a very less time, there is a reduced chance of device failure even for bad devices. Moreover, it eliminates the human errors in measurements. Since the data are fed directly to the PC, quick mathematical calculations, easy data processing and analysis are possible. We have followed the virtual instrumentation approach for the automation of laser diode characterization facility.

2.3.1 L–I–V Characteristics Measurement

Figure 2.14 shows a schematic diagram of experimental setup for laser diode characterization [70]. A high-power (65 A) laser diode current-driver (Newport-5600) and a low-power (3 A) precision pulse current-driver (ILX-Lightwave LDP-3840) have been used to drive current in the laser diodes depending on the types of the laser diode i.e. either high-power or low power. We have used the 818-SL silicon detector and 818-IR germanium detector with specific attenuator in case of high intensity light, to detect the light output. The optical power is measured using Newport's integrating sphere and Lock-in amplifier (SR-530). The detector used to detect the light output is 818-SL silicon

photodetector. The current driver and Lock-in amplifier have been interfaced with PC using PCI-GPIB (IEEE-488.2). These instruments are controlled by a VI made in LabVIEW-8.2. The actual photograph of L–I and I–V measurements setup is shown in Fig. 2.15. The laser diode chip/bar was mounted on a probing stage attached with thermo electric cooler (TEC) module and an individual laser diode stripe was probed using gold coated Tungsten Carbide tip as shown in Fig. 2.16. TEC module is arranged on a heat sink with a cooling fan. The probing arm is assisted by an XYZ mount as shown in Fig. 2.16.

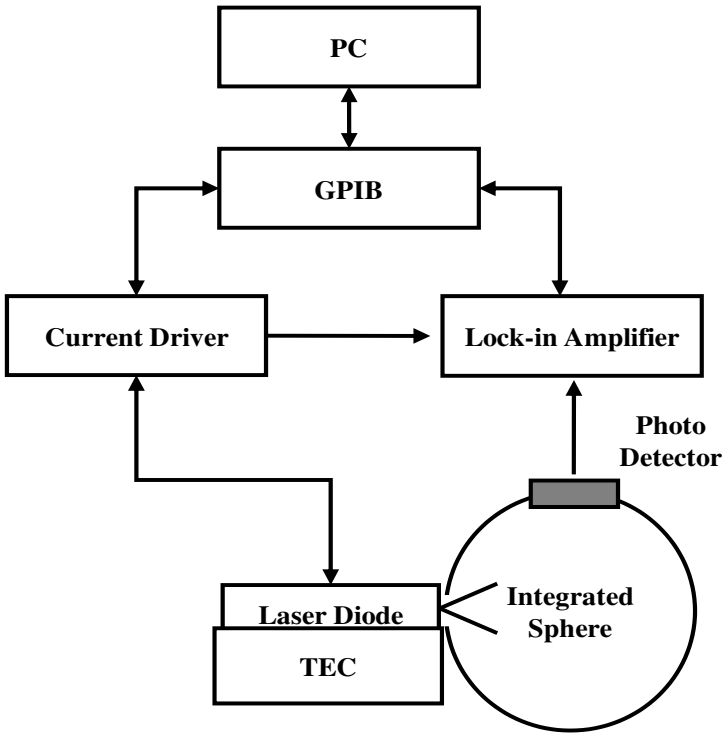

Figure 2.14: A schematic diagram of experimental setup for laser diode L–I and I–V characterization. Photo-detector attached to the integrated sphere detects the light output of the laser. The electrical signal corresponds to the light power form the detector fed in to the lock-in amplifier and hence to the computer by means of GPIB.

A LabVIEW program (VI) measures L–I and I–V characteristics simultaneously. The VI features input current control with desired step increase, time delay, lock-in amplifier sensitivity, current driver mode selection viz. constant output current (I_O), constant monitor photodiode current (I_m) and constant optical power (P_O), and data storage. One can also choose to operate the current driver in either pulse mode or continuous wave (CW) mode. While measuring the L–I–V characteristics the VI

initializes instruments and checks for their status and controls the current output using PCI-GPIB IEEE 488.2 commands.

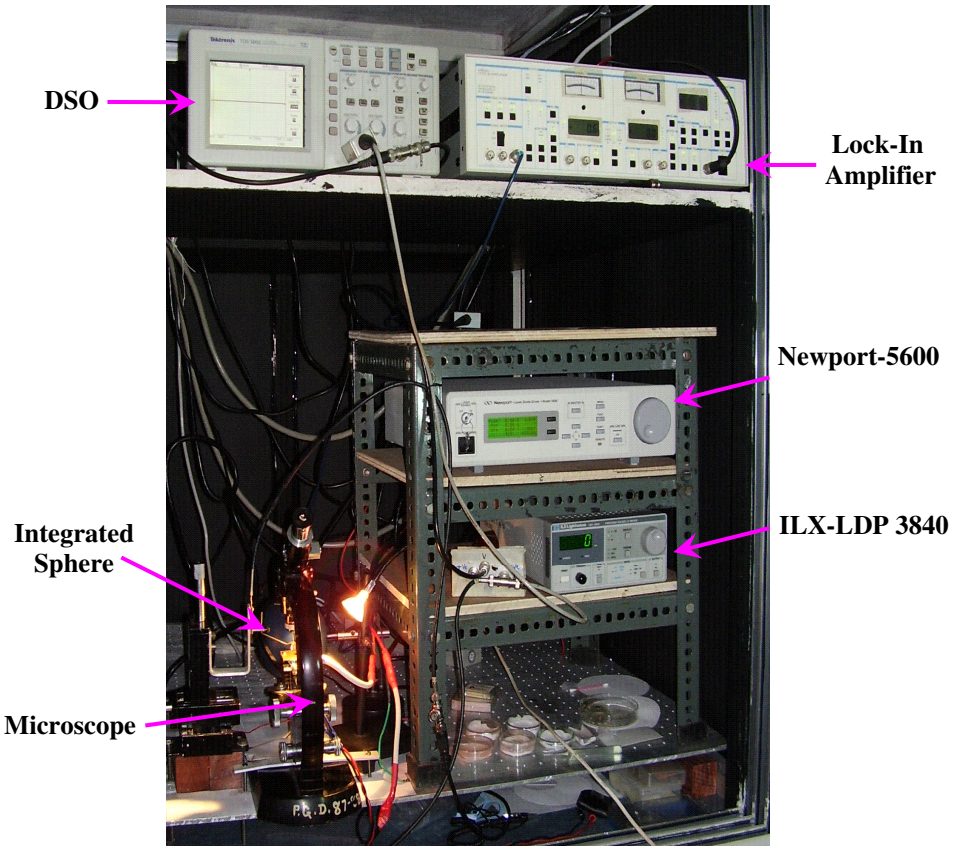

Figure 2.15: L–I and I–V characteristics measurement setup photograph.

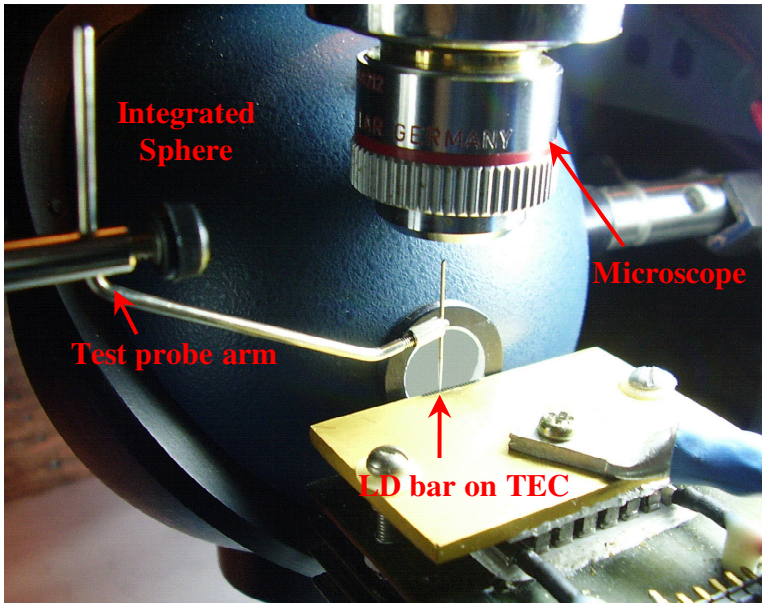

Figure 2.16: Laser diode chip/bar mounted on the probing stage attached with TEC probed for L–I and I–V characteristics measurements [70].

The light emitted by Laser Diode is collected by the integrated sphere and corresponding photocurrent, generated by photodiode is measured using a Lock-in amplifier whose output is read by the VI. The optical power and laser voltage are dynamically plotted against the input current. The linear portion of L-I and I-V curves are separated using the double differentiation of L-I and I-V curves. The post threshold portion is then fitted using "Linear Curve Fit" to get the slope and intercept. The Differential Quantum Efficiency of laser diode is obtained from the slope of linear portion of the L-I curve. However, the optical power obtained from L-I curve is the power emitted by the front facet. To calculate the differential efficiency, the total power generated inside the cavity is used, which is calculated from front facet output using known values of front and back facet reflectivities. The slop of the I–V curve gives the series resistance of laser diode.

In addition to the dynamic data acquisition and display the program also analyzes the data and computes essential parameters like threshold current, turn-on voltage and differential quantum efficiency for the laser diode. The results are displayed graphically as well as numerically. The programming code of the VI for laser diode characterization is shown in Fig. 2.17 (a). Figure 2.17 (b) shows controls and indicators of graphical user interface (GUI) for the L-I and I-V characteristic measurement. The L-I curve plot on the GUI is shown in Fig. 2.17 (c). Figure 2.17 (d) illustrates GUI for laser diode spectral response measurement.

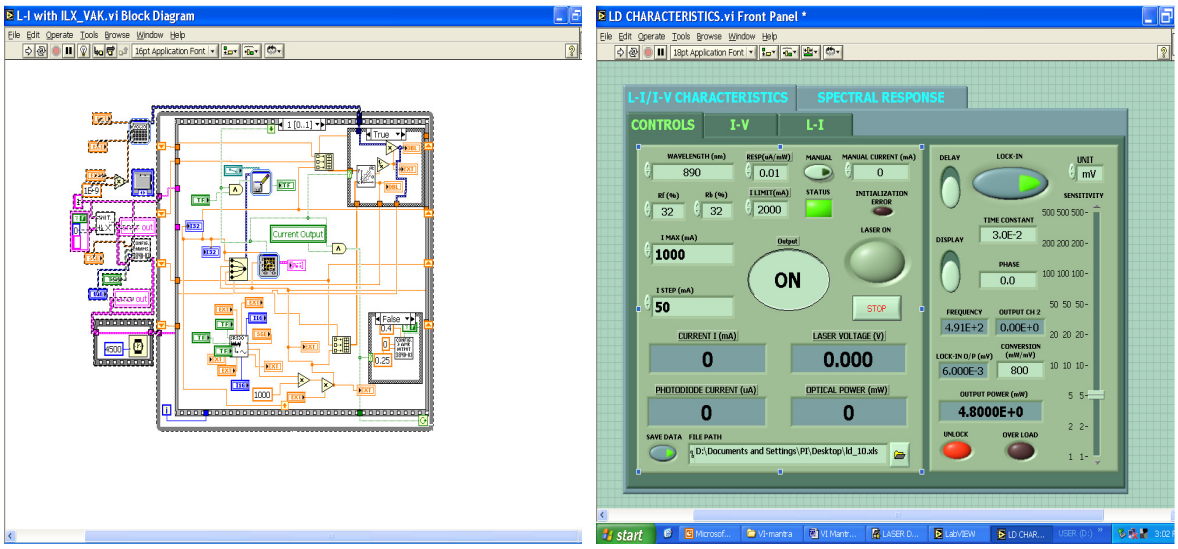

(a) **(b)**

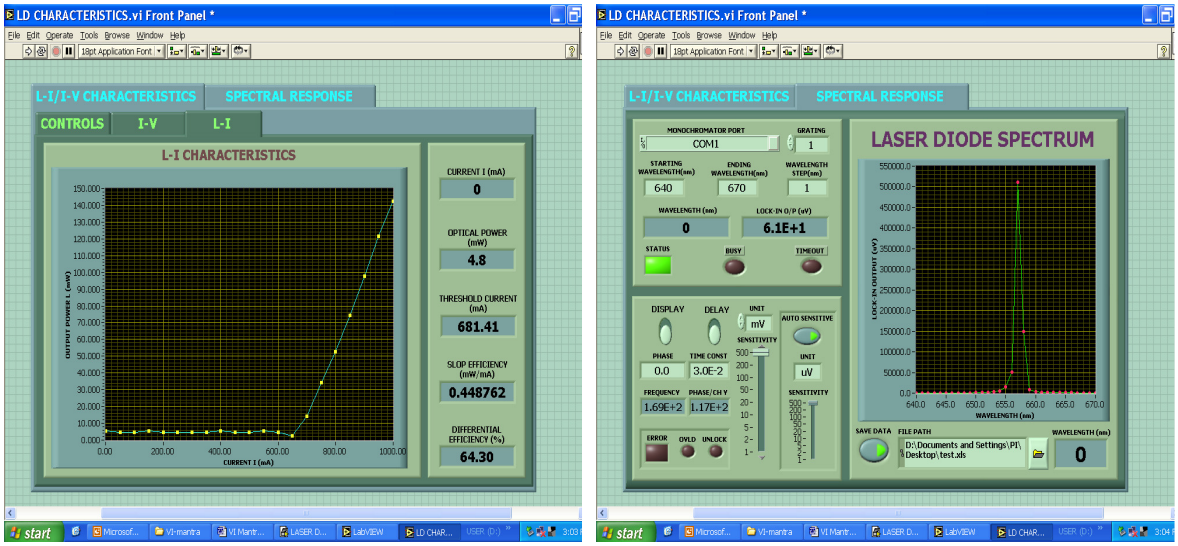

(c) **(d)**

Figure 2.17: (a) Block diagram of VI and GUI screen shot for (b) controls of L–I and I–V characteristics (c) L–I characteristics plot and (d) Spectral response measurement.

Figures 2.18 (a) and (b) show the experimental L–I–V Characteristics and the spectral response of the 808 nm TO (transistor outlook) package high-power laser diode. The diode emission, in this case, was recorded from 640 nm to 670 nm with 1 nm step size and 2 nm band-pass of the monochromator.

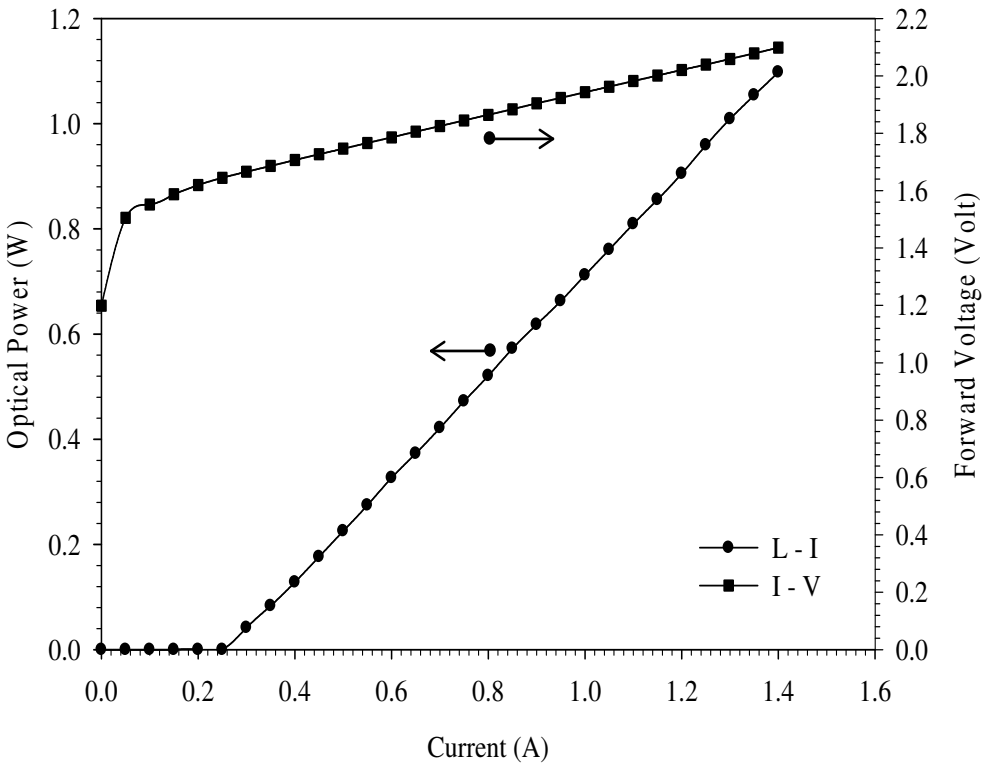

(a)

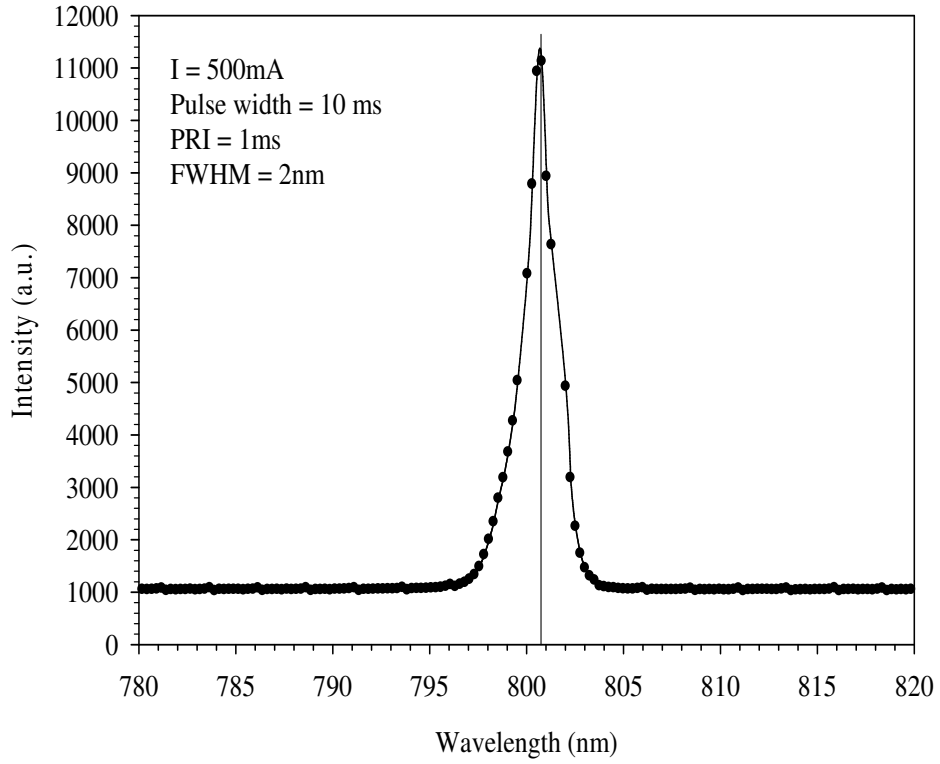

(b)

Figure 2.18: (a) L–I–V characteristics and (b) spectral response of 808 nm TO package high-power laser diode.

The VI allows the user to carry out two main characterization of laser diode in a same program viz. L–I–V characteristics. Thus, it is very useful in the field of research and other areas where frequent characterization of laser diode is required. Beside its obvious advantages over manual measurements like less time and effort consumption, the automated setup has many beneficial features including precision, consistency and uniformity in data acquisition, especially because these measurements have to be carried out in the dark room. Accuracy of L–I measurements is better than ± 2 % mainly decided by the photodiode whereas the wavelength accuracy is ± 0.2 nm.

The limitation of this setup lies in the hardware side. As Newport's 5600 current driver is typically a high-power laser diode driver, it cannot measure the voltage for low power laser diode below 1.5 V. Moreover, in the pulse mode, the duty cycle and frequency cannot be controlled by the program. Similarly the minimum scanning step for spectral response is limited by the resolution of Monochromator.

Further, slight modification in the VI with required change in measurement conditions of experimental setup allows determination of more laser diode parameters as discussed earlier. Experimental setups and necessary modifications in VIs for measurements of parameters like Characteristic temperature (T_0), Thermal Impedance (R_{th}), degradation rate and life time of laser diodes are described here.

2.3.2 Spectral Response Measurement

In case of spectral response measurement, the light from laser diode is made to focus at the input of the monochromator. A monochromator (CVI-CM110) has been interfaced using serial port (RS232) with PC. The monochromator wavelength is controlled by the VI. Again the output of monochromator is fed to the photo detector through an optical chopper. This chopper provides the triggering to the Lock-in amplifier. A picture of this setup is shown in the Fig. 2.19.

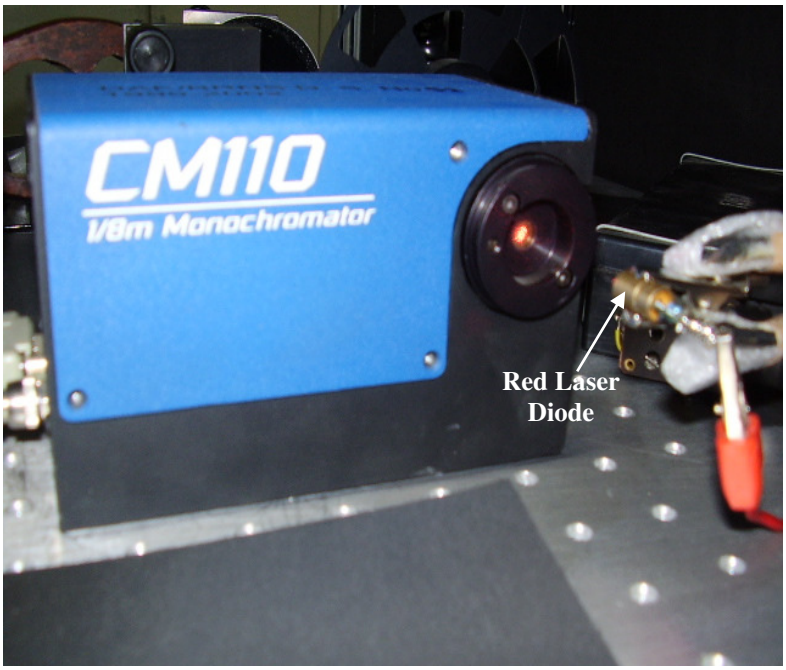

Figure 2.19: Spectral response measurement setup.

The VI corresponding to the spectral measurement provides control over monochromator grating selection, wavelength range, scanning steps and delay. GUI controls and plot of spectral response measurement of laser diode is shown in Fig. 2.17 (d).

Though the monochromator gives the laser spectral response with quite good accuracy, the time consuming data acquisition process to scan the entire spectrum restrict the utilization of this experimental setup. Because one has to run the laser diode for longer time until the whole spectral scan is over. The continuous device operation causes device heating and hence the shift in the output spectral mode, as the wavelength of the laser diode strongly depends on the temperature. To overcome this restriction we have used the high resolution miniature fiber optic spectrometer (HR2000, Ocean Optics).

2.3.3 Junction Temperature Measurement

High-power laser diodes are finding extensive application due to their small size, low threshold current and high electrical to optical efficiency. Low value of junction temperature is required for high-power operation of laser diode. The operating characteristic and lifetime of semiconductor laser are also strongly affected by junction temperature. It affects the laser diode performance in many ways. Light output, center wavelength, spectrum, power magnitude, and diode reliability are, all directly dependent on junction temperature.

Junction temperature can be deduced from the laser threshold and the stimulated emission. However, these techniques are weakly accurate and of low sensitivity. The thermo reflectance techniques provides high sensitivity and high spatial resolution but it works excellently only for low power laser diodes where the temperature distribution in the laser is weak. Other methods like Electroluminescence (EL), Photoluminescence (PL), and Non-contact method are also reported [71]. The Raman scattering spectroscopy provides temperature profile with high resolution of 1 μm. However, Raman spectroscopy needs a sophisticated experimental setup and the precision of temperature is as low as 10 K. Nematic liquid crystal with infrared (IR) laser illumination has also been reported, however, the experimental setup is quite difficult and expensive [71].

In this study, forward voltage is employed in the measurement of the junction temperature of laser diode. Because it is quite easy, simple instrumentation is used and the results are very precise with the accuracy of ±3 °C. The experimental setup to determine the junction temperature of laser diode was optimized. The current–voltage

characteristic measurement of laser diode at different temperature gives voltage–temperature relation. Using this relation one can directly get the junction temperature at a particular operating current. The relation between temperature (T) and forward voltage (V_f) of device is linear with negative slope.

$$\Delta V_f = \alpha \Delta T_j \quad (2.9)$$

where, α is correlation factor [72].

The 650 nm InGaP quantum well laser diode chip was used for the measurement of junction temperature. Figure 2.20 shows the schematic and experimental set up for measurement of the laser diode junction temperature. We have used Precision Pulse Current Source (ILX Lightwave LDP-3840) for low power pulse measurements of laser diodes. The laser diode was operated in pulse mode with in the current range of 0-80 mA with 1μs wide pulse width and 0.25 % duty cycle. Lower valued pulse width and duty cycle prevents the self-heating of the diode. Laser diode was kept on a heater for voltage measurement at different temperatures. A digital oscilloscope (Tektronix TDS 2002) measures the voltage across the diode. Entire measurement is done at ambient temperature. For I-V measurement in CW mode the constant operating current is supplied to the laser diode through source meter (Keithley 2420C).

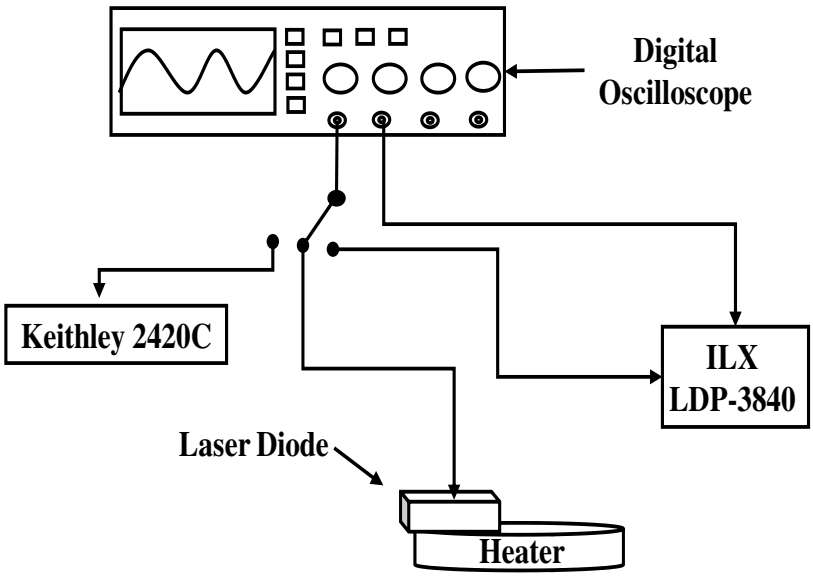

(a)

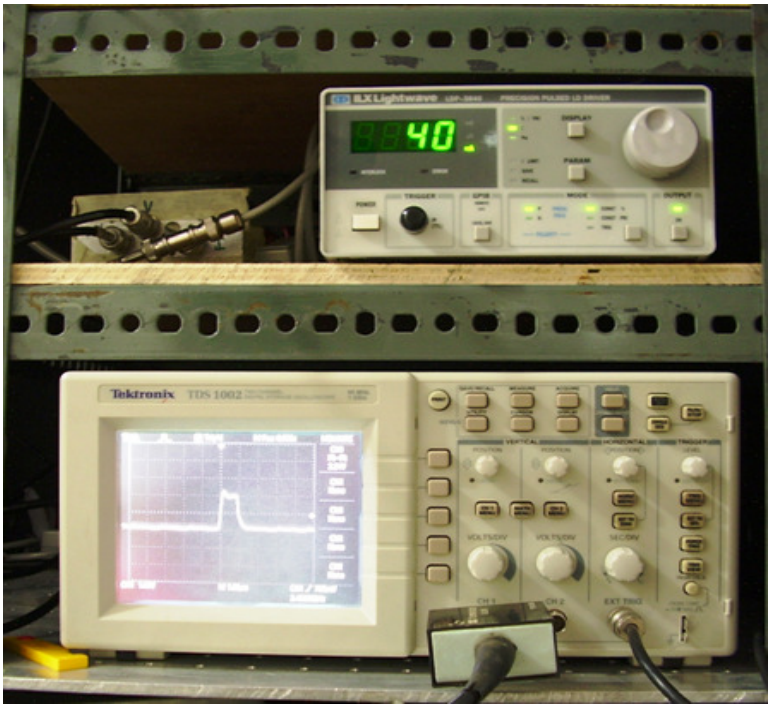

(b)

Figure 2.20: (a) Schematic and (b) measurement set up to find laser diode junction temperature.

We had found that the decrease in forward voltage for given constant operating current with increasing junction temperature, as shown in Fig. 2.21 (a). These results are quite good in agreement to the Eq. 2.9.

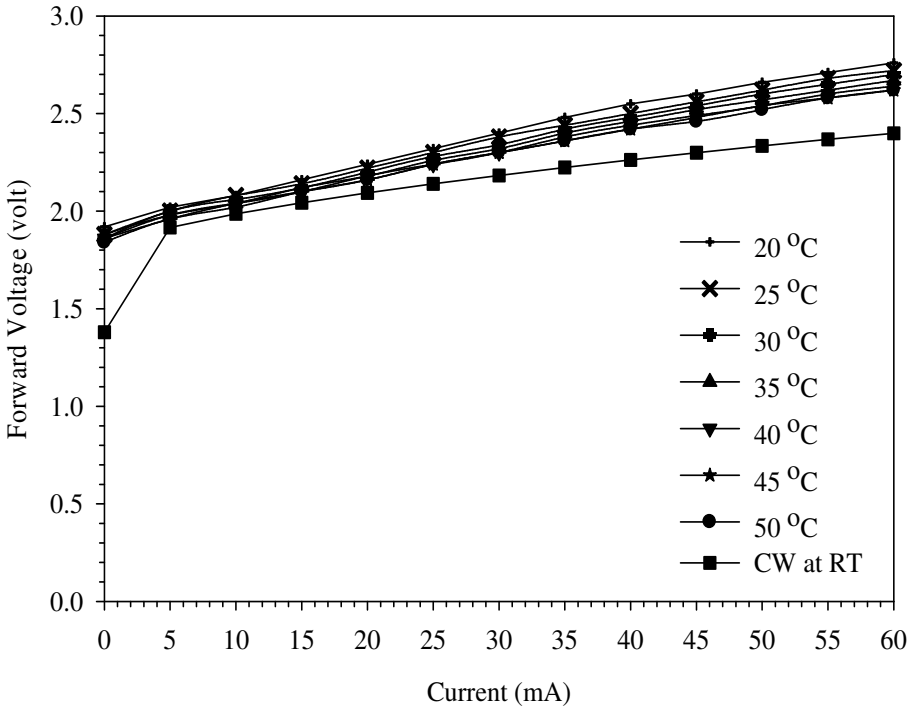

(a)

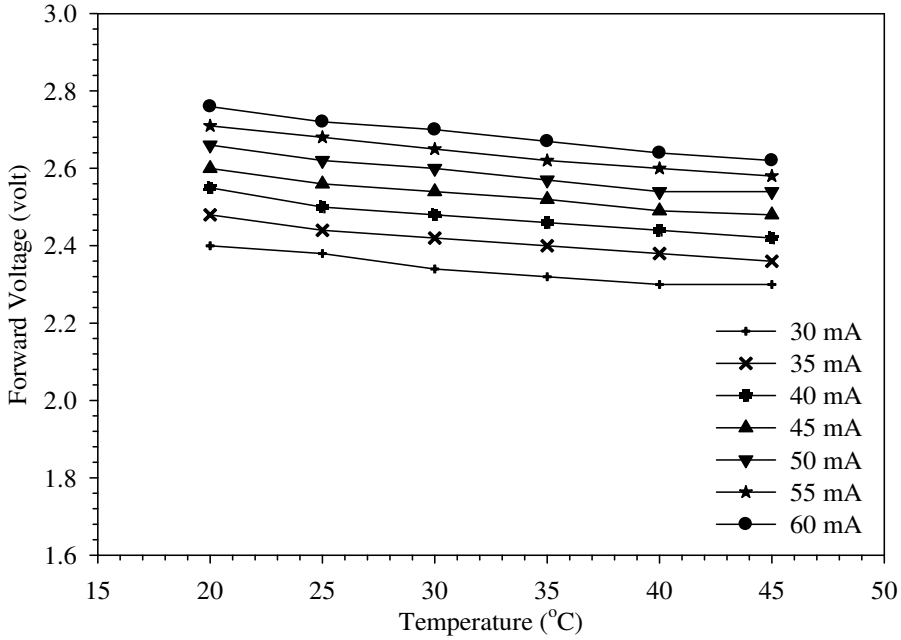

(b)

Figure 2.21: (a) Voltage vs. Current at different ambient temperature, (b) Forward Voltage vs. Temperature at different operating current.

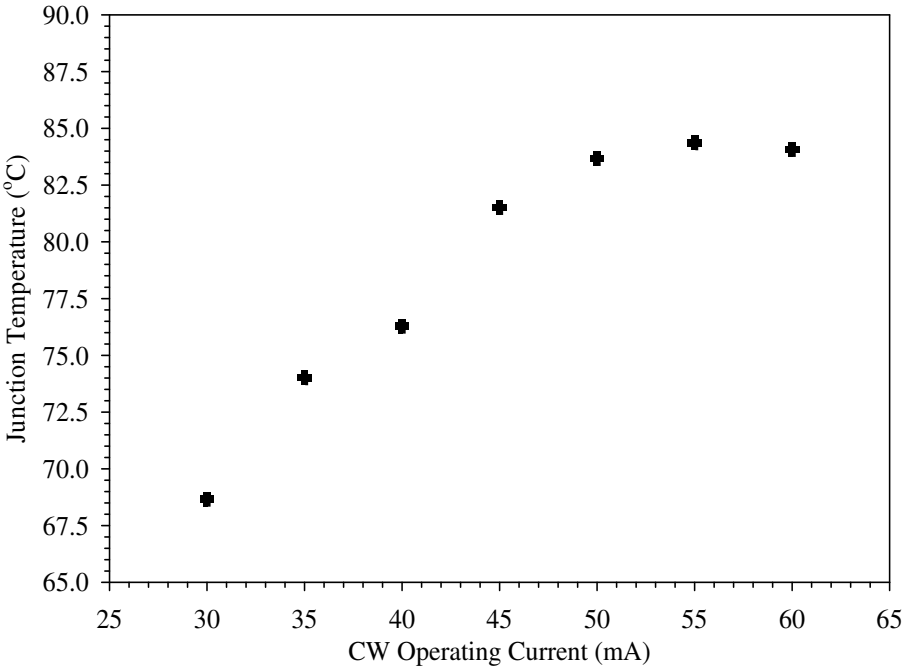

Figure 2.22: Junction temperature vs. operating current.

Fitting the experimental data of voltage – temperature relation, shown in Fig. 2.21(b), linearly to the type of, $Y = m\,X + c$, we get the value of junction temperature for

constant operating current in CW mode. From this we can get the calibrated relation between junction temperature and operating current of laser diode, shown in Fig. 2.22.

2.3.4 Estimation of Maximum Power (P_{max}) for COMD

One of the major issues associated with the high-power operation of the laser diode is the mirror facet damage. We have optimized an experimental setup to measure the P_{max}, maximum optical output power, at catastrophic optical mirror damage (COMD). Generally COMD occurs at low operating temperature (< 40 °C). Figure 2.23 shows the schematic of P_{COMD}, power density at COMD.

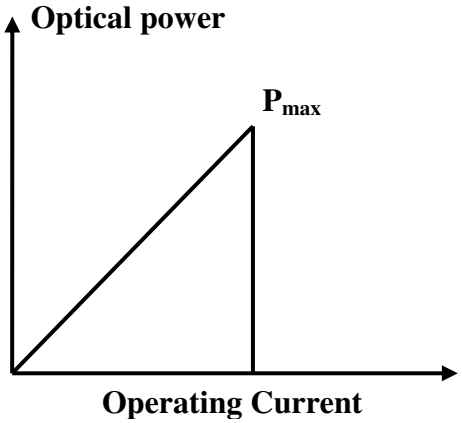

Figure 2.23: Schematic of L-I for P_{COMD}.

The L–I measurement at room temperature has been carried out in pulse, with essential higher repetition rate and duty cycle, or CW mode. Gradual increase in operating current leads non-radiative recombination and we could observe sharp decrease in optical output power. The P_{COMD} was calculated using equation.

$$P_{COMD} = \frac{P_{max}}{\left[w \times \left(d/\Gamma \right) \right]} \times \left(\frac{1+R}{1-R} \right) \tag{2.10}$$

Here, P_{max} is the maximum power just before COD, (in *Watt*), (d/Γ) is the equivalent/transverse spot size, (in μm), d is quantum well width, Γ is fraction of optical power residing in quantum well, R is front facet reflectivity, and P_{COD} is power density at COD.

The experimental was optimized to measure the P_{max}, the maximum power just before the COD occurs. The precision pulse laser diode driver (ILX Lightwave LDP – 3840) and Lock-in amplifier (SR 530) was connected to computer by GPIB. Whole

operating and measurement system was automated using VI (Virtual Instrument) program of LabVIEW. For the temperature stability the device was mounted on TEC. The operating current was gradually increased up to the sharp decrease in the optical output power of the laser diode under the test. For the initial optimization we have used the commercially available class-2A laser pointer diode. An experimental setup and the VI user interface are shown in Fig. 2.24 and Fig. 2.25.

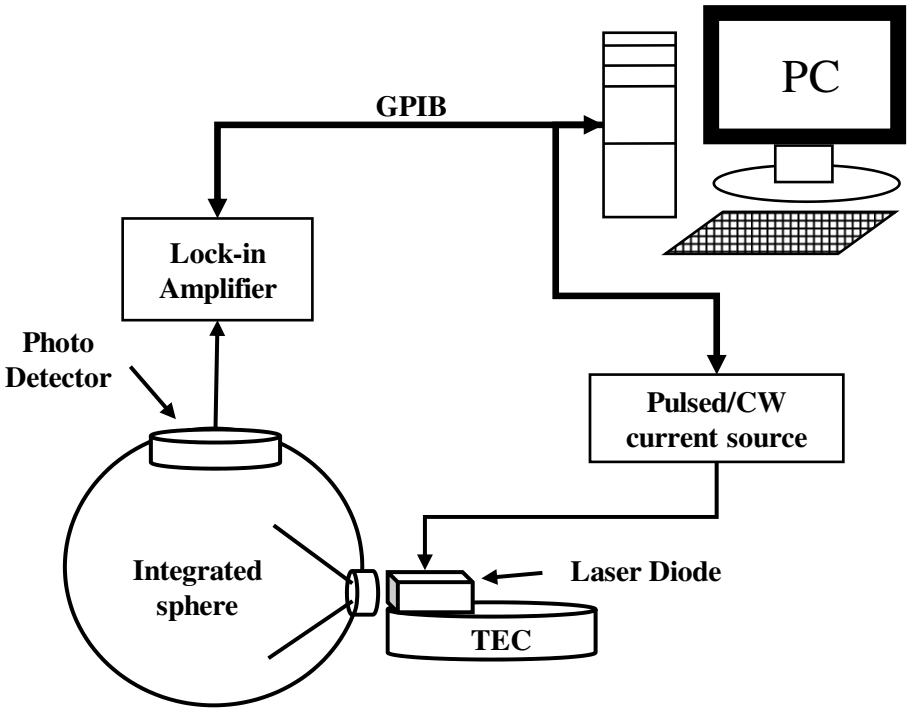

Figure 2.24: Experimental Schematic for P_{max} measurement.

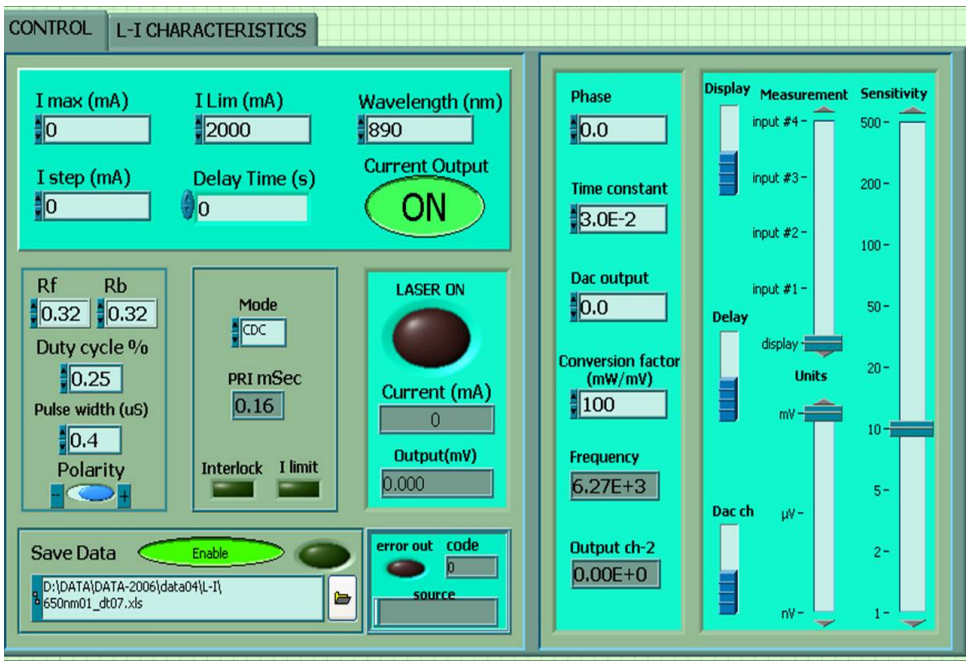

(a)

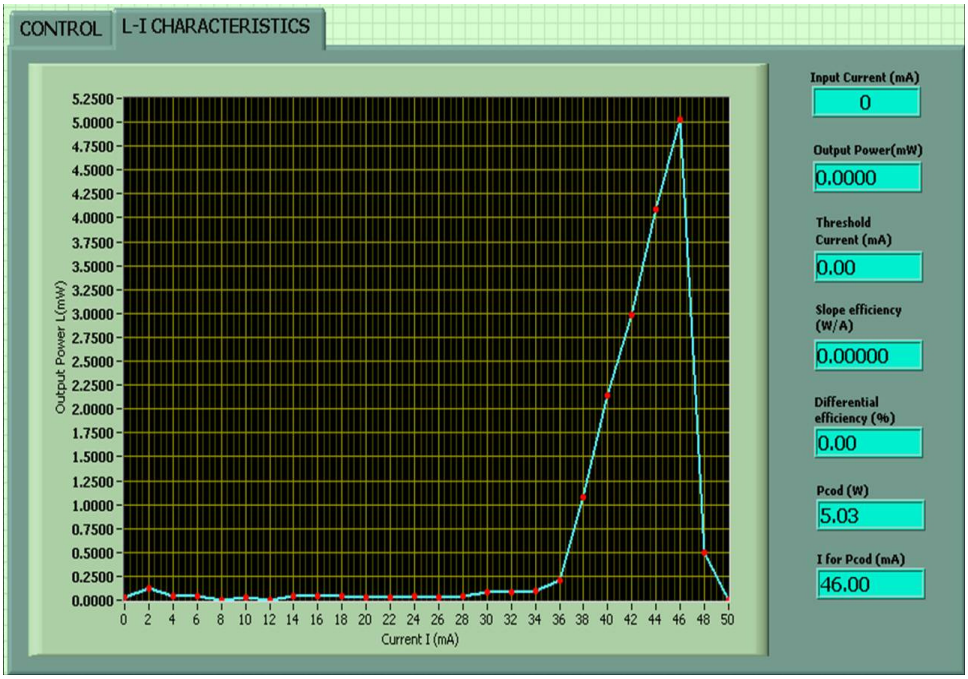

(b)

Figure 2.25: (a) Front panel of Lab-VIEW VI user interface to control the diode operation of L-I measurement. (b) The graph shows the sudden drop in optical output power and we have P_{max} value.

* * *

Chapter 3

Growth Structure and Device Processing of DQW InGaAs/GaAs Laser Diode

3. Growth Structure and Device Processing of DQW InGaAs/GaAs Laser Diode

Fabrication of high-power laser diode requires a multilayered structure of semiconductor materials having excellent electrical and optical quality, which is realized by the epitaxial growth. A series of processing steps are required for the fabrication of laser diode bars and devices out of the epitaxially grown laser diode structures. Post-growth processing is a crucial issue for device fabrication and demands very careful optimization, since threshold current and external efficiency depend on internal structures and the device processing of laser diode. This chapter presents a brief report on the laser diode structure and the processing steps used for the fabrication of edge-emitting high-power laser diodes.

3.1 Introduction

Laser diodes have been realized over a wide range of lasing wavelength with a variety of material systems. Since the first demonstration of the GaAs based homojunction laser diode in 1962 [73], the threshold current densities have been brought down by more than three orders of magnitude due to the advancement in the crystal growth technologies. In the early 1970's, improvements in Liquid Phase Epitaxy (LPE) enabled the realization of the double heterostructure (DH) and continuous-wave (CW) operation of the laser diode at room temperature [12]. Further, the development of quantum-well (QW) and quantum-dot (QD) lasers, which are essential for realizing high-power laser diodes today, is possible due to the advancement in molecular-beam epitaxy (MBE) and metalorganic vapor phase epitaxy (MOVPE).

Most high-power laser diodes are based on III-V semiconductor QW structure having an active layer thickness of about a few nanometers, which consists of precisely controlled composition and good homogeneity throughout a wafer. The photon, generated by the band-to-band recombination in the QW active region, is vertically (transversely) confined by means of the waveguide layer comprising of the cladding and confinement layer. The waveguide layers are much thicker, having thickness of 3-5 μm, and in order to assure the economic feasibility of the process they have to be grown at a reasonable

growth rate. All of these have to be achieved while maintaining high crystalline quality with minimal defects, with a tight control of the doping profile, and requiring optimized epitaxial growth conditions for the individual layers of the laser structure. On the other hand, lateral optical confinement is usually achieved by various post-growth processing steps that define the laser device geometry viz. gain-guiding or index-guiding.

3.2 Epitaxial Growth of Semiconductor Materials

A lattice matched single crystal layer with controlled thickness and doping can be achieved by means of an epitaxial growth process. The identical crystalline symmetry between the substrate and the epitaxial layer is crucial for good quality epitaxial growth of the layers. Selection of epi-layer composition to achieve lattice-matching, while providing good carrier and optical confinement, is particularly important for the heterostructures used in laser diodes. The lattice mismatch, i.e. the difference between the lattice constants of the substrate and the epitaxial layer, should not exceed a critical limit. The large value of lattice mismatch usually results in the generation of dislocations and defects, degrading the quality of the grown layer. The lattice-mismatch also determines the onset of three-dimensional (3D) growth-mode, commonly known as the Stranski-Krastanov growth-mode [74].

3.3 Epitaxial Growth Techniques

There are several epitaxial growth techniques viz. liquid phase epitaxy (LPE), molecular beam epitaxy (MBE) and vapor phase epitaxy (VPE), of III-V compound semiconductor materials and their heterostructures. Table 3.1 shows a comparative of various merits and demerits of aforementioned epitaxial growth techniques [75].

3.3.1 Vapor Phase Epitaxy (VPE)

Vapor phase epitaxy (VPE), also known as chemical vapor deposition (CVD), refers to the formation of a thin film on a crystalline substrate from a gaseous medium of different chemical composition. Unlike physical vapor deposition (PVD), where condensation occurs in the absence of a chemical change, the thin film growth takes place in VPE as a

result of thermo-chemical vapour-solid reaction. In VPE, a mixture of gases flow through a reactor and interact on a heated substrate to grow an epitaxial layer. There are three different CVD techniques used for the growth of III-V and other compound semiconductors. These are the halide process, hydride process, and the organometallic or metal-organic vapor phase epitaxy (OMVPE or MOVPE).

Table 3.1: The comparison of epitaxial growth techniques.

Technique	Merit	Demerit
Liquid Phase Epitaxy (LPE)	• Simple • High purity	• Commercial production • Limitation to achieve low-dimension
Molecular Beam Epitaxy (MBE)	• Uniform layer • Simple process • Abrupt interface • In-situ monitoring	• As/P alloy difficult • 'Oval' defects • Expensive • Low throughput
Hydride Vapor Phase Epitaxy (HVPE)	• Well developed • Large scale production	• No aluminium alloys • Complex process • Control difficult • Hazardous sources
Metal Organic Chemical Vapor Deposition (MOCVD)	• Most flexible • Large scale production • Uniform layer • Abrupt interface • Simple reactor • High purity	• Expensive sources • Hazardous precursors

❖ Metal-Organic Vapor Phase Epitaxy (MOVPE)

Metal-organic vapour phase epitaxy (MOVPE), also known as organometallic vapour phase epitaxy (OMVPE) or metal-organic chemical vapour deposition (MOCVD) is an improvised form of VPE technique where the growth is carried out from the vapor phase using organometallic and hydride sources [76]. It was first developed extensively by Manasevit in 1968 for the growth of a variety of materials including III-V semiconductors [77]. Since then, it has been advancing as a significant technique for the growth of high-quality low- dimensional structure for fundamental semiconductor physics and for semiconductor photonic devices such as single layers, heterojunctions, and QW structures with excellent control over layer thickness, doping, and formation of hyper-abrupt isotype and anisotype junctions. It was the MOVPE technique, which led to the room-temperature operation of QW lasers for the first time [78] by means of the high-quality epitaxial layer structures.

A typical MOVPE growth system, shown in Fig. 3.1, consists of a gas-mixing system, a reactor, and a pump, and an exhaust handling system. In the gas-mixing system, the metal-organic (MO) precursors are kept in stainless steel container at a precisely controlled temperature and pressure. Flowing hydrogen, carrier gas, through these cylinders of liquid (TMGa, TEGa, TMAl, DMZn) or solid (TMIn) precursors results in a controlled transport of their saturated vapor into the reactor. The reactants can be switched into the reactor or bypassed directly into the exhaust by switching manifolds [79]. The fluxes of hydrogen and the other precursors for epitaxial growth are metered by mass-flow controllers, actually measures the thermal conductivity of the flowing gas. Capacitance or piezoelectric pressure transducers control the pressure. For the reactor design a variety of different concepts are being used, either horizontal linear reactor [80] or vertical reactor [81]. A most common design found extensively for the production of high-power laser diode is horizontal reactor where the gas stream enters on one side, is passed over the lying substrate and leaves the reactor on the other side. The reactor chamber is followed by a pumping system consisting of a rotary pump, a throttle valve for pressure control, and traps for particles or condensable materials. Wet or dry chemical scrubbers are used to remove the toxic materials from the effluent gas coming out of the reactor.

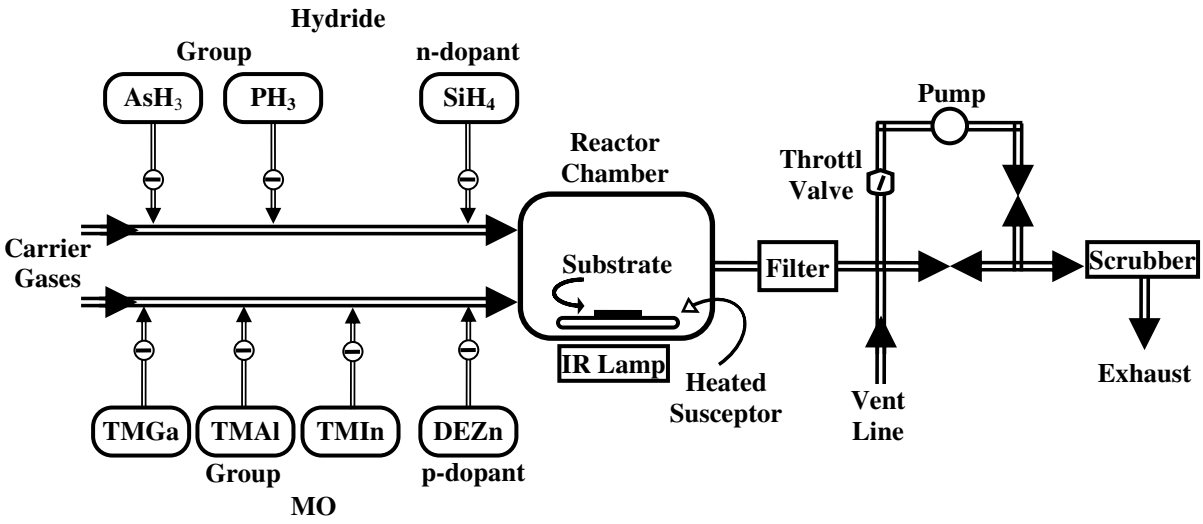

Figure 3.1: A typical MOVPE growth system.

Figure 3.2 illustrates the process in MOVPE reactor during the epitaxial growth. The reaction is carried out in a gas flow with hydrogen, as a carrier gas, and nitrogen, as a pure gas, at atmospheric or reduced pressures. The pure gas decontaminates all the system components from toxic gases and inflammable sources. In this process, chemically active species, or metal-organic precursors, usually the alkyl compounds of group III elements, i.e. Al, Ga or In, interact with sources of group V element, i.e. As and P usually the hydrides arsine (AsH_3) and phosphine (PH_3), on a substrate by means of adsorption, surface diffusion, and surface reaction to produce a corresponding epitaxial layer, either in the vapor phase or on a solid surface of the substrate. The substrate is placed on a heated graphite susceptor. The hot susceptor has a catalytic effect on the decomposition of gaseous products and the growth takes place on this hot surface. The byproducts are removed through diffusion.

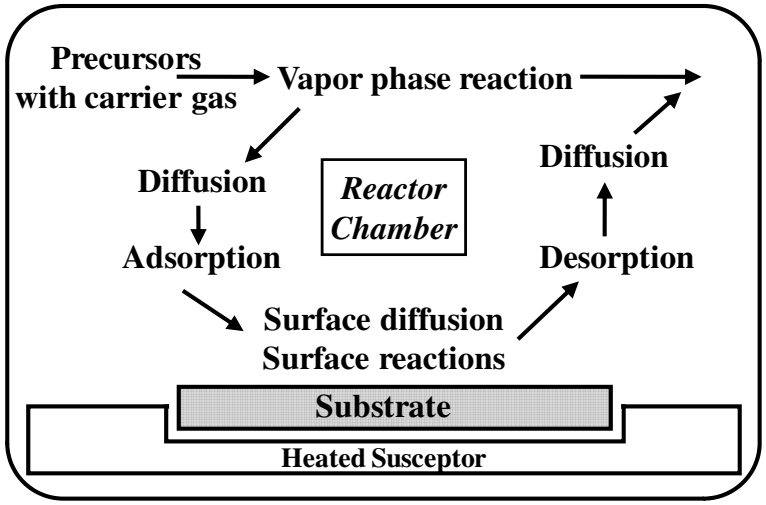

Figure 3.2: Processes in MOVPE reactor during the epitaxial growth.

In MOVPE growth process, the basic chemical reaction is irreversible pyrolysis that takes place in the vapor phase of a volatile metal-organic compound and a gaseous hydride, and forming some intermediate compounds, given by, Eq. 3.1 [76]

$$R_n A + DH_n \longrightarrow AD + nRH \tag{3.1}$$

where, R_n indicates a lower order organic radical, such as a methyl- or ethyl-radical; A and D are, the group III and V constituent species for the deposited solid, respectively. An important example of this case is given by, Eq. 3.2,

$$\left(CH_3\right)_3 Ga + AsH_3 \xrightarrow{600\ ^\circ C} GaAs + 3CH_4 \tag{3.2}$$

Finally, the constituent elements are released and get incorporated into the lattice on the semiconductor surface.

The growth rate is one of the main parameters to be controlled during epitaxial process, and is mainly decided by the growth temperature. The kinetics and thermodynamics of the growth process play an important role, which defines the growth rate and determines the driving force for the overall growth process, respectively. If the reaction rate limits the growth rate, it is called kinetically limited case wherein the growth rate increases with increase in temperature. Moreover, the processes like diffusion, called mass transport, too, limit the growth rate, which is inversely proportional to pressure and is independent of temperature. Growth rate is usually controlled by reaction kinetics in low-temperature range and by mass transport in high-temperature range. The growth rate is given as r_g = (const.) $p_{TMGa}(V/P)^{1/2}$ for the growth process of GaAs, as in Eq. 3.2, where, p_{TMGa} = partial pressure of TMGa, V = gas velocity, P = reactor pressure.

A number of important and beneficial features are offered by the MOVPE growth technique. Compounds, such as GaAs, can be grown with different As to Ga ratio (V/III ratio) simply by varying the relative vapor pressure of arsine hydride (AsH_3) and trimethyl gallium (TMGa) as there is no need of establishing equilibrium with source materials. This allows the study of native defects and trap states, which are supposed to be related to the stoichiometry. It is possible to grow almost all the III-V semiconductor compounds, their ternary and quaternary alloys, using MOVPE. Growth of high purity, ultra-thin layers, and abrupt junctions with precise composition and doping control makes this technique more prevalent in the field of optoelectronic device fabrication.

3.3.2 Materials for High-Power Laser Diodes

The direct energy bandgap and lattice constant of the material are the most crucial parameters in the material selection for laser diodes. Hence, the elementary semiconductors e.g. silicon or germanium are not used for lasers because of their indirect energy bandgap. The III-V compound semiconductor materials are widely used for the fabrication of high-power laser diodes. The III-V binary compounds are formed by combining elements form group III and group V of the periodic table while, ternary or quaternary compounds are formed through alloyed binary compounds. The energy bandgap and the lattice constant of ternary and quaternary compounds depend on the mole fraction of the constituent binary compounds. For example, the lattice constant of any ternary compound ($A_xB_{1-x}C$) is calculated with the help of Vegard's law [82] using Eq. 3.3.

$$a_{A_xB_{1-x}C} = xa_{AC} + (1-x)a_{BC} \tag{3.3}$$

where, *AC* and *BC* are binary compounds such as InP, GaP. Similarly, the energy bandgap of any ternary compound ($A_xB_{1-x}C$) can be calculated as,

$$Eg_{A_xB_{1-x}C} = xEg_{AC} + (1-x)Eg_{BC} + x(1-x)C_1 \tag{3.4}$$

where, C_1 is the Bowing parameter of ternary material [83].

As the alloy composition changes the band structure and hence electronic and optical properties of the alloy changes. Thus by choosing appropriate compounds or alloys, it is possible to select and tune the emission wavelengths for laser diodes. The choice of material system for the fabrication of laser diode is determined by the emission wavelength (λ) of interest and hence by the energy bandgap (E_g) of the active region in the laser structure as,

$$E_g\ (\text{eV}) = \frac{hc}{\lambda} = \frac{1239}{\lambda\ (\text{nm})} \tag{3.5}$$

where, *h* is Plank's constant and *c* is velocity of light. Therefore, the lasers having wavelength in the range of 600-700 nm can be assessed using ternary or quaternary compound viz. AlGaAs, InGaP, AlGaInP. Also, lattice matched AlGaAs grown on GaAs can realize laser emission wavelength in the range 700-870 nm, whereas using InGaAs/GaAs strained quantum well system the wavelength range can be extended

further up to 1100 nm by varying the thickness and indium content. The energy bandgap and lattice constant for various semiconductors at 0 K [84] is shown in Fig. 3.3.

Laser diode often faces rapid degradation in its performance due to formation of misfit dislocations in the crystal. The density of point defects, which act as centers for non-radiative recombination and reduces the efficiency, should be as low as possible. To avoid this problem, thick waveguide and cladding layers have to be grown lattice matched to the substrate. Moreover, the crystalline quality of the layers can be adversely affected by ordering as in the case of GaInP or by phase separation as observed for certain compositions of quaternary GaInAsP [81]. These require optimal growth conditions for each material.

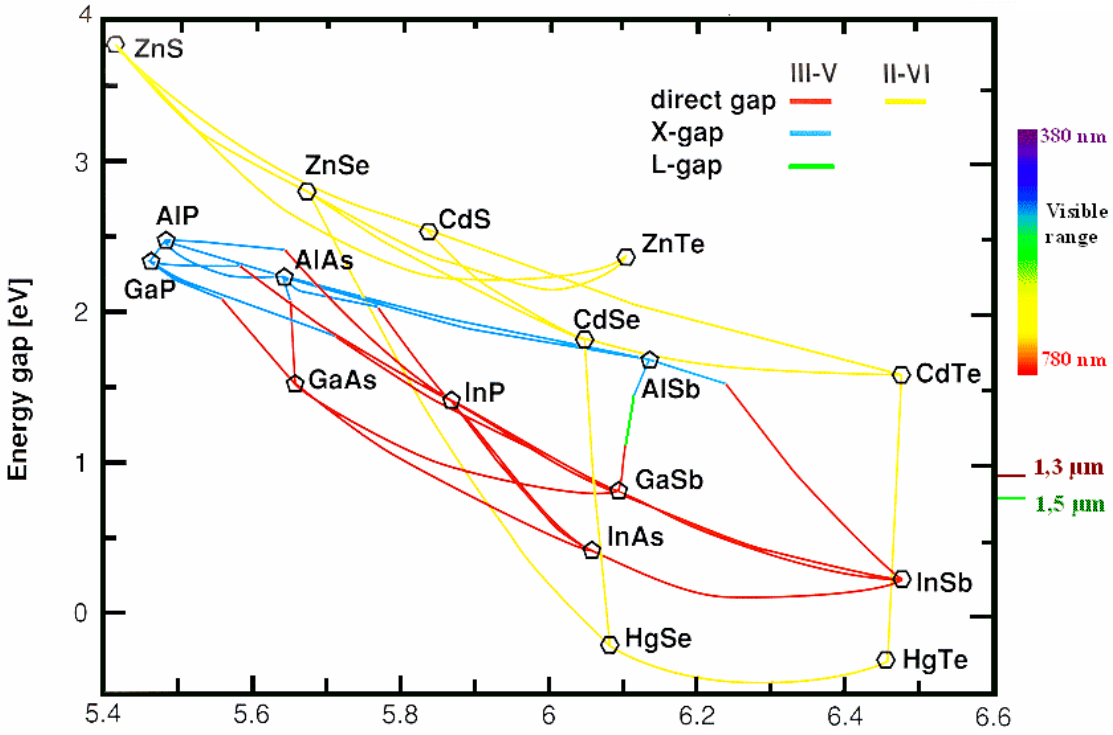

Figure 3.3: Bandgap versus lattice constant for conventional III-V semiconductors at 0 K.

3.3.3 Growth of a Complete Laser Structure

After optimizing individual layer parameters, complete laser structure has been grown by MOVPE (AIX-200) at RRCAT Indore [37]. The laser structure was grown for the fabrication of 980 nm high-power laser diode. Figure 3.4 (a) shows schematic of

complete laser structure with thickness of each layer. The energy band diagram corresponding to the laser diode structure is shown in Fig. 3.4 (b).

Further processing of this MOVPE grown laser was carried out for the structural growth of laser diode. The device processing is crucial in the high-power laser diodes. Since the high-power operation of the laser diode involves high-current density and high light intensity, the processing procedures must be optimized for these devices to achieve the following viz. (i) to improve the optical and electrical confinement, (ii) to minimize the series resistance of the device and, (iii) to reduce the amount of stresses and damages experienced by the laser diode structure during the processing steps.

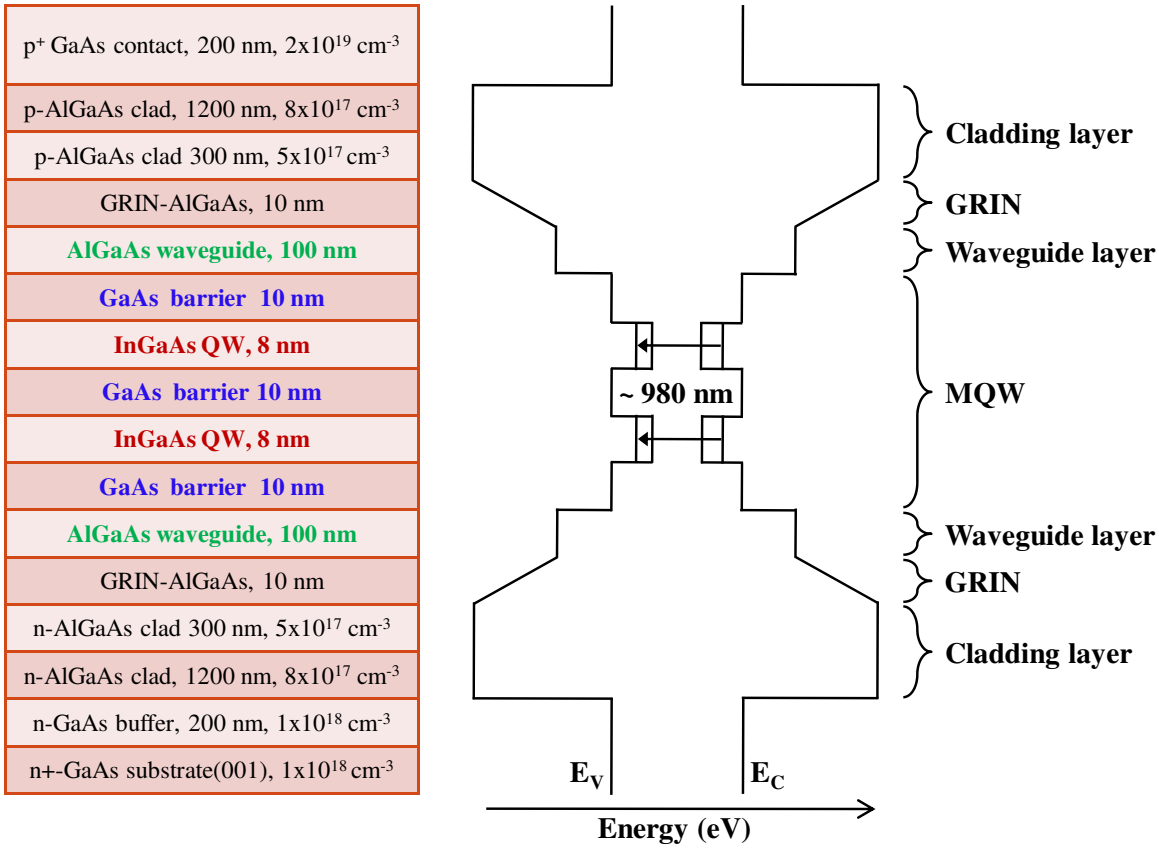

Figure 3.4: (a) Schematic structure for 980 nm high-power laser diode. (b) Energy band diagram for the grown laser diode structure.

3.4 Various Laser Diode Geometries

The edge emitting laser diodes are fabricated mainly in two device geometries. These are broad-area geometry and stripe geometry.

3.4.1 Broad-Area Laser Diodes

The broad-area laser diodes are the most elementary form of edge-emitting laser diodes. In these lasers, the stripe-width is much larger than the thickness of the laser structure, which allows uniform distribution of the injected current and the optical field in lateral direction. Nevertheless, due to large lateral dimensions many transverse modes can sustain this type of laser structure. Moreover, the filamentation, i.e. lateral beam distortions due to increase in refractive index, in broad-area devices is very well-known, and limits the high-power operation of the device.

3.4.2 Stripe Geometry Laser Diodes

As the name suggests, laser diodes with a few μm wide narrow stripe for lateral current confinement are known as stripe geometry injection lasers. This current confinement into the device can effectively overcome the issues like filamentation. The stripe geometry laser diodes can again be categorized into gain-guided, index-guided and buried heterostructures, according to different types of lateral confinement mechanisms viz. current, optical or photon, and carrier confinement, respectively.

Laser diodes, which only have current confinement, are called gain-guided lasers. In case of gain-guided lasers the lateral wave-guide is defined simply by the contact geometry. The current confinement is provided by an aperture, which is mostly realized by a dielectric isolator as shown in Fig. 3.5 (a). Though the fabrication of this laser is easy, there are some disadvantages as well. The threshold current in this devices is high compared to the index-guided one because of optical loss in waveguide.

The waveguiding in index-guided laser diode is achieved by means of lateral effective refractive index step difference formed by a very small mesa-structure in the

thickness of the upper cladding layer. A single lateral mode operation can be attained by optimizing the index step and the width of the waveguide. A typical example of an index-guided laser is the mesa- structure or ridge-waveguide laser shown in the Fig. 3.5 (b). Since, the current is injected at the top of the ridge, current confinement is also realized. A precise and reproducible control of ridge dimensions is necessary during device fabrication as the beam quality of the ridge-waveguide laser strongly depends on ridge dimension. The main advantage of the mesa- structure or ridge waveguide is well-defined current and optical confinement, which results in a lower threshold current, especially for stripe widths smaller than 100 µm.

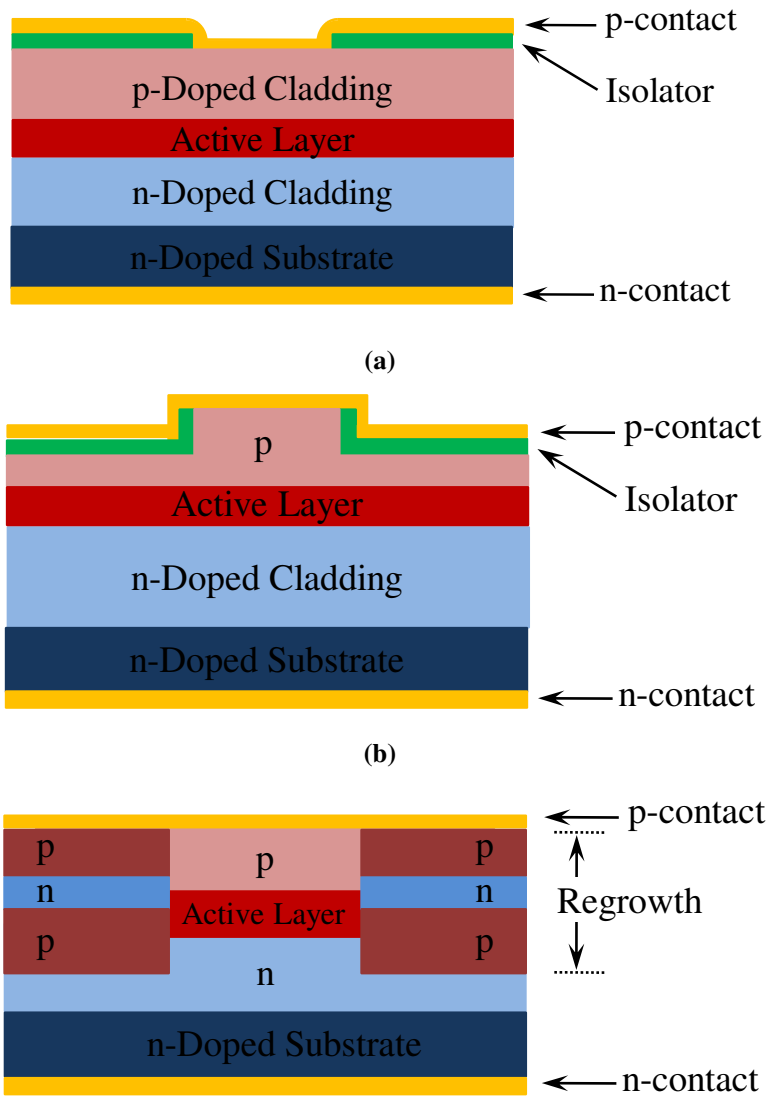

Figure 3.5: Stripe laser structures with different lateral confinement. (a) A gain-guided stripe laser, (b) The ridge-waveguide laser and (c) The buried-heterostructure laser.

The third type of stripe-geometry laser diode is a buried heterostructure, having all three types of lateral confinement, shown in Fig. 3.5 (c). The buried heterostructure is composed by an epitaxial re-growth technique, provides index guiding and carrier confinement. The p-n-p structure in the vertical direction works as a current-blocking layer providing carrier confinement. Buried heterostructure lasers are mostly used in communication systems where low- power consumption is required.

The stripe geometry laser provides no optical confinement and has large optical losses hence higher threshold current. On the other hand, the buried heterostructure, providing low threshold current indeed, is quite difficult to fabricate and need to optimize precisely for its reproducibility. Hence, the ridge-waveguide laser structure having both current and optical confinement with moderate threshold current and low optical loss is easy to optimize. We have processed the epitaxially grown wafer to grow mesa structure ridge waveguide laser. The optimization of all processing steps is discussed in detail in following section.

3.5 Fabrication of Laser Diode Bar with Mesa-Stripe Geometry

After the MOVPE growth of laser diode structure, the epitaxially grown wafer was processed to make laser diode bars using mesa-stripe geometry. For the device processing, the grown wafer is first cleaned by means of organic cleaning. The next step is to form the top ohmic contacts. The metal patterning in laser diode processing is usually attained by the photolithography and lift-off process. The photolithography involves applying an organic compound, called photoresist, on the wafer followed by baking, ultraviolet (UV) exposure through a pattern mask, and development of pattern to determine the desired exposed patterns. The device-isolation to form mesa-structure is usually carried out by wet chemical etching and coating of dielectric oxide e.g. SiO_2. The wafer is etched down to the appropriate layer of multilayered laser diode structure in the unmasked areas.

Further, the laser diode wafer has to be thinned down to desired thickness by lapping and polishing of substrate. Finally, the laser diode bars with desired cavity length

are scribed and cleaved. The processing is generally carried out in the class-10,000 clean-room, i.e., the room contains less than 10,000 particles of size more than 0.5 μm in a cubic foot of air. All these steps for fabrication of laser diode bars with mesa stripe geometry and their optimization for our structure is discussed in the next section in their processing sequence.

3.6 Optimization of Various Steps in Laser Diode Processing

The post-growth device processing of laser diodes were carried out at Semiconductor Laser Section, SSLD, RRCAT, Indore. The wafers were first cleaved into small pieces of about 1 inch area. Here, it is important to identify the crystalline direction lying within the surface plane since the etching profile is good in the primary flat direction and it is easy to cleave the sample in the direction perpendicular to the primary flat in order to obtain the cavity mirrors.

3.6.1 Organic Cleaning

The organic cleaning is preliminary practice to clean the semiconductor wafer from various contaminants e.g. dust, greases and other oily impurities. The sample was first cleaned in warm trichloroethylene (TCE) which removes oily impurities from the sample. Furthermore, the sample was cleaned in acetone and methanol, respectively, to remove the effect of previously used chemical, i.e. acetone to remove TCE and methanol for acetone. Finally, the sample was cleaned by de-ionized (DI) water. These organic solvents are effective in removing oils, greases, waxes and organic materials such as photoresists from the sample surface. The sample was then dried under nitrogen flow, and made ready for photolithography, which defines the transverse dimension of laser diode.

3.6.2 Photolithography

Photolithography is a process to form desired pattern on semiconductor surface by means of pattern-masking on an intermediate photosensitive polymer film called photoresist. The semiconductor surface, coated with photoresist, is then exposed through mask and developed to realize desired pattern by removing excess photoresist. The remaining

pattern can then be replicated in other materials in subsequent processing, using techniques such as etching, metallization, etc. The resolution is limited by the diffraction effect, which increases with the square root of the wavelength and with the gap between the mask and the wafer [85]. Various steps involved in photolithography are given below.

❖ Spin Coating

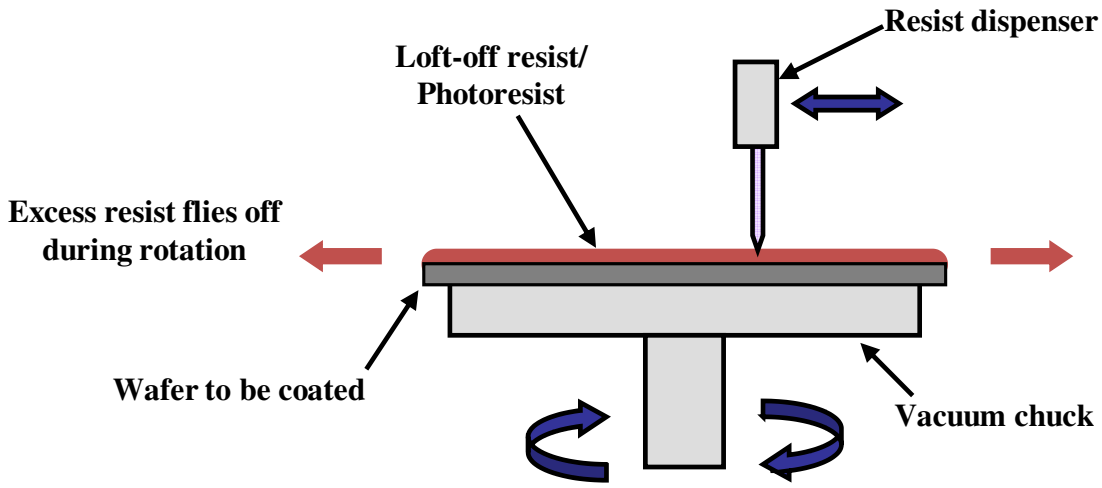

Figure 3.6: Schematic diagram of Spin coating process

➢ Lift-off Resist Coating

Prior to photoresist coating, the lift-off resist (LOR) has been spin-coated for the subsequent lift-off process to remove excess metal coat on the photoresist. It is used for making undercut in the photoresist layer. Since, LOR do not contain any photosensitive material it does not decompose on exposure to UV light. The LD samples were spin-coated with LOR at 4000 rpm for 30 sec following to the backing for 5 minute at 150 °C.

➢ Photoresist Coating

Generally, photoresist materials are classified into two types according to their solubility in a developer after UV exposer, i.e. positive photoresist (PPR) and negative photoresist (NPR).

- **Positive photoresist material**

The positive photoresist (PPR) becomes more soluble in a developer after exposure to the ultraviolet (UV) light. It consists of two parts, resin and photoactive compound. It decomposes on exposure to the UV light, through patterned mask, and makes the resin

more soluble in developer. Hence, the exposed resist is then washed away, leaving windows of underlying material.

- **Negative photoresist material**

As the name suggest, the negative photoresist (NPR) behaves exactly opposite to the PPR. It becomes less soluble in developer after exposure to the UV light. It consists of chemical inert rubber and photoactive agent. Exposure to the UV light causes the negative resist to become polymerized, and more difficult to dissolve in developer. Hence, developer solution can only remove the unexposed photoresist. Masks used for NPR, therefore, contain the inverse (or photographic "negative") of the pattern to be transferred.

Both PPR and NPR have their merits and demerits, listed in Table 3.2. We have used PPR for lithography, as it provides good step coverage and dissolve in aqueous developer. It is deposited on the semiconductor surface by means of spin coating.

Table 3.2: Differences between positive photoresist and negative photoresist.

NPR	PPR
Swells during develop	No swelling during develop
Marginal step coverage	Good step coverage
Organic solvent developer	Aqueous developer
Sensitive to O_2	Operate well in air [86]

We used OiR-960 positive photoresist (S1813) for photolithography of laser diode samples. The samples were coated with PPR, having thickness about 1 μm, at 3500 rpm and soft baked at 95 °C on a hot plate for one minute.

❖ Alignment & Exposure

A photomask consists of desired pattern, i.e. alternate transparent and opaque stripes, to realize laser diode mesa structure was aligned to the wafer. The photomask, having stripe width 100 μm, used for patterning is shown in Fig. 3.7, having opaque Fe_2O_3/chromium stripe pattern on a soda lime glass substrate.

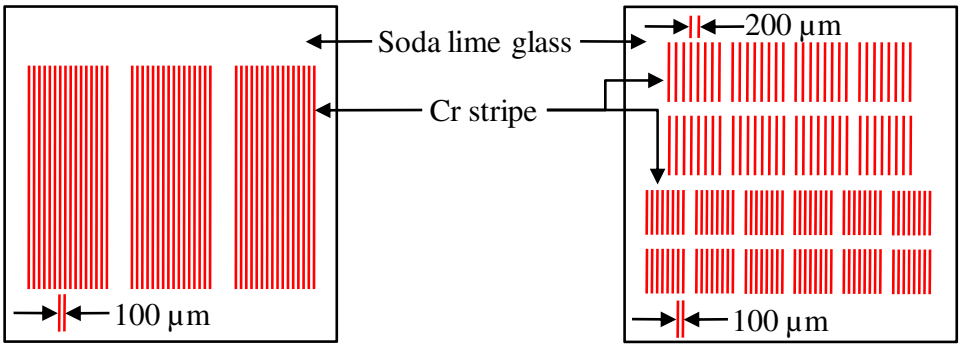

Figure 3.7: Masks used in lithography

In optical lithography, the formation of images with visible or UV radiation occurs on the photoresist using contact or proximity printing. We have used contact printing, in which the mask (M1-MESA (N)) was brought into contact with a resist coated wafer. This prevents the diffraction losses and we get high resolution. However, there is a drawback of this method in that it may produce defects in both, the wafer and the mask. The sample was exposed using a Quintel 4TL mask aligner for 10 s with 10.6 mw, 365 nm UV radiation.

❖ Development

The exposed photoresist is now dissolved into a suitable developer which is different for different photoresists. When the wafer is dipped into a developer the exposed photoresist dissolves in developer (MFCD-26) while lower LOR remains unaffected. After exposure and development, a hard bake at 120 °C for 1 minute is applied to the sample, which makes photoresist hard and prevents the further dissolution of the photoresist in developer. Once again the sample is dipped in MFCD-26 for 1 minute to realize undercut by removal LOR. Finally, the wafer cleaned in DI water and dried with N_2 gas

3.6.3 Top Metal Contact Deposition

The purpose of top and bottom metal contact is to provide an ohmic contact to the laser diode which allows the flow of electric current through the device. Hence, the series resistance of the device due to contact layer should be as small as possible. Also, the contact layer should be a stable with respect to ambient temperature and over the long

period time. Therefore, low contact resistance, ease of fabrication, better adhesion, and thermal stability are the primary quality requirements of the metal to realize a good quality contact layer.

The metallization is also the basis for the laser diode mounting on a heat sink which allows soldering, also known as die-bonding, and wire bonding. Generally, for high-power diode lasers based on GaAs substrates, the semiconductor contact layer consists typically of heavily doped *p*- and *n*-type GaAs. Almost any metal placed in intimate contact with these heavily doped GaAs surface will result in an ohmic contact without any alloy formation. We have deposited multilayer of Titanium (Ti) (~10 nm)/ Platinum (Pt) (~5 nm) / Gold (Au) (~200 nm) in sequence to deposit p-type ohmic contacts. Here, Ti and Pt are used for the better adhesion of top Au layer, which provides a very high conductivity and a soft surface quality for device bonding. The front contacts to the p+ GaAs capping layer of the laser structures were deposited using a metal coating unit with thermal evaporation system at high vacuum (3×10^{-6} mbar pressure)

3.6.4 Lift-off Process

Lift-off process is a simple method for patterning films which are deposited on the sample. In this step, we remove the metallic layer from the top of mesas, by means of warm (65 °C) PG remover bath. The PG remover reacts with LOR and causes swelling and losing adhesion to the wafer and hence excess metal deposited on the photoresist is removed while metal directly deposited on wafer remains unchanged. Figure 3.8 shows the final structure of the top p-contact surface.

Any deposited film can be lifted-off provided that the substrate does not reach the temperature high enough to burn the photoresist during the deposition and the film is thin enough to allow solvent to seep underneath. Various mechanisms from resist coat to lift off are shown in Fig. 3.9 [87].

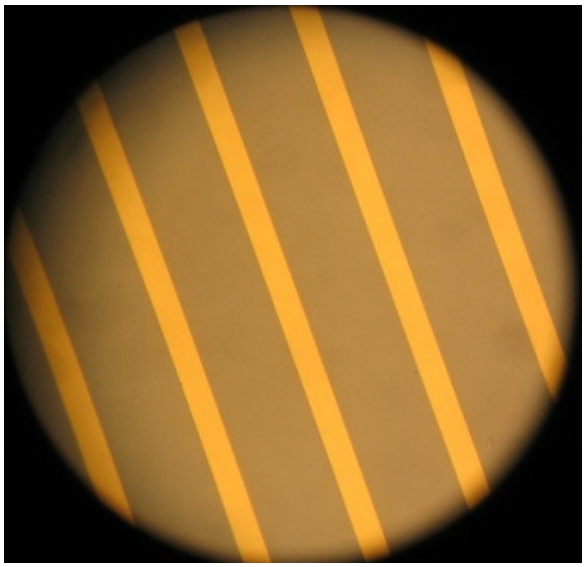

Figure 3.8: Photograph of metal contacts on laser structure after lifting-off.

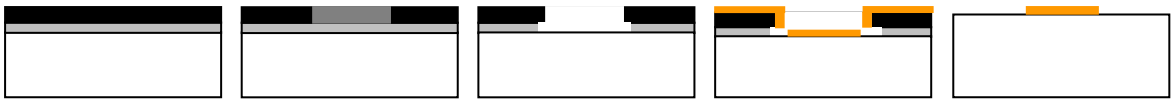

Figure 3.9: Lift-off technique: (a) overlying layer of photoresisr (OiR 960), soft baked at 95 °C for 1 minute and (b) exposed to UV light (λ = 365 nm) (c) developed resist with formation of undercut (d) metal deposition on sample (e) lift-off and clean.

3.6.5 Rapid Thermal Annealing of Top Contact

Rapid thermal annealing (RTA) is very crucial for obtaining good metal-semiconductor ohmic contacts [88]. It helps the diffusion of the metal into the GaAs crystal, and reduces the barrier-height at the junction by alloying the semiconductor and the metal at the junction. This results in the reduction of series and thermal resistance of the devices. The annealing should be very rapid to avoid unwanted processes like redistribution of impurities and increment in escape probability of volatile materials. The RTA also provides good adhesion for metal to semiconductor contacts.

Heating by an array of incandescent lamps is a popular method for RTA. In this method, many incoherent lamp sources like tungsten–halogen lamps are mounted in a cylindrical box containing a quartz tube in which samples are placed on the Silicon wafer. Silicon wafer has high absorption for infrared radiation, which is emitted by tungsten halogen lamps and hence causes the heating of the sample up to desired temperature. We

have carried out RTA at 375 °C for 45 s. Rapid heating of a sample with temperature and desired dwelling time is a difficult job and this is achieved by a computer controlled PID temperature controller. A thermocouple is used to measure the temperature of wafer. For abrupt cooling, proper coolant like N_2 gas is used. The temperature profile graph of RTA process is shown in Fig. 3.10.

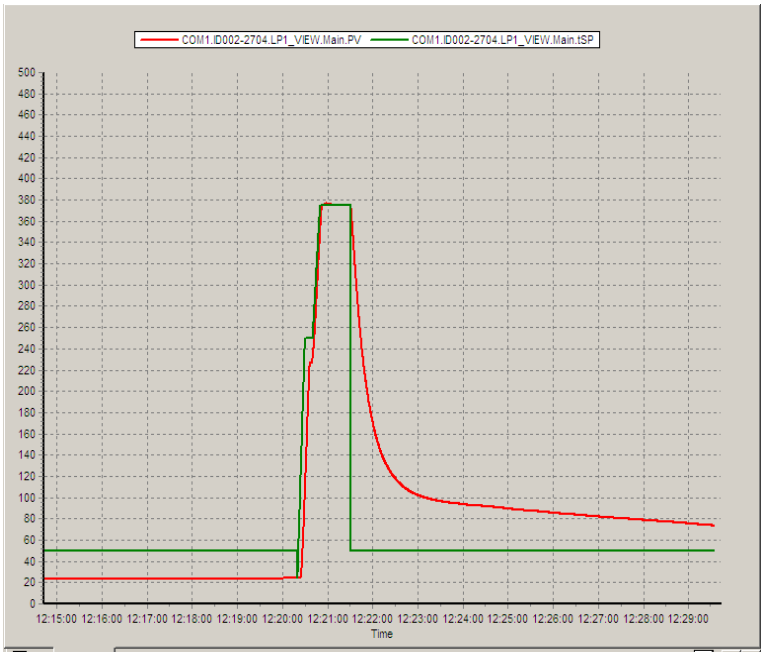

Figure 3.10: Temperature profile with respect to time during RTA process.

3.6.6 Etching

The etching is required to isolate individual devices in a laser diode bar and to form mesa structure. The wafer is etched till the upper cladding layer by using suitable etchant which reduces the current spreading in the devices. The etching of the mesa can be carried out either by wet etching or dry etching methods. In wet etching, areas of the wafer outside the desired stripe are removed by dissolving them in a wet chemical solution. The dry etching involves reaction of materials in such areas, to be removed, with gases in plasma to form volatile products. In this work, because of its simplicity [89,90], and depth control, wet etching was preferred giving reliable results for laser diode devices.

In the case of wet chemical etching, only solutions which exhibit anisotropic etching and strictly proceed downwards into the material are preferred. If the etching is

isotropic, a large undercut occurs resulting in breaks and degradation of metallization films and the structure [85]. Though the wet etching forms an undercut and hard to control it is mostly used due to its low cost, easy to implement, high etching rate, good selectivity for most materials and produce better electronic properties.

The etching solution for GaAs and AlGaAs usually contain hydrogen peroxide (H_2O_2), to oxidize the semiconductor surface, and phosphoric acid (H_3PO_4), to dissolve the oxidized components of mixture. In the present study, H_3PO_4 etching solution has been used. The H_3PO_4 / H_2O_2 / CH_3OH system is used to etch GaAs and AlGaAs at controlled rates. This is due to high viscosity of H_3PO_4, so that diffusion of the hydrogen peroxide to the semiconductor surface becomes the rate - limiting step. In this study, a mixture of CH_3OH / H_3PO_4 / H_2O_2 in 6:3:1 ratio is made as an etching solution for GaAs and AlGaAs. The etching rate was determined with the help of surface profilometer by etching on the dummy samples and desired etching depth was achieved by controlling time of etching, shown in the Fig. 3.11. After etching, the wafer was dried by N_2 gas.

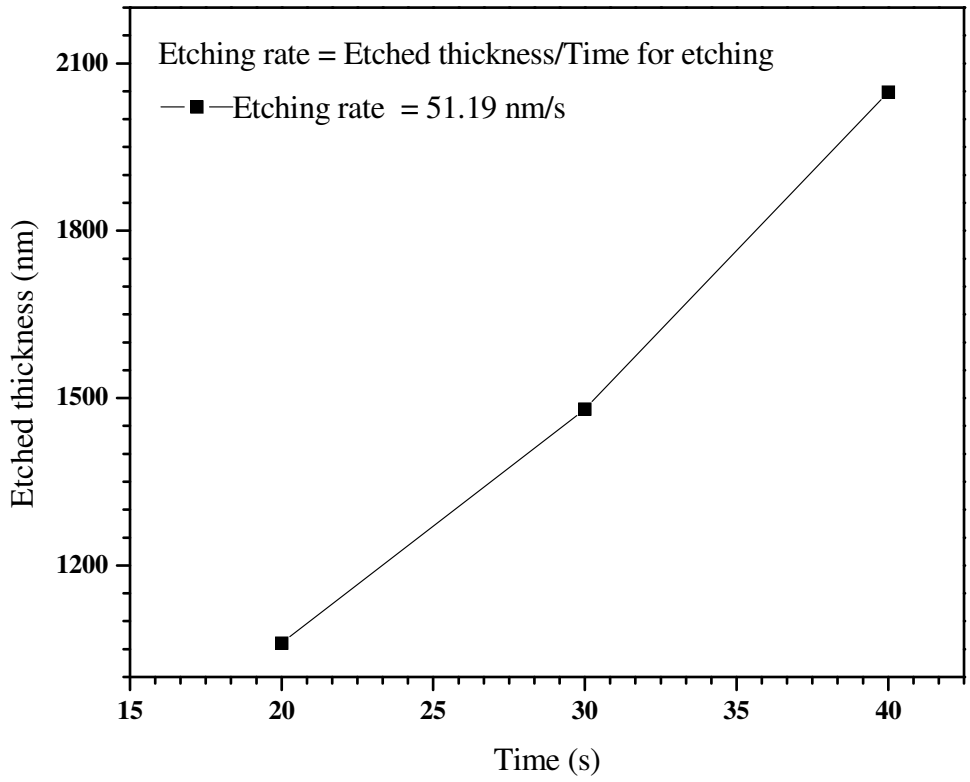

Figure 3.11 - Etched thickness vs. time

3.6.7 SiO_2 Deposition and Window Opening

For better isolation and surface state passivation of laser diode, dielectric layers are used as a current barrier between isolated laser diodes after GaAs/AlGaAs etching. The oxide deposition improves the performance of the laser diode because it isolates the devices completely and prevents tunneling of carriers from one diode to other. So the carrier loss is reduced and directly injected to the active region. Thus the injection efficiency of the laser diode is also improved. We have deposited SiO_2 dielectric layer of ~200 nm on GaAs/AlGaAs etched mesa laser diode structure. After SiO_2 deposition it is necessary to remove the SiO_2 from the top of metal contact region. To do so we have again used photolithography and selective etching of SiO_2 with following sequential process execution.

- 200 nm thick SiO_2 deposition on etched laser diode wafer.
- Spin coating of PPR for 30 s at 3500 rpm.
- Soft baking at 95 °C for 1 min.
- Mask alignment in such a way that only exposed PPR coated on metal stripe.
- Exposure to UV light for 10 s.
- Etching of selective SiO_2 Buffer Hydro-Fluoric acid (BHF).
- Develop for 1 min with developer, to remove PPR from SiO_2.
- Then clean with acetone, methanol, and DI water.
- Dry it with N_2 gas.

To make the Buffer Hydro-Fluoric acid (BHF), 40 g of ammonium fluoride (NH_4F) is dissolved in 60 ml of DI water. The solution is then mixed with HF acid in a ratio of 6:1. The overall chemical reaction for SiO_2 etching is: $SiO_2 + 6HF \rightarrow H_2SiF_6 + 2H_2O$, where H_2SiF_6 is water-soluble complex. The pattern sample was dipped into the BHF solution for 15-20 s for etching. After SiO_2 etching and complete lithography process we get SiO_2 window open from the metal contact region as shown in Fig. 3.12.

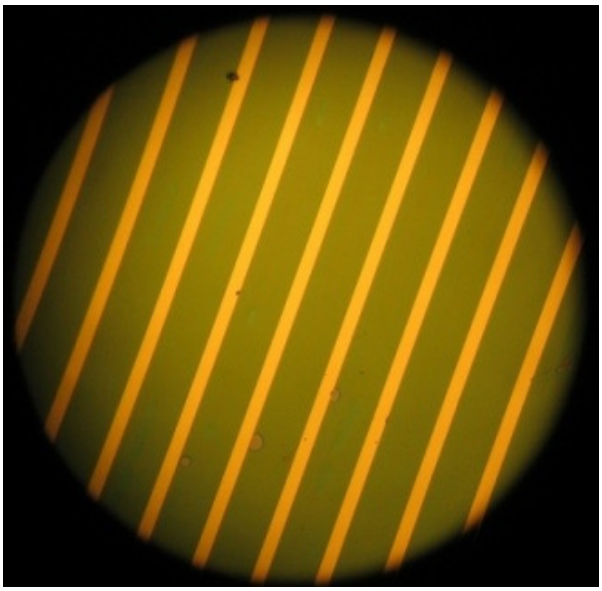

Figure 3.12: Sample photograph after window opening by removal of SiO_2 with BHF.

3.6.8 Lapping and Polishing

In order to reduce the thermal resistance of the device and to facilitate the scribing procedure, it is necessary to thin down the wafer by reducing the substrate thickness. This is accomplished by reducing the thickness of n^+ GaAs wafer to around 150 μm by mechanical lapping and polishing the wafer manually. Lapping was done using alumina powder or diamond pest, having particle/grain size 5 μm and 1 μm, to reduce thickness followed by polishing with alumina slurry, having particle size 0.5 μm, to mirror polished the surface. Polishing is necessary to achieve uniform surface with minimum roughness which reduces the device resistance and helps to get void-free die-bonding. After lapping and polishing, the wafer was cleaned organically and the bottom surface of the wafer was chemically polished by means of etching using CH_3OH / H_3PO_4 / H_2O_2 etching solution. Finally, the wafer was cleaned with DI water and dried under nitrogen flow.

3.6.9 Bottom Metal Contact Deposition

After the samples are thinned by lapping and polishing, it is necessary to cover this surface entirely, for the n-contact of the laser devices. The most common approach of fabricating ohmic contacts on n-GaAs is to apply an appropriate metallization to the wafer, and then alloy the metal into the GaAs. During the alloying and cooling period, a

component of the metal enters into the GaAs and highly dopes the surface layer. This doping decreases the Schottky barrier and the tunneling dominates the conduction mechanism. The doping agent is generally chosen to be germanium (Ge). Gold-germanium (Au-Ge) is usually applied with an overlay of another thin metal layer such as nickel (Ni). Addition of Ni to Au-Ge leads to lower contact resistance as well as serving to maintain a smooth surface morphology after alloying the contact metallization [91]**.** The Au-Ge alloy has a poor sheet resistance, is very difficult to wire-bond and is not solderable to a heat sink. This requires an additional gold layer to be deposited on the Au-Ge alloy. The sequence for bottom ohmic contact deposition on n-type substrate is Au-Ge (~ 5 nm) /Ni (~ 5 nm) /Au (~ 100-200 nm). To achieve intimate contact formation between GaAs substrate and the deposited metals, we have carried out RTA at 375 °C for 45 s.

3.6.10 Scribing

Finally, the wafer is cleaved along the cleavage plane, i.e. (110) for GaAs, perpendicular to laser diode stripes using Micro Suss HR 100 manual scriber to get laser diode bars with different cavity lengths ranging from 0.5 mm to 2 mm. Each bar contains several laser diodes with stripe width of 100 µm.

The complete process layout for the processing of laser diode is given in Fig. 3.13.

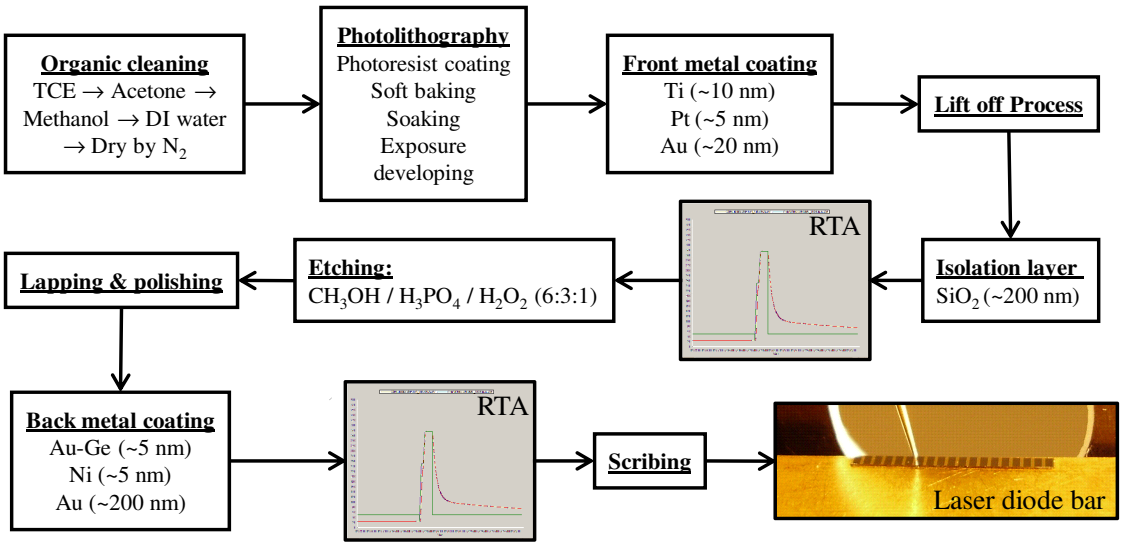

Figure 3.13: A complete procedure of device processing.

* * *

Chapter 4

Laser Diode Facet Coating Using Al_2O_3, SiO_2, TiO_2, and ZrO_2

4. Laser Diode Facet Coating Using Al_2O_3, SiO_2, TiO_2 and ZrO_2

The facet coating is one of the most important aspects of the high-power laser diode post-fabrication technologies. It protects laser diode from facet degradation and enhances the power level of catastrophic optical mirror damage (COMD) and eventually ensures long-term reliable operation. The facet coating is realized by an appropriate dielectric thin-film coating on the facets. This chapter discusses the optimization conditions for thin-film coating of various dielectric materials viz. Al_2O_3, MgF_2, SiO_2, TiO_2. Study of anti-reflection (AR) and high-reflection (HR) coating on front and rear laser facets, respectively, and its effect on laser diode characteristic has been studied. Additionally, an in-situ reflectivity measurement technique has been optimized and described in detail.

4.1 Importance of the Facet Coating

Laser diode facet coating is one of the most important phases in device fabrication technology. The laser mirrors are achieved by a three-step process: (1) Cleaving of the wafer into laser bars/chips, (2) Passivation of the cleaved surfaces, and (3) Coating for the desired reflectivity. The cleaved facets of the semiconductor crystal form the resonator cavity in a laser diode. Hence, the natural reflectivity of both the pure cleaved facets is nearly 32 % [6] and the laser diode emits an equal amount of light output from both the facets, as illustrated in Fig. 4.1 (a). However, in most of the practical applications, it is generally not possible to use the light from both facets of the laser. In order to make light emission from only one of the facets, one facet of the laser is coated with an antireflection (AR) coating and the other with a high reflection (HR) coating.

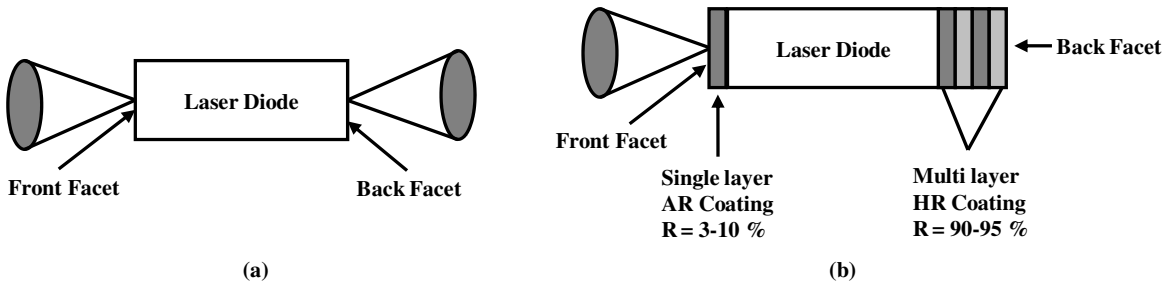

Figure 4.1: Schematic of facet coating on a (a) bare, without facet coating, laser diode chip with (b) single layer anti-reflection (AR) and multilayer high-reflection (HR) coating having reflectivity 3-10 % and >90 %, respectively.

The operation of the laser diode with a bare facet will lead to the facet oxidation, which causes the device degradation and sudden failure. The mirror coatings are deposited for passivation and protection of the sensitive laser facets. Consequently, one can either reduce or eliminate the laser diodes facet degradation by suitable coating. On the other hand, the facet coating will change the facet's reflectivity, allowing the light emission from the front facet and reducing the optical density inside the cavity, and hence, increasing the optical output power. Moreover, it also ensures long term and reliable device operation without affecting the mirror facet.

The facet coating must fulfill three crucial requirements: First, the preferred reflectivity should be realized, typically from 3 % to 10 % at front facet and > 90 % at the rear facet, as shown in Fig. 4.1 (b). Second, for higher mechanical and optical stability of lasing, the facet coatings have to exhibit a number of mechanical properties, viz. good adhesion to the facet surface, low mechanical stress, chemical and mechanical stability, and an excellent behavior with respect to lifetime and catastrophic optical mirror damage (COMD). In addition, for optical communication systems it is necessary that the beam characteristics of the laser devices do not change by facet coating. That means a stable optical operation and high transparency at the wavelength of emission is required after the facet coating. The third requirement is that the facet coating process must be cheap, reproducible, and technologically worthy for mass-production.

The dielectric thin film coating to the laser diode facets not only protects it from environmental influences but also reduces further chemical and thermal effects to the facets and eventually increases the device lifetime. Nonetheless, the electronic states at the interface between the laser facet and the coating can act as traps for minority carriers and cause nonradiative recombination of the carriers. Therefore, an appropriate material selection having good chemical and mechanical stability with sufficiently large bandgap than laser material can improve the laser performance. The particular characteristic viz. self-passivation, high density, and having an ability to withstand exposure to heat and humidity, of the facet coating makes it a low-cost alternative to the hermetic packages for the laser diode, indeed [92]. Facet coating reduces the degradation rate significantly [93,94]. The reflectivity modulation to the laser facets can lead to the better side modes suppression and show a narrower width of the spectral peak. *T. Guhne et al.* [95] has

demonstrated the reduction in beam divergence off the axis perpendicular to the active region by 30 % by means of SiO_2 (silicon oxide) AR coating application. Also by proper design of the facet reflectivity the lasing transition of the quantum well can be tailored to take place either between the n = 1 or n = 2 sub-band [96].

4.2 Optical Thin Film Coatings

The reflectivity modulation works on the principle of interference in thin films. Optical interference in a thin film can be explained in terms of the wave theory of light. When a light wave traveling in a certain medium having refractive index, n_0, encounters a medium having different index of refraction, n_1, a portion of light reflects at the interface. The amplitude of this reflected light wave, which is equivalent to the electric field strength, depends on the refractive indices of a medium at the interface and can be given for normal incidence as

$$\rho = \frac{n_0 - n_1}{n_0 + n_1} \tag{4.1}$$

This Eq. 4.1 was developed by the French physicist *Augustin Jean Fresnel* in 1896 and also known as the Fresnel Equation. The Fresnel reflection coefficient ρ in the above equation is real. The sign of this coefficient determines that whether there is a phase shift between the incident and reflected wave or not and it depends on the difference between n_0 and n_1. One can modify the reflectance of a surface by coating the surface with single or multilayer dielectric thin films. In a multilayer coating, a portion of the incident wave is reflected at each of the interfaces. The phase difference between the incident and reflected light causes either constructive or destructive interference, accordingly, the reflectance of the coated surface increases or decreases, respectively. This phase difference depends upon the film's thickness and its refractive index, also known as *optical thickness*.

There are basically two types of coatings namely antireflection (AR), and high reflection (HR) coatings needed on a laser chip/bar facets to make them functional. A wide range of coating design and materials to be used in the coating has been studied. The most common material for laser facet is GaAs. This material has a high refractive index at various wavelengths. As discussed above, the reflectivity of pure cleaved facet is

nearly 32 %. This value can easily be modified by coating of the facets with an appropriate layer or a stack of layers; particularly, the front facet coating should have a negligible absorption for the laser emission wavelength.

4.2.1 Antireflection Coating

Anti reflection (AR) coating is one of the essential processing technologies for realizing high-power operation of the laser diode. It is also essential to realize super luminescent diodes (SLDs) and semiconductor laser amplifier. For the amplifier application, it is necessary to achieve maximum optical power for minimum electrical consumption and to minimize the modal reflectivity at the end facets. The simplest method to obtain high-power is the AR facet coating to one of the laser facets [97,98]. Laser diodes with one or both of their facet reflectivity reduced by AR coating are transformed from oscillating cavities into gain media. Since the laser diodes with AR coating are continuously tunable over a wavelength range of more than 25 nm and having mode stability, they can be used as external cavity diode laser (ECDL) by means of coupling with a grating [99]. The wavelength stabilization on high-power laser diode can be achieved with an additional AR coating to the facets [100]. The catastrophic optical mirror damage (COMD), permanent damage to the laser mirrors by local facet heating, is the most prominent damage mechanism of the high-power laser diode. The non-absorbing facet coating to the device is the easiest way to suppress the COMD and increase device reliability [101,102] as it reduces the optical density at the front facets and reduce the facet heating effect.

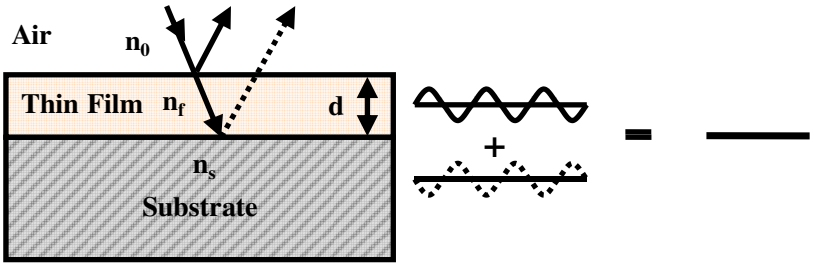

Figure 4.2: Destructive interference between light beams reflected from the upper and the lower surface of the deposited dielectric thin film for AR coating.

The antireflection coating works on the principle of the destructive interference of the light waves, reflected from the layer interfaces of the thin film. The coating is design

in such a manner that the phase shift between the reflected light wave from the front and back surface of the thin film is 180°. If the light waves recombine destructively then there will be no reflection of the light at the front facet, as shown in Fig. 4.2, and hence the AR coating ensures the maximum light transmission form the front facet.

The simplest way to design AR coating is that the quarter-wave optical thick (QWOT) film deposition, where the optical thickness of the film should be quarter of the lasing wavelength i.e. $\lambda/4$, of the laser diode. Hence, the physical thickness, d, of the coating layer, for normal incidence of light, will be $\lambda/4n_f$, where n_f will be refractive index of the thin film. Beside the lasing wavelength and the thickness of the coating layer to optimize the AR coating, one has to look out for refractive indices of the substrate, n_s, and the thin film, n_f, and angle of incident , θ. For minimum reflectance, the refractive index of the film, n_f, should be chosen so that, $n_f = \sqrt{n_0 n_s}$ where, n_0 is the refractive index of medium, usually air. The normal reflectance, R, of a single layer AR film is given by the Eq. 4.2 [5]. One can easily adjust the reflectivity minimum according to the laser emission wavelength by varying the film refractive index or in other words by changing the coating material.

$$R = \frac{(1-n_s)^2 \cos^2(\delta) + \left(\frac{n_s}{n_f} - n_f\right)^2 \sin^2(\delta)}{(1-n_s)^2 \cos^2(\delta) + \left(\frac{n_s}{n_f} + n_f\right)^2 \sin^2(\delta)} \tag{4.2}$$

where,

$$\delta = 2\pi \frac{n_f d}{\lambda} \tag{4.3}$$

Normally, the single layer AR coating does not provide very low reflectivity that can be realized by multilayer AR coating. However, in case of laser diode the reflectivity achieved by a single layer AR coating is usually sufficient. In addition to that, the design and optimization a single layer AR coating is very simple and cost effective. Therefore, we have used single layer AR coating for reflectivity modulation for our laser diodes.

4.2.2 High-Reflection Coating

The high-reflection (HR) coating is used to prevent the light emission from the rear facet of the laser diode and to reflect most of the light back into the cavity. To increasing the reflectivity of the laser facet, a multilayer dielectric thin film is utilized in general. Therefore, the HR coating consists of a number of bi-layer pairs of low and high refractive index materials. As its name suggests the basic working principle of HR coating is exactly opposite to the principle of AR coating, i.e. constructive interference. The light waves reflected from each consecutive surface of the multi-layer coating, all in phase, recombine constructively and this superposition of the light makes the coating highly reflecting. So, one can achieve very high reflective coating simply by increasing number of bi-layers. The HR coating consisting of a stack of alternating bi-layer films pair. Each pair consists of a QWOT low refractive index- (n_L) and high refractive index- (n_H) material layer according to laser diode wavelength. The actual structure of the multilayer HR coating is, Substrate (GaAs for most of the laser diode)-LH…LH-Air, where L be the low refractive index material, and H be the high refractive index material. The reflectance at the wavelength,λ, is given by [103],

$$R = \left[\frac{n_s^F - n_0}{n_S^F + n_0} \right]^2 \tag{4.4}$$

where, $F = \left(\frac{n_H}{n_L} \right)^{2p}$ and p is the number of bi-layer pairs. From the Eq. 3.4, it is clear that higher the ratio of (n_H/n_L) is, the required number of bi-layers for HR coating will be less. The reflectivity increases with the number of bi-layers. To reduce mechanical stress and to increase the stability of the coating, it is necessary to choose a material pair that exhibit good adhesion and reduces the number of bi-layers necessary to reach the desired reflectivity.

4.2.3 Materials for AR – HR Coatings

In order to meet the demands of the laser diode facet coating and the coating process, the evaporation materials should fulfill a number of requirements viz. it should be depositable on the facets without causing any damage to the underneath layer, having a suitable refractive index and should be transparent for the lasing wavelength. The coating

material should have refractive index equal to the square root of the effective refractive index of the laser facets at the particular wavelength to realize single layer antireflection coating having minimum reflectivity. Above all, the chemical purity of the material is to be of concern as it influences the properties of the coating. The impurities in the coating generate defects and causes optical losses in film e.g. scattering or absorption by changing the film stoichiometry. Normally, the material having 99.99 % purity can be utilized for the optical coating.

The first choice of the coating materials is based on its refractive index value and the transmission range, of course. As it is known, low absorption is obviously required so as the material do not absorb light at the wavelength of interest. The transmission range of materials is limited by the bandgap and the molecular vibrational absorption, at shorter and at longer wavelengths, respectively. Thus, the bandgap of the material should be much higher than the laser photon energy. Moreover, this is the reason why dielectric stack of low and high refractive index materials is preferred over metals for HR coating despite the fact that metals provides high reflection easily. Moreover, one also cannot ignore the possibility of shorting of the laser diode contacts due to the metal coatings to the facets. Above all, the coating material should exhibit a long-term stability over the atmospheric effects and even under the high-power operation of the laser diode.

The desired value of the modified laser diode facet reflectivity is about 3-10 % for the front and >90 % for the back facet. There are many materials suitable to modify the laser facet reflectivity. Typically, a single layer QWOT Al_2O_3, SiO_2, MgF_2, is used as antireflection coating at the front facet, and to increase the reflectivity at the back facet one of these materials will be paired with a material having higher index of refraction, say Silicon (Si), than that. Many materials have been reported for the AR coatings on the laser facets. For example, silicon nitride [104], and gallium oxide (Ga_2O_3) [105] were used to obtain single layer AR coating. In case of multilayer HR coating, the performance is strongly bound to the ratio of the refractive indices of the materials making up the stack. High refractive index value ratio provides wider bandwidth and requires fewer layers to obtain specific reflectance. Thus, for multilayer HR coating, one of the materials should have high refractive index compared to the other.

We have used QWOT Al_2O_3 and ZrO_2 for AR coating to 808 nm and 980 nm laser diode, respectively, while HR coating for these devices realized by means of multilayer QWOT pairs of Al_2O_3/TiO_2 and SiO_2/ZrO_2, respectively for 808 nm and 980 nm. Here, Al_2O_3 and SiO_2 are low-refractive index material in comparison to the TiO_2 and ZrO_2 being high-refractive index material. Table 4.1 (a) & (b) show the physical and optical properties of the bulk material used for facet coatings [24], respectively.

Table 4.1 (a) – Physical properties of the bulk materials used for AR – HR facet coating.

Material	Symbol	Color	Melting Point (°C)	Density (gm/cm^3)	z – factor
Aluminum Oxide	Al_2O_3	Clear white	2072	3.97	0.999
Titanium Oxide (IV)	TiO_2	White	1830	4.26	0.4
Silicon Dioxide	SiO_2	White	1610	2.65	1.00
Zirconium Oxide	ZrO_2	White	2700	5.89	1.00

Table 4.1 (b) – Optical properties of the bulk materials used for AR – HR facet coating.

Material	Refractive index	Wavelength range	Dielectric constant	Energy band-gap (eV)
Aluminum Oxide	~ 1.75 (at 808 nm)	50 nm – 6 μm	~ 10	10
Titanium Oxide (IV)	~ 2.48 (at 808 nm)	220 – 720 nm	~ 30	5.6 – 1.1
Silicon Dioxide	~ 2.00 (at 980 nm)	0.18 – 3.5 μm	~ 3.9	5.65
Zirconium Oxide	~1.45 (at 980 nm)	0.25 – 9 μm	~ 25	9

The refractive index of the Al_2O_3 is about 1.66, nearly same as to optimize single layer AR coating for the wavelength of our interest. As mentioned in Table 4.1(b), the useful transmission range of the Al_2O_3 extends from 50 nm to 6 μm. The Al_2O_3 has relatively high dielectric constant, $k \approx 10$, wider bandgap, ~10 eV and high chemical stability [106]. It too exhibits high resistivity, high thermal conductivity, and stability with a thermal expansion coefficient of 8.4×10^{-6} /°C. In addition, the hardness and the high corrosion resistance favor Al_2O_3 as a passivation layer. Titanium dioxide (TiO_2) has been used in optical coating for many years as it provides high refractive index for the visible region i.e. 2.2 – 2.4 at 550 nm and it is hard and stable in comparison with other oxide materials. These features of the TiO_2 can be used for multilayer HR coating in

combination with Al_2O_3 as low refractive index material, which gives more than 90 % reflectivity with only three bi-layer pairs of Al_2O_3-TiO_2. The deposition of AR and HR coatings on the facets of laser diode involve thin film deposition technology. We have carried out the facet coating on laser diodes using e-beam evaporation technique. The next section discusses issues related to optical thin film deposition using e-beam and optimization of coating conditions for laser diode facets.

The most widely used materials for 980 nm laser diode are aluminum oxide (Al_2O_3), silicon nitride (Si_xN_y) and silicon dioxide (SiO_2) for single layer AR coatings while silicon (Si) is used as high refractive index material in combination with Al_2O_3 or SiO_2, having low refractive index, to realize HR coating [6,97,107,108]. The sputtered Si_xN_y suffers from its reproducibility in the film index [109]. Although having very high laser damage threshold, the SiO_2 thin film prepared by ion assisted electron-beam (e-beam) evaporation shows quite variation in film refractive index with oxygen partial pressure and also continues to oxidized in air so the refractive index reduce with time [109]. The refractive index of Si strongly varies with wavelength and, for wavelength range up to near infrared the absorption becomes significant, leading to facet heating [6]. Moreover, contamination to the Si may cause device sorting.

Leading to these facts we have used zirconium oxide (ZrO_2) to realize the AR coating and HR coating in combination with SiO_2. The refractive index of ZrO_2 (i.e. ≈2 at 980 nm) is quite near to the geometric mean value of the refractive index needed for single layer AR coating. It is best suited material for GaAs (refractive index, n ~ 3.6) based laser diodes, because it has high dielectric constant ($\varepsilon \approx 25$), large bandgap ($E_g \approx 5.65$) [110] and high stability which prevents degradation of the devices. Further, stoichiometry in zirconia films can be achieved without the addition of oxygen into the vacuum chamber. It is also known that the laser damage threshold of ZrO_2 is higher than TiO_2, usually used as high refractive index (H) material in combination with Al_2O_3 or SiO_2 for HR coating of laser diode, so ZrO_2 will be more suitable material for HR coating for HPLDs. Similarly, SiO_2 ($n = 1.45$, $E_g \approx 9$ eV) [111] have low refractive index (L) and easy to evaporate. It also provides a high threshold for laser induced damage and it has good environmental stability, besides this SiO_2 also has compressive intrinsic stress [112]. Also, QWOT SiO_2/ZrO_2 multi layers are widely used for the facet coating of GaN

based ultraviolet (UV) laser diodes, due to very high laser damage threshold [113]. To the best of our knowledge the combination of these materials for AR and HR coating on the facet of 980 nm laser diode is not reported.

4.3 Thin Film Deposition Technique

Generally, the term *thin film* is related to the layers having thickness ranging from few atomic layers i.e. nanometers to several microns or less (1 μm) [114]. On the other hand, thin film can also be defined in terms of the production process, i.e. material created initially by the random nucleation and growth processes of individually condensing atomic or molecular species on a substrate [115]. Any thin film deposition technique involves a controlled transfer of atoms and an atomistic growth of the overlay material to the substrate atom-by-atom. Thin films can be realized by various deposition techniques like physical vapor deposition (PVD), chemical vapor deposition (CVD), sol-gel technique, etc. The detail classification of the thin film deposition techniques is given in the Fig. 4.3.

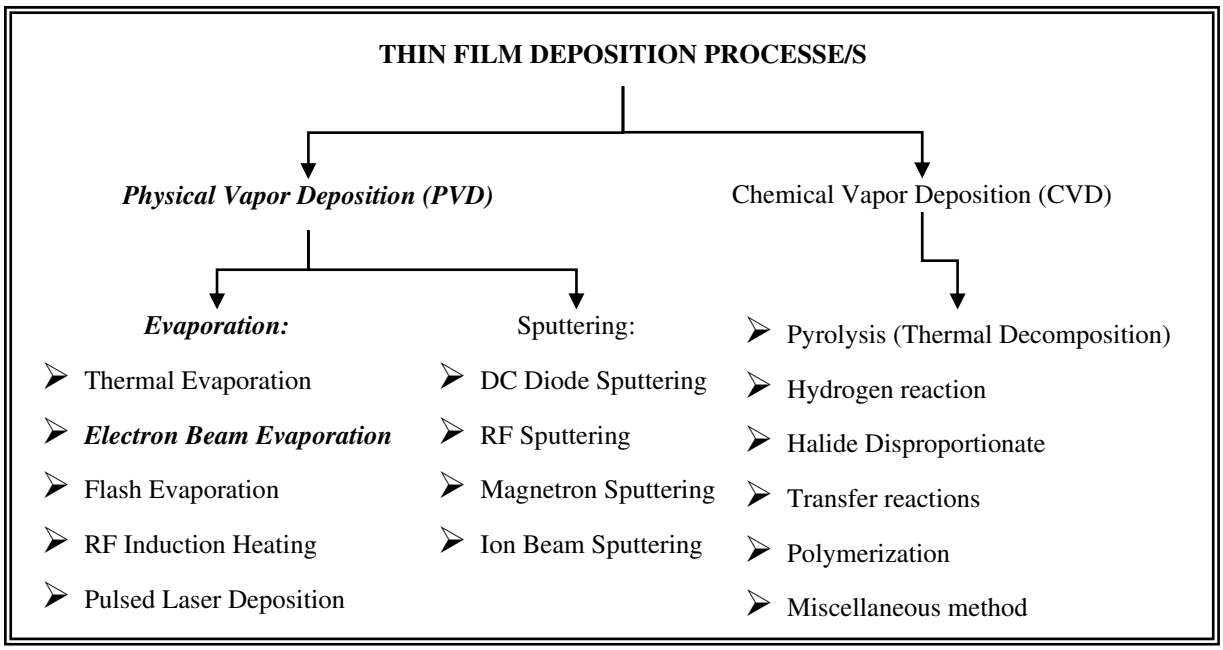

Figure 4.3: Classification of the thin film deposition techniques. Here, a suitable technique for the laser diode facet coating is the electron beam evaporation.

4.3.1 Physical Vapor Deposition

The Physical Vapor Deposition (PVD) involves three fundamental processes: (1) the vaporization from the solid or liquid source materials in form of atoms or molecules, (2) the transfer of vapor through vacuum ambient to the substrate and, finally, (3) the condensation of the vapor on the substrate and create overlay. Typical PVD deposition rates are 10–100 Å per second. The deposition is carried out essentially in a vacuum of the order of 10^{-5} to 10^{-9} mBar for the following reasons. First, it increases the mean free path length of the vaporized source material and thus easily reaches the substrate with little or no collision. Second, it reduces the boiling point of most of the materials. Third, it provides a very low level of gaseous contamination in the deposition system and reduces the probability of the reaction of the source and substrate materials. PVD processes generically involve individual atoms or perhaps small clusters of atoms, which are not normally found in the gas phase [116]. Typically, these atoms are removed from a solid or liquid source, transit an evacuated chamber, and impinge on a solid surface at which point the atoms stick and form a film. The main categories of PVD processing are vacuum evaporation, sputter deposition, and ion plating, classified by the method of removing the atoms from the original source. Depending on the method of applying heat to the source material, the PVD can be further classified in various techniques such as thermal evaporation, electron-beam (e-beam) evaporation, sputtering, pulsed laser deposition, etc.

❖ Electron Beam Evaporation Technique

AR coatings on laser diodes have previously been demonstrated using radio frequency (RF) sputtered Al_2O_3, silicon [97], and lead silicate [117]. RF sputtering is a convenient PVD method since the deposition rate is slow, enabling easy control over the thickness, and the films are uniform and show good adhesion properties. However, the high reflection multilayer coating cannot be carried out easily using RF sputtering, as it requires very complex system. Moreover, it is difficult to incorporate in-situ reflectivity monitoring in the system since the plasma is complex and easily disturbed. In addition, dielectric target for RF sputtering systems tend to be non-uniform, making it difficult to maintain reproducibility in the film refractive index. Deposition by e-beam evaporation

is an alternative method, which can solve some of these problems. A large variety of dielectric materials can be deposited by e-beam evaporation and it allows multilayer deposition. In addition, the incorporation of in-situ monitoring system is easy in e-beam system.

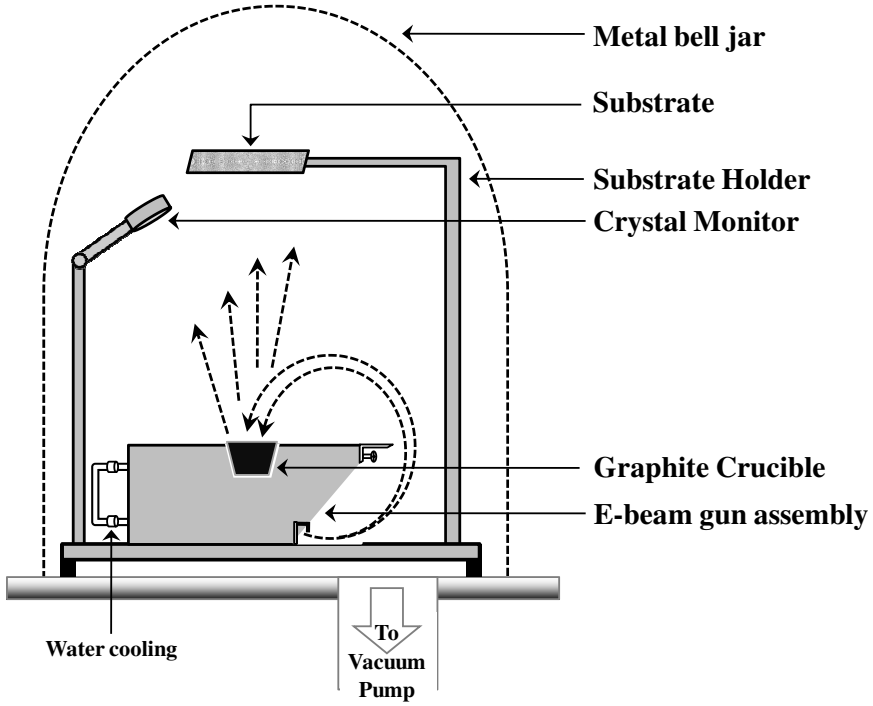

Figure 4.4: The above schematic diagram shows the e-beam evaporation using 270° bent e-beam gun assembly installed in a high vacuum chamber.

In the e-beam evaporation system, the source-material is placed either into a graphite crucible or in water-cooled metal (generally copper) cup, called hearth. Figure 4.4 shows the schematic diagram of the e-beam evaporation of the material, using a 270° bent e-beam gun assembly installed in a high vacuum chamber. The high energetic e-beam is thermionically emitted from a heated tungsten filament, which is shielded from the direct line-of-sight of the source material and the substrate. The emitted e-beam from the e-beam gun assembly is accelerated by means of the bias voltage, ranging 4-20 kV. In addition, a transverse magnetic field is applied to the e-beam, which provides the beam deflection in a 270° arc and is focused onto the source material using a permanent magnet and/or an electromagnet. The energetic e-beam imparts energy to the source material, melts it, and evaporates it. The emitting flux of the evaporant material is having almost a cosine distribution. Generally, there is a modest distance of about 10 to 50 cm between

the source and substrate to cover larger deposition area and limit sample heating by optical radiation from the source. As discussed earlier, most evaporative deposition systems require high vacuum to operate efficiently. Aside from the issue of incorporation of impurity, it is desired that the mean free path of the evaporant-flux exceeds the distance from the source to the sample. This reduces in-flight scattering with the background gas, which can lead to reduced deposition rates. The scattering, which defines the mean free path, is related to the density and pressure of atoms and molecules in the gas phase. From the kinetic theory of gas, the mean free path, mfp, is calculated as [118]:

$$mfp = \frac{k_B T}{\sqrt{2}\,\mathrm{Pr}^2\,\pi} \tag{4.5}$$

where k_B is Boltzmann constant, T is absolute temperature, r is molecular diameter, and P is pressure in Pascal. The scattering probability is given as fraction N/N_0 of molecules that are scattered in distance, d, during their travel through gas.

$$\frac{N}{N0} = 1 - e^{\frac{-d}{mfp}} \tag{4.6}$$

where, N_0 is total number of molecules, N is number of molecules that suffers collisions, d is distance between source and substrate.

- **Advantages of E-beam Evaporation Technique**
  1. In practice, one can evaporate most of the materials viz. metals, oxides, and compounds at almost any rate as the temperature at the focused spot can be raised to as high as 3000 °C.
  2. Since the temperature is high only at a focused spot, rest of the material including the crucible remain cool and thus there is reduced contamination.
  3. Multi-source hearth makes parallel or multi-layer evaporation possible and thus it is very useful in multilayer coatings.
  4. Offers many desirable characteristics such as high evaporation rate, relatively highly dense coating, good composition control, columnar and polycrystalline microstructure, good surface finish and a uniform microstructure.

- **Disadvantages of E-beam Evaporation Technique**
  1. The electron energy is sufficient to ionize residual gas or evaporant molecules encountered along the way. Since ionization causes loss of beam-energy and

beam-focus, the pressure in the vacuum chamber must be below 10^{-4} torr, preferably 10^{-6} torr.

2. Generation of X-rays by the e-beam.

4.3.2 Substrate Preparation

It is essential to clean the substrate thoroughly before the deposition process, as the thin film growth and adhesion is primarily related to the initial substrate surface conditions. In industry, this is often done by using the etching chemicals or plasma etching. We have used GaAs substrate to optimize facet coating reflectivity. Any impurity on the surface may cause poor film quality and lead to the false reflectivity value. The substrate was cleaned by means of organic cleaning process consisting of trichloroethylene (TCE), acetone, and methanol. The substrate was cleaned thoroughly in a hot vapor bath of these chemicals one by one, respectively. The TCE removes most impurities, like grease and oil particles, from the substrate, which comes from the manufacturing process. Later, acetone and methanol were used to remove the preceding chemical effect, respectively, followed by drying the substrate under nitrogen flow.

4.4 Facet Coating Optimization

Optical coating on laser diode facets requires careful designing and a high degree of control over the deposited thin film parameters namely optical quality, film structure, morphology and stoichiometry. Low absorption coating requires compositionally pure starting materials and clean vacuum ambient. The e-beam evaporation offers high purity films and avoids contamination because only a small amount of energy can melt or sublime the source materials. The material exposed to the e-beam spot is only gets melted while the adjacent material remains at relatively low temperature and form an effective crucible of the source material itself. Therefore, the molten material is only in contact with an existing crucible made of the same material, and hence any chemical reactions with contaminants are eliminated.

The thin film structure plays a vital role in determining the optical properties of the films. Normally, thin films produced by the e-beam evaporation have columnar

structure, which causes generation of channels for moisture incorporation cracks. These cracks can influence local electric field distribution surfaces, which are chemically active, and boundaries, which may be mechanically unstable. The substrate is rotated with a constant rpm during evaporation using a dc motor inside the vacuum chamber to attain a uniform film thickness on the substrate and to avoid columnar growth.

Optical coating for laser diode should be morphologically isotropic and compositionally stoichiometric to provide homogeneous material properties. The substrate temperature and the deposition rate affect the morphology and stoichiometry of thin film, respectively. Substrate temperature affects thin film properties viz. composition, nucleation growth, absorption, and diffusion. We have optimized the dielectric thin film for the facet coating at high substrate temperature by means of a radiant heater. The e-beam evaporation is known for causing 'spatter' from the source during deposition. At high e-beam power, the temperature is higher underneath the free surface, generating pressure differentials that are revealed via explosions. Under certain conditions, molten particles can be seen ejected from the source. The spattering is minimized by reducing the e-beam surface intensity and thereby reducing the evaporation rate. Thus, facet coating is carried out at a low evaporation rate. In addition, by controlling the beam intensity by means of either increasing the surface area of beam foot-print or by decreasing the beam energy, we can reduce the film thickness non-uniformities over the substrate and control the coating layer thickness. To improve these conditions, we used a sweeping e-beam at a high frequency on the material surface instead of steady electron beam.

4.4.1 Experiment: Al_2O_3 (AR) and Al_2O_3/TiO_2 (HR) Coating

The facet coatings were optimized in an electron beam evaporation system using 6 KW electron beam evaporator in a high vacuum coating unit (Hind High Vacuum Co. (P) Ltd.). The coating unit is equipped with 270^0 bend e-beam gun facility. As shown in the picture (Fig. 4.5), the e-beam evaporation system is interfaced with SQC-122c SIGMA Thin Film Deposition Controller to precisely monitor and control the thickness and deposition rate of the thin film. The thickness measurement involves piezoelectric quartz crystal placed inside the vacuum chamber. The oscillating frequency of the quartz crystal

declines from its original frequency, i.e. 6 MHz, as coating materials are deposited on the crystal.

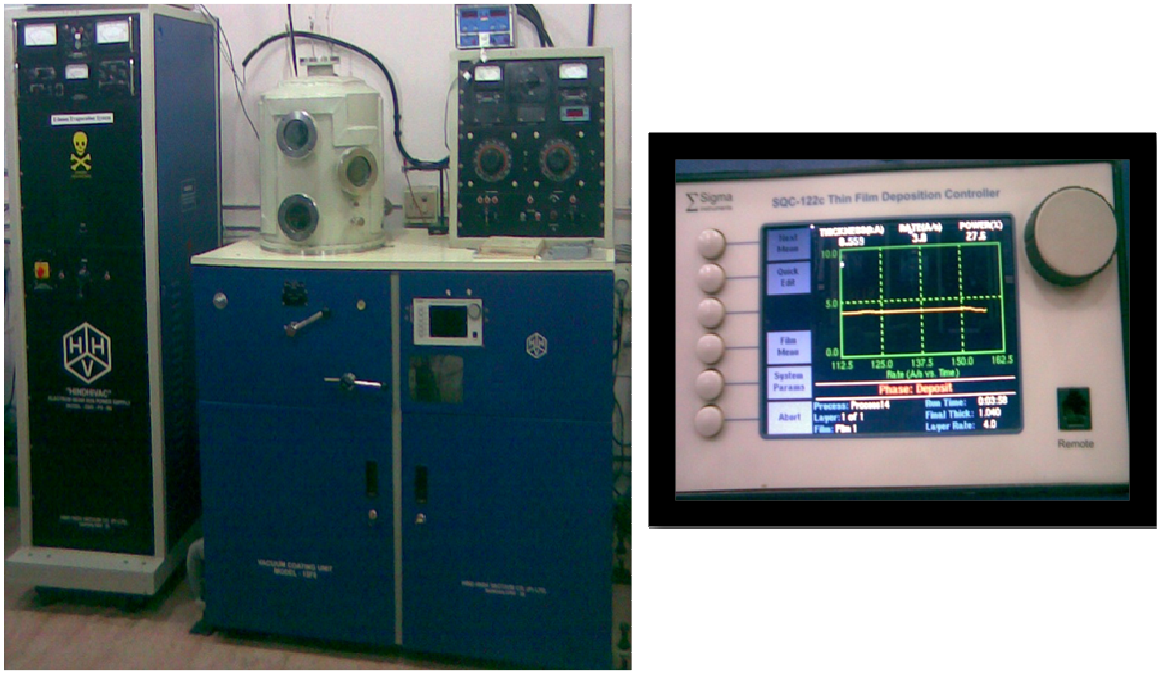

(a) **(b)**

Figure 4.5: (a) High vacuum coating unit assembled with 270° bent e-beam gun, (b) Thin film deposition controller, USA SQC-122c.

The rate of change of the crystal frequency depends on the mass of the deposited material. Consequently, the thickness of the coating on the crystal can be calculated by measuring the fall of the crystal's oscillation frequency, area of the crystal exposed to the film, and the density data of the material. The crystal is positioned at the center of the coating chamber to estimate the coating thickness on the substrate. The vacuum coating chamber is pumped down to achieve a pressure upto $1x10^{-5}$ mbar using an oil diffusion pump backed by a rotary pump. A special jig has been fabricated to coat the end facets of the laser bars. The jig uses two silicon wafers to hold the laser diode bar with a spring action of two springs. Figure 4.6 shows the pictures of jig to hold laser diode bar for facet coating.

The substrates are rotated with 120 rpm inside the vacuum chamber during deposition with the help of a dc motor in order to get uniform coating. The films have been deposited at 100 °C substrate temperature with a constant rate of 4 Å/s for the both Al_2O_3 and TiO_2. The substrate temperature is attained using a radiant heater.

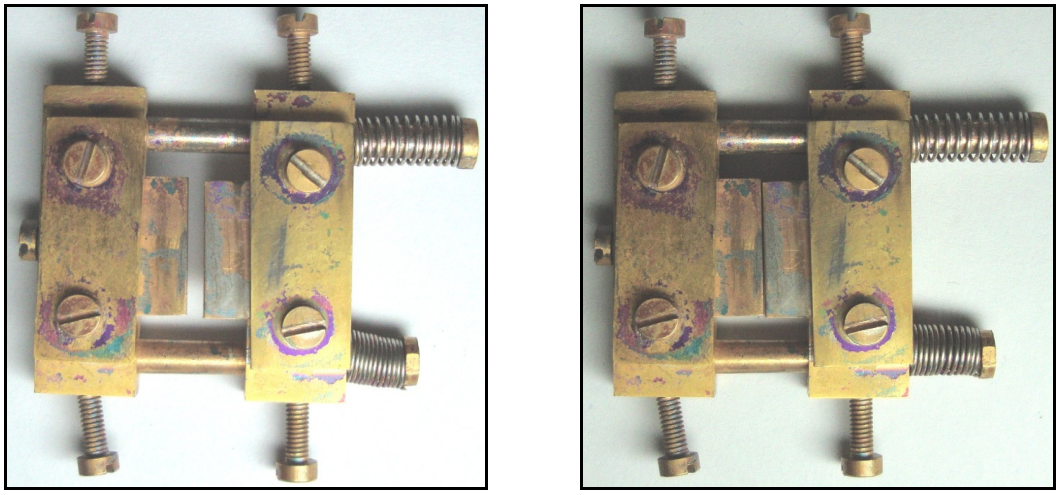

Figure 4.6: Jig to hold laser diode during facet coating.

4.5 Reflectivity Measurement

Since we are applying thin film optical coating for the reflectivity modulation, the main characterization necessary for our films is the reflectivity measurement. The facet coating is to be deposited on the facet of laser diode, which is made up of GaAs based materials. However, it is not convenient to measure directly the reflectivity of the facet. Therefore, we use GaAs substrate for the optimization of reflectivity. We have used the ex-situ reflectivity measurement setup for the optimization of facet coating.

4.5.1 Ex-situ Reflectivity Measurement

In ex-situ reflectivity measurement a tungsten-halogen lamp is used as a polychromatic light source. The light from the lamp is focused on the monochromator input slit using convex lens. We have used 1/8-m monochromater, CVI-CM 110. The output beam from the monochromater is chopped using a mechanical chopper. This chopped beam is then aligned on the sample and/or reference gold coated mirror, through a cube-beam splitter, near-normal geometry and the reflected beam is directed to the photo detector. The detector assembled with lock-in amplifier, SR-530, measures the intensity of the reflected beam. Figure 4.7 shows the schematic of the experimental set up to measure the reflectivity.

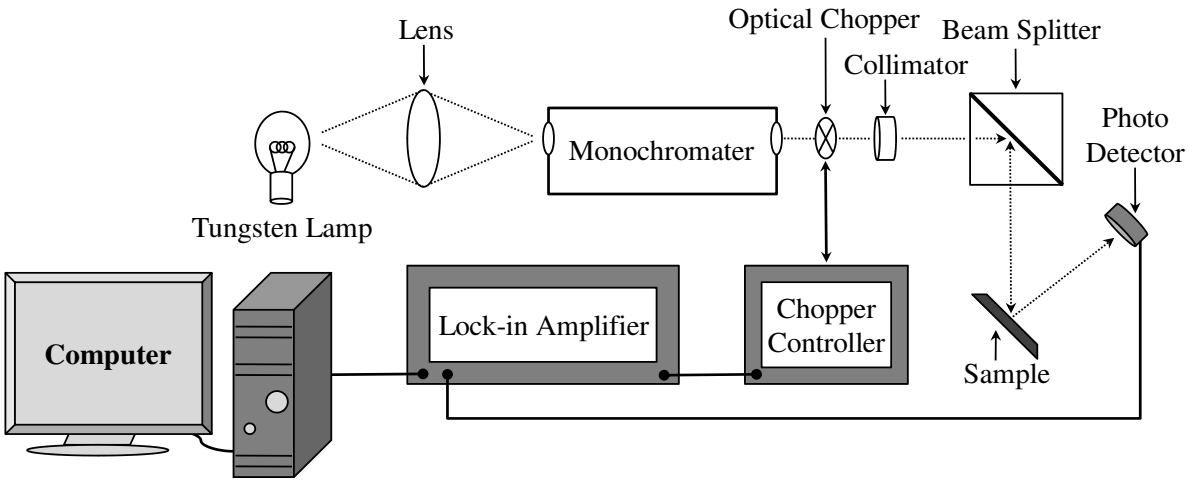

Figure 4.7: The above is a schematic of the ex-situ reflectivity measurement setup. The reference beam from the optical beam chopper, passing through the beam splitter, falls on to the reference Gold mirror and then on the sample, and, finally, on the detector, which gives the reflectivity.

The reflectivity of the sample at particular wavelength is found using the Eq. 4.7:

$$R_S = \frac{S_S}{S_{GM}} \times R_{GM} \ \% \tag{4.7}$$

where, R_S is the percentage reflectivity of the sample, S_S is signal from the sample, S_{GM} is signal from the reference gold mirror, and R_{GM} is the known reflectivity of the gold-mirror. The monochromator and the lock-in amplifier have been interfaced with the computer via communication (COM) port (RS-232) and general purpose interface bus (GPIB), respectively. The experiment is automated using LabVIEW-8.2 (laboratory virtual instrument engineering workbench–version 8.2). However, in this setup, since the reflectivity of the sample is measured with reference to the standard reflectivity gold mirror, we need to take two scans for complete spectral range of interest viz. one with slandered gold mirror and the other with the unknown sample.

The dedicated virtual instrument, made in LabVIEW-8.2, computes and displays the reflectivity spectrum simultaneously with data acquisition and storage. Figure 4.8 (a) and (b) show the front panel (control and displays) of the virtual instrument (VI) for reflectivity measurement displaying reflectivity spectrum of reference gold mirror and HR coated test substrates.

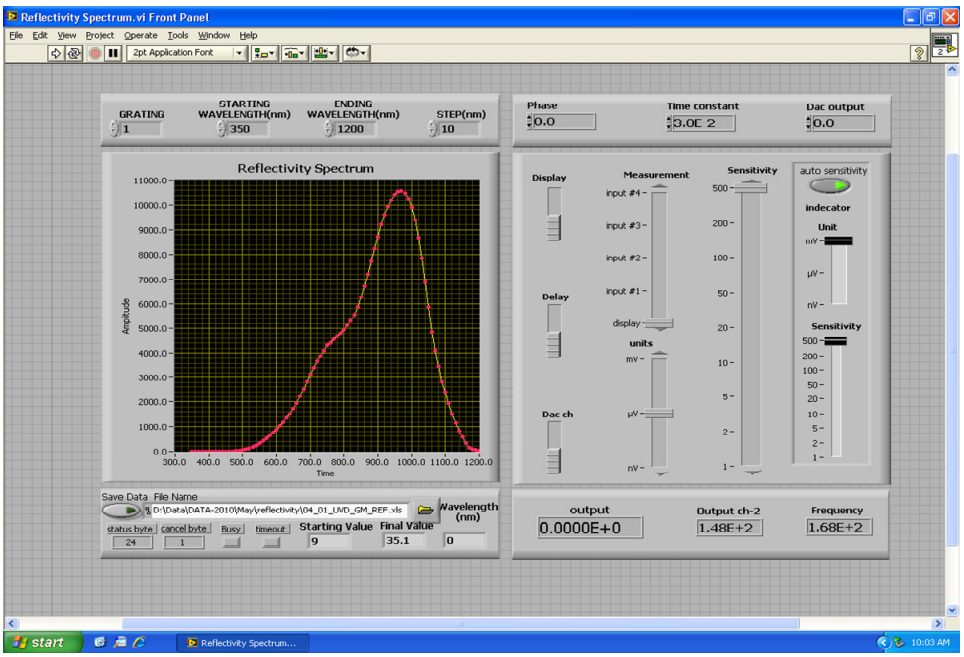

(a)

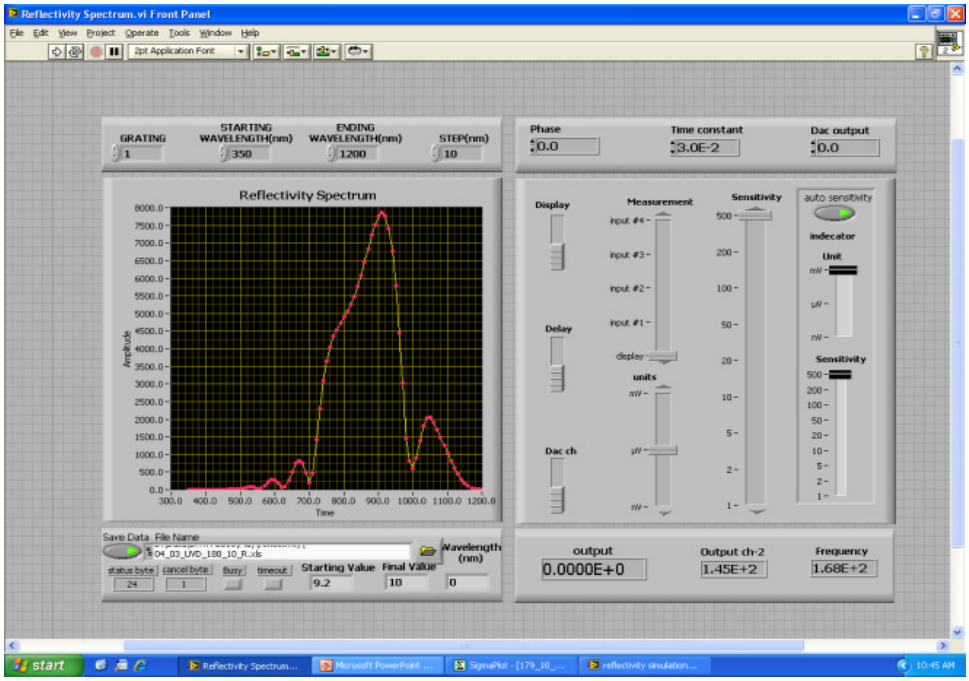

(b)

Figure 4.8: Graphical user interface for reflectivity measurement. (a) Reference signal from the standard gold mirror and (b) signal from HR coated GaAs test substrates with 5 bi-layer pair of Al_2O_3 – TiO_2.

As mentioned earlier, the reflectance of the multilayer non-absorbing dielectric films depends on constructive and/or destructive interference of the light from each consecutive boundary of the film interface. Therefore, the choice of an appropriate

sequence of these layers with suitable dielectric materials and their thickness that best satisfy the desired spectral response for the application is a crucial issue. Thus, to design the multilayer dielectric thin films and to optimize their coating conditions, a reflectivity spectrum simulation of these optical thin films is an essential tool. We have used a LabVIEW-8.2 based simulator, that determines the 2 x2 '*characteristic matrix*' elements for each layer of the stack at particular wavelength and angle of incidence [119].

In addition, the refractive index and the physical thickness of the film are most important parameters for facet coating optimization. We have matched experimental data with simulation to optimize the process. Moreover, the thickness of the film was also optimized using simulation [119].

4.5.2 In-situ Reflectivity Measurement

We have optimized and automated the experimental in-situ reflectivity measurement system for the laser diode (LD) facet coating. The deposition of single layer MgF_2 and a QWOT three bi-layer pairs of MgF_2 - Si on GaAs test substrate were carried out under the high vacuum (10^{-5} mbar) using e-beam evaporation system (EBG-6K, HINDHIVAC). The quartz crystal monitor was used for measuring the thickness of the sample. The e-beam evaporation system is interfaced with the thin film deposition controller (SQC-112C, Sigma Instruments) for the better control of the deposition parameters viz. thickness and deposition rate. The substrate was rotated with 120 rpm inside the vacuum chamber during the deposition with the help of a dc motor in order to get uniform coating. The substrate was maintained at 100°C using a radiant heater during the deposition. The deposition rate was 4 Å/s.

Figure 4.9 shows a schematic diagram of the experimental setup for in-situ measurement of reflectivity. The laser beam enters into the vacuum chamber through a glass-view-port of the chamber and reflects back on the photo-detector (BPW-34) from the sample at normal incident angle. We have used a commercially purchased red laser diode (λ=650 nm) as a probe light source for the experiment. To check the stability of the optical power of the laser diode, we operated the laser diode in CW mode continuously for a few minutes before starting the deposition and monitored its optical power as a

function of time. The signal from the photo-detector is fed to a computer through data acquisition card (NI-USB-6251). Figure 4.10 shows the acquired data in the front panel of the program built-in LabVIEW-8.2.

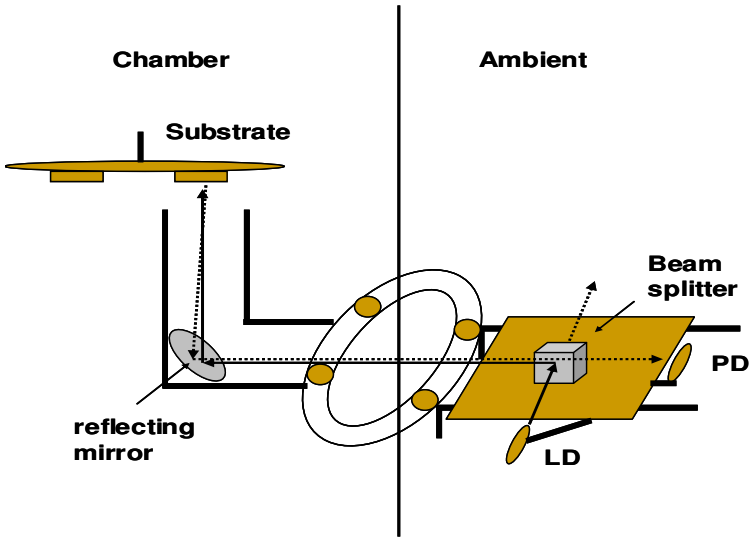

Figure 4.9: The above schematic shows the experimental setup for in-situ measurement of reflectivity.

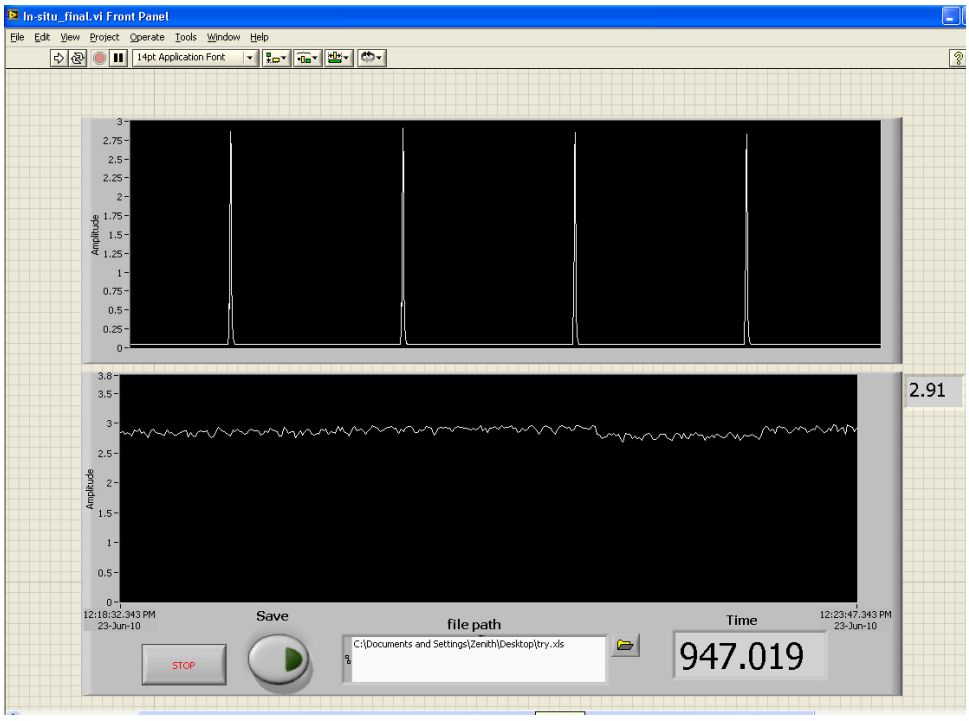

Figure 4.10: The LabVIEW-8.2 front panel showing real time data acquisition as the light reflects from the sample and is detected by the photodetector.

We have also developed a reflectivity-simulator program, based on LabVIEW-8.2, which gives the reflectivity data as a function of the thickness of the film (single or multi-layer) for a given wavelength. It aids in optimizing the deposition parameters while monitoring the coating of the films in-situ. The light reflected from the air-film and the film-substrate interface give rise to the interference phenomenon, which results in the change in the reflected beam intensity as the film grows on to the substrate.

Figure 4.2 shows light incident on an air-film interface. The light reflected from the air-film and the film-substrate interface give rise to the interference phenomenon, which results in the change in the reflected beam intensity as the film grows on to the substrate. The reflectance co-efficient, *r*, of a non-absorbing multilayer dielectric thin-film is given as [5, 119]:

$$r = \frac{Y_0 m_{11} + Y_0 Y_S m_{12} - m_{21} - Y_S m_{22}}{Y_0 m_{11} + Y_0 Y_S m_{12} + m_{21} + Y_S m_{22}} \tag{4.8}$$

where, $Y_0 = \sqrt{\varepsilon_0/\mu_0 n_0'}$ and $Y_S = \sqrt{\varepsilon_0/\mu_0 n_S'}$ with n_0' and n_s' being the effective refractive indices of the incident medium and the substrate, respectively, and are given as $n_0' = n_0 \cos\theta_0$ and $n_S' = n_S \cos\theta_S$ for *s* or perpendicular polarization. In case of *p* or parallel polarized light, n_0' and n_s' are given as $n_0' = n_0/\cos\theta_0$ and $n_S' = n_S/\cos\theta_S$. Here, n_0 and n_s are the refractive indices of the incident medium and the substrate whereas θ_0 and θ_s are the angles of incidence in the incident medium and the substrate, respectively. In Eq. 4.8, m_{11}, m_{12}, m_{21}, and m_{22} are the elements of characteristic matrix, *M*, of the entire system with *p* layers in a multilayer stack, which is the resultant of the product (in proper sequence) of the individual *2x2* matrices for each layer in the multilayer stack, that is:

$$M = M_1 M_2 M_3 \ldots\ldots M_P = \begin{bmatrix} m_{11} & m_{12} \\ m_{21} & m_{22} \end{bmatrix} \tag{4.9}$$

However, the layer matrix is a complex matrix [119]. Hence, elements m_{12} and m_{21} in above equations are purely complex whereas the other two elements, i.e. m_{11} and m_{22}, are real. Thus, the reflectance coefficient *r* is an imaginary quantity. So, the reflectance, $R = r \cdot r^*$ gives,

$$R = \frac{(n_0' m_{11} - n_S' m_{22})^2 + (n_0' n_S' m_{12} - m_{21})^2}{(n_0' m_{11} + n_S' m_{22})^2 + (n_0' n_S' m_{12} + m_{21})^2} \tag{4.10}$$

Equation 4.10 determines the reflectance of the non-absorbing multilayer dielectric thin-film. This equation is used in the computer simulation program. Figure 4.11 shows the front-panel of the LabVIEW program for reflectivity simulation of the optical thin film.

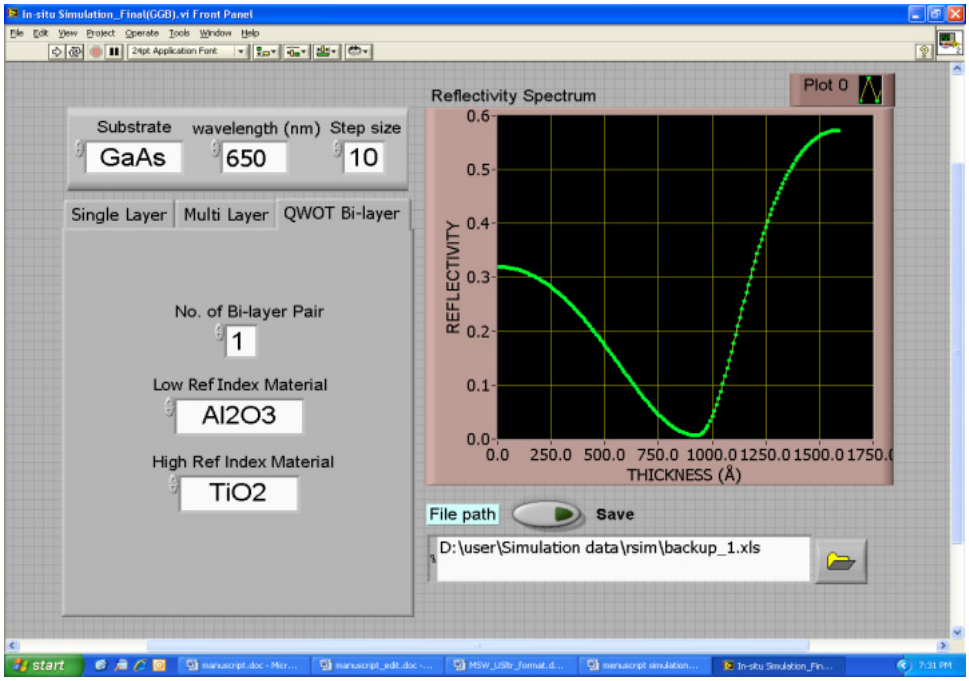

Figure 4.11: The front-panel of the LabVIEW program for reflectivity simulation of the optical thin film.

❖ Program execution

In the case of optical films, two parameters are necessary to determine the reflectivity of the thin film viz. the physical thickness and the refractive index of the material [120]. The other input parameters are the refractive index of the substrate material, wavelength of interest, and thickness (step size). All these parameters are provided on the front panel of the program, shown in Fig. 4.11. Figure 4.12 shows the other control parameters to be fed as the input. The program executes as per the data flow arranged using the graphical programming code in the back panel of the program viz. block diagram.

4.6 Facet Coating Optimization for 808 nm Laser Diode

The design of multilayer high-reflection (HR) coating and simulation of corresponding reflectivity spectra are carried out for 808 nm laser diode. The high reflection at the back

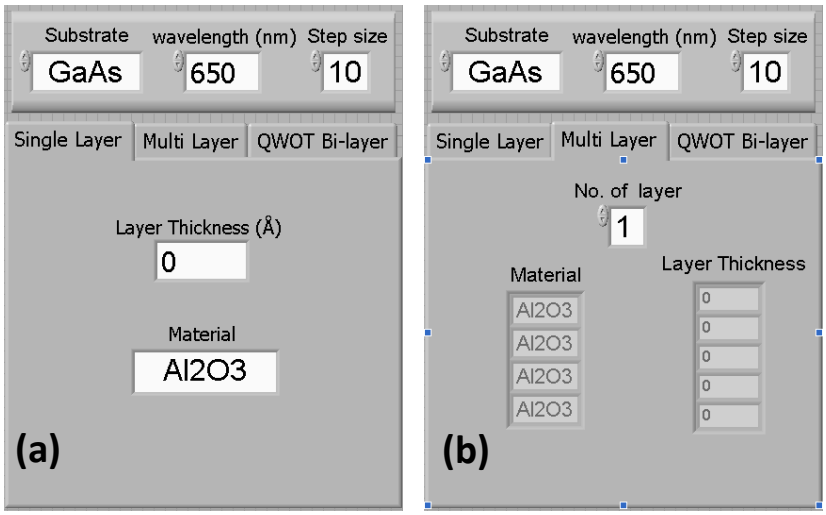

Figure 4.12: The input parameters for single layer (a) and multi layer (b) in-situ reflectivity simulation.

-facet of the diode laser is achieved by multilayer stack of alternating films. The structure of multilayer stack consists of alternating films of Low (L) and High (H) refractive index layers of quarter wave optical thickness (λ/4) at lasing wavelength. In our previous work, we used silicon (Si) as high refractive index material for HR coating [121]. However, Si has some limitation such as poor resistivity and finite absorption coefficient in visible and near IR. To overcome these limitations we replace Si with TiO_2 as high refractive index material in design of HR coating.

TiO_2 has been optimized as a high refractive index (H) material in combination with Al_2O_3 as a low refractive index (L) material for HR coating. The GaAs test substrate was used for the film deposition. The films were deposited at room temperature on the test substrates under high vacuum during optimization. The substrates were rotated with ~120 rpm during the deposition. In order to monitor and control the deposition rate and thickness of the film the vacuum coating unit had been facilitated with a thin film deposition controller. Also for the better adhesion, substrate temperature about 100 °C was attain by means of a radiant heater. The results of reflectivity measurement were compared with the simulated results.

4.6.1 Results and Discussion

The laser facet coating structure is substrate – n (L H) – Air (here, integer *n* shows the no. of bi-layer pair of low and high refractive index material). As mentioned, Al_2O_3 was used as a low refractive index layer and TiO_2 as a high refractive index layer for HR coating. For the 808 nm, the quarter wave optical thickness was 202 nm for each layer. Hence, the physical thickness for Al_2O_3 layer (L) was 126.25 nm and that for TiO_2 layer (H) was 84.16 nm.

Figures 4.13 (a) and (b) show the reflectivity spectra for the optimized single layer TiO_2 and Al_2O_3 quarter wave optical thickness and deposition parameter, respectively. The reflectivity achieved so far for the five bi-layer pairs of Al_2O_3 – TiO_2 is about 94 %, as shown in Fig. 4.14. The difference between the simulated and experimental reflectivity is because of dispersion in refractive index value of the material. Furthermore, the refractive index value of the e-beam evaporated film changes with deposition conditions, which leads to the difference in simulated and obtained reflectivity.

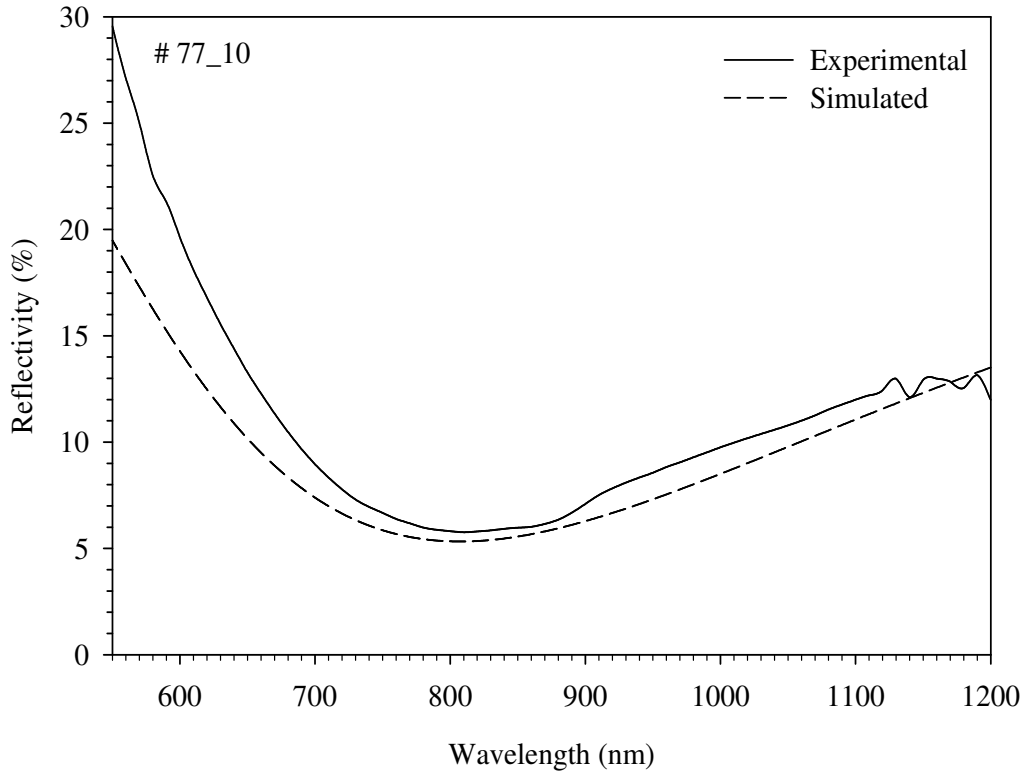

(a)

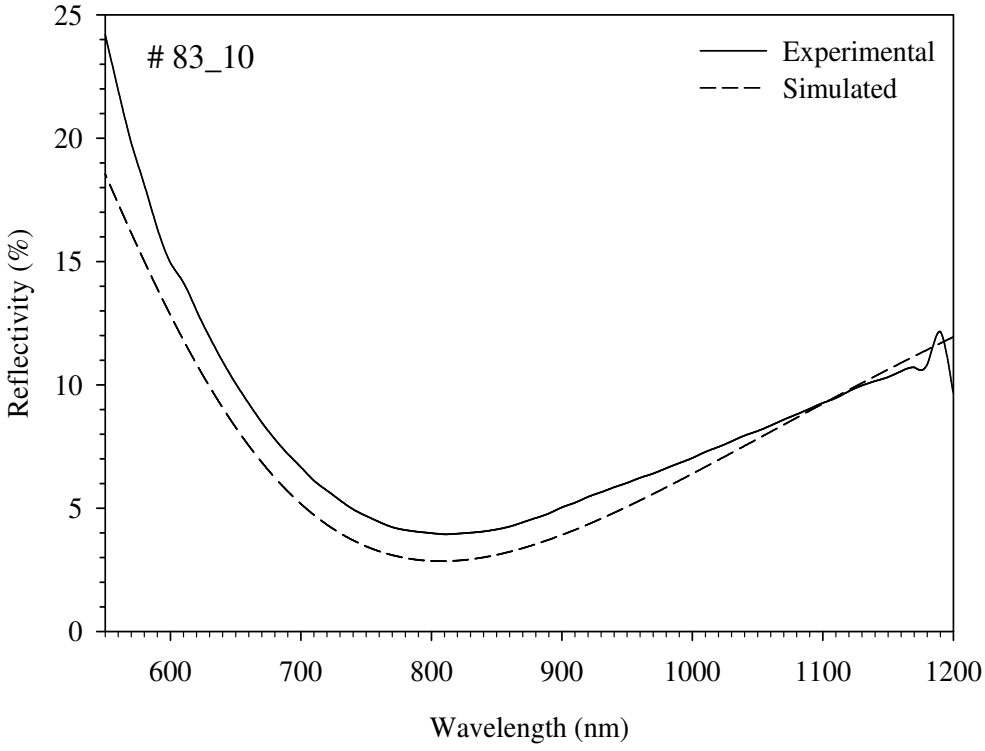

(b)

Figure 4.13: Reflectivity spectra of optimized single QWOT layer (a) TiO_2 and (b) Al_2O_3 for 808 nm.

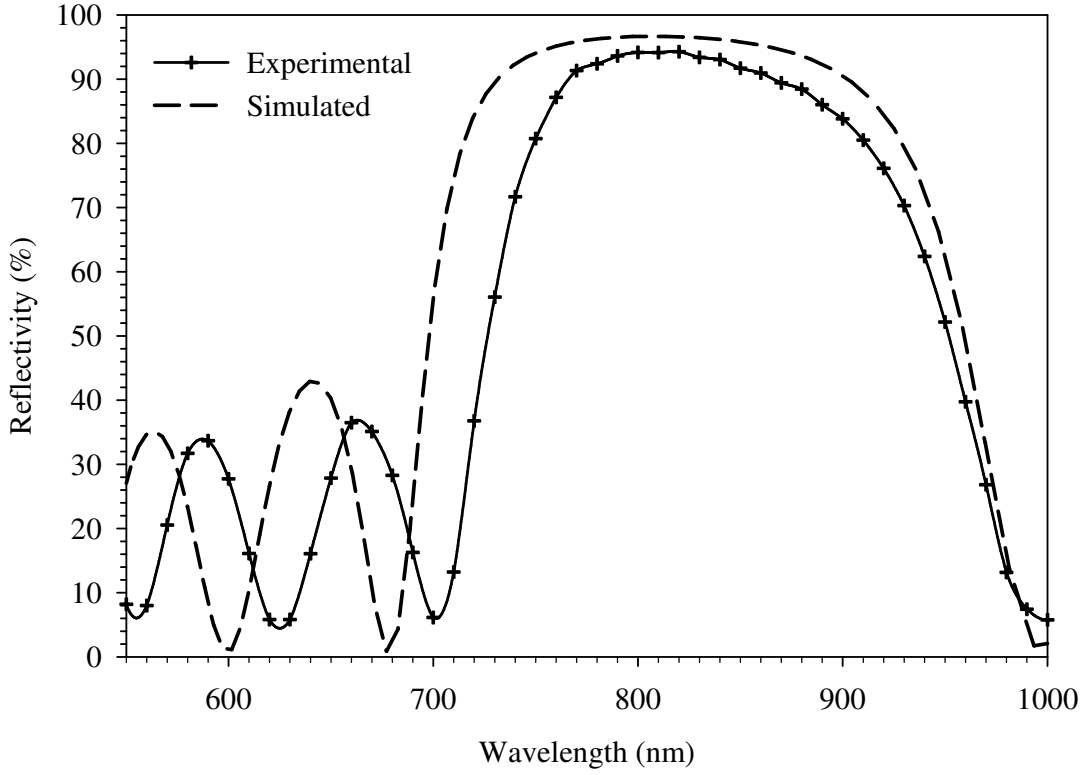

Figure 4.14: Experimental and simulated reflectivity spectra of HR coated GaAs test substrates optimized for 808 nm laser diode.

❖ In-situ Facet Reflectivity Measurement

Thin film optical coating is used for modulating the reflectivity in different kinds of optical components viz. beam splitters, optical filters, polarizers, lenses of cameras and telescopes, including anti-reflection (AR) and high-reflection (HR) coating on the laser diode facets [122]. Owing to its importance, it is essential to monitor the thin film deposition parameters like the deposition rate, substrate temperature, and thickness of the thin film during the deposition.

We have developed an in-situ reflectivity measurement system for optimization of facets-coating process for laser diodes. We have performed in-situ reflectivity measurements on single layer MgF_2 and a quarter-wave optical thick (QWOT) three bi-layer pairs of MgF_2 and silicon on GaAs as a substrate for both the cases. The measurements were optimized using a simulation program that gives the reflectance of non-absorbing dielectric single or multi layer, or QWOT bi-layer optical facet coatings for the Laser Diode (LD) using LabVIEW-8.2 Since the set-up is custom-built for our specific application, it is quite simple, cost-effective, and an efficient tool for quick optimization and automation of the process.

The single layer MgF_2 film was deposited at room temperature on the GaAs substrate at the deposition rate of 4 Å/s. Figure 4.15 shows the acquired data of the reflected laser light intensity versus time.

It is known that there is a direct relation between the film's thickness and the film's deposition rate. So, one can easily estimate the thickness of the deposited film. Moreover, the natural reflectivity of the substrate GaAs is ~32 % and which modifies as the film grows on it. Hence, we can directly get the film reflectivity from the reflected intensity. Figure 4.16 (a) and (b) shows the experimental as well as the simulated data of the reflectivity of single layer MgF_2 and multilayer stack of three QWOT bi-layer pair of MgF_2 and Si where the former has a low refractive index and the latter has a high refractive index.

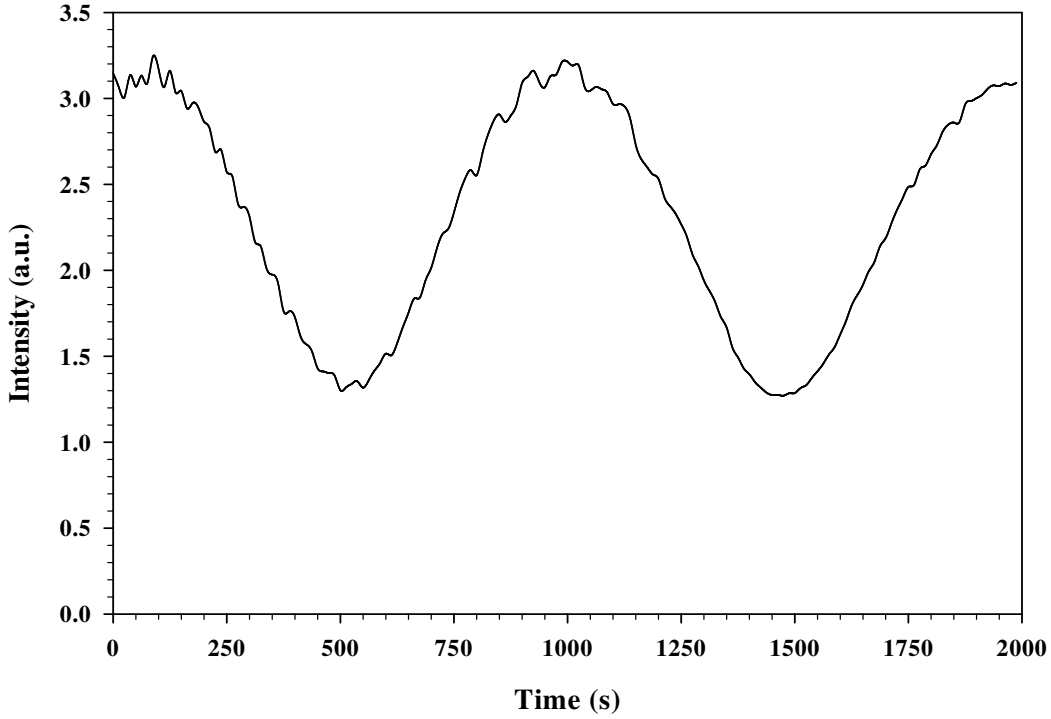

Figure 4.15: Intensity measurement curve as a function of time for the MgF_2 thin film deposited on GaAs substrate.

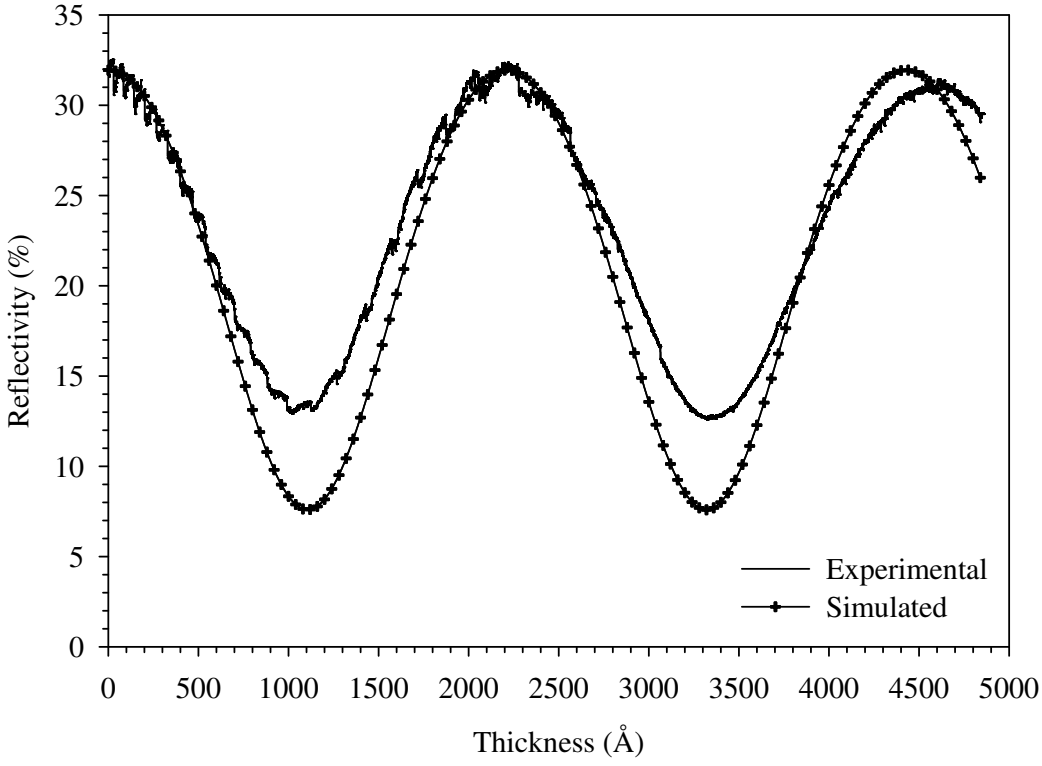

(a)

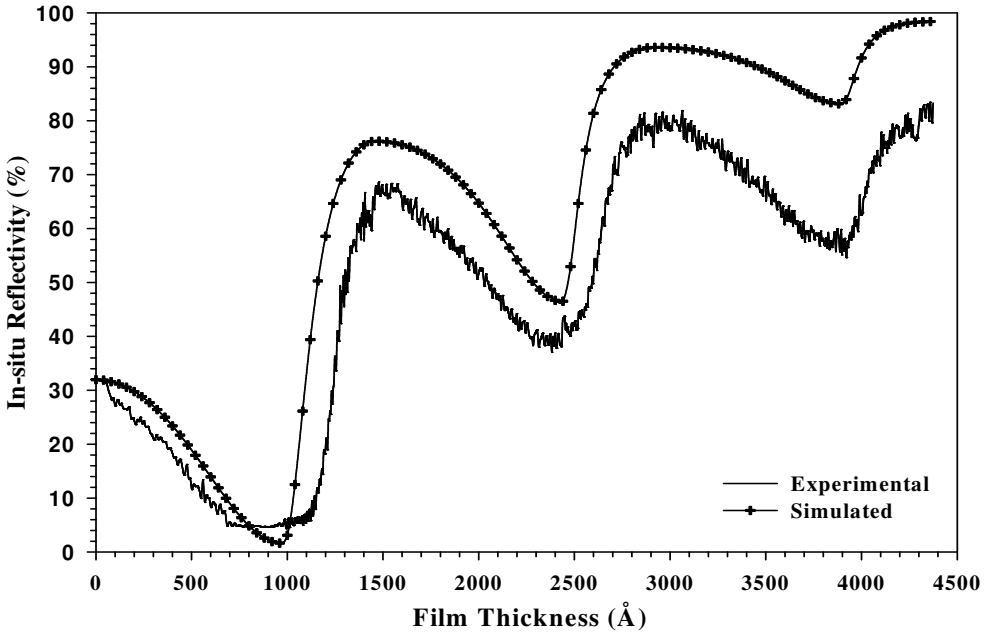

(b)

Figure 4.16: In-situ reflectivity and simulated reflectivity plots, (a) for a single layer MgF_2 and (b) for three QWOT bi-layer pairs of MgF_2-Si, deposited on GaAs substrate.

In order to confirm the obtained results, we measured the reflectivity spectrum of the coated samples ex-situ with the standard setup using a broad-band light source, a monochromator, photo-detectors and a lock-in amplifier. Figure 4.17 shows the reflectivity spectrum for a three QWOT bi-layer pairs of MgF_2-Si measured ex-situ.

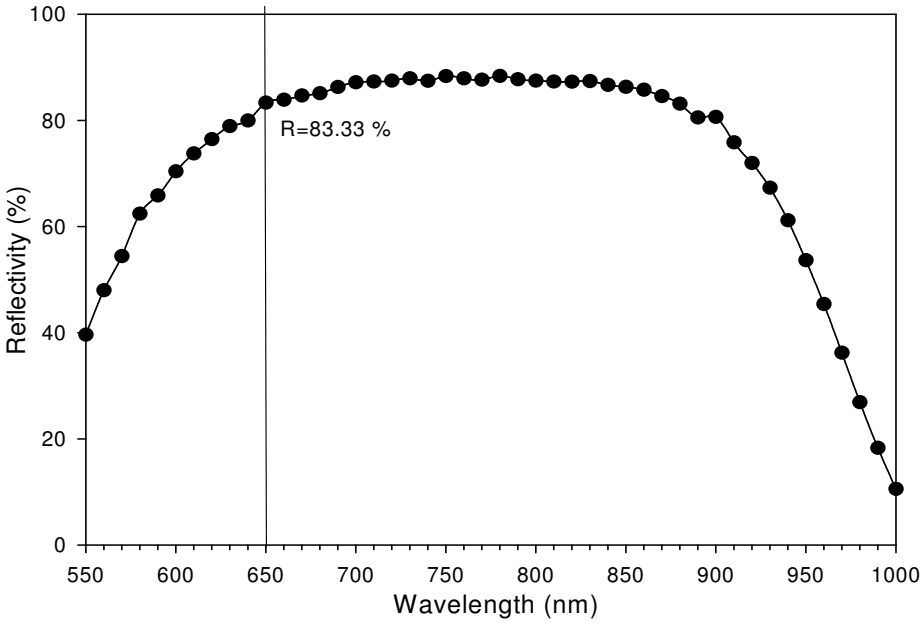

Figure 4.17: Reflectivity spectrum for three QWOT bi-layer pairs of MgF_2-Si measured ex-situ.

We have optimized and automated the experimental in-situ reflectivity measurement system for the laser diodes facet coating [39]. We have also developed a reflectivity-simulator program that gives the reflectivity data as a function of the thickness of the film (single or multi-layer) for a given wavelength, which aids in optimizing the above parameters while monitoring the coating of the films in-situ. We report the results for the in-situ reflectivity of a single layer MgF_2, and a quarter-wave optical thick three bi-layer pairs of MgF_2 and silicon, on GaAs as a substrate for both the cases. We have achieved up to 83 % experimental reflectivity for the latter case.

❖ Laser Diode Facet Coating

In order to study the effects of facets coating on optical power output, we deposited AR and HR films on, respectively, front and back facet of laser diodes with 808 nm lasing wavelength. Figure 4.18 shows the L-I characteristic of laser diodes before and after the facets coating. The L-I measurements were carried out in pulse-mode with 400 ns pulse-width and 0.25 % duty-cycle. The collective effect of AR and HR coating leads to boost the optical power output from front facet by almost 40 % at 850 mA input current [36].

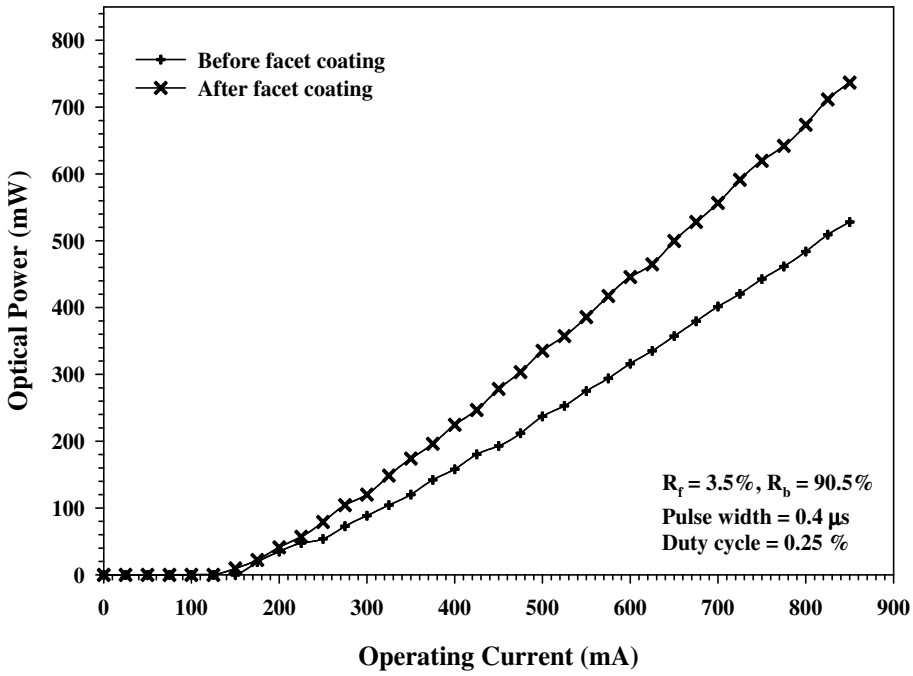

Figure 4.18: L-I characteristics of 808 nm laser diode before and after facets-coating.

❖ Conclusion

The in-situ reflectivity measurement of the single and multilayer optical thin films has been demonstrated. The change in intensity of the laser light after reflection has been measured to obtain the reflectivity as a function of thickness. In addition, we have developed an in-situ reflectivity simulation for the optimization of the in-situ film deposition. The reflectivity simulator provides a very good tool for designing the optical thin films with desired reflectivity response. Moreover, one can use the simulator for determining the material and the deposition conditions viz., film thickness, and deposition rate for single or multi layer films.

4.7 Facet Coating Optimization for 980 nm Laser Diode

The high power laser diodes (HPLDs) emitting at 980 nm are the key components for applications such as pump source for erbium-doped fiber amplifiers (EDFAs) or solid state lasers because of their low noise characteristic and high efficiency [123,124,125]. It is also utilized in medical therapy viz. dentinal surgery, due to handling flexibility and ease of operation [126]. An another advantage of the 980 nm laser diode is that there is no excited state absorption exists for this wavelength and hence high pumping efficiency is achieved [127]. The simplest way to achieve high power operation is to fabricate a simple ridge waveguide structure and dielectric facet coating.

4.7.1 Experiment: ZrO_2 (AR) and SiO_2/ZrO_2 (HR) Coating

Recently we have developed InGaAs/GaAs/AlGaAs based laser diode for 980 nm with output power of 670 mW/facet at the injection current of 2 A. These results are from the bare surface of cleaved facet of laser diode. To increase the output power and the stability of the spectrum, suitable dielectric materials single and multilayer coatings are desired. In view of this single layer of ZrO_2 and five pairs of SiO_2/ZrO_2 (L/H) multilayer are coated on the front and rear facet of laser diode for AR and HR respectively. The e-beam evaporation method is used for deposition of these thin films to minimize damage to the semiconductor surface. The properties of facet coated laser diode were compared with that of the bare devices.

Metalorganic Vapor Phase Epitaxy grown laser diode structures based on InGaAs/GaAs double quantum well were processed through conventional optical lithography, n- and p-type metal contact by e-beam/thermal evaporation, lift-off process and rapid thermal annealing of metal contacts. After making a smooth walled mesa-structure using H_3PO_4:CH_3OH:H_2O_2 etchant solution, electrical isolation and side-wall passivation was realized by SiO_2 layer deposition between the metal stripes. Details of growth and processing parameters of the device structures were presented elsewhere [25,37,128]. Finally, the structure was thinned down to ~150 μm and several laser stripes of different dimensions were cleaved.

The AR and HR coatings were carried out using e-beam evaporation method. The e-beam evaporation system is interfaced with a thin film deposition controller (SQC-310C, Inficon) to precisely monitor and control the thickness and deposition rate of individual dielectric layers. Initially the thin films of ZrO_2, SiO_2 and multilayer's of SiO_2/-ZrO_2 were deposited on chemically cleaned GaAs substrates with a typical deposition rate of ~3-4 Å/s at 80 °C using e-beam source (EBG-PS-3K, Hind HIVAC) in a vacuum coating unit (12A4T, Hind HIVAC) at a pressure of ~6 X 10^{-6} mbar. The thickness of individual layer is monitored in-situ using quartz crystal. Subsequently, thickness of the films is measured from stylus (Dektak 150, Veeco) and also estimated from the theoretical fitting (FILMETRICS) [19] of the measured reflectivity data that is recorded using UV-VIS-NIR spectrophotometer (Cary 5000, Varian). After achieving the desired results of reflectivity on the GaAs substrates, the cleaved laser diode bar is clamped in the appropriate mounting jig that is placed in the vacuum chamber for antireflection and high reflection coatings in sequence. The laser diode characteristics are evaluated in the home made testing setup that is equipped with precision pulse laser diode driver (LDP-3840-3B, ILX Lightwave), power meter (OPHIR), spectrometer (HR 4000 CG, Ocean Optics), mounting stage, microscope etc [70].

4.7.2 Results and Discussion

❖ Anti-Reflection and High-Reflection Coatings

➢ ***AR Coating***

The AR coating is typically a single layer coating. The laser diode in the present studies is mainly grown on GaAs substrate that has a fairly high refractive index. This substrate can be perfectly antireflection coated with a low refractive index material equal to the square root of the refractive index of substrate at the particular wavelength. Thus single layer of QWOT ZrO_2 (≈117 nm) is deposited on the GaAs substrates. Subsequently, reflectivity of deposited ZrO_2/GaAs heterostructure is measured from 200 to 1000 nm. Figure 4.19 (a) shows the measured and simulated curves of reflectivity of ZrO_2/GaAs heterostructure. The measured value of reflectivity is about 2 % at 980 nm and good enough to be used as AR coating material on the facet of laser diode with lasing wavelength of 980 nm. Reflectivity of single layer of SiO_2 (≈170 nm) deposited on GaAs is shown in Fig. 4.19 (b). The combination of these single layers of SiO_2 and ZrO_2 are used for HR coatings.

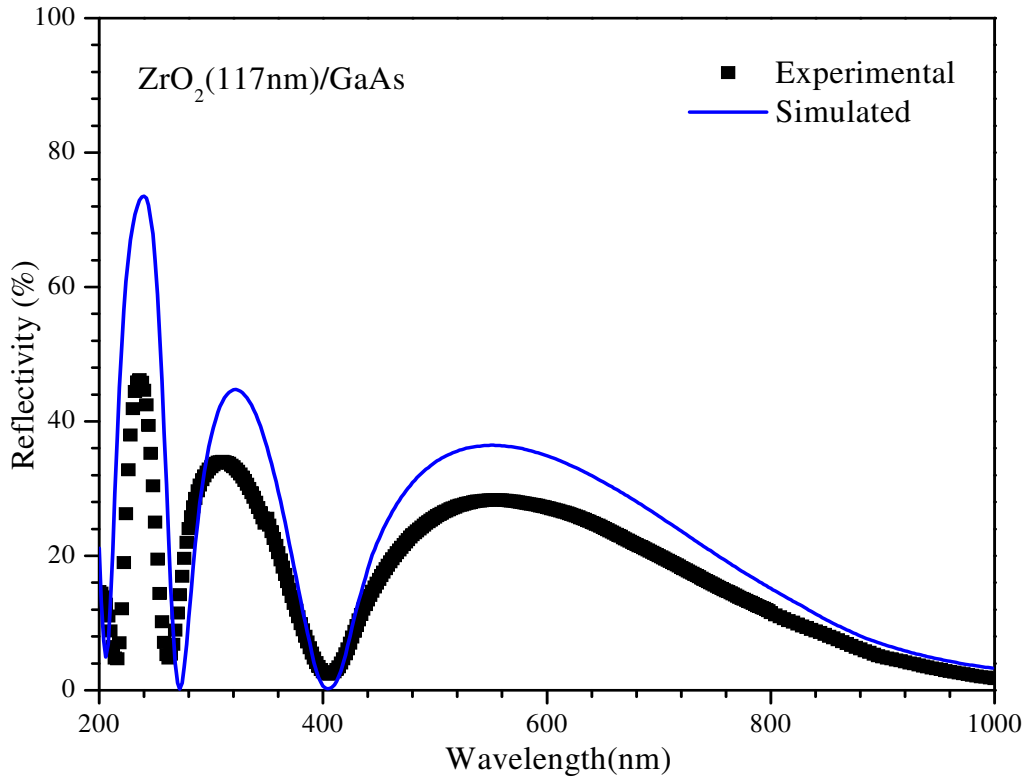

(a)

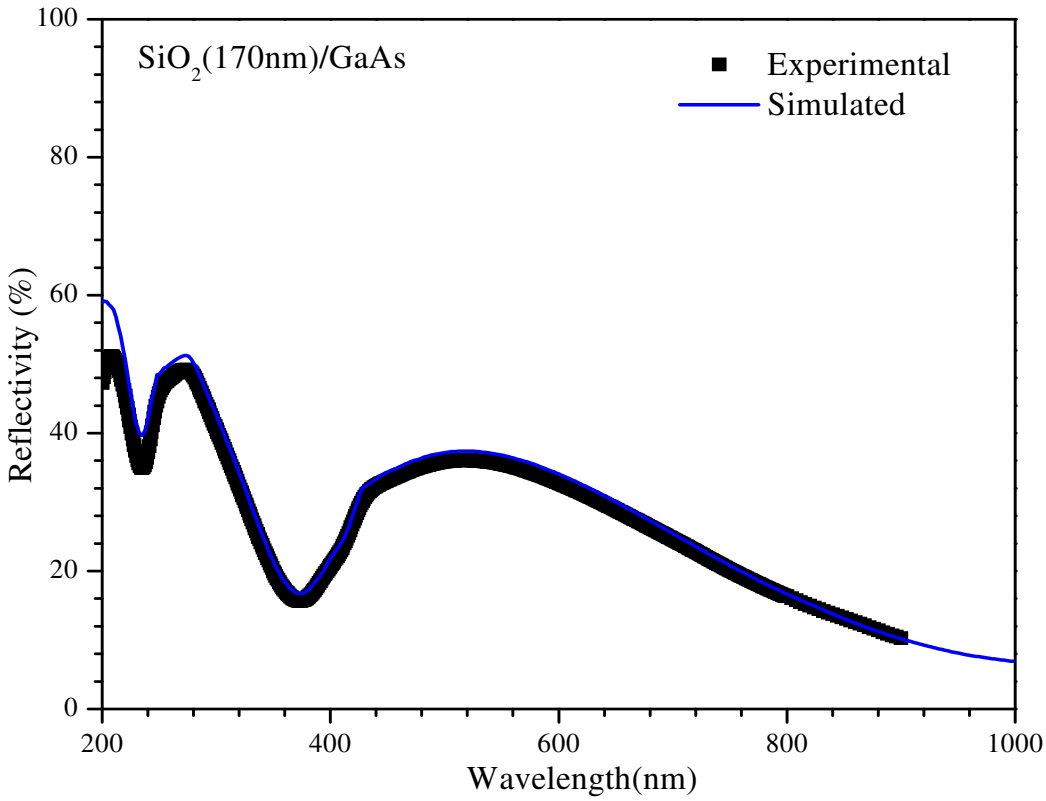

(b)

Figure 4.19: Reflectivity as a function of wavelength for (a) ZrO_2/GaAs (b) SiO_2/GaAs.

➢ ***HR Coating***

HR coating is based on the constructive interference of light reflected from successive boundaries of multilayer dielectric thin films and gathers in phase at the emergence of one surface to provide the maximum reflectance. The designed HR coating consists of multi-layer stack of alternating films of 170 nm thick low SiO_2 (L) and 117 nm thick high ZrO_2 (H) refractive index layers. The thicknesses of the layers were estimated from the optical thicknesses ($\lambda/4$) at the lasing wavelengths. The complete optimized structure consists of five pairs of LH layers. Figure 4.20 shows the relative increase of reflectivity from single to five pairs of LH layers.

As can be seen from Fig. 4.20 the reflectivity value is ~ 90 % for five pairs of LH layers. It is also noted that the values of measured reflectivity for AR and HR coated substrates are lower by around 5 to 10 % as compared to the simulated value of the reflectivity. This is predominantly due to the usage of bulk values of the material parameters during reflectivity simulations. Also, oxides film grown using e-beam evaporation exhibit a variation in refractive index with film thickness. Thus single layer

with optimum thickness 117 nm of ZrO_2 is used on the laser diode facet coating. Similarly five pairs of SiO_2 (L)/ZrO_2 (H) layers are used for HR coatings. The complete structure on laser diode with partial reflectivity of 2/90 is "Air-AR-front facet-rare facet-$(LH)^5$-Air".

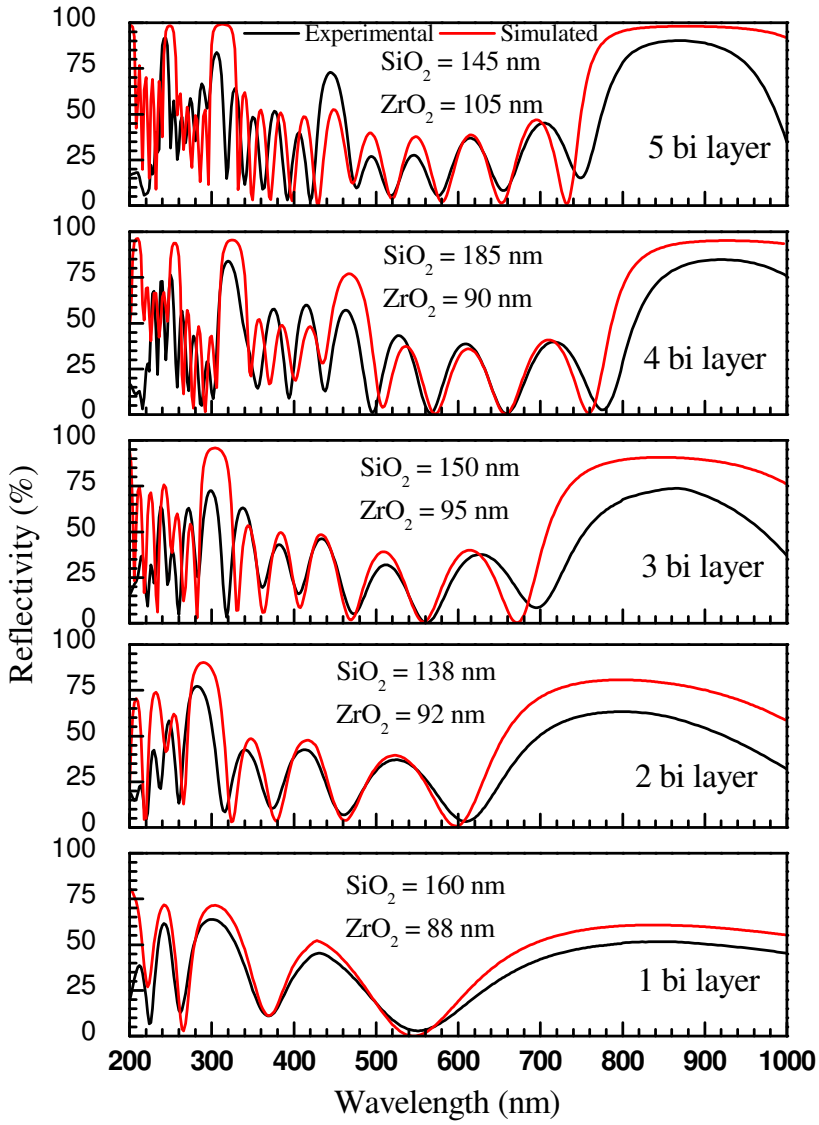

Figure 4.20: Reflectivity as a function of wavelength for ZrO_2/SiO_2/GaAs multilayer.

❖ Optical Light Output Power vs. Current Characteristics of AR/HR Coated Laser Diode

The optical light output power-injection current (L-I) characteristics and spectral response of the lasers without AR/HR coatings and with AR/HR coatings are shown in the Fig. 4.21 (a) and (b), respectively.

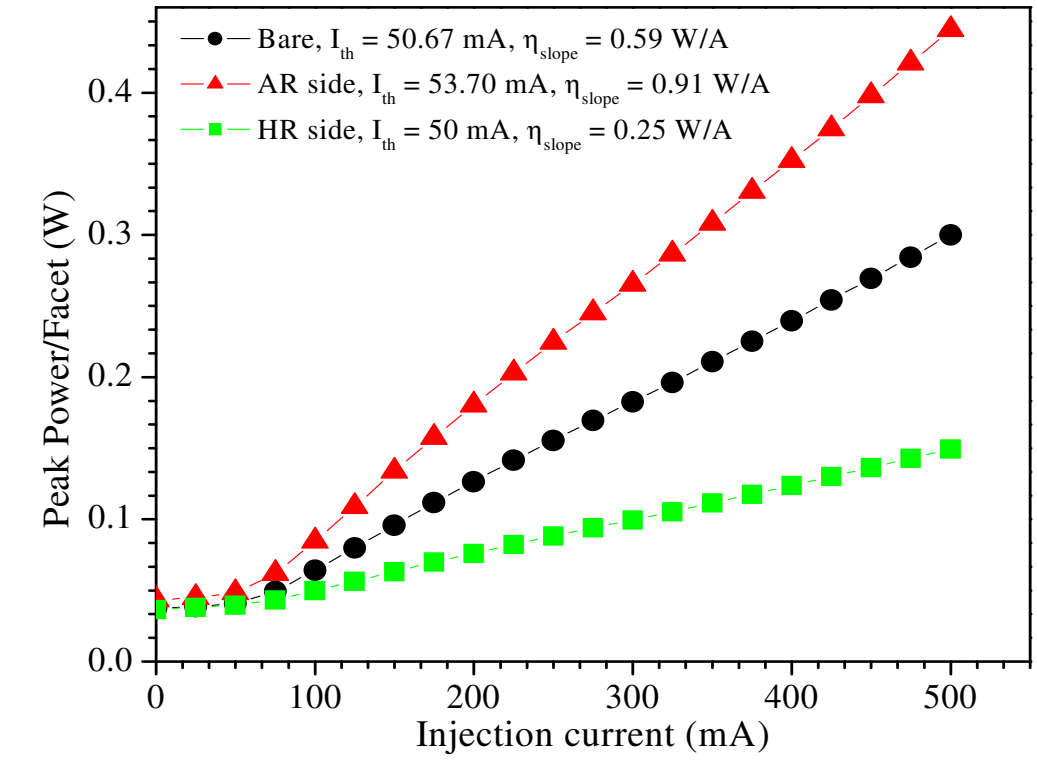

(a)

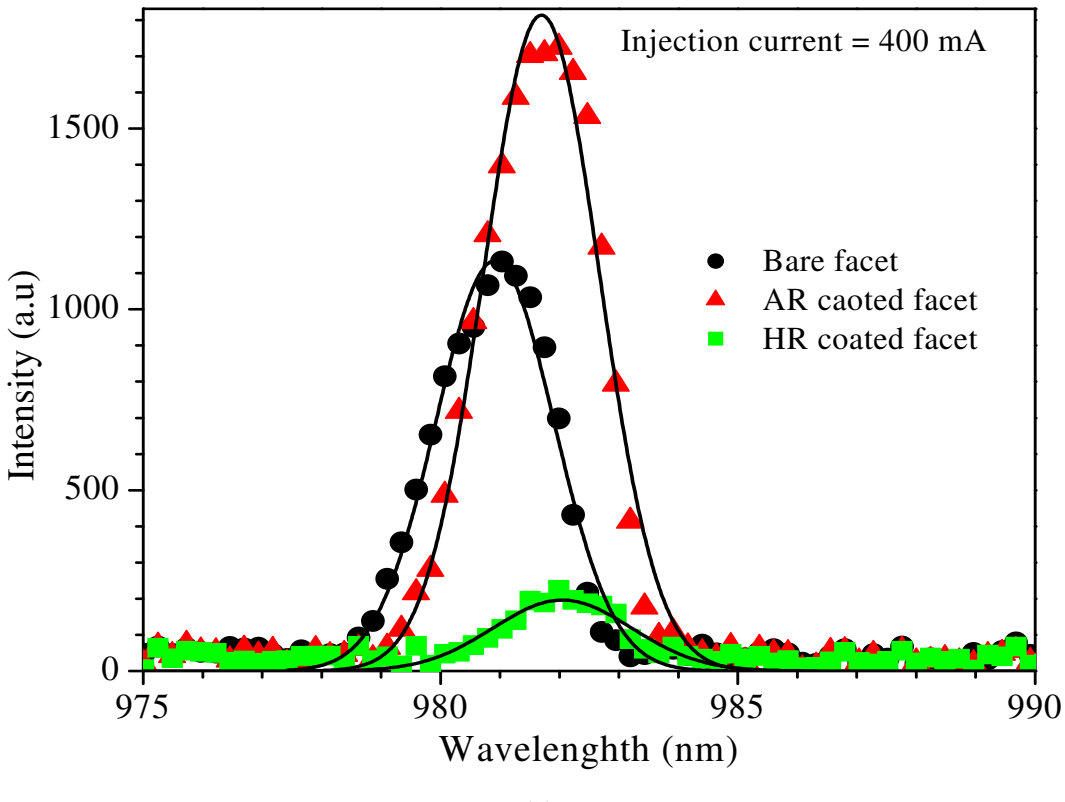

(b)

Figure 4.21: (a) L-I characteristics of laser diode (b) Emission spectra of laser diode

The threshold current of lasers with AR/HR coatings did not change compared to the uncoated ones, however the slope efficiency (*dP/dI*) increased by 1.5 times. This is due to the fact that a laser diode provides equal optical power from both the front and the back facets. However, in most instances, only the power output from one of the facet is useful. The optical power output from the front facet of laser diode is given by, $P^{T}_{out} = P_c (1-R_f) (1+R_r)/2(1-R_fR_r)$ where R_f, R_r are the reflectivity of the front and back facet of laser diode, respectively. The total optical power generated in the cavity (P_c) is calculated as a function of input current. In the present structure considering the 2 % and 90 % reflectivity $P_{out} = 0.94 \times P_c$, thus justifying the pertinent facet coating of laser diode by Eq. 4.11 [38].

$$dP_{out}^{T} / dI = (dP_c^{f} / dI + dP_c^{r} / dI)_{coated}^{T} = 0.94 \times (dP_c / dI + dP_c / DI)_{uncoated} \quad (4.11)$$

Figure 4.21 (b) shows the emission spectra of laser diode without and with coating. It is noted that the position of emission spectrum of the facet coated surfaces are nearly similar to that of uncoated surface. The small shift of ~1 nm may be due to the variation of the operating temperature of the peltier cooler assembly. Subsequently, these laser diodes (die bonded p-side down with indium (In) preform on a gold plated copper package) were also operated under continuous wave (CW) mode of operation. The total output power from the facet coated laser diode was 745 mW at ~3.3 A injection current.

❖ Conclusion

Single layer of QWOT ZrO_2 (AR) and multilayer stack of SiO_2/ZrO_2 (HR) coatings on the front and rear facets of high power InGaAs QW laser diodes are deposited using e-beam methods. Reflectivity of 2 % and 90 % of the front and rear facet, respectively, are achieved in the configuration "Air-AR-front facet-rare facet-$(LH)^5$-Air" of laser diode. L–I characteristics have been measured before and after facet coatings. Significant output power enhancement for laser diodes due to AR and HR coatings is achieved. The slope efficiency is increased and the experimental results are in good agreement with the theoretical estimated.

* * *

Chapter 5

Packaging and Testing of 650 nm and 980 nm High-Power Laser Diodes

5. Packaging and Testing of 650 nm and 980 nm High-Power Laser Diodes

The packaging is the final and the most important processing step of laser diode fabrication technology that significantly affects the laser diode performance, especially in continuous-wave (CW) mode. The packaging of the laser diode includes die- and wire-bonding. It provides electrical and thermal conduction to the device and makes it applicable to the outer world. The present chapter discusses optimization of bonding process for high-power laser diodes.

5.1 Introduction

The packaging of the high-power laser diodes (LD) is the most essential process of the device production. It provides not only the mechanical support but also the electrical and thermal conduction to the device and makes it applicable to the outer world. The leading factor in the laser diode packaging is the die-bonding and wire bonding. The process to solder the laser chip or bar to the appropriate substrate by means of any solder material, viz. Indium (*In*), gold tin (*AuSn*), is known as die-bonding. While further electrical interconnection of the laser chip/bar to the contact lead of the package by means of gold wire or ribbon is known as wire bonding. This chapter discusses optimization of bonding process for laser diodes. The packaging of high-power laser diode is demonstrated.

Laser diode must be bonded and sealed in a suitable package depending on its application, which can be hermetic or non-hermetic. Hermetic type sealing is impervious to dust and moisture and prevents ambient contamination to the laser. Hermetic packages are very robust and provide long term reliability to the laser diode. However, hermetic packaging technique is quite expensive, which increases the manufacturing cost significantly. Non-hermetic packaging, though not as reliable as hermetic one, is extensively used in a number of applications due to cost effectiveness and ease of implementation. Thus, selection between hermetic and non-hermetic packaging can be seen as a compromise between cost and performance. We have utilized a co-axial type non-hermetic type gold plated copper packages to optimize the packaging of the laser

diode. The following sections discuss the solder material, the packaging substrate, and the die-bonding process for optimization the laser diode.

5.2 Die-Bonding

The packaging of laser diode includes die-bonding and wire-bonding of the laser diode chip/bar to the appropriate package. The bonding process affects the electrical and thermal properties of the laser diode [129] and need to be optimized in order to meet the requirements like, reliable operation with high output power and longer lifetime. The electrical and thermal resistance of the laser diode assembly should be as low as possible to efficiently reduce the device heating and better heat dissipation from the laser diode active layer under high-power operation. Thus, the overall efficiency and reliability depend largely on packaging techniques. Further, due to the mismatch in the coefficient of thermal expansion (CTE), the thermo-mechanical stresses generated at the interfaces of dissimilar materials during packaging are a big challenge to the realization of a durable system [130].

As discussed earlier, the operation of attaching the semiconductor chip (laser diode in our case) to the package is known as die-bonding. The semiconductor laser chip/bar is placed at an appropriate position in the package, at the edge in case of edge-emitting laser diode. There are some important requirements which have to be taken into account while optimizing the die-bonding process: (1) High electrical and thermal conductivity are essential, (2) Void- free contact formation between laser chip and package, which means good adhesion, and (3) Good matching of CTE between the laser chip and package material. A wide range of solder types and techniques are available for the die-bonding.

5.2.1 Types of Die-bonding

❖ Adhesive Bonding

As the name suggest, an adhesive bonding is formed by adhering the die to the package by means of some adhesive material. Adhesive bonding is conducted at room-

temperature and widely used for die-bonding of semiconductor chips. The adhesive material can be electrically conducting or insulating depending on the application of the device. It mainly consists of metal particles having size in microns, viz. silver flakes, suspended in a carrier like epoxy resin. The carrier provides adhesion and cohesion to make a bond with the correct mechanical strength, while the metal particles provide electrical and thermal conductivity. The adhesive bonding gives reduced void propagation underneath the die, with better heat transfer, leading to enhanced device reliability [131].

❖ Soldering

Soldering is the process in which die-bonding takes place by formation of the inter-metallic layer of solder material viz. soldering paste or solder preform. The formed inter-metallic layer not only provides mechanical integrity but also provides good electrical and thermal conductivity to the laser diode. The simplest method to perform the solder reflow is to heat the solder material by means of any heater. The reflow of solder material is usually performed under inert gas flow to prevent oxidation. To achieve good inter-metallic contact formation, the essential condition is to remove the surface oxide from the semiconductor chip, substrate, and solder material. This surface oxide makes a barrier on the semiconductor and solder surface and prevents the formation of intimate contact between them. Typical reflow of solder materials on a heater in air usually requires flux. The flux could be in form of either solid, liquid, or gas. The most widely used flux in semiconductor chip bonding is liquid type. This is a rosin based liquid that promotes wetting between two surfaces by removing surface oxide and also inhibiting further oxidation of the surfaces during the bonding process. However, use of liquid fluxes is questioned in the case of laser diode bonding since it produces residual impurities which may cause electrical and mechanical degradation of the device [132]. Moreover, it also requires further cleaning treatment to remove additional flux and residual contaminants which is not desirable in case of laser diode bonding. Hence we have used the no-clean liquid flux to remove the surface oxide from the semiconductor, solder and metal surfaces. The liquid fluxes may be eliminated through the use of gaseous flux like forming gas, mixture of nitrogen (N_2) and hydrogen (H_2), cover over a heater. The forming gas atmosphere provides a sufficient environment to inhibit oxide formation

during the reflow operation. Generally, solder materials are classified into two types according to their yield strength i.e. soft solder and hard solder. Hence, the soldering can be achieved by soft soldering or by hard soldering (or eutectic bonding), depending on the solder material used.

- **Soft Soldering**

As the name suggest, the soft soldering has low yield strength compared with eutectic soldering. It is used for high-power devices, especially in power electronics where good electrical and thermal conductivity is required. Alloys like lead-tin (*PbSn*), silver epoxy, and indium (In) preform are most likely used soldering materials. Being soft in nature it is quite ductile and can undergo large plastic deformation before any mechanical damage, while device operation. Hence, they can withstand in case of thermal mismatch by plastic deformation and can help relieve the stress due to plastic strain or deformation. However, due to plastic strain soft soldering may suffer from the thermal fatigue and creep movement within the joint [133,134]. The most widely used solder materials in device packaging are *PbSn* and silver epoxy to reduce the effective production cost. However, at present, due to an environmental hazard of lead [134] and lower thermal and electrical conductivity of silver epoxy limit their utilization in laser diode packaging.

- **Hard/Eutectic Soldering**

The hard/eutectic solder consists of eutectic mixture generally an alloy of two or more dissimilar metals. The critical melting point of eutectic solder material is much below than that of the constituent material. The hard soldering has very high yield strength and exhibit only elastic strain while device operation. Therefore, it does not have thermal fatigue and creep movement like soft soldering. The eutectic bonding gives very good electrical and thermal contact and high mechanical strength. However, it does not help to release stresses generated in a joint structure because of lack of plastic deformation. Also, one has to take care about the temperature control and mechanical stability of the whole experimental setup because of the critical melting temperature of the solder material. An abrupt solidification may lead to cracks and voids in the joint. Moreover, the eutectic bond is brittle and the thermal mismatch may also cause the chip to crack during the bonding process or during thermal cycling.

There are plenty of new materials and alloys that are being developed to achieve good mechanical strengths and high thermal fatigues because die-bonding is still a major source of faults during assembly fabrication and require lots of process optimization. The bonding must be free of voids to attain minimum electrical and thermal resistance. Large number of voids in bonding causes an increase in thermal resistance and hence increases in the junction temperature. Also, high electrical resistance causes thermal roll-over due to device heating while operating under high-power operation. Moreover, solder voids near the front facet are not desirable as they can raise the facet temperature significantly and cause catastrophic optical mirror damage (COMD) [135]. However, it is almost impossible to achieve void-free bonds, since air-films are always trapped at the interfaces. The solder does not flow sufficiently to displace all this air to the die periphery and much of it remains trapped after soldering as voids within the bond. Thus, quality of void-free soldering depends on the wettability of the surfaces, the accuracy of the solder volume, and on protecting the process from oxygen. In addition, structural damage may also occur to the laser diode chip while mounting and bonding it on the package. Thus, mounting and die-bonding of a high-power laser diode on a package must be optimized to ensure satisfactory thermal and electrical coupling between the package and the laser diode chip.

5.2.2 Bonding Configuration

There are two basic configurations in which a laser diode chip can be bonded on the package; junction (or p-side) -up and junction-down configuration. Figure 5.1 shows the schematic of the laser diode bonding configuration. Die-bonding processes for p-side up bonding is much explored and well established by the packaging industry [136]. The heat generated in the active region of the laser diode spreads laterally over the entire laser width and has to flow through the entire substrate (GaAs) before reaching to the heat sink. Due to the low thermal conductivity of ternary alloys and multiple hetero structures [137] of the laser diode, the heat generated in the active region cannot be dissipated onto the heat sink efficiently. As shown in Fig. 5.1 (b) the junction down bonding is more efficient in removing heat from the device since the epitaxial layers containing the active region are typically much thinner than the substrate [138,139,140] and the active region is only within the proximity of a few microns from the package surface. However, the

reliability of a laser diode bonded in p-side down configuration is significantly impacted by electromigration in the die attach solder [135]. The electromigration can create and enlarge voids as well as accelerate the propagation of preexisting voids [141], which leads to the device failure. Also the stress associated with p-side down bonding may cause damage to the active layer and hence the device due to the mismatch in the coefficient of thermal expansion between the laser diode and the heat sink material. Above all, the technique to configure p-side down bonding is quite complex and requires special die-bonding tools which are some of the discouraging factors in the adoption of this technique [142]. Considering these facts and the unavailability of sophisticated instrumentation for die-bonding, we have employed the conventional junction-up method, which is relatively simple and provides sufficient heat dissipation up to moderate power. We experimented with different solder materials to die-attach identical laser diode chips on specially design packages [143].

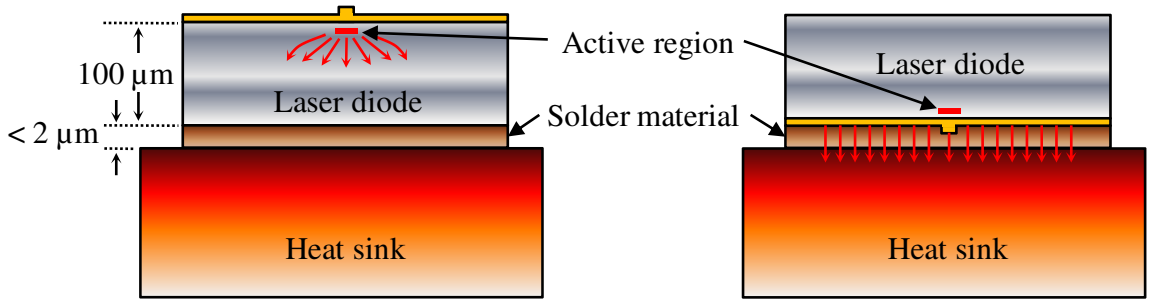

Figure 5.1: Different bonding configurations of ridge-waveguide laser diodes. (a) For p-side up bonded laser diode, the heat generated in the active region is ineffectively transferred through the substrate; (b) For p-side down bonded laser diode, the heat flux is effectively reached the heat sink within several microns.

5.2.3 Solder Materials for Die-bonding

A wide variety of solders are available for die-bonding of semiconductor components on the heat sink. However, selection of the most appropriate solder material is very important and involves many parameters such as die and package materials, operating conditions and reliability requirements. The most widely used solder materials in device packaging are *PbSn* and silver epoxy to reduce the effective production cost. However, at present, due to an environmental hazard of lead [134] and lower thermal and electrical

conductivity of silver epoxy limit their utilization in laser diode packaging. We have used *In* and *AuSn* solder preform to bond the devices.

- **Indium (*In*) Preform**

Indium preform is one of the most widely used solders in die-bonding of high-power laser diodes. Indium solder has some advantages in laser diode die-bonding. Indium, being a soft solder, relaxes stress caused by mismatch of coefficient of thermal expansion (CTE) between the chip and package material effectively. Moreover, it is a low cost material with low melting point of 157 °C. It also has some concerns, however, especially in terms of reliability [134]. The thickness of the In-preform used in our experiment is 55 μm.

- **Gold-Tin (*AuSn*) Preform**

Gold-tin (*AuSn*) is the alloy most commonly used in the industry for GaAs assemblies due to its compatibility with gold-based components and its long-term reliability. The composition of the alloy used for the experiment is 80 % gold - 20 % tin, which is a eutectic alloy and has a melting point of 283 °C. Being a hard solder, *AuSn* overcomes the disadvantageous thermal-fatigue and creep-rupture properties of the soft solders, such as *In*, by staying in elastic deformation. However, the same property demands that the mismatch of CTE of the package material should be within the acceptable range. Large mismatch in the CTE may induce large strain and subsequently produce stresses during the thermal cycling, which may cause cracks in the die or detachment of the die.

5.2.4 Package Material and Design

The design of laser diode packages is one of the most extensive research areas in laser diode bonding and packaging. The packaging material and design selection for the laser diode is depends on the specific requirements of different cooling techniques viz. active or passive cooling. The package with active cooling consists of water cooled, micro-channel heat-sink while passive or conductive cooling to the package will provide by means of heat-sinks, generally made of copper, mounted on thermo-electric coolers. The packaging materials commonly having high thermal conductivity and the coefficient of

thermal expansion (CTE) matched with the device's substrate material i.e. usually GaAs, is used for laser diode.

The standard heat sink material mostly used in all commercially available packages is copper, because of its good thermal and mechanical properties, and its low price. However, the mismatch in CTE between the laser bar and the copper has a major influence on the operation lifetime of the laser bars, as it causes a severe stress in to a laser bar. In addition to that, the increasing demand of high-power laser requires heat sink material with even high thermal conductivity with less CTE mismatch. Hence, the compound materials having moderate thermal conductivity like copper-tungsten (CuW) or diamond are used for laser packaging. Unfortunately, these materials are much costlier than copper and having moderated thermal conductivity. In addition, the mechanical machining properties of these materials are poor and hence it is too difficult to achieve desired package design. Hence, we have used gold plated copper (*Cu*) and KOVAR (Ni:Co:Fe::29:17:54 wt% [144]) as packaged substrate to optimize the bonding process. To compensate the difference of CTE between laser diode and package, we have used indium soft solder as bonding material. The laser diodes were die-attached on specially designed co-axial type gold-plated copper packages as shown in Fig. 5.2 (a). Gold leads, flattened at the front edge as shown in Fig. 5.2 (b), were inserted and fixed in the packages through ceramic isolators to carry out wire-bonding. Such a package, ready to be die- and wire-bonded, is shown in Fig. 5.2 (c).

(a) **(b)** **(c)**

Figure 5.2: (a) Gold platted copper package, (b) flattened-ended gold lead and (c) package with gold lead inserted and isolated through ceramic.

Here, in this work, we present the successful optimization of the high-power laser diode bonding process using *In* and *AuSn* soldering material on gold plated *Cu* and

KOVAR substrates. We have used uncoated laser diode chips with lasing wavelength of 650 nm, 808 nm, respectively for die-bonding process-optimization. The 980 nm GaAs/InGaAs double quantum well high-power laser diode element and bars were bonded using optimized bonding process parameters. Results of bonded and un-bonded devices are compared during the CW high-power operation.

5.3 Wire Bonding

Once the laser diode chip is attached on the package, the next step in the packaging is assembly interconnection. The most common method for electrical interconnections is wire bonding. It provides the electrical connection on p or n-type metallization of the laser diode. Thin metal wires are connected one by one between the contact stripe on the laser diode chip (die bonded p-side up) and the corresponding contact-lead on the package. For laser diode assembly, gold wires are normally used.

Wire bonding is a very delicate procedure. The machine bonds one end of the wire, usually gold, to the metalized substrate using an ultrasonic pulse, creates a loop with the wire, and makes a second bond, cutting the wire at that end. Normally the wire bonding techniques can be categorized into three major processes: thermo-compression bonding (T/C), ultrasonic bonding (U/S), and thermosonic bonding (T/S), depending on the bonding parameters i.e. ultrasonic power and/or heat. As the name suggest, T/C and U/S bonding process are accomplished by means of only bonding force/pressure aided by temperature and ultrasonic power, respectively. The most commonly employed technique to achieve wire bonding is the thermosonic (T/S) bonding, performed at elevated temperature by ultrasonic power. The wire bond is formed with heat, pressure, and ultrasonic energy. The heat is provided through the bonding stage consists of heater. The bond head movement in vertical direction exerts pressure on the wire and ultrasonic energy from the transducer through the bond tool to the wire altogether form a wire bond, as shown in Fig. 5.3.

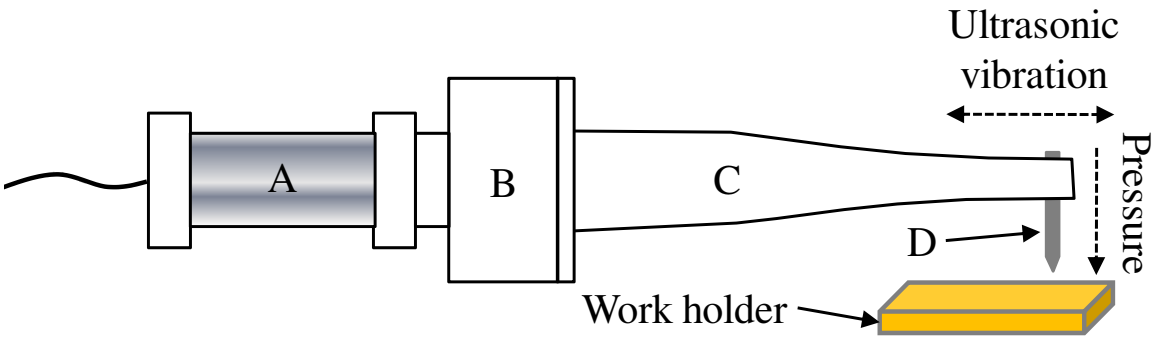

Figure 5.3: Typical ultrasonic transducer used for manual wire bonding: (A) the ultrasonic transducer element; (B) the mounting clamp, which is located on a vibration node and is clamped to the bonding machine; (C) referred to as the horn (tapered to amplify the ultrasonic wave); (D) the tool/capillary, which is clamped perpendicular to the axis of the horn.

The various bonding parameters like ultrasonic power, pressure or force, temperature, and bond-time, determine the bond quality. Force, time, and ultrasonic power are critical for consistent wire bond and hence the reliability of the bonded device. There are two basic wire-bonding techniques: ball-bonding and wedge-bonding, as shown in Fig. 5.4, depending on that the bonding loop formation take place either in ball-wedge or wedge-wedge loop configuration. In case ball-wedge configuration first bond of the loop on the device is formed by a ball bonding following with the second bond as a wedge type. While, on the other hand, for wedge-wedge type bonding both the loop ends are formed by wedge bonding. The merits and demerits of both ball and wedge bonding are discussed in Table 5.1

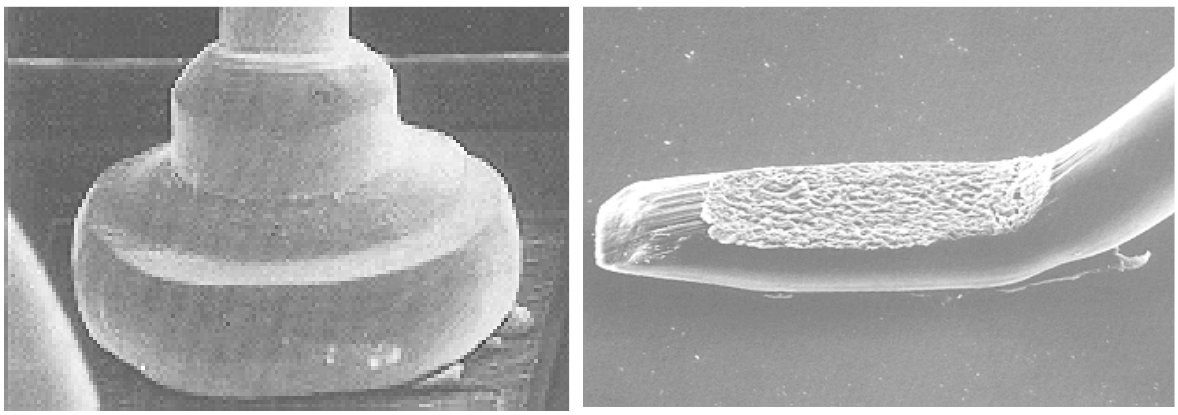

(a) **(b)**

Figure 5.4: The SEM image of (a) Ball bond, and (b) wedge bond [145].

Table 5.1: Wedge bonding vs. Ball bonding

Wedge bonding	Ball bonding
Unidirectional bonding	Multi-directional bonding
Creates small bonds (1.1 to 2 times wire diameter)	Bond sizes range from 2.5 to 4 times wire diameter
Usually used with aluminum wire, however it is also used with gold wires.	Used mostly with gold wires
No electronic flame off (EFO) is employed	Requires EFO to form ball
Being unidirectional the wedge bonding is slower	It is comparatively faster than wedge bonding.

5.3.1 Wire Bonding Process

The wire bonding process consists of applying ultrasonic energy to form a strong, reliable, intermetallic connection between the wire and the pad, as well as between the wire and the lead. This is accomplished by inserting the wedge tool in the bonding head, which is coupled to a precision ultrasonic generator. The main phases of the wire bonding, i.e. wedge-type in our case, bond-cycle is: 1^{st} bond, loop formation, 2^{nd} bond, and wire termination, respectively. Each phase is the result of several operations performed by the wedge. These operations can be presented by stages that complete the bonding cycle given below in Fig. 5.5.

The commercially available die and wire bonder comprise of automated parameter control and designed for dedicated device assembly bonding. All the bonding parameters like, bond location, bonding time, temperature can be programmed in this type of automated bonded and we can have definite quality bond. However, these commercial bonders for both die-bonding and wire-bonding are quite expensive. Hence, we have indigenously designed and developed the setup for die-bonding of the laser diode, while manual wire bonder is used to carry out wire bonding.

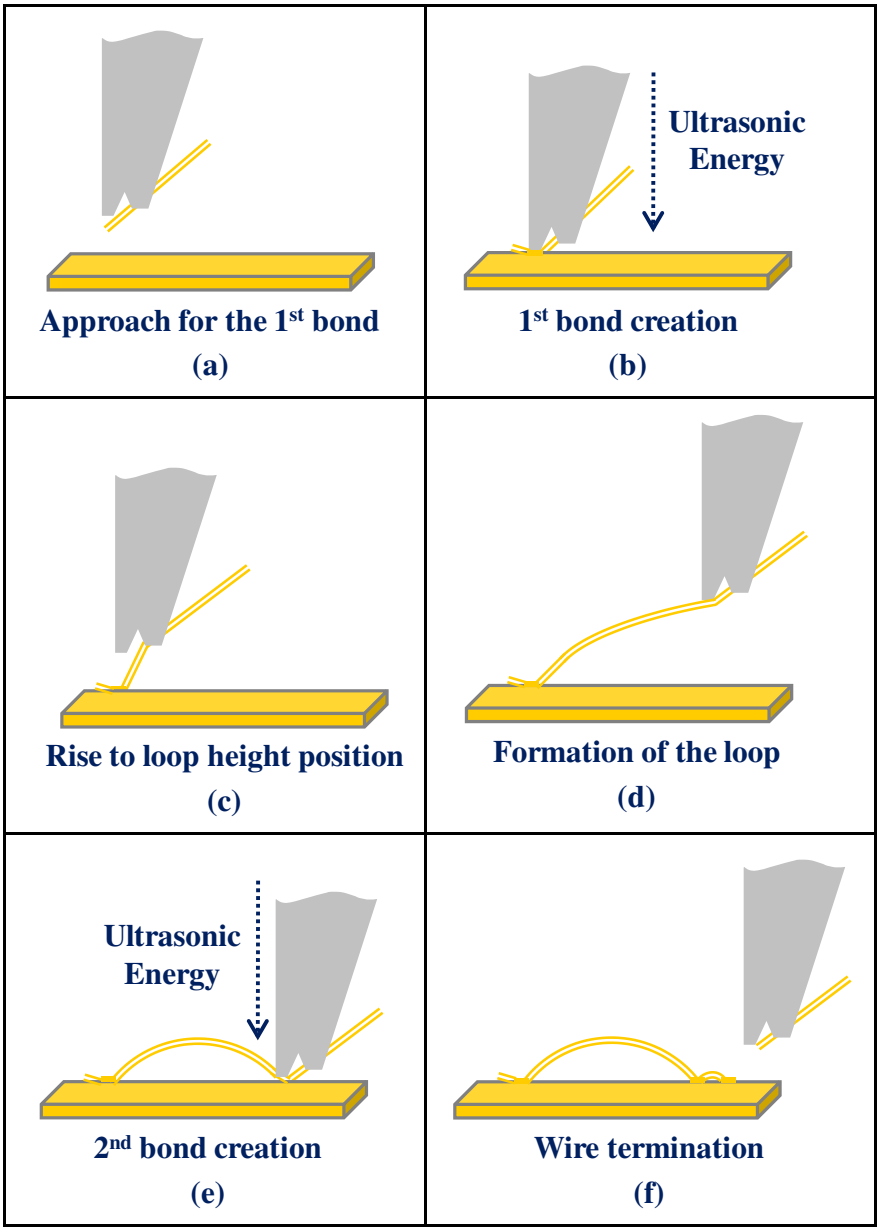

Figure 5.5: Wire bond loop formation steps for wedge bonding.

5.4 Experimental

5.4.1 Die-Bonding

We have used two types of bare facet, without facet coating, 650 nm and 980 nm laser diodes for die-bonding optimization. The 650 nm lasers are commercial devices while 980 nm devices are fabricated at RRCAT, Indore [25]. The die-bonding is carried out using an indigenously developed setup. The experimental setup consists of bonding pad (Heater), the bonding tool with inert gas (N_2) flow outlet mounted on travelling stage and

the microscope for better alignment to view the device and solder preforms i.e. *In* and *AuSn*. Figure 5.6 (a) shows the schematic of the experimental setup for the die-bonding process. The bonded laser diode bar and *AuSn* preform on the edge of the laser diode package is shown in Fig. 5.6 (b).

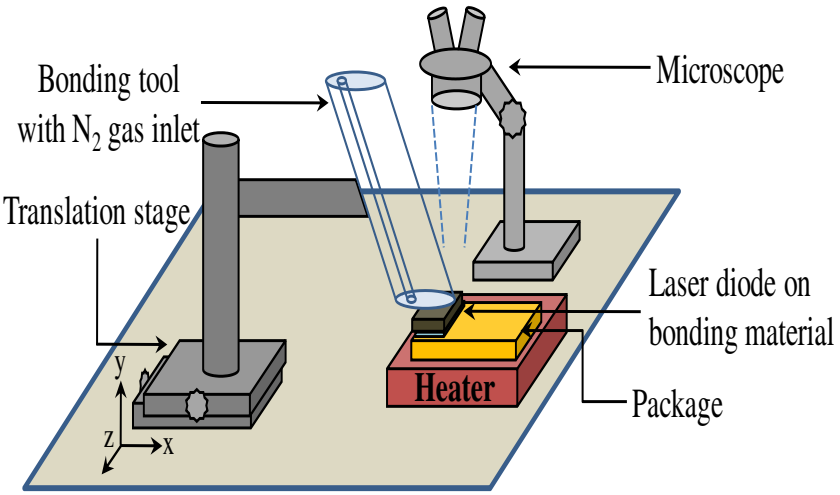

(a)

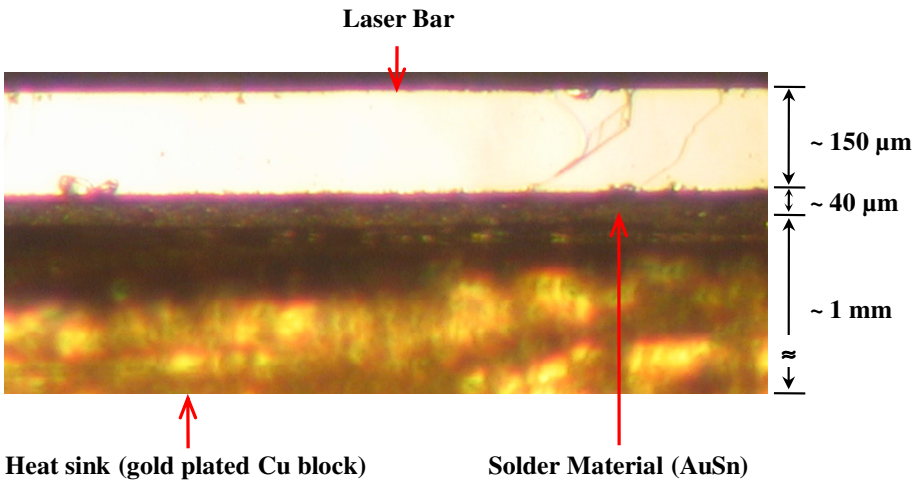

(b)

Figure 5.6: (a) The schematic diagram of the experimental setup of the self assembled manual die bonder. (b) p-side up die-bonding configuration of the 980 nm InGaAs/GaAs ridge waveguide laser diode bar.

The bonding tool was made to press laser diode with controlled force on a substrate in such a manner that it neither disturbs the alignment nor damages the device as well. After proper alignment, the assembly was heated up to the melting point of the soldering material and kept for curing. The whole experiment was done under nitrogen

ambient (N_2 flow at pressure 0.25 Bar) to reduce the environmental oxygen effect on the bonding quality. To achieve good bonding between device and substrate, soldering flux (*Kester #952-D6*) was used. The optimized parameters of die-bonding along with physical and electrical parameters of the materials used are shown in Table 5.2 and Table 5.3.

Table 5.2: Physical and electrical parameters of the materials [51,146].

#	Melting Temperature (^oC)	Thermal Conductivity (W/m ^oC)	Thermal Expansion Coefficient (ppm/^oC)	Electrical resistivity ($\mu\Omega$.cm)
GaAs	1238	54	6.5	~10000
In	157	80	32.1	8.8
AuSn	283	57.3	15.9	16
Cu	1085	400	17.8	1.68
KOVAR	1450	15	5.8	40-50

Table 5.3: Optimized bonding parameters for *In* and *AuSn*.

Curing Temperature (^oC)	Curing Time (s)	Natural cooling in presence of N_2 gas
170	80	Till 70 ^oC
300	57	Till 100 ^oC

In addition to that we also have bonded 650 nm laser diode bar to the c-type gold plated copper module package, where both contact ends of the bar are die bonded to the package as shown in Fig. 5.7. The base to hold this packaging module is alumina substrate having conductive stripe. This module die-bonding process is carried out in rapid thermal annealing (RTA) furnace in presence of forming gas, i.e. a mixture of 92 % nitrogen and 8 % hydrogen at elevated temperature. Specially fabricated jig for facet coating was used to hold the module package along with device and bonding material inside the furnace, shown in the Fig. 5.8. The optimized bonding parameters are shown in Table 5.4. One of the features of this type of bonding is that there is no need to wire bond the device further.

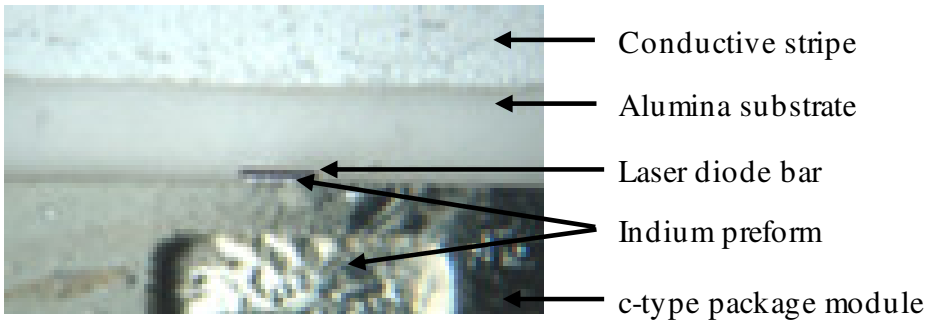

Figure 5.7: 650 nm laser diode bar bonded on c-type package with indium preform. The base for the bonding of this module is alumina substrate with conductive stripe.

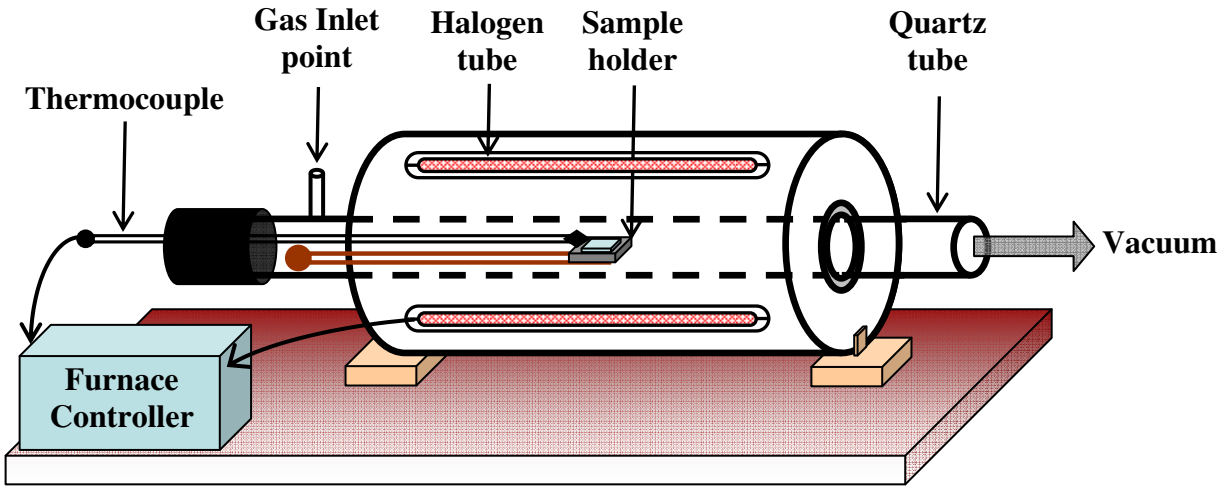

Figure 5.8: Schematic of vacuum based rapid thermal annealing (RTA) furnace [147].

Table 5.4: Optimized bonding parameters for module type package with In preform in RTA furnace.

Temperature (^{o}C)	275
Bonding time (m)	7
Forming gas flow rate (sccm)	70

5.4.2 Wire Bonding

After the die-bonding of the laser diode, the top contact on the chip/bar was provided through wedge-type wire bonding. The 1 mil (25.4 µm) diameter gold wire was used to connect device and contact lead. The wire bonding was achieved using manual wire bonder (K & S make universal bonder) shown in Fig. 5.9. The wire bonder mainly consists of ultrasonic power supply, transducer, bonding head, bonding tool, heating

stage, temperature controller, and microscope. Figure 5.10 shows the photograph of bonding tool for wedge bonding.

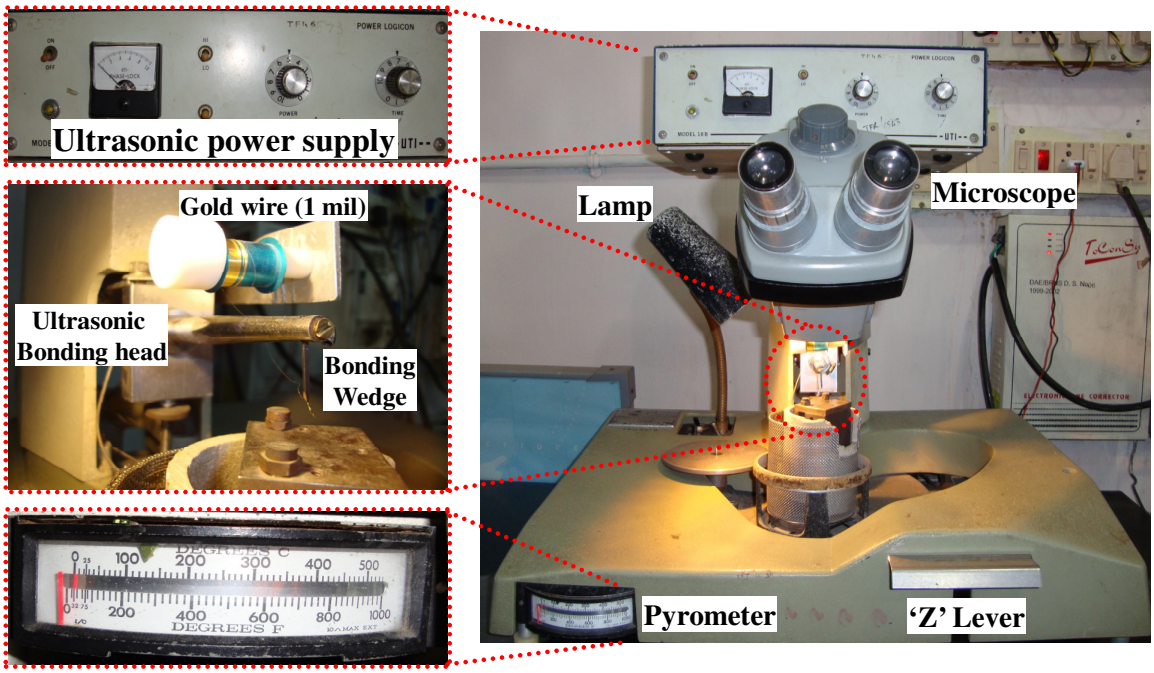

Figure 5.9: K & S make universal ultrasonic wire bonder.

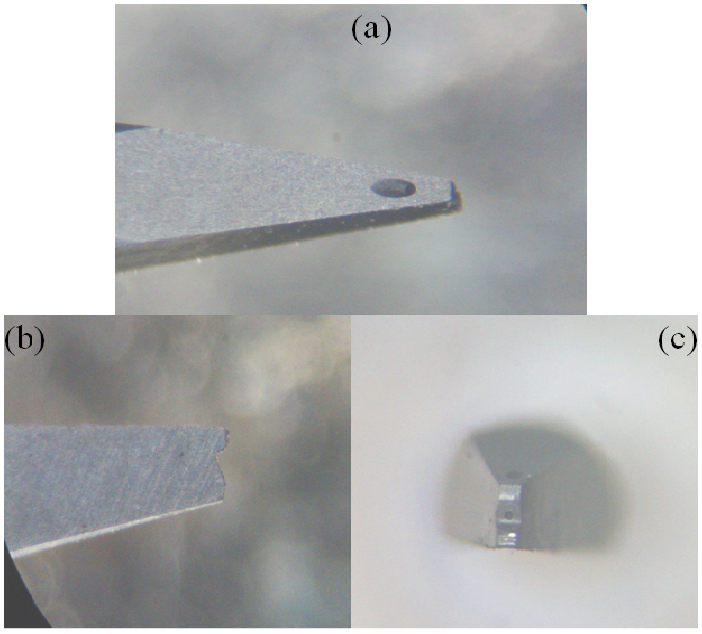

Figure 5.10: A microscopic view of the wedge used for the bonding. (a) Wedge tip, (b) Side view Wedge tip, (c) Front view Wedge tip

A good wire bonding can only be attained by optimizing the parameters viz. bonding force, temperature, ultrasonic power, and finally the bonding time in a sequential

manner. The complete bonding process was optimized on a specially fabricated and organically cleaned gold plated printed circuit board (PCB), shown in Fig. 5.11. The bonding optimization was carried out with different conditions of possible combinations of different parameters and finally observing the foot-prints of the formed bond-loop under microscope. Table 5.5 shows the experimental and optimized wire bonding parameters.

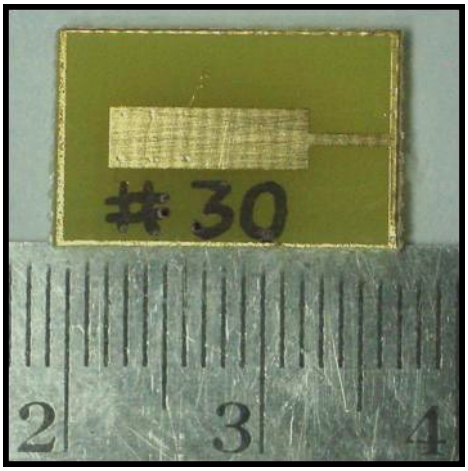

Figure 5.11: Elecroless Ni-Au coated PCB used as the wire bond pad.

Table 5.5: Optimized wire bonding parameters on PCB.

Parameters	**Experimental**	**Optimized**
Bonding force (gm)	8 – 12	11 – 12
Temperature (^{o}C)	RT, 50 & 100	RT & 50
Ultrasonic power (unit)	0.3 – 1.0	0.5 – 0.7
Bonding time (unit)	1 – 10	4 – 6

Here, the whole range of optimized parameters is known as the process window. If the value of bonding parameters set below or above this process window, it will result in either no bonding or wire breakage and further damage to the substrate. Figure 5.12 (a) shows the optimized bond footprint while Fig. 5.12 (b) shows the bond neck break due to excess ultrasonic power applied during wire-bonding process.

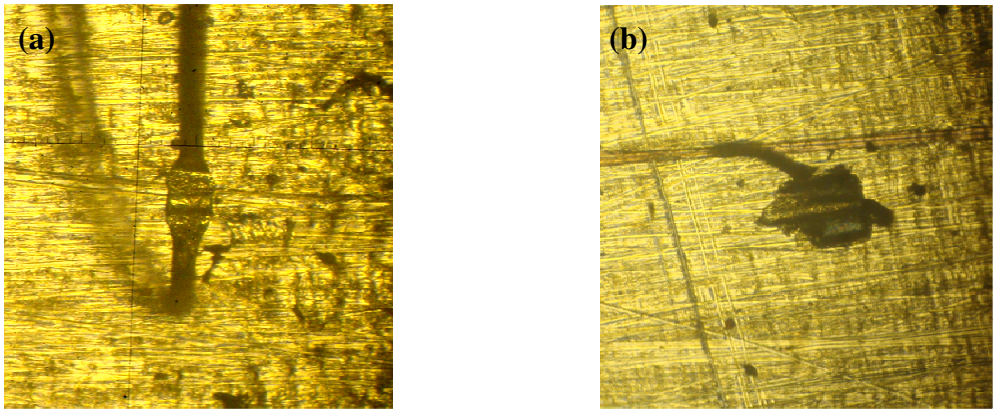

Figure 5.12: Wedge bond foot prints under microscope: (a) Optimized bond, and (b) Failed bond due to excess ultrasonic power, which results in bond neck-break.

5.5 Results and Discussion

The laser diodes with emitting wavelengths 980 nm and 650 nm have been bonded with two different methods and tested for its L-I-V characteristics after the successful optimization and implementation of all bonding parameters. The detail results are discussed in subsections, mentioned below.

5.5.1 Mechanical Properties (Adhesion)

❖ Effect of Flux Application

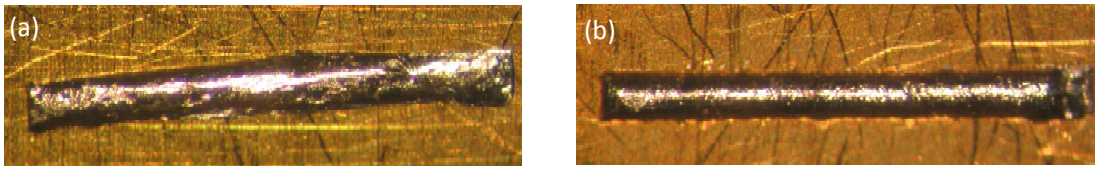

Figure 5.13: The photograph shows effect of flux applied on melting of Indium preform. (a) While melting 'In' without flux application only shrink and don't show adhesion, on the other hand (b) 'In' melted with flux applied shows uniform melting and better adhesion to the substrate.

The die-bonding of the laser diode to the substrate was done by means of the intermetallic compound formation and further diffusion of the bonding material to the both contact layers i.e. LD's n/p- contact layer and substrate. To achieve good intermetallic contact formation, the essential condition is to remove the surface oxide from the substrate and

solder material. This surface oxide makes the barrier between the semiconductor and solder surface. It also prevents the formation of intimate contact between them. In order to remove the surface oxide from the semiconductor, solder, and metal surfaces flux was used. Figure 5.13 shows the effect of applied flux on melting indium preform.

❖ Effect of Packaging Material

The effect of bonding on L-I characteristics of the device with different packaging material was measured by operating it under pulse mode and continuous wave (CW) condition. In case of high-power laser diode the heat generation within small volume is too large and should be removed effectively. Hence, high-power laser diode was configured to bond p-side down to reduce the heat diffusion path. However, one has to take care of the coefficient of thermal expansion (CTE), which should match with the composition material of the device. An epitaxially grown thin layer will experience the strain due to the mismatch in CTE and hence will leads to poor device performance. Here two laser-diode bars are bonded on different gold plated substrates i.e. Cu and KOVAR. The *Cu* is most widely used material in laser diode packaging due to its high electrical and thermal conductivity. However, the high CTE mismatch with GaAs (laser substrate) makes it less favorable in packaging, especially in case of p-side down configuration. On the other hand, KOVAR has moderate electrical and thermal conductivity compared to *Cu*, but its good matching of CTE with GaAs makes it more suitable material for laser packaging. The device was bonded p-side up with *In*-preform on gold plated substrates (*Cu* and KOVAR).

5.5.2 Output Power versus Injection Current Characteristics

❖ Pulse Operation

Initially, the bonded lasers were operated with 0.5 ms pulse repetition interval (PRI) and 2 µs pulse width (PW). The output parameters of the bonded laser are shown in the Figure 5.14 (a). It is noted that there is no distinguished effect of different substrates (*Cu* and KOVAR) during pulse mode operation. This is due to the fact that during the pulse mode operation there was no excess device heating. In addition to that we have also bonded a

laser bar having three elements on *Cu* package with p-side down configuration. This laser diode bar operated under pulse mode with duty cycle = 1:5000 has given total integrated output power 7.5 W, shown in the Fig. 5.14 (b).

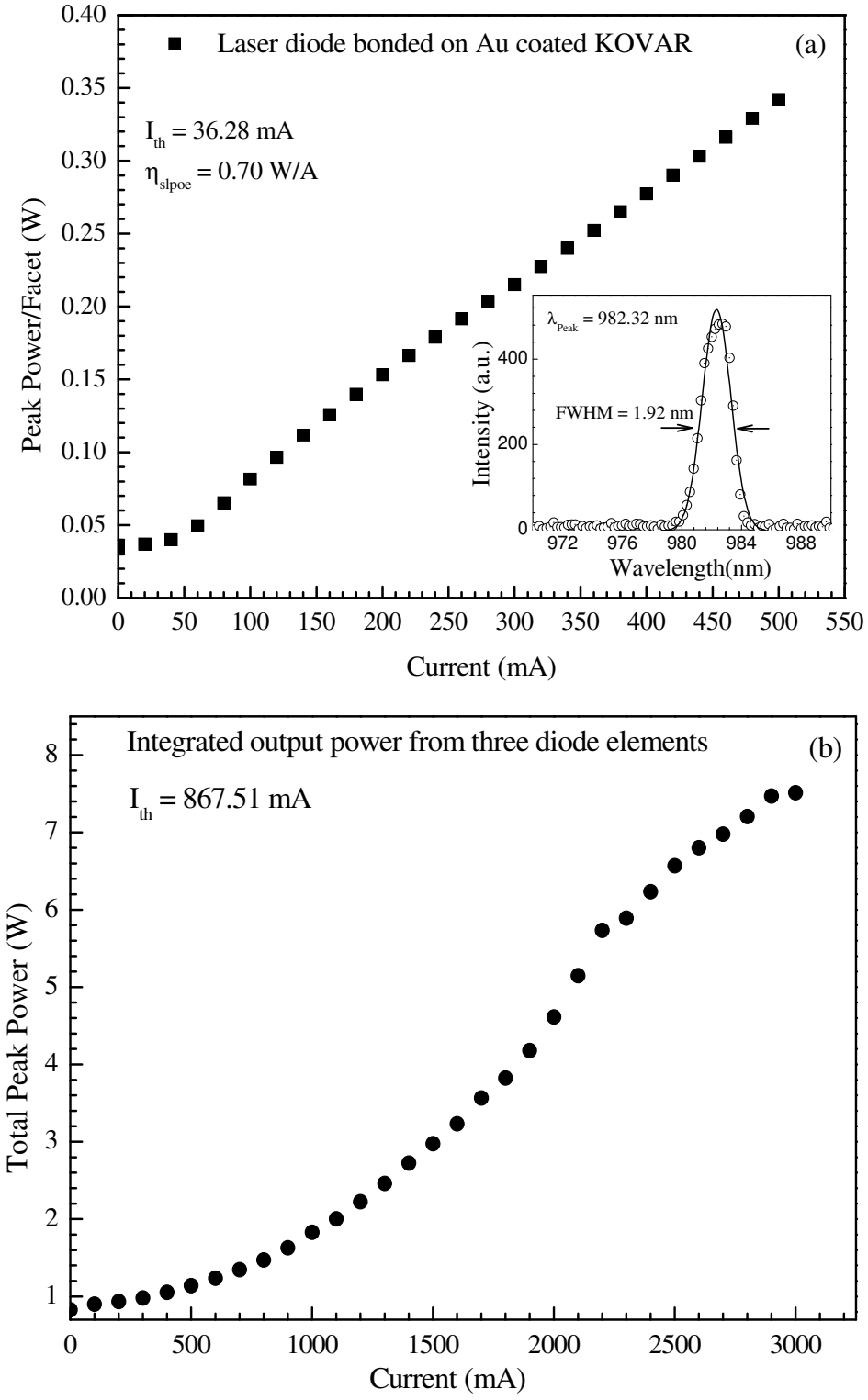

Figure 5.14: (a) Pulse L-I characteristic curve of laser diode elements bonded p-side up with In preform on gold plated KOVAR, inset figure shows typical emission spectrum. (b) Pulse L-I characteristic curve of laser diode bar with three elements bonded p-side down configuration.

❖ Continuous Wave Operation

Figure 5.15 (a) & 5.15 (b) shows the comparative results of output power, voltage and wall plug efficiency as a function of injection current of un-bonded and bonded devices under CW operation. Inset photographs of Fig. 5.15 (a) & 5.15 (b) shows the emitted output power for the bonded and un-bonded devices. The bonded laser diode could be operated at high injection current i.e up to 2 A in comparison with 1.5 A of un-bonded one. Thus the output power of bonded device is ~ 28 % higher than un-bonded one. This indicates more effective heat removal from the bonded laser diode mounted on the thermoelectric cooler (TEC). The comparative results of laser diode parameters are given in Table 5.6.

Table 5.6: Comparative results of laser diode parameter.

Parameters	Without die-bonding	With die-bonding
Threshold Current I_{th} (mA)	94	94
Maximum Power/Facet P_{max} (mW)	520 at 1.5A	670 at 2A
Slope Efficiency η (W/A)	0.82	0.81
Differential quantum efficiency η_d (%)	65	65
Wall plug efficiency W (%) at 700 mA	53	51

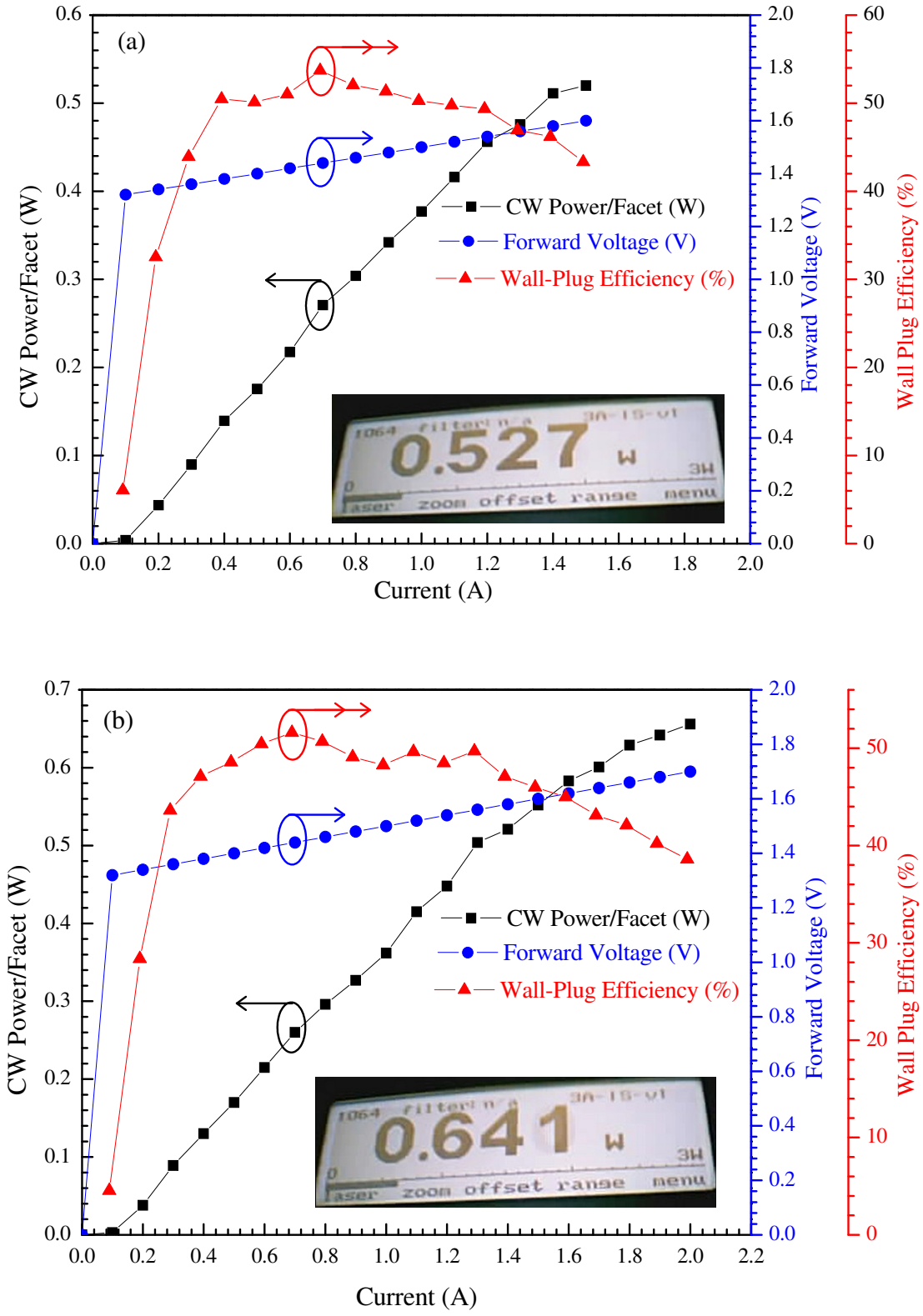

Figure 5.15: Optical output power/facet of the 980 nm GaAs/InGaAs quantum well laser (a) un-bonded and (b) bonded as a function of CW current. The device was bonded p-side up on the gold plated Cu package with indium preform.

5.5.3 Dynamic Resistance Calculation

The low dynamic resistance of the die bonded laser diode exhibits good bonding quality. Consequently, the lower electrical resistance implies low thermal impendence of the bonded device, and hence lower device heating, which makes it reliable for long term operation. We have tested the bonded device for its I-V characteristic in CW mode and found out the dynamic series resistance is about 1 Ω for the 980 nm laser diode bonded on gold plated copper mount with indium preform. Though the series resistance we have find is quite low, this measurement was not completely precise because it also consists of lead and external circuitry resistance. Hence, we have measured this external circuitry resistance, by connecting only the package, having value of about 810 mΩ, shown in Fig. 5.16.

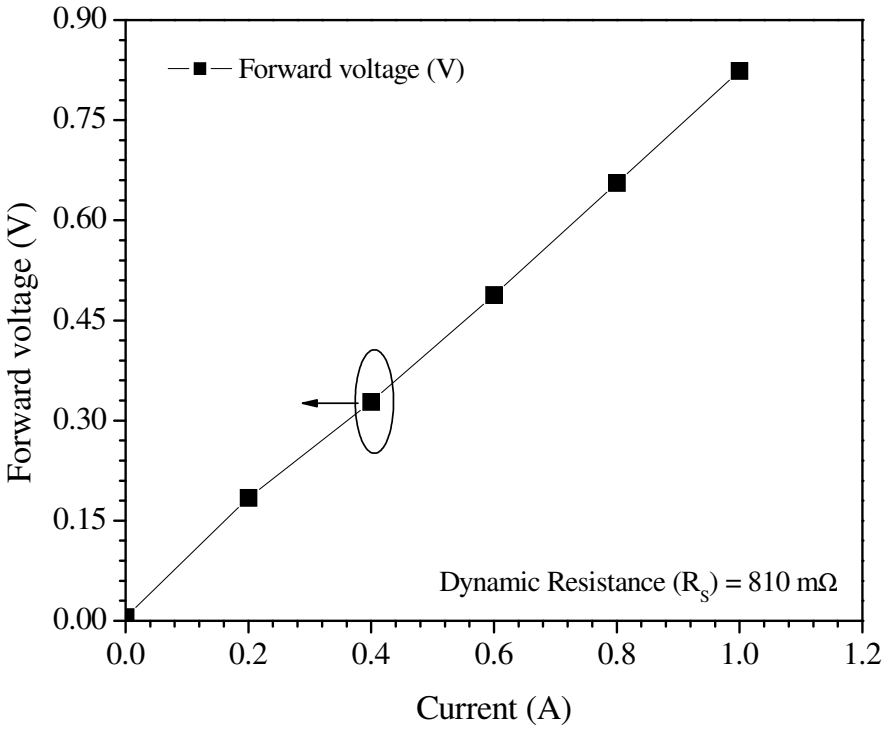

Figure 5.16: Dynamic resistance of the L-I-V measurement circuit, to be subtracted from the total resistance measured while device under operation.

Therefore, by subtracting the external circuitry resistance we have extremely low dynamic series resistance value, i.e. ≈200 mΩ. To verify this we also have calculated the resistance (R) of the device by means of existing resistivity (ρ) values of each layer, from Eq. 5.1, of the laser diode structure discussed in Chapter 3. The resistivity was estimated

trough Eq. 5.2 where the value conductivity (σ) and mobility (μ) was taken from the standard available literature.

$$R = \frac{\rho l}{A} \tag{5.1}$$

where, l = length of the layer, i.e. laser cavity length, A = area of the layer.

$$\rho = \frac{1}{\sigma} \tag{5.2}$$

where, σ = conductivity of layer. For intrinsic semiconductor, $\sigma = q\,(\mu_n n + \mu_p p)$. For extrinsic semiconductor, $\sigma = q\,(\mu_n n)$ for n-type semiconductor and $\sigma = q\,(\mu_p p)$ for p-type semiconductor. Here, μ is mobility of the carrier, n and p is the carrier concentration.

5.5.4 Testing of the Laser Diode Bar Package Module

The commercially purchased 650 nm laser bar having 11 elements on it was bonded on c-type gold plated copper package module with indium preform. The LD bar was sandwiched between two pieces of package and bonded together as an assembly with indium on an alumina substrate having conducting strips, as shown in Fig. 5.17. The bonded device was tested in both CW and pulse operation. The CW operation and I –V of the bar is shown in Fig. 5.18. The low series resistance value, i.e. 6.78 Ω, implies the good bonding quality. Also, the laser was tested under pulse mode with 1 % duty cycle and 5 μs pulse width, shows very low threshold current and total output power of about 50 mW. Figure 5.19 shows the pulse L-I characteristics of the LD bar package module.

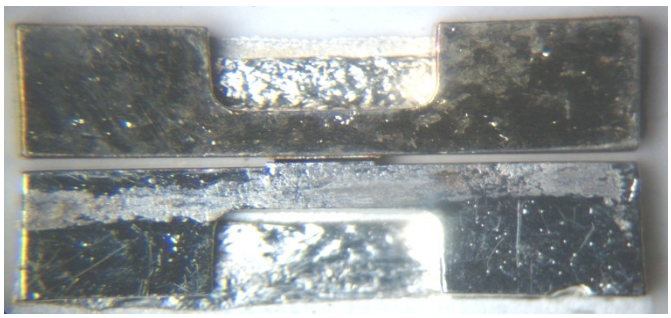

Figure 5.17: Laser diode bar is die bonded on c-type package using indium preform on an alumina substrate.

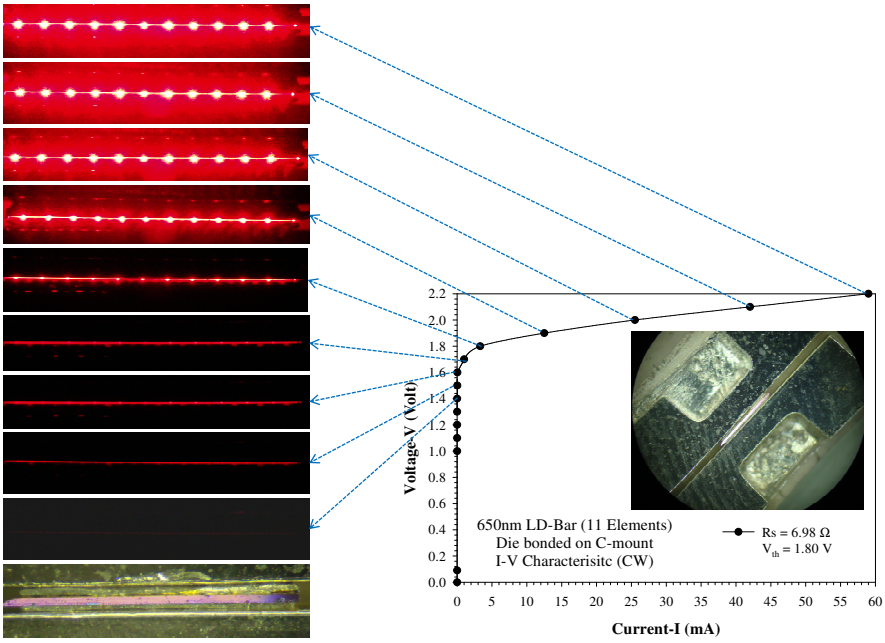

Figure 5.18: CW I-V characteristics and luminescence at different electrical power from the 650 nm laser diode bar package module (illustrated in inset photograph).

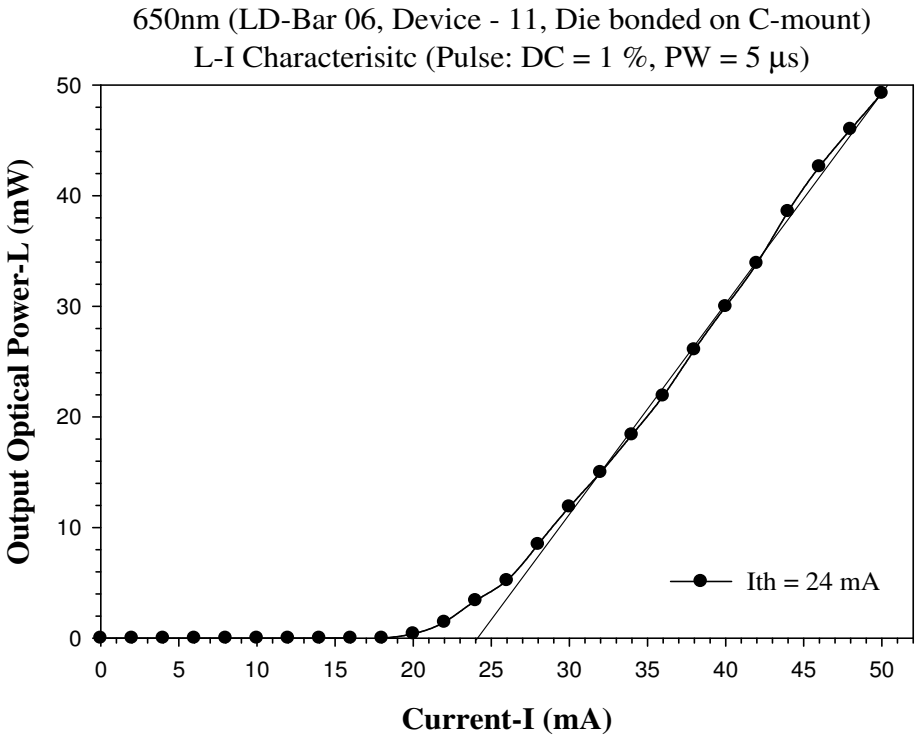

Figure 5.19: Pulse L-I characteristics of Laser diode package module

❖ Conclusion

The successful optimization of the high-power laser diode die-bonding and wire bonding process parameters has been demonstrated. The solder material used for the die-bonding was *In* preform and *AuSn* eutectic alloy. The effect of the die-bonding on the device performance can easily be observed from the L-I characteristic measurement while operating it under CW mode. We have utilized the liquid soldering flux for surface wetting and better adhesion of the device to the substrate. In addition to that, we also have used the forming gas as gaseous flux for laser diode bar package module to remove surface oxide and proper adhesion. Single laser diode element with effective die-bonding gave an output power of ~ 670 mW/facet at ~ 2 A under CW operation with the dynamic resistance of ~ 200 mΩ. Identical characteristics of the three elements, such as threshold current density, and emission wavelength, L-I characteristics, were also achieved under pulse mode operating condition. The integrated pulse output power of ~ 7.5 W from these three devices was also achieved. Subsequently, the developed semi-packaged laser diode was used for characterization of electronic transitions of InAsP/InP quantum well in photoluminescence spectroscopy whose details will be discussed in the next chapter.

* * *

Chapter 6

Life-time and Damage Threshold Estimation and Application of the High-Power Laser Diode

6. Lifetime and Damage Threshold Estimation and Application of the High-Power Laser Diode

The main factor which limits the high-power operation of the laser diode is the facet degradation. To overcome this limitation, optimization of the facet coating and packaging for the high-power laser diode has been done over here. However, while applying this coating to the high-power laser diode the quality of the thin-film has to be examined. The laser induced damage threshold (LIDT) of the optimized single layer QWOT dielectric films using high-power solid state Nd:YAG laser was carried out. The effect of packaging on the reliability and performance of laser diode by measuring the device life-time is also discussed in this chapter. Finally, the device application in photoluminescence spectroscopy of InAsP/InP quantum well samples was demonstrated.

6.1 Introduction

High-power laser diodes (HPLDs) cover a broad range of applications starting from a simple laser pointer to a pump source in solid state lasers. These applications requires long lifetime of the device and hence, the reliability is a common critical issue for HPLDs. The reliability of semiconductor lasers has been in constant improvement for about four decades, since continuous wave (CW) lasing at room temperature was achieved [81]. From the scientific point of view, the situation of strong competition, and the requirement of the commercial and technological secrecy, was not helpful for accelerating the research on the degradation mechanisms existing in HPLDs. Hence, reliable devices are available in the market however the knowledge of the degradation mechanism responsible for degradation is very poor.

In general, laser diode reliability may be defined as *"the ability to operate the device satisfactorily in a defined environment for a specified period of time"* [148]. Unfortunately, there are few industry standards that address laser diode reliability [149]. The problems resulting from this situation include issues such as the calculation of laser reliability (from accelerated life test data) and the interpretation of subsequent reliability claims. The chapter discusses in brief about various degradation modes and estimation of device lifetime. Also, the laser induced damage threshold (LIDT) measurements of

different dielectric films has been demonstrated as an alternative to catastrophic optical mirror damage (COMD) testing to the device. Finally, we have demonstrated a successful application of indigenously developed laser package in photoluminescence (PL) spectroscopy of InAsP/InP quantum well.

6.2 Degradation Phenomena in High-Power Laser Diodes

The state of the art in applications of the high-power laser diodes (HPLD) are the forces that drive the growing importance of understanding the reliability and the degradation phenomena of laser diodes. Hence, for any application of laser diodes, the major degradation mechanism has to be recognized. There are several types of degradation modes depending on the initial period of degradation, degradation rate and the degree of degradation. Figure 6.1 illustrates various degradation mechanisms generally observed in laser diodes. These modes can be classified by location of degradation viz. internal or external degradation. The internal degradation occurs only inside the laser crystal which includes degradations of the active layer and p-n junction, whereas the external degradation occurs outside the laser i.e. degradation of facets, solder material, and contact electrodes.

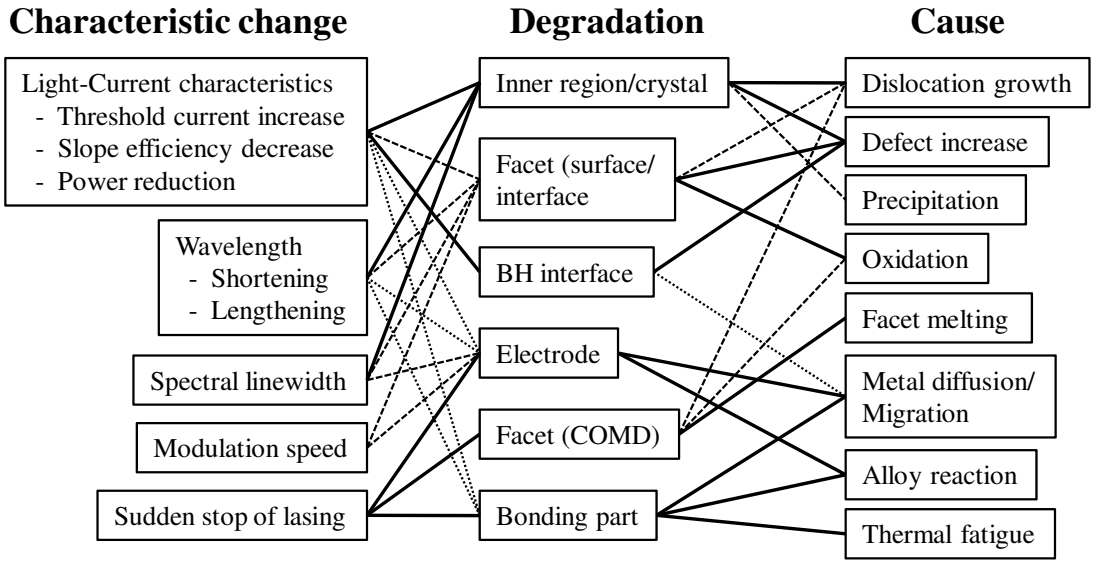

Figure 6.1: Main degradation mechanism of edge-emitting laser diode. The bold-lines, dashed-lines and dotted lines, respectively, indicates strong, moderate and weak correlation [150].

During the operation of the HPLD, usually decrease in the optical output power under a constant driving current or an increase in operating current during constant power operation indicates the device degradation. Typically, these changes are mainly caused by an increase in internal optical losses and decrease in injected carrier lifetime. These parameters directly affect the performance parameters of the laser viz. threshold current and differential or external quantum efficiency. Basically, based on the rate of change in device characteristic, for example optical output power, one distinguishes between three main failure modes: rapid, gradual, and catastrophic degradation, shown in Fig. 6.2 [151].

The rapid degradation occurs in the very initial phase of the device operation that can be detected by a very fast decrease in output power at a constant driving current or device efficiency. Basically the rapid degradation is characterized by an abrupt (< 50-100 hr) change to zero efficiency and is usually accompanied by the presence of dark-line defects–so called because they appear as regions of reduced efficiency in luminescence or lifetime plots.

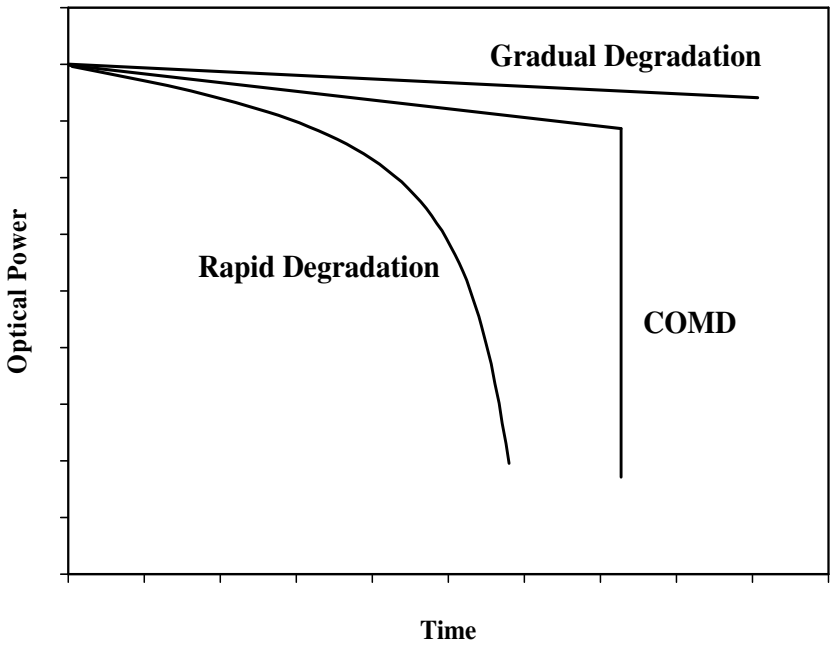

Figure 6.2: Various degradation modes of laser diode.

In today's high-quality quantum well (QW) lasers, rapid degradation phenomena rarely occur and the lifetime of lasers is generally limited by the other two mechanisms, i.e., gradual or catastrophic degradation. The gradual degradation can be described as a slow (~ 0.1-10 % per khr) decrease in efficiency which is, however, spatially uniform.

The point defect generation is responsible for this degradation mode. The ultimate lifetime of the laser diode is determined by gradual degradation which occurs over a long period. The lifetime can be estimated by extrapolating the power versus time curve at constant current or the drive current versus time curve for constant power until a definite change in value of respective entity is exceeded [152]. The maximum optical power of HPLD, however, is mostly limited by the catastrophic optical mirror damage (COMD). It is the irreversible failure of the device due to instantaneous melting at the facet at excessive power levels. The understanding of COMD mechanism is crucial, since it is one of the major killing factors for HPLDs.

6.2.1 Rapid Degradation

The rapid degradation process occurs in the active region, because of an increase in nonradiative recombination. The high-power operation of laser diodes at high input current densities creates high-energy carriers and thermal gradients, which have the potential to generate nonradiative recombination inside the active region. This increase in nonradiative recombination causes an increase in internal absorption loss and shortens the injection carrier lifetime. In general, when a laser diode is operated with constant output power or input current, there are cases in which operating current or optical power rapidly increases or decreases, respectively, within few hundred hours, known as '*rapid degradation*'.

The root cause for this degradation is generation and growth of the dislocations within the active region, and also formation of precipitate like defects of host atoms. The basic characteristics of the rapid degradation are: (1) rapid decrease in the optical output power of the laser diode during constant current operation (or increase in operating current while operating the laser diode at constant output power), (2) formation of the non-emitting regions within active layer viz. dark-spot defects (DSDs) [153], dark-line defects (DLDs) i.e. linear regions of significantly reduced radiative efficiency [154], and dark regions [155]. Here, in case of rapid degradation the life time of the laser diode is ≤ 100 hours at room temperature. This type of degradation is due to either recombination enhanced dislocation climb (REDC) or recombination-enhanced dislocation glide (REDG) [156].

6.2.2 Gradual Degradation

In contrast to rapid degradation, gradual degradation is characterized by a slow decrease in optical power or efficiency while operating the laser diode in constant current mode or increase in operating current in constant optical power mode of operation. The gradual degradation remains extent even after the complete removal of the rapid degradation and continuous over a long period. The rate of degradation depends on a variety of factors starting from device fabrication to its operating conditions viz. crystal growth parameters, material systems, strain, operating temperature and drive operation mode. The characteristic of the gradual degradation is a uniform darkening in the active region along with a gradual increase in deep level concentration [157]. The self destructing loop of nonradiative recombination generation at existing point-defects (vacancies and/or interstitial atoms of host elements) and development of new point-defects increase with time and this leads to reduced quantum efficiency. Point defects generated in the process can migrate and merge into defect clusters and micro-loops [158]. Ultimately, it is this mode that determines the lifetime of a component.

6.2.3 Catastrophic Optical Mirror Damage (COMD)

The maximum output optical power of HPLDs is mostly limited by the catastrophic optical mirror damage (COMD). The COMD mechanism can be illustrated by a number of related degradation feedback loops at the cleaved laser diode facets as shown in Fig. 6.3.

At high optical output power, facet heating leads to the third degradation process, namely COMD. Todoroki et al. [159] and Brugger et al. [160] have measured the laser mirrors temperature up to 450 °C by means of Raman scattering spectroscopy during CW operation of the device. Such high temperatures drive the facet degradation process which is triggered by oxidation of the facets. Figure 6.3 shows the self-destructing feedback loops at the cleaved laser diode facets leading to the damage of the facet and so the failure of the device. All the processes leading to a degradation of a diode laser are described in detail in [161]. The reason for the initial absorption of stimulated emission at facets is that there are interface states at the semiconductor–insulator interface. These interface

states are increased by oxidation of the semiconductor material. This absorption induces the nonradiative surface recombination of the excitons, electron-hole pairs, in the facet regions and hence the facet heating followed by bandgap reduction. This bandgap reduction increases the light absorption at the facets, and a feedback loop develops. This effect will be enhanced by current crowding at the facet due to the lower bandgap [162]. Finally, if the absorbed energy is high enough, a self-destructing feedback loop generates which leads to spontaneous facet damage, known as COMD.

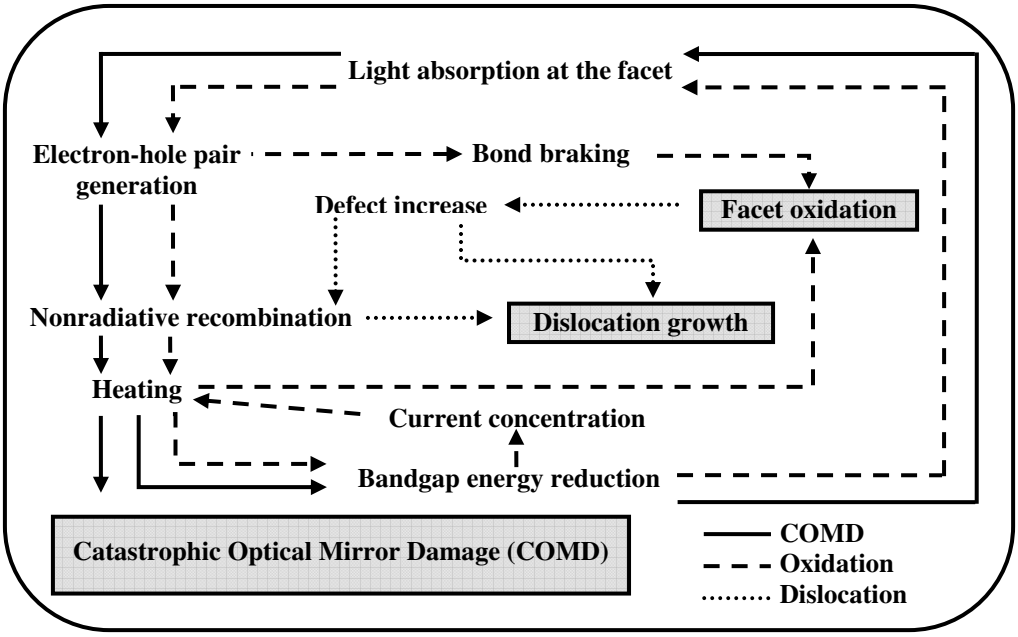

Figure 6.3: Degradation mechanism in edge-emitting laser diode. This self-destructing cycle of laser diode degradation finally comes to an end with catastrophic optical mirror damage (COMD). [163, 164]

In case of the HPLD the high-power density in a small volume can easily reach up to the order of MW/cm^2 at the facets region. This high-power is near to the damage threshold of the laser facet. To reduce the probability of the facet damage, various approaches have been reported. To decrease the initial light absorption at the facet, the bandgap near the facet has to be broadened. Also one can protect the facet from degradation by reducing the surface recombination velocity by means of cleaving the wafer into bars in ultrahigh vacuum or in a protective atmosphere and to evaporate an appropriate passivation layer on the surface [165]. The surface heating takes place by forward current due to the nonradiative recombination. This phenomenon will lead to

decrease in bandgap at the facet. One can put off the supply of the carriers to the area close to the facet [166].

6.3 Laser Induced Damage Threshold Measurement

The utilization of the HPLDs increases with technological advancements. The application of the HPLD systems is not only limited to the consumer electronics but also used in high energy systems [167]. Hence the HPLD is required to operate over a long period of time without any significant degradation in performance. The high-power operation of the laser diode is primarily limited due to the thermal rollover and/or the laser facet damage. The thermal limitations of the laser diode can be eliminated by various laser structure designs e.g. quantum well intermixing [168,169] while the laser facet damage can be improved by facet coating with appropriate dielectric materials besides the laser structure improvement [164].

The laser diode performance improvement can be achieved by single-layer ($\lambda/4$ thick) anti-reflection (AR) and $\lambda/4$ thick multi-layer high reflection (HR) coatings at front-and-back facet, respectively [170]. This dielectric facet coating serves as passivation and protection against external effects viz. oxidation, moisture effects, etc. It also enhances the maximum output power and efficiency by modification in facet reflectivity [171,172], and shows good stability during the long term operation [173]. Hence, with the development of HPLD the facet coating with high damage resistance need to be optimized.

The most common practice to investigate the laser diode facet coating properties is the pre- and post-laser diode characterization viz. Optical power(L)–Current(I)–Voltage(V) testing. In addition to that some researchers put efforts to measure the long term reliability and catastrophic optical mirror damage (COMD) test of the laser diode after facet coating. The COMD of the laser diode is a spontaneous (occurs without prior significant) event due to the high-power density at the facet region. The COMD event is random and the theoretical models proposed for the damage mechanism are device dependent. The probability of COMD occurrence in most of the applications of the laser diode is infrequent, especially in case of longer wavelength devices. So it is good to

characterize the facet only for its damage threshold rather than characterize it after device facet coating, which costs not only the material processing but also the whole device failure.

One possible way to find the damage threshold of the optical thin-film is the laser induced damage testing. The laser damage threshold (LDT) is defined as the fluence (energy density per unit surface area, J/cm^2) at which an irreversible damage/change occurs in the optical material as a result of laser illumination [174]. Various methods have been demonstrated for measuring the laser induced damage threshold (LIDT) of the thin-film optical coating viz. 1–on–1, S–on–1, R–on–1 etc. A common method is to expose a focused laser beam on to the sample and after illumination the coating is inspected for the damage using microscopy [175].

The present thesis discusses the LDT measurement of the optical thin-films deposited on to the GaAs samples with varying thicknesses viz. λ/4, 3λ/4, and 5λ/4. The diode pumped Q-switched Neodymium Yttrium Aluminum Garnet (Nd:YAG) laser (1064 nm) was used to damage the samples. The sample prepared for LDT was characterized for its reflectivity before the damage test. The laser induced damage was observed initially by visible flash and finally under microscopic observation. The preliminary results show that the damage on the samples was only due to the heating effect rather than optical absorption into the sample. Moreover, there was no significant effect observed on LDT as a function of film thicknesses.

6.3.1 Experimental

The single layer anti reflection (AR) coatings of the Al_2O_3, MgF_2 and SiO_2 (MERCK) were deposited in a 270° bend 6 kW electron beam evaporation system in a high vacuum coating unit (Hind High Vacuum Co. (P) Ltd.). The system is equipped with thin film deposition controller (SQC-122c SIGMA) to precisely monitor and control the thickness and deposition rate of the thin film. The single layer coatings were carried out on GaAs substrate and optimized for the wavelength ~1060 nm. The substrate was cleaned thoroughly using trichloroethylene (TCE), acetone, and methanol. The AR films have been deposited with constant rate of 2 Å/sec on a rotating substrate (30 rpm). Radiant

heater was used to maintain the desired substrate temperature of 200 °C. The reflectivity of the deposited film on a GaAs substrate was measured ex-situ.

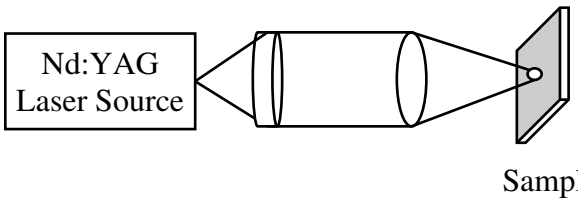

Figure 6.4: The schematic of the laser damage threshold measurement of single layer QWOT antireflection thin films deposited on the GaAs substrate.

The standard methods for the laser damage threshold measurement are 1–on–1, and S–on–1 tests [174]. The limitations of these methods are complex implementation and data analysis is time-consuming and each experimental condition requires exposing a sample to the new damage site. Hence, an unconventional laser damage test has been performed as per the available facility. Figure 6.4 shows the schematic of the laser damage threshold measurement of the single layer QWOT antireflection thin films deposited on the GaAs substrate. The LDT test was carried out using diode pumped Q-switched Nd:YAG laser system (Model. Hallmark Diode, Sahajanand Laser Technology Ltd., INDIA). The laser produced a beam with a gaussian spatial profile. The detail technical specification of the laser system used for pulse LDT is mentioned in Table 6.1.

Table 6.1: Laser system specification used for the pulse LDT measurement

Laser Source	Diode Pumped, Q-switch Nd:YAG
Wavelength	1064 nm
Beam Mode	TEM_{00}, M2 < 1.2
Laser Power (Avg.)	0.5 to 1.5 W
Pulse width	100 ns
Pulse Frequency	200 Hz
Resolution	1 μ
Output beam diameter	6 mm ($1/e^2$)

The beam spot size was set by adjusting the distance between the sample and positive/focusing lens (focal length = 70 mm) i.e. 1.17 mm for pulse mode and 0.39 mm for continuous wave (CW) LDT measurement. (Focal length = 77 mm). To avoid the

effect of interference and reflection of the irradiated laser from the sample to the source, the sample was adjusted slightly displaced from the normal. The average output power of the collimated laser beam was measured with power meter (Laser power meter, OPHIR Photonics). The servo-motor enables the sample to travel across the laser path (with speed of 200 mm/s) that irradiates the laser with frequency of 200 Hz. The damage sight on the coated sample was observed using a polarization microscope (LABOURLUX 11, Leitz).

6.3.2 Results and Discussion

❖ Reflectivity Measurement

The mirror polished GaAs sample was coated with single layer quarter wave optical thick (QWOT) of different dielectric materials viz. Al_2O_3, MgF_2, and SiO_2. The LDT was measured for the samples with different material thickness viz. λ/4, 3λ/4 and 5λ/4 optimized for the wavelength ~1060 nm. The reflectivity of the coated thin films on GaAs substrate was measured using self assembled reflectivity measurement setup. The experimental reflectivity was measured with reference to the standard gold mirror and compared with simulated results. Figure 6.5 shows the experimental and simulated reflectivity of the optimized sample. The reflectivity simulation was discussed by V. A. Kheraj et al. in detail [119]. The reflectivity measured for other samples with different thickness is shown in Table 6.2.

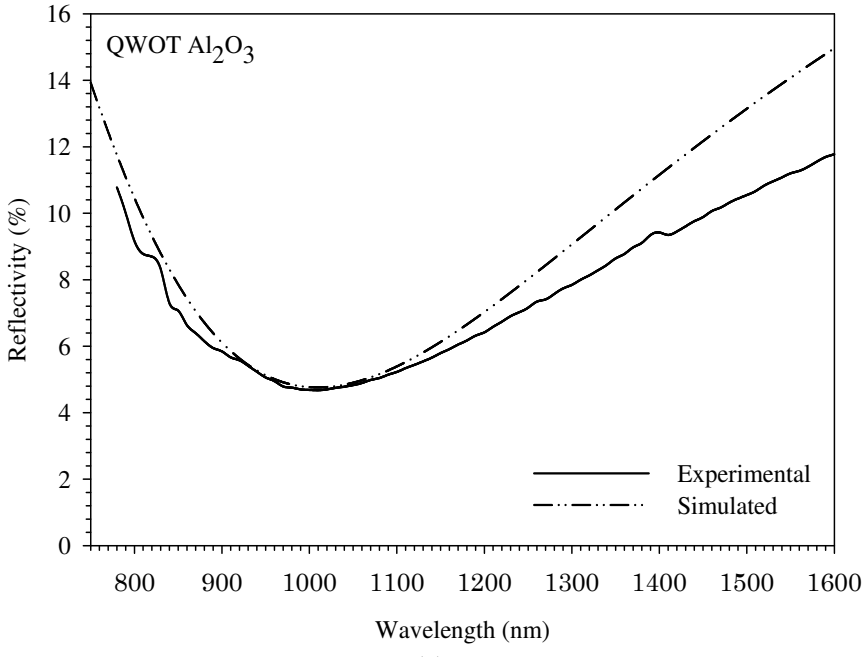

(a)

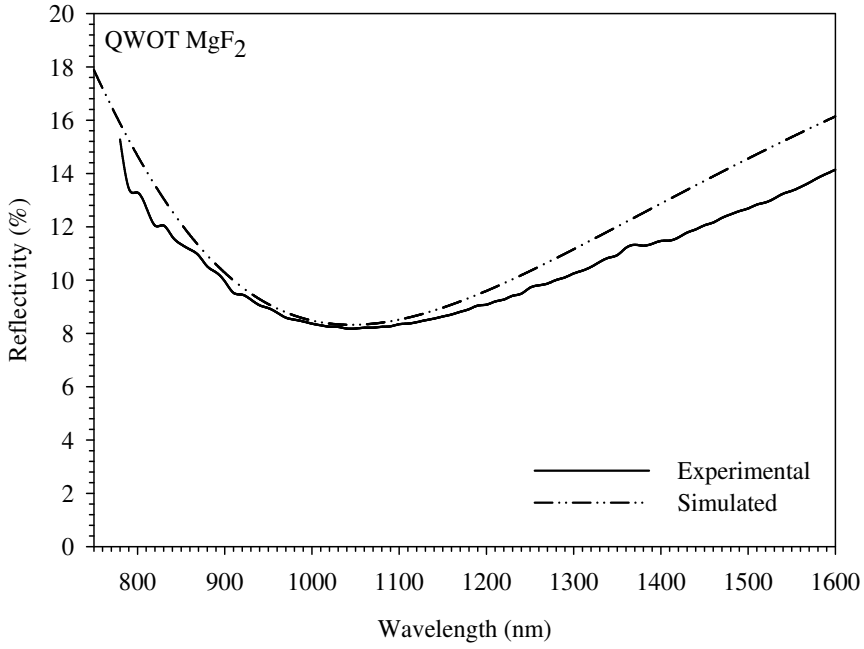

(b)

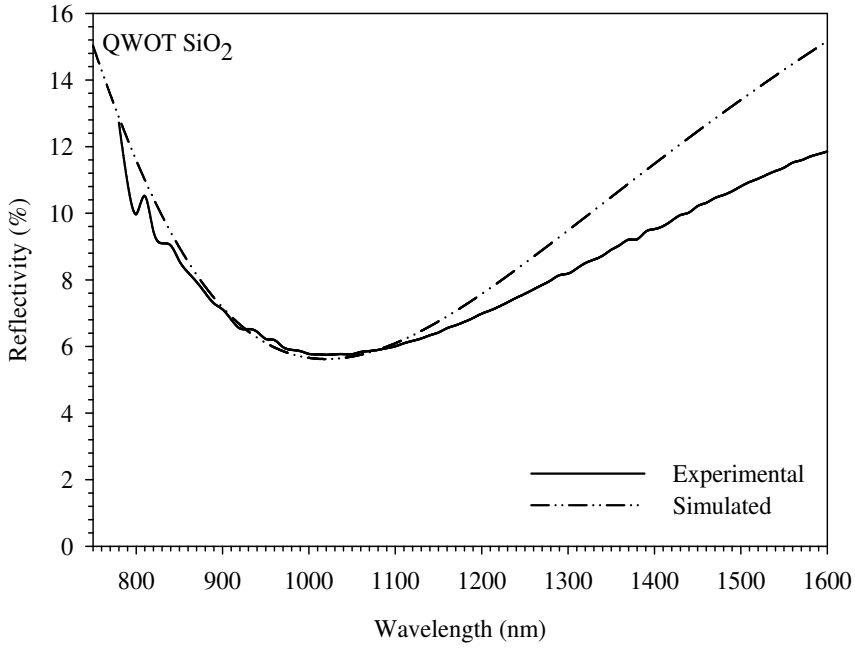

(c)

Figure 6.5: Optimized QWOT single layer facet reflectivity curve for (a) Al_2O_3, (b) MgF_2 and (c) SiO_2

Table 6.2 – The measured and calculated thin film parameters.

Material	Thickness (Å)	Reflectivity (%)	
		Exp.	Sim.
Al_2O_3	λ/4n	4.89	4.97
	3λ/4n	6.63	7.09
	5λ/4n	5.63	6.32
MgF_2	λ/4n	8.21	8.33
	3λ/4n	7.04	8.24
	5λ/4n	6.60	6.75
SiO_2	λ/4n	5.83	5.75
	3λ/4n	5.20	5.32
	5λ/4n	6.57	6.61

❖ LDT Measurement

The samples were irradiated with increasing beam fluence up to 1.5 W average power (starting from 0.1 W with 0.1 W step increase) for pulse LDT. In case of CW LDT measurement the power was increased up to the damage with 1 W step increase. The spacing between consecutive damage spot with different fluence was kept enough to avoid the intermixing of damage conditioning on nearby damage spots. The preliminary confirmation of the damage to the samples was by observing spark/flash during irradiation and also using CCD camera (75X zoom) mounted on the laser system. After each irradiation to the sample the damage site's snap shot was taken to compare the influence of the increasing damage fluence.

In case of pulse LDT measurement increase in the diameter of the damage spot with increasing laser power was observed for all samples, as shown in Fig. 6.6. Tables 6.3 and 6.4 contain the LDT data of Al_2O_3, MgF_2 and SiO_2 measured in pulse mode and CW operation, respectively.

Table 6.3: Laser damage threshold (Pulse mode) of materials with beam diameter = 1.17 mm, frequency = 200 Hz, Pulse width = 100 ns

Experimental Parameters	Materials		
	SiO_2	Al_2O_3	MgF_2
Average Power (W)	0.85	0.8	0.7
Energy / pulse (mJ)	4.25	4.00	3.50
Peak power (kW)	42.5	40.0	35.0
Peak power density (MW/cm^2)	3.95	3.72	3.26

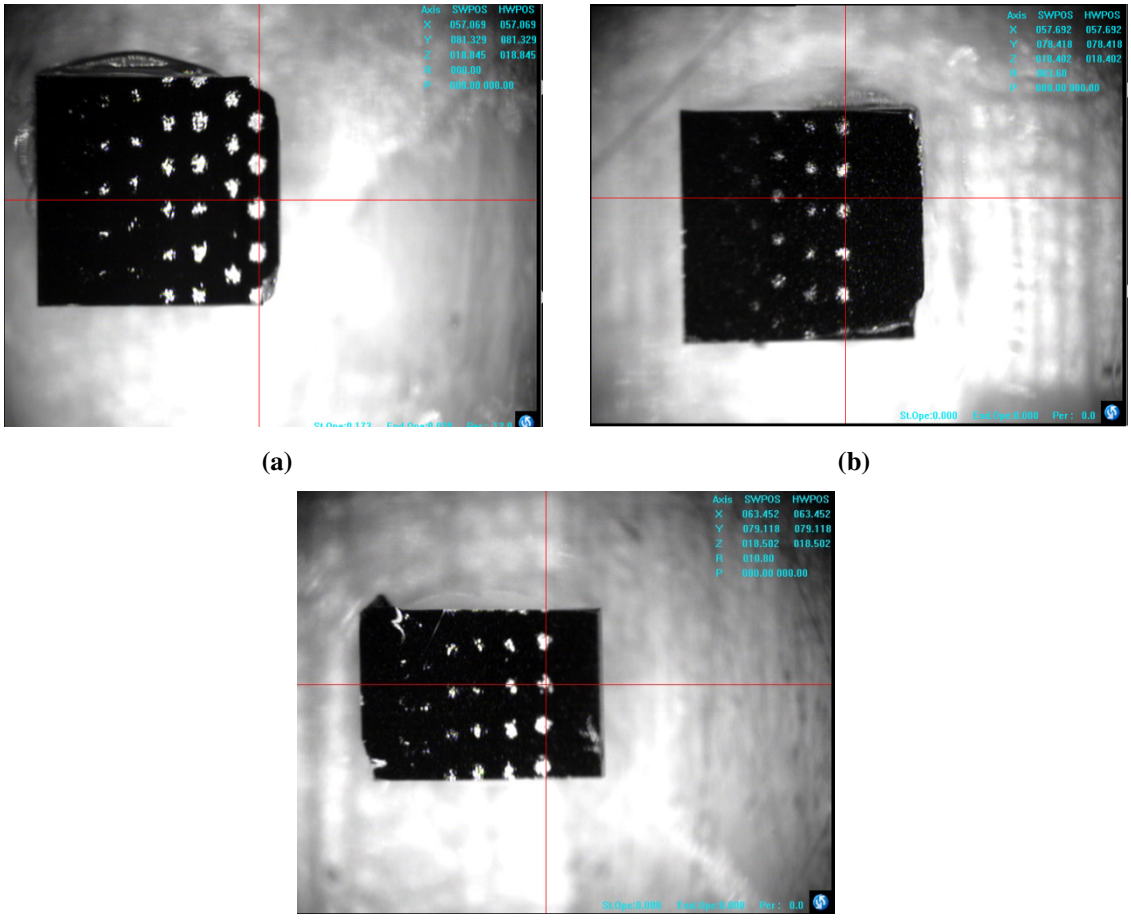

(a) **(b)**

(c)

Figure 6.6: Photographs of pulse laser induced damage for single layer QWOT (a) Al_2O_3, (b) MgF_2, and (c) SiO_2 on GaAs substrate

The damage threshold of the sample with different thickness is almost equivalent and there is no observable difference found on the sample observed under the microscope. It has been reported by T. W. Walker et al. [175] that the LDT of the oxide materials shows no significant change as a function of thickness while MgF_2 shows small variation in LDT with thickness. The microscopic observation of the CW laser induced damaged site clearly illustrates the melt substrate material as shown in Fig. 6.7.

Table 6.4: Laser damage threshold (CW mode) of materials with beam diameter = 0.39 mm

Experimental Parameters	Materials		
	SiO_2	Al_2O_3	MgF_2
Average Power (W)	10	16	11
Power density (kW/cm^2)	8.37	13.39	9.21

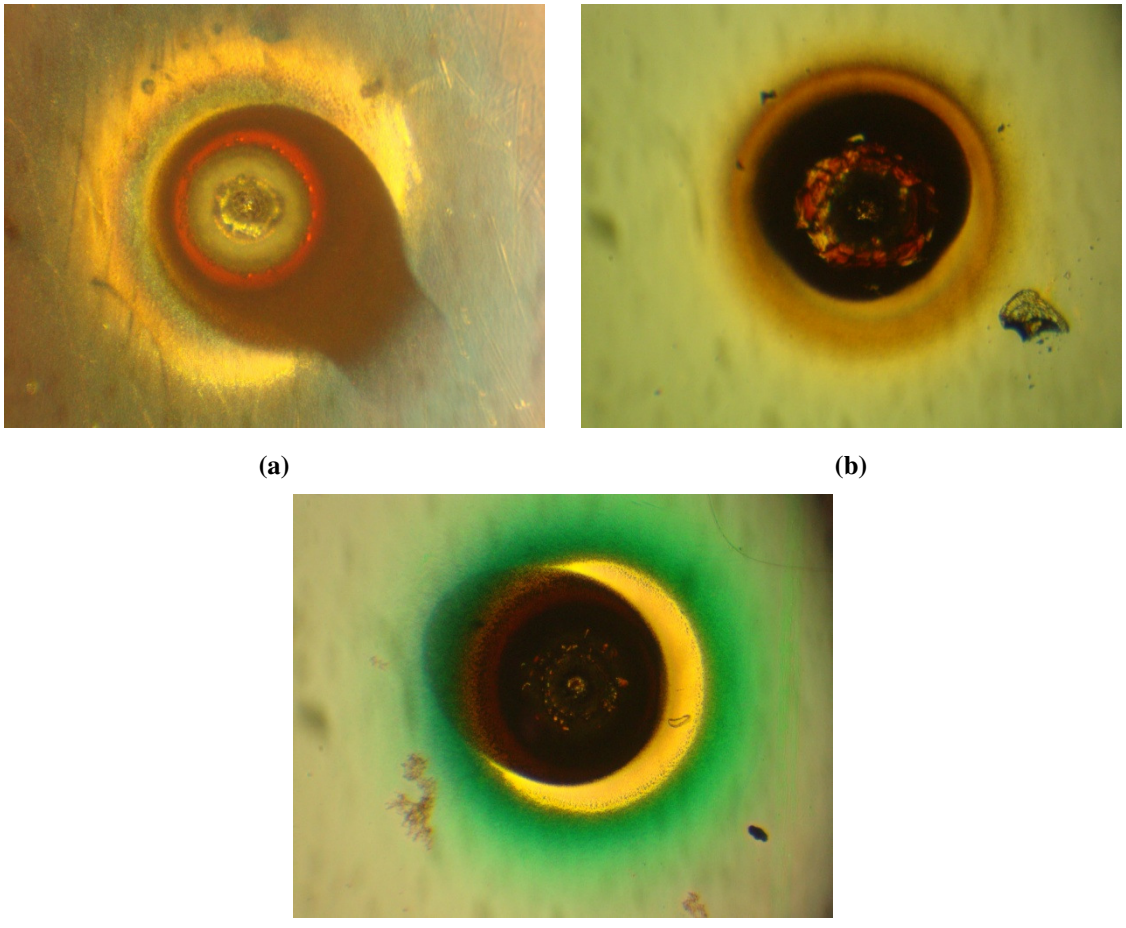

(a) **(b)**

(c)

Figure 6.7: Microscopic view of the single layer QWOT (a) Al_2O_3, (b) MgF_2, and (c) SiO_2 CW laser induced damage site.

The damage to the sample is entirely because of the heating effect. The impurity percentage and surface defects in the substrate and the deposited material play a vital role in absorption and hence heating into the sample. The absorption of the laser energy leads to the nonradiative relaxation on excited electrons and hence causes the heating. The heat around the irradiated area cause expansion of material and finally melts it. Also, A.V. Kaunar et al. have reported that the GaAs with mirror polished surface has less surface absorption than other rough surfaces and hence higher laser damage threshold [176]. The average damage spot site diameter was ~150 μm, which leads to CW LDT >55 kW/cm^2. The catastrophic optical damage (COD) limit of the commercially available bare HPLDs is of the order of few hundred watts. Hence we can certainly utilize this facet coating to improve laser diode COD limit.

6.4 Lifetime Measurement

Lifetime measurement is an important phase for the study of device degradation as well as reliability testing during the fabrication process of laser diodes. Life tests generally involve monitoring the operation of a laser diode under carefully controlled conditions. Degradation is observed and recorded throughout the test by precise measurement of changes in the laser's operating characteristics. However, it is not possible to obtain sufficient amount of test data within specific time period while operating the device under normal use condition, especially when device having high reliability and long lifetime. Therefore it seems impractical to run the device over a long period of time only to measure its lifetime. Hence, the lifetime measurements are performed at high stress conditions to get enough data within relatively small time period and that can be fitted to various empirical models depending on stress parameters. Usually stress parameters includes in lifetime testing are temperature, current, power, voltage, humidity and ambient pressure either taken singly or in combination.

We have developed the VI using LabVIEW (ver. 8.2) that allows the life time measurement. Generally the lifetime of the laser diode can be measured in either automated current control (ACC) or automated power control (APC) mode. In ACC mode the laser drive current should remain constant while in APC mode the laser output power should remain constant. Moreover, for accelerated aging, the experiment can be carried

out at higher temperature. We have estimated the lifetime of the laser diode using ACC mode under accelerated aging condition. The constant operating current is supplied to the laser diode using constant current source meter (Keithley 2420C). The voltage across the diode is also measured by Keithley 2420C. The output light is made to fall into the integrated sphere and the signal from the photodetector is measured with the help of PCI-6024E Data Acquisition (DAQ) card. The laser diode is kept at constant temperature using a TEC (Thermo Electric Cooler) to avoid temperature instability during the experiment. The experiment is carried out in a dark room to avoid effects of other light sources. The VI records and displays the current, the voltage across the laser diode and the optical power at the desired interval of time.

The whole experiment is provided with the UPS backup system in order to avoid problems of electrical power failures during the experiment which runs for a few days. Further, Laser diode life test studies require the accurate measurement of changes in laser operating parameters as small as a few percent over thousands of hours. Consequently, the stability of the measurement equipment must be very high, typically on the order of 0.1 % per 1000 hours. The DAQ card PCI-6024E provides the stability of 0.01 % per 1000 hours.

In ACC mode, when user stops the experiment, the VI plots the optical power over the complete experiment time and the power versus time curve is fit to the exponential decay curve of the type

$$y = A\exp[-Bx] \tag{6.1}$$

Thus, from Eq. 6.1, we get the life time of the laser diode as

$$\tau = \frac{1}{B} \tag{6.2}$$

The final result of life time is displayed on the front panel and recorded in the file along with the sample details and measurement mode. The front panel and the block diagram of the VI are shown in Figs. 6.8 (a) and (b) respectively.

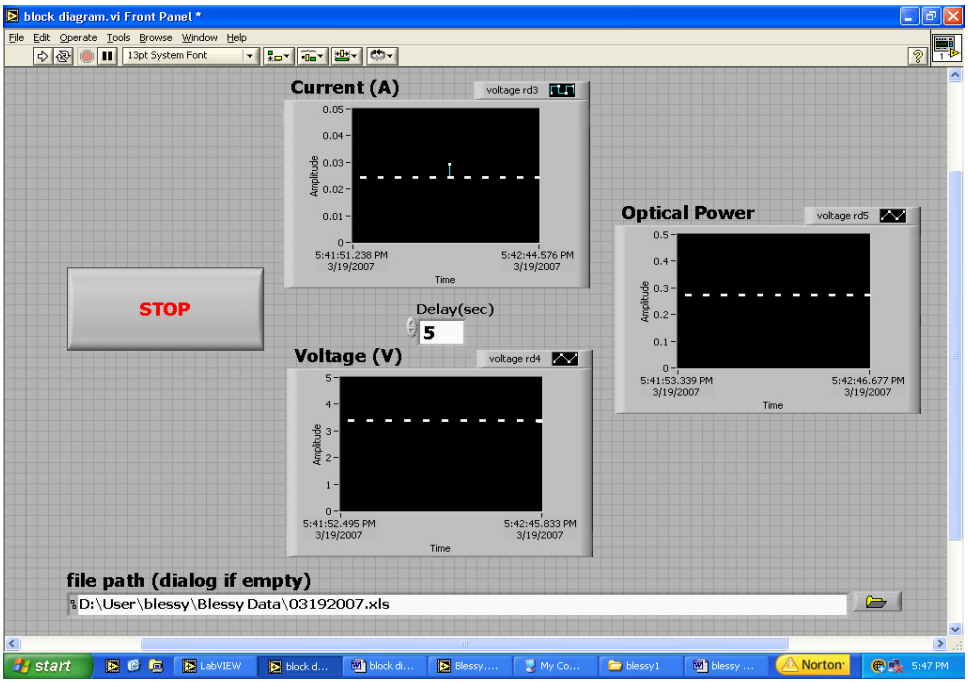

(a)

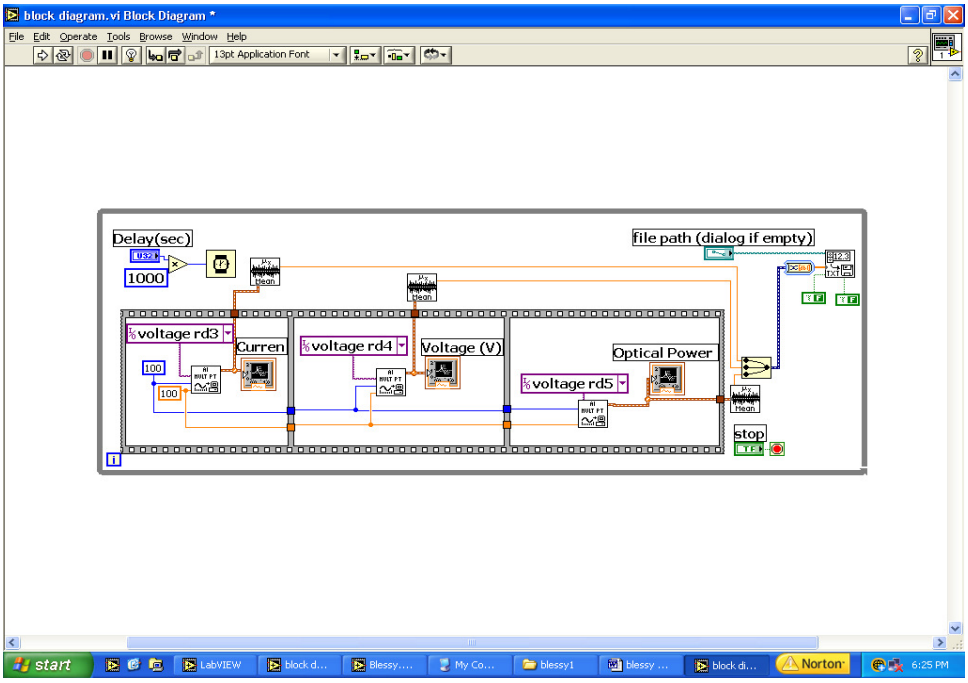

(b)

Figure 6.8: (a) Front panel and (b) block diagram of the laser diode life-time measurement VI.

6.4.1 Upgradation in Lifetime Measurement

We have upgraded an automated lifetime measurement facility for testing of laser diodes. The InGaP quantum well laser diode (λ = 650 nm) was tested for the optimization of the setup. Program itself monitors the input parameter viz. operating temperature and current.

The optical output power data will be stored and the extrapolation of this optical power as a function of time gives device life-time. The device was degraded by means of ACC mode, for measurement of laser diode lifetime. As the name suggest in ACC mode laser current is held constant for the duration of the test and the optical output power is monitored continuously. We have developed a (VI) using LabVIEW (ver. 8.2) that allows the measurement of output power being the function of time for accelerated aging.

The experiment was carried out at temperature, 80 °C. The applied constant operating current and device operating voltage across the diode was monitored using source meter (Keithley 2420C). The output light was made to fall into the integrated sphere (Lab-sphere 819IS) and photo-detector (Newport 818SL) assembly and output power was measured through PCI 6024E DAQ card. The laser diode was kept at constant temperature to avoid temperature instability during the experiment. The experiment was carried out in a dark room to avoid effects of other light sources. The schematic and photograph of the experimental setup is shown in Fig. 6.9.

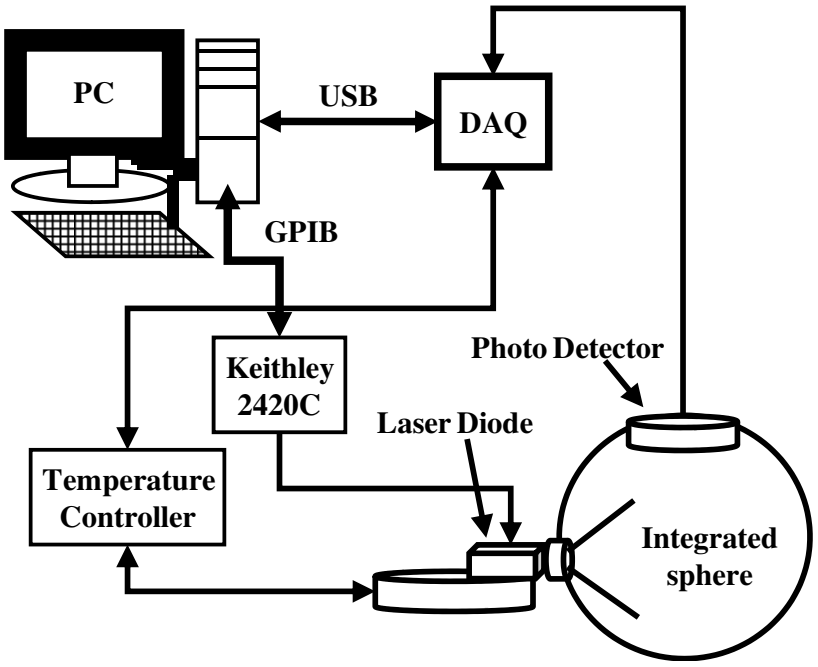

(a)

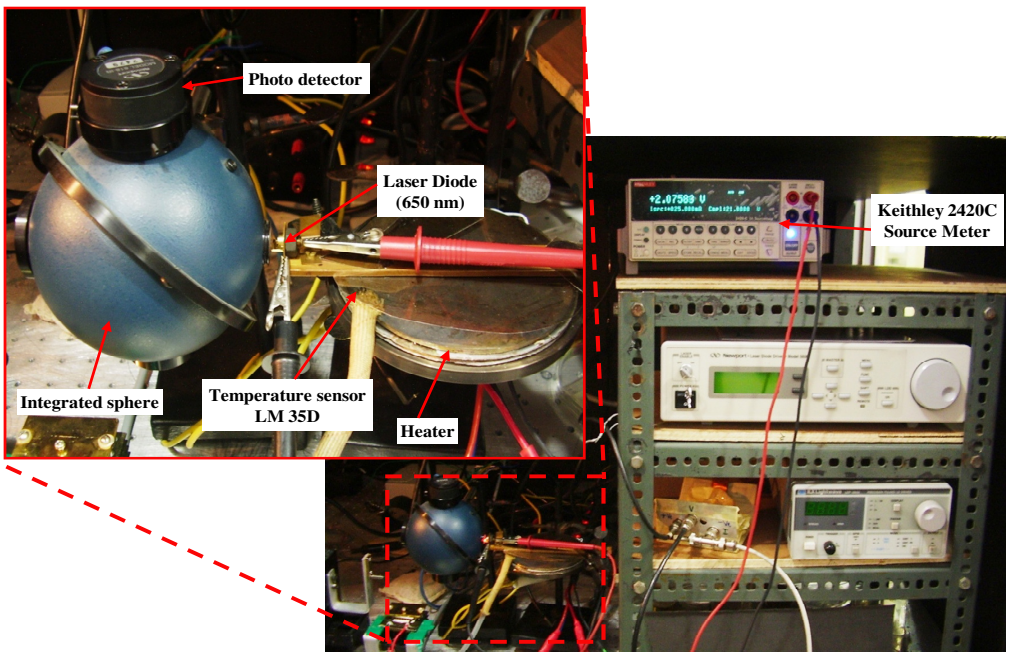

(b)

Figure 6.9: Experimental setup to find device lifetime, (a) Schematic and (b) photograph.

The developed program flow for the automation of the experiment and data acquisition follows the flowchart shown in Fig. 6.10. The front user panel and the LabVIEW block diagram are shown in Fig. 6.11 (a) and (b), respectively.

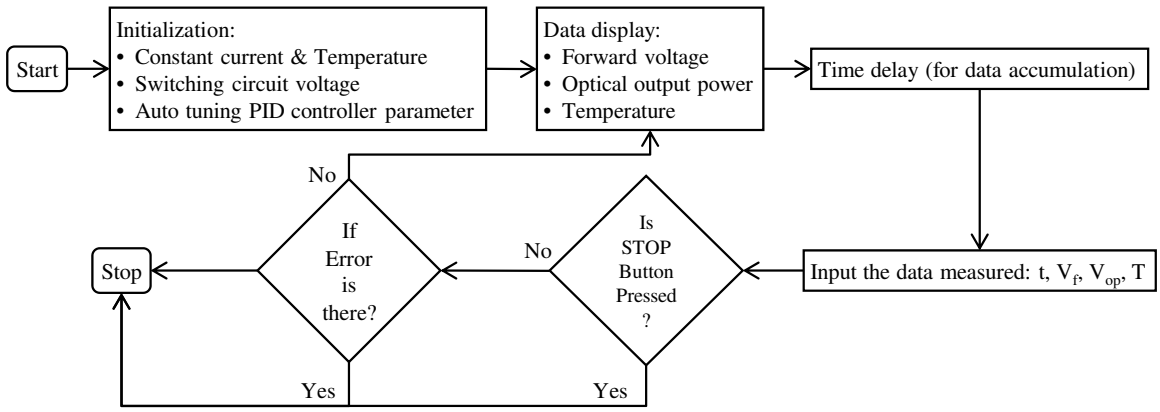

Figure 6.10: Flow of the program shows programming initialization as well as conditions to fulfill user requirement of the instrument automation and data acquisition.

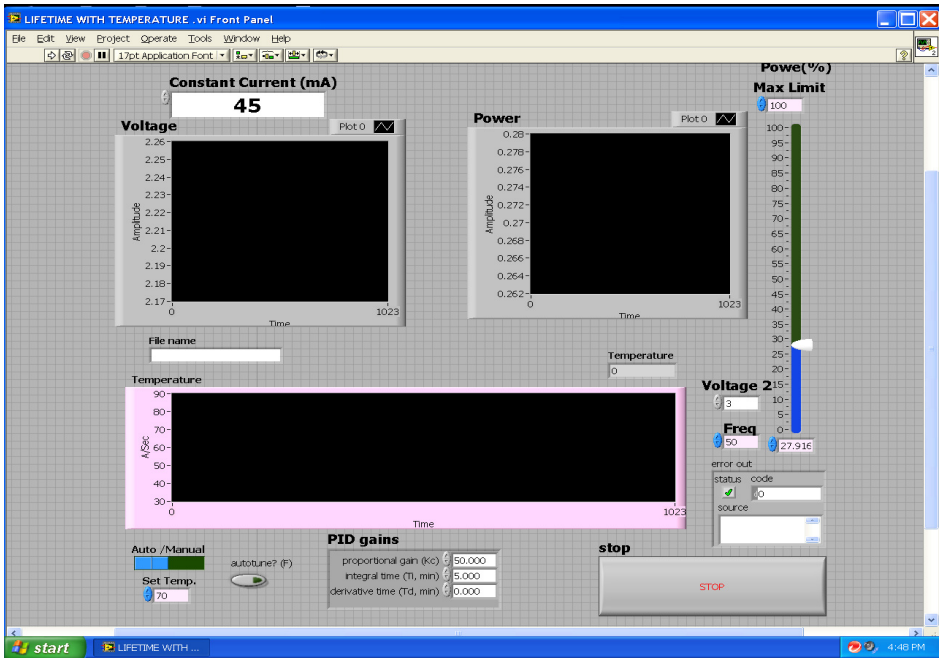

(a)

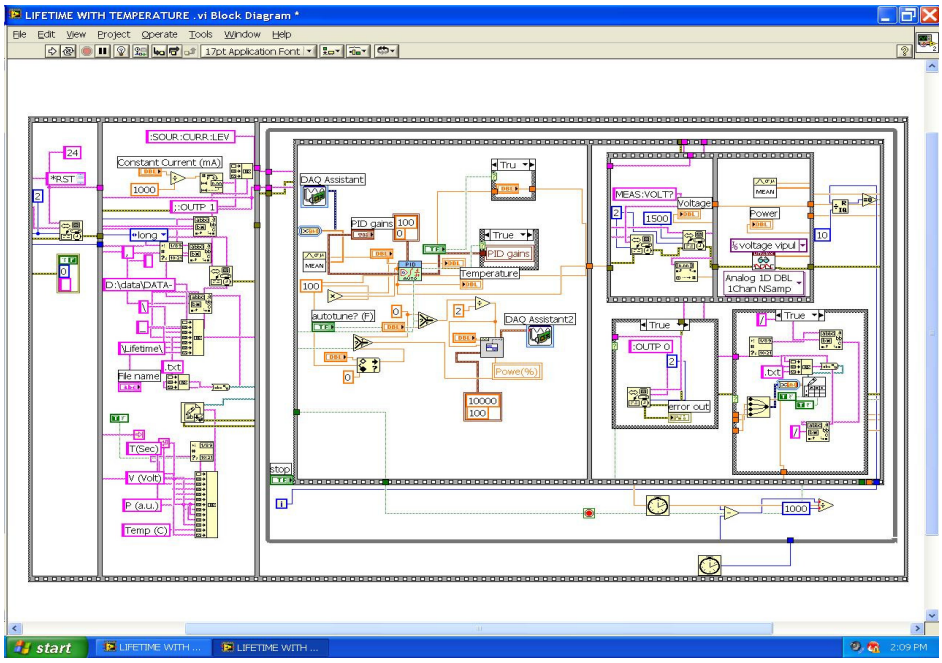

(b)

Figure 6.11: LabVIEW VI for Automated Lifetime Measurement: (a) User front panel enables the user to control all attached instruments and experimental parameter. (b) Block diagram shows graphical user interface and programming facility of LabVIEW.

6.4.2 Results and Discussion

Pre and post L–I–V tests at room temperature (24 °C) produced typical, well-behaved parametric curves for output optical power and voltage vs. operating current. These L–I–

V tests were performed before and after the 80°C burn-in. The results of these tests are shown in Fig. 6.12 (a) and (b).

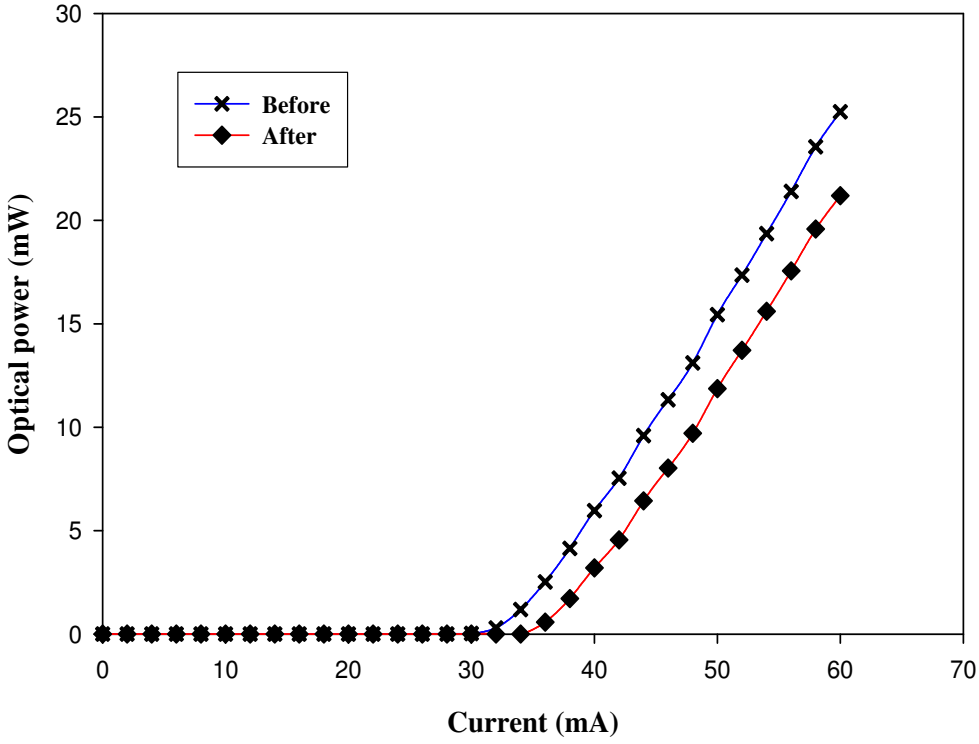

(a)

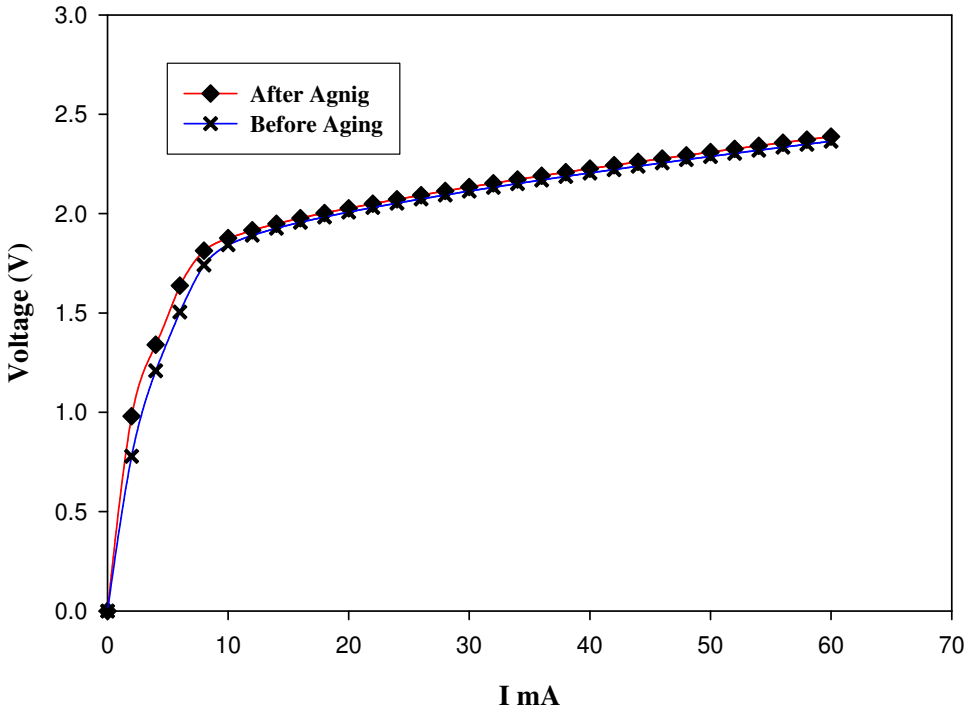

(b)

Figure 6.12: (a) L–I curve, (b) I–V curve of LD at room temperature before and after the reliability test.

Usually, the lifetime of laser diode is defined as the time period for 20 % decrease in optical output power or 20 % increase in operating current while operating the device under ACC or APC mode, respectively. Considering the same end-of-life criterion of 20 % increase of laser operating current over its initial value, Yajun Li [177] has reported lifetime extrapolation of 650 nm InGaAlP laser diodes measured at 70 °C for 1000 h under APC mode. Similarly, the lifetime of the 100 μm stripe width 650 nm broad area lasers has been estimated about 100,000 h at room temperature [178]. In our case, an aging test of 195 hr of the laser diode shows the degradation of device, as shown in Fig. 6.13, operating at 80 °C in automatic current control mode. By extrapolation of the data using Eq. 6.2 we find the device lifetime is ~ 35,000 hr, at 45 mA operating current and 80 °C ambient temperature.

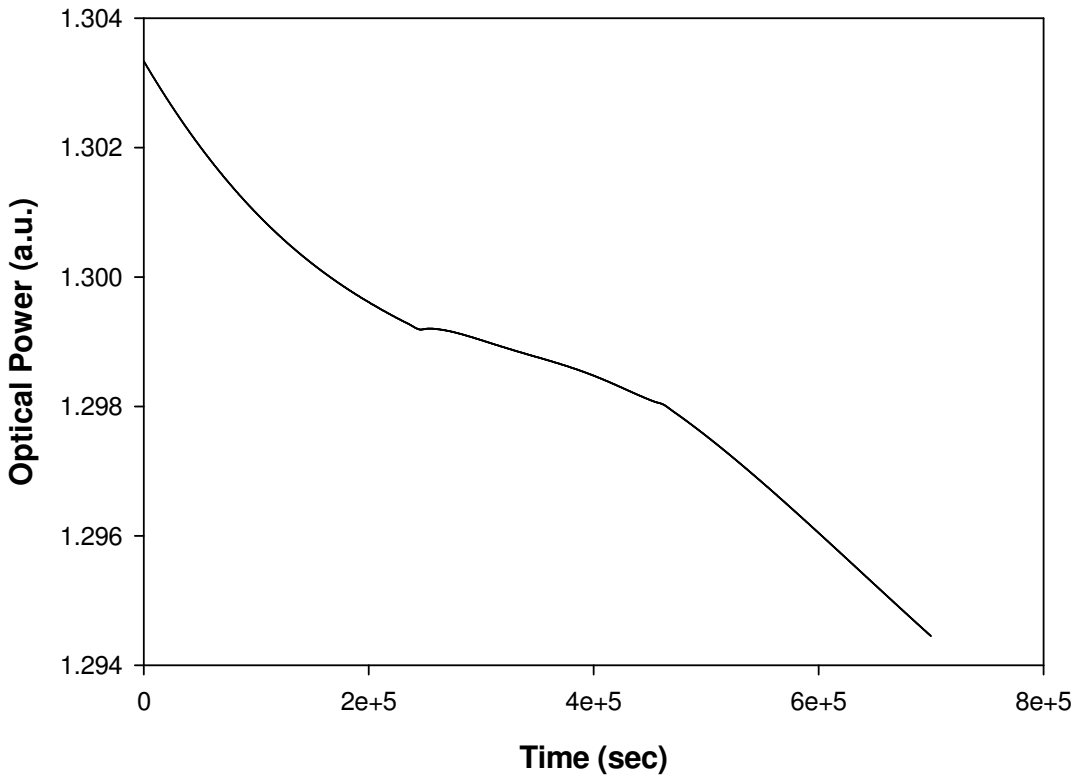

Figure 6.13: Optical output power of laser diode at constant operating current, 45 mA, as a function of time at 80 °C in ACC mode.

❖ Conclusion

The reliability of the 650 nm InGaP quantum well laser diode was measured using automated constant current (ACC) mode with accelerated aging. Extrapolation of the data for optical output power versus time gives the lifetime of device of the order of 10^5 hour at room temperature. The junction temperature was measured using electrical test method. Though the variation in forward voltage with respect to temperature is very small we find the quite good relation between junction temperature and operating current. We also observed that for the higher injection current value the linear relation does not hold true.

6.5 Application of 980 nm Laser Diode in Photoluminescence (PL) Spectroscopy

6.5.1 Photoluminescence

Photoluminescence (PL), as its name suggests, is define as the photon assisted spontaneous light emission from the material. Or, in other words, we can say that the excitation of an electron from ground state to higher energy state by absorbing a photon of energy $h\nu \geq E_g$ and subsequent emission of light when electron return to the ground state. Photoluminescence (PL) has been developed as a sensitive technique for semiconductor material analysis as the energy of the light emitted from the material corresponds to the difference in energy between the excited state and the equilibrium state involved in the electronic energy transitions. Hence, it is used to characterize semiconductor material for bandgap determination, detect and identify impurity level, recombination mechanism analysis, material quality measurement, etc. The radiative emission intensity is proportional to the impurity density. Impurity identification by PL is very precise because the energy resolution is very high.

Figure 6.14 shows usually observed transitions with PL. Excitation of a sample occurs via absorption of a photon and create electron-hole pair, called excitons. Eventually, these excitons will de-excite/recombine either radialtively or non-radiatively. Here, the primary interest in PL is the radiative recombinations since it is observable with

very high sensitivity. These various possible radiative recombination processes are illustrated in Fig. 6.14.

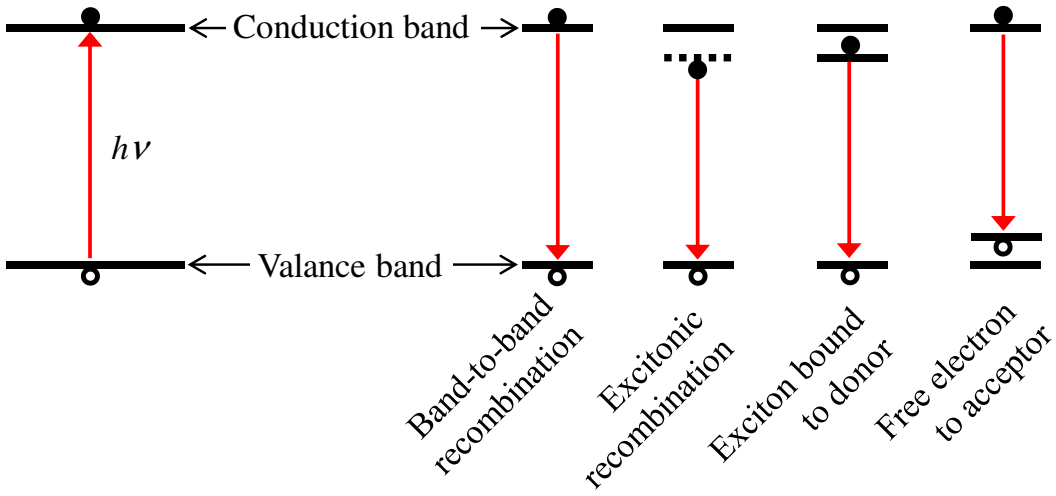

Figure 6.14: Transition during Photoluminescence. [179]

The analysis of PL data will give the following information.

1. The peak intensity gives information about the optical quality of sample. Higher the intensity better is the quality.
2. Bandgap related information.
3. The full width half maximum (FWHM) of the peak tells about the uniformity of layers (compositional and spatial). Narrower the FWHM better is the layer uniformity.

The main strength of the PL spectroscopy lies in its sensitivity to detect very weak signals (high signal to noise ratio), which depends on the quality of the sample. Its main limitation is weak or no PL signal for indirect bandgap materials. It provides only the lowest excited state information for quantum structures and requires low temperatures to suppress the luminescence from defects in case of low quality samples.

6.5.2 Experimental

A typical PL spectroscopy setup is illustrated in Fig. 6.15. Usually, the experimental set up of PL spectroscopy consists of an excitation source, a monochromator, photo detector and lock-in amplifier. Lasers are generally used as excitation source in most cases since

they are capable of delivering monochromatic and highly collimated beam. Also laser allows localized spatial resolution and determination of the penetration depth. The optics used in the set up is such a way that to ensure maximum light collection from the sample. The apparatus shown in Fig. 6.15 has a lens system which is closely matched to the f-number (in our case, 4) of the monochromator. Here, C is chopper, F is filter, L is lens, S is sample, S_1 and S_2 are input and output slits of monochromator respectively, G is grating and D is detector (in our case Ge detector).

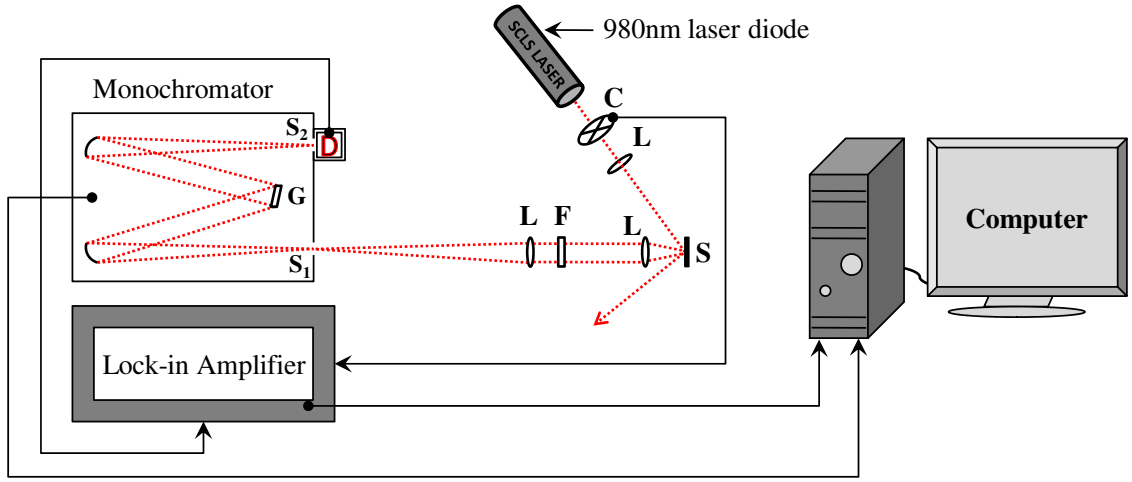

C – chopper, D – Ge detector, F – filter, G – grating, L – lens, S – sample, S_1 & S_2 – slits

Figure 6.15: Block diagram of Photoluminescence set up.

In this setup is we have used laser that we have developed having wavelength 980 nm operated at 4.7 mW/facet CW power and germanium (Ge) detector is used which detect wave length ranges from 1050 nm to 1600 nm. This laser beam is chopped using a mechanical chopper (whose frequency is set using a lock-in amplifier). Chopping is necessary to improve the signal to noise ratio (~ 10^{-6}). The chopped beam is focused on the sample using lenses. We have used triplet lens which is a combination of two convex and one concave lens to collect and concentrate the beam coming out of the laser diode.

6.5.3 Sample Detail

We have done PL spectroscopy by using indigenously developed laser diode package on two InAsP/InP quantum well (QW) samples having thickness of 28 Å and 38 Å, as shown in Fig. 6.16. The structure of sample consists of $InAs_xP_{1-x}$ sandwiched between two undoped InP barrier layers. Then there are cap layers on the top side and the buffer layer

on substrate is of InP which is doped with Si with doping density 2.6 x 10^{17} cm^{-3}. The whole structure is grown on n^+ InP (001) substrate having doping density is of 1x 10^{18} cm^{-3}. Further details regarding the sample growth and characterization are discussed elsewhere [180].

n^+ InP, 1470 Å, 2.6 x 10^{17} cm^{-3}
Undoped-InP, 50 Å
Undoped-$InAs_xP_{1-x}$ QWs, 28 & 38 Å, x = 0.38
Undoped-InP, 50 Å
n^+ InP, 1470 Å, 2.6 x 10^{17} cm^{-3}
n^+ InP (001), Substrate 1 x 10^{18} cm^{-3}

Figure 6.16: InAsP/InP single quantum well sample structure.

6.5.4 Photoluminescence Measurement

The laser diode, developed in semiconductor laser section (SCLS), Raja Ramanna Center for Advance Technology (RRCAT), Indore, has been used as a source of excitation in photoluminescence (PL) spectroscopy. The PL of InAsP/InP single QW has been measured with CW power 4.7 mW at low temperature, 10 K. The measurement has been carried out at low temperature to reduce losses due to scattering and leakage of carriers. Two different laser sources, one 532 nm commercial laser and the second one is 980 nm semi-package LD developed at SCLS. Figure 6.17 shows the PL with SCLS laser as a source of excitation to find the electronic transition in the QW samples which is confirmed with reproduction of the results using commercial laser.

As shown in the Fig. 6.17, the first peak at 1000 nm corresponds to source wavelength itself. There is shift in source laser wavelength may be due to continuous use and thermal degradation of device. The recorded peaks at ~1120 nm and at ~1230 nm corresponds to the sample with QW thickness 28 Å and 38 Å, respectively.

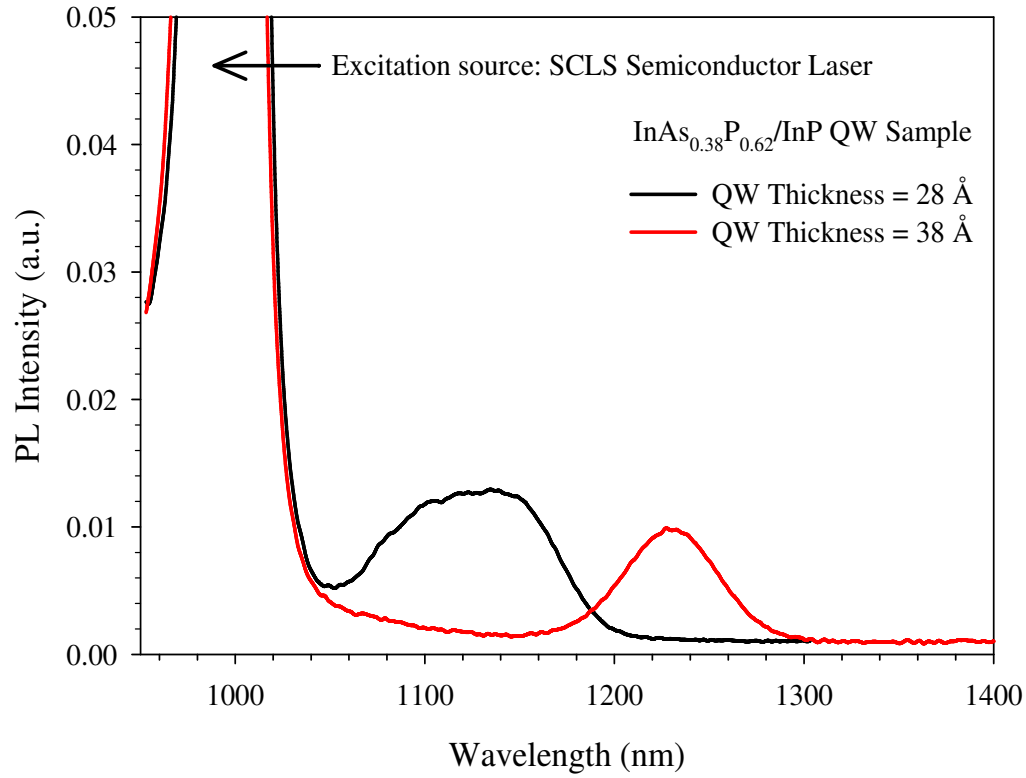

Figure 6.17: PL with 980 nm SCLS Laser

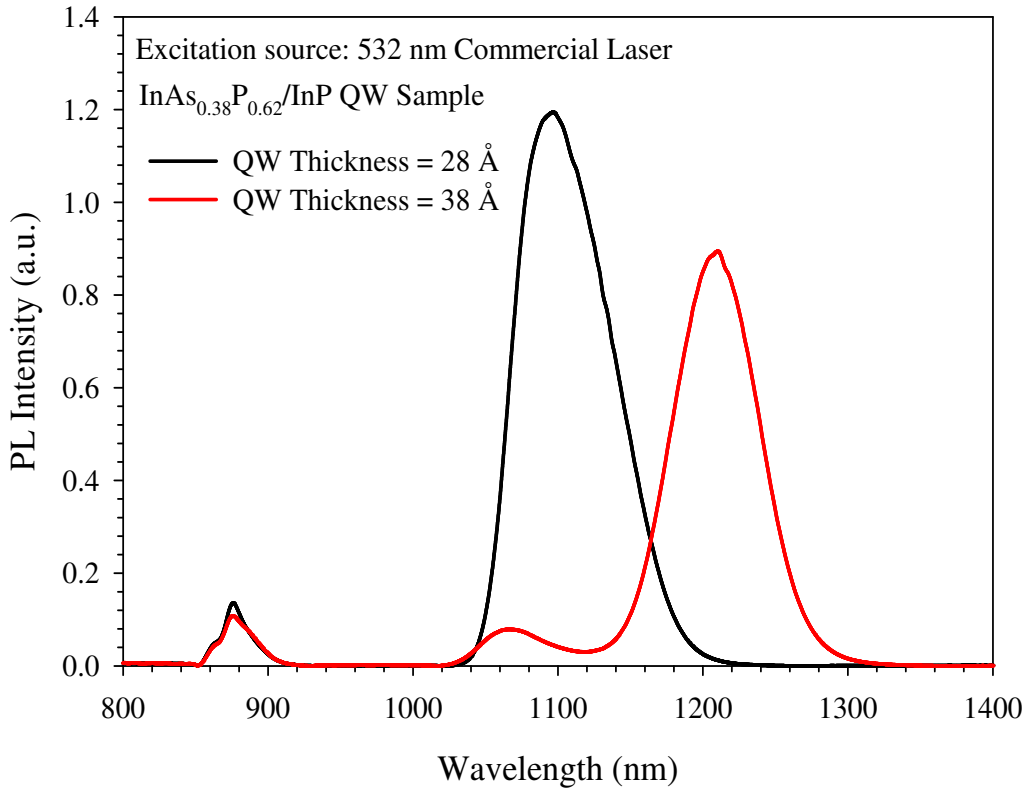

Figure 6.18: PL with 532 nm Commercial Laser

It is known that the bandgap of InP is 1.42 eV at 10 K and on adding InAs, bandgap of material reduces. Calculated bandgap, from Eq. 6.3, related to the wavelength

1120 nm is about 1.107 eV which corresponds to 28 Å thick $InAs_{0.38}P_{0.62}$ QW. Further, there is decrease in energy bandgap of QW sample if we increase the thickness of the QW. Hence the peak observed for 38 Å thick QW sample is at 1230 nm, which corresponds 1.01 eV.

$$E = \frac{1.24 \times 10^{-6}}{\lambda} \tag{6.3}$$

The similar results have been verified with PL measurements using commercial 532 nm source. As the source energy is high we can also able to excite the barriers i.e. InP. The energy bandgap of InP at 10 K is about 1.40 eV, which is related to the 880 nm, shown in Fig. 6.18, for both the samples irrespective of the QW thicknesses. The subsequent peaks from the QW samples, 28 Å and 38 Å, in Fig. 6.18 is 1067 nm and 1208 nm which correspond to energies by Eq. 6.3, 1.162 eV, and 1.02 eV, respectively. This verifies the results we have achieved using 980 nm SCLS laser.

❖ Conclusion

We have successfully measured the laser induced damage threshold (LIDT) of single layer Al_2O_3, MgF_2, and SiO_2 thin films deposited on the GaAs. The measurement was done by using Q-switched Nd-YAG laser in both pulse mode and CW mode. The laser induced damage on the samples was only due to the heating effect. The effective damage radius on the samples was ~150 μm and average continuous wave laser induced damage threshold was found >10 W. Hence, we can say that the optimized single layer QWOT thin films have potential for laser diode facet coating application. In addition to that we have demonstrated the design of experimental setup to measure laser diode accelerated lifetime in ACC mode and estimated the device lifetime about ~ 35,000 operated at 80 °C. Finally, we have successfully demonstrated an application of indigenously developed laser diode (980 nm) package for PL spectroscopy.

* * *

❖ Summary and Future Outline

➢ Summary

The present thesis deals with the various laser diode (LD) post growth fabrication technologies and process optimization viz. structure processing, facet coating, packaging, and the development of characterization facilities. Finally it improves the device life-time and its reliability. In addition we also have successfully demonstrated an application of indigenously developed a complete LD package in photoluminescence (PL) spectroscopy.

It is of much importance to have appropriate LD characterization facilities to evaluate the LD performance after each process optimization and its application to the laser. Hence, the development and upgradation of the LD characterization technique is an inevitable part of the research. Here various LD characterization systems has been developed and are automated using LabVIEW GUI for proper and accurate real time data acquisition and analysis as well. The characterization techniques are developed to measure: L-I-V characteristic, spectral response, junction-temperature and life-time estimation, P_{max} at COMD level, ex-situ and in-situ reflectivity and LIDT measurements of various thin films.

We have successfully processed and developed LD mesa-stripe structure of MOVPE grown double QW InGaAs/GaAs high-power laser diode. The experiments were optimized for post growth processing includes photolithography, lift-off processes, mechanical lapping and polishing, insulation and metal contact layer deposition. A 980 nm laser bar with 100 µm stripe width and 150 µm thickness was operated very well under pulse mode and CW operation.

The second step to improve LD performance is the laser facet coating which not only prevents the device facet degradation but also enhances the laser output power from respective facet depends on the coating type either AR or HR. We have optimized QWOT single layer of various dielectric materials for facet coating viz. Al_2O_3, SiO_2, MgF_2, TiO_2, and ZrO_2. The QWOT single layer Al_2O_3 and ZrO_2 AR coating has been optimized for 808 nm and 980 nm laser diodes, respectively. For HR coating to the device is released by

multilayer QWOT pair of Al_2O_3/TiO_2 for 808 nm LD bar and SiO_2/ZrO_2 for 980 nm LD bar. Laser diode with AR and HR facet coating shows improvement in output power level than the bare, without coated, devices. The optimized facet coating have also been tested for laser-induced-damage threshold (LIDT) measurements and proved to be a suitable facet coating for HPLD

Finally, the laser diode packaging has been realized by means of laser diode die-bonding and wire-bonding. The die-bonding of the 980 nm laser diode with indium and gold-tin (AuSn) preform has been optimized using indigenously developed setup. The substrates used for die-bonding were of copper and KOVAR with gold plating on them. After die-bonding, wire bonding on the device is also optimized using manual wire bonder for thin gold wire (diameter - 1 mil). A complete package has been successfully tested and the measured dynamic series resistance of the device is low enough (200 mΩ) to confirm quality bonding. Beside this, we also have optimized a bonding process to make laser diode package module with die-bonding on the electrodes for 650 nm laser diode bar.

The device performance to estimate its life-time using accelerated aging technique with constant CW current and high temperature (80 °C) has been tested. The life-time of the device has been estimated about 10^5 h at room temperature. The improved device performance has successfully been demonstrated after applying various optimized post growth process to the HPLDs. Single laser diode element with effective packaging gave an output power of ~670 mW/facet at ~ 2 A under CW operation with the dynamic series resistance of ~ 200 mΩ. Subsequently, the developed semi-package, non hermetic, laser diode was used for the characterization of electronic transitions of InAsP/InP quantum well in photoluminescence (PL) spectroscopy.

- **Future Outline**

The field of research is its own kind of ocean of information, so, as we go deep into it we can get more and more information and hence there is a huge scope of improvement in future. We have tried our best to improve the device performance but still there are some aspects needed to be kept in attention for technological development of more reliable

device package.

The following topics could be considered in future technological development of high-power laser diode fabrication.

- Internal structure of the device can be improved by using strained QW or QD based laser structure growth.
- Contact layer deposition while device processing can be done and optimized by means of electroless gold plating instead of thermal evaporation.
- Cleaving of laser diode bar or chip with proper facets is the most crucial job of laser diode processing and can be improved with wafer cleaver.
- Conventional method of facet coating, i.e. QWOT film coating, can be improve by multilayer coating of varying thicknesses for AR and HR coating.
- Different dielectric materials, such as Hafnium Oxide (HfO_2), Tantalum oxide (Ta_2O_5), and other rare-earth oxides can also be tested and studied for facet coating.
- Thermal management is one of the main aspects of the laser diode packaging. Hence, simulation of the heat dissipation through the device package can improve the understanding of thermal management.
- One can choose the materials like diamond or copper tungsten (CuW) having higher thermal conductivity than copper, used as a submount, for device packaging.
- Degradation study of the laser diode itself is a subject that needs deep and concentrated research. Research on causes of degradation can lead us to improve the device structure and hence the better performance of the device.
- Study of degradation can also help researchers to improve the reliability of the device further.

* * *

❖ References

[1] G. P. Agrawal, N. K. Dutta, "*Semiconductor Lasers*", 2nd Edn., Van Nostrand Reinhold, New York, (1993).

[2] P. S. Zory, Ed; "*Quantum well lasers*", Academic Press, Boston, (1993).

[3] Pallab Bhattacharya, "*Semiconductor Optoelectronic Devices*", Prentice-Hall, India, (1999).

[4] H. Jiang, J. Lin, *Proc. 14th Annual Meeting of the IEEE Lasers and Electro-Optics Society (LEOS-2001)*, **2** (2001) 758.

[5] H. A. Macleod, "*Thin Film Optical Filters*", 2nd Edn., Adam Hilger Ltd, Bristol, (1986).

[6] Peter Unger, "*Introduction to power diode lasers*", High Power Diode Lasers, Ed.: R. Diehl, *Topics Appl. Phys.*, **78**, Springer-Verlag Berlin Heidelberg, (2000).

[7] T. H. Maiman, *Nature*, **187** (1960) 493.

[8] R. N. Hall, G. E. Fenner, J. D. Kingsley, T. J. Soltys, R. O. Carlson., *Phy. Rev. Lett.*, **9** (1962) 366.

[9] M. I. Nathan, W. P. Dumke, G. Burns, F. H. Dill, Jr., G. Lasher, *Appl. Phys. Lett.*, **1**, (1962) 62.

[10] N. Holonyak, Jr., S. F. Bevacqua, *Appl. Phys. Lett.*, **1** (1962) 82.

[11] T. M. Quist, R. H. Rediker, R. J. Keyes, W. E. Krag, B. Lax, A. L. McWhorter, H. J. Zeigler, *Appl. Phys. Lett.*, **1** (1962) 91.

[12] Alferov Zh. I., V. M. Andreev, D. Z. Garbuzov, Yu. V. Zhi-lyaev, E. P. Morozov, E. L. Portnoi, and V. G. Trofim, *Sov. Phys. Semicond.*, **4** (1971) 1573.

[13] I. Hayashi, M. Panish, P. W. Foy, S. Sumski, *Appl. Phys. Lett.*, **17**, pp. 109 (1970).

[14] H. Kroemer, *Proc. IEEE*, **51** (1963) 1782.

[15] Zh. I. Alferov, R. F. Kazarinov, *U.S.S.R. Patent,* **181737**

[16] J.P. van der Ziel, R. Dingle, R.C. Miller, W. Wiegmann, W.A. Nordland Jr., *Appl. Phys. Lett.*, **26** (1975) 463.

[17] R.D. Dupius, P.D. Dapkus, N. Holonyak, E.A. Rezek, R.Chin, *Appl. Phys. Lett.*, **32** (1978) 295.

[18] R.D. Dupius, P.D. Dapkus, P.D. Chin, N. Holonyak, S.W. Kirchoefer, *Appl. Phys. Lett.*, **34** (1979) 265.

[19] R.D. Dupius, P.D. Dapkus, N. Holonyak, R.M. Kolbas, *Appl. Phys. Lett.*, **35** (1979) 487.

[20] W. Huang, F. Jain, *J. Appl. Phys.*, **87** (2000) 7354.

[21] Shu-man Liu, Masahiro Yoshita, Makoto Okano, Toshiyuki Ihara, Hirotake Itoh, Hidefumi Akiyama, Loren N. Pfeiffer, Ken W. West, Kirk W. Baldwin, *J. Appl. Phys.*, **102** (2007) 043108.

[22] A. Salhi, L. Fortunato, L. Martiradonna, R. Cingolani, M. De Vittorio, A. Passaseo, *J. Appl. Phys.*, **100** (2006) 12311.

[23] R. L. Byer., '*Diode laser-pumped solid-state lasers*', Science, **239** (4841), (1988) 742.

[24] http://en.wikipedia.org/

[25] V. K. Dixit, S. Pal, R. Jangir, S. K. Khamari, P. Babudayal, S. D. Singh, S. Porwal, R. Kumar, S. Mishra, K. Alexander, T. Ganguli, C. Mukherjee and S. M. Oak, *Proceedings of National Laser Symposium-19 (NLS-19)*, RRCAT (Indore), (2010).

[26] M. Fukuda, M. Okayasu, J. Temmyo, J. Nakand, *IEEE J. Quant. Electron.*, **30** (1994) 471.

[27] K. H. Park, J. K. Lee, D. H. Jang, H. S. Cho, C. S. Park, K. E. Pyun, J. Y. Jeong, S. Nahm, and J. Jeong, *Appl. Phys. Lett*. **73** (1998) 2567.

[28] R. E. Mallard and R. Clayton, *Proc. SPIE*, **3004** (1997) 145.

[29] A. Moser and E.-E. Latta, *J. Appl. Phys*. **71** (1992) 4848.

[30] A. McKee, C. McLean, G. Lullo, A. Bryce, R. De La Rue, J. Marsh, and C. Button, *IEEE J. Quantum Electron*. **33** (1997) 45.

[31] B. Corbett, P. Lambkin, J. O'Callaghan, S. Deubert, W. Kaiser, J. P. Reithmaier, and A. Forchel. *IEEE Photon. Technol. Lett.*, **19** (2007) 916.

[32] H. Horie, Y. Yamamoto, N. Arai, and H. Ohta, *IEEE Photon. Technol. Lett.*, **12**(1), (2000) 13.

[33] F. Rinner, J. Rogg, M. T. Kelemen, M. Mikulla, G. Weimann, J. W. Tomm, E. Thamm, and R. Poprawe, *J. Appl. Phys.*, **93**(3), (2003) 1848.

[34] C. L. Walker, A. C. Bryce, and J. H. Marsh, *IEEE Photon. Technol. Lett.*, **14**(10), (2002) 1394.

[35] H. Taniguchi, H. Ishii, R. Minato, Y. Ohki, T. Namegaya, and A. Kasukawa, *IEEE J. Select. Topics Quant. Electron.*, **13**(5), (2007) 1176.

[36] **G. G. Bhatt**, Vipul Kheraj, M. S. Desai, and C. J. Panchal, *Proceedings of National Laser Symposium-19 (NLS-19)*, RRCAT (Indore), (2010).

[37] T. K. Sharma, Tapas Ganguli, V.K.Dixit, S.D.Singh, S.Pal, S.Porwal, Ravi Kumar, Alexander Khakha, R. Jangir, V. Kheraj, P. Rawat and A. K. Nath, *KIRAN,* **17**(3), (2006) 86.

[38] Archana Marathe, **Gopal Bhatt**, S.K Khamari, S.Pal, K.Rajiv, C. Mukharjee, C.J Panchal, V.K Dixit, T.K Sharma and S.M Oak, *Proceedings of National Laser Symposium-22 (NLS-22)*, Manipal University, Manipal (Karnataka), (2014).

[39] **G. G. Bhatt**, Vipul Kheraj, M. S. Desai, C. J. Panchal, *J. Nano- Electron. Phys.*, **3**(1), (2011) 721.

[40] **G.G. Bhatt**, A.L. Patel, M.S. Desai, C.J. Panchal, *J. Nano- Electron. Phys.*, **5**(2) (2013) 02016.

[41] **G. G. Bhatt**, C. J. Panchal, M. S. Desai, V. A. Kheraj and T. K. Sharma, *Proceedings of XV - International workshop on Physics of Semiconductor Devices*, Jamia Millia Islamia University, New Delhi, (2009) 1047.

[42] **G. G. Bhatt**, V. A. Kheraj, C. J. Panchal and T. K. Sharma, *Proceedings of National Laser Symposium-08 (NLS-08)*, LASTEC, DRDO, New Delhi, (2008).

[43] **Gopal Bhatt**, M. Shrivastava, A. Marathe, S. K. Khamari, A. Khakha, S. Porwal, V. Agnihotri, S. Pal, C. J. Panchal, V. K. Dixit, T. K. Sharma and S. M. Oak, *Proceedings of National Laser Symposium-22 (NLS-22)*, Manipal University, Manipal (Karnataka), (2014).

[44] H. Kressel, J. K. Butler, "*Semiconductor Lasers and Heterojunction LEDs*", Academic Press, New York, (1977).

[45] Berthold E. Schmidt, Stefan Mohrdiek, Christoph Harder, *"Pump Laser Diode", Optical Fiber Telecommunications IV-A*, Ed.: Ivan P. Kaminow, Tingye Li, Academic Press, (2002).

[46] G.P. Agrawal and N.K. Dutta, "*Long-Wavelength Semiconductor Lasers"*, NY: Van Nostrand Reinhold Company, New York, (1990)

[47] L.A. Coldren and S.W. Corzine, "*Diode Lasers and Photonic Integrated Circuits"*, NY: John Wiley & Sons, Inc., New York, (1995).

[48] Tyll Hertsens, "*Measuring Diode Laser Characteristics*", ILX Lightwave-Application note-**5**, (2000).

[49] Greg Pakulski, Laser Designer, Nortel Networks, interview with author, Ottawa, (April 2001).

[50] Mool Chand Gupta and John Ballato, Ed.; "*Hand-book of Photonics*", 2nd Edn., CRC Press, (2006).

[51] S. M. Sze, "*Physics of Semiconductor Devices*", Wiley-Interscience, New York, (1969).

[52] Y. Nakano, Y. Ushida, K. Tada, *IEEE Photon. Tech. Lett.*, **04**(04), (1992) 308

[53] D. A. Yanson, E. U. Rafailov, G. S. Sokolovskii, V. I. Kuchinskii, *J. Appl. Phys.*, **95(3)**, (2004) 1502.

[54] C. H. Henry, *IEEE J. Quantum Electron*., **18** (1982) 259.

[55] M. Aoki, K. Uomi, T. Tsuchiya, Shinji Sasaki, M. Okai, N. Chinone, *IEEE J. Quantum Electron*., **27** (1991) 1782.

[56] S. L. Chuang, "*Physics of Optoelectronic Devices*", Wiley, New York, (1995).

[57] Toshio Higashi, Tsuyoshi Yamamoto, Shouichi Ogita, Masahiro Kobayashi, *IEEE J. Quant. Electron.*, **34**(9), (1998) 1680.

[58] Peter Blixt, John E. Bowers, Erik Bodtker, O. Sahlen, Roy S. Smith, *IEEE Transact. on Microwave Theory and Tech.*, **43**(9), (1995) 2214.

[59] Hiroshi Hatakeyama, Koji Kudo, Yoshitaka Yokoyama, Koichi Naniwae, Tatsuya Sasaki, *IEEE J. Sel. Topics Quantum Electron*, **8**(6) (2002) 1341.

[60] Scott T. McCain, Michael E. Gehm, Yanqia Wang, Nikos P. Pitsianis, Michael E. Sullivan and David J. Brady, Proc. of SPIE, **5864**, "*OSA Biomedical Optics, Novel Optical Instrumentation for Biomedical Applications II*", Eds.: Christian D. Depeursinge, (2005).

[61] N. Beverini, G. Del Gobbo, G. L. Genovesi, F. Maccarrone, F. Strumia, F. Paganucci, A. Turco, M. Andrenucci, *IEEE J. Quant. Electron.*, **32**(11), (1996) 1874.

[62] Xinlu Zhang, Yuezhu Wang, Youlun Ju, *J Opt. Laser Technol*, **39**(1), (2007) 78.

[63] Johnson, L.A., *IEEE Communications Magazine,* **44**(2), (2006) 4.

[64] Melanie Ott, "*Capabilites and Reliability of LEDs and Laser Diodes*", Report no. 301-286-0127, NASA Goddard Space Flight Center (1997).

[65] Nam Hwang, Min-Kyu Song, Seung-Goo Kang, Hee-Tae Lee, Kyung-Hyun Park, Dong-Boon Jang, Seong-Su Park, Hak-Soo Han, Dong-Goo Kim, and Hyung-Moo Park, *IEEE Proc. 45th Electronic Components and Technology Conference*, (1995) 318.

[66] Konstantin Boucke, "*Packaging of Diode Laser Bars*", High Power Diode Lasers: Technology and Applications, Ed. Friedrich Bachmann, Peter Loosen, Reinhart Poprawe, Springer Series in Optical Sciences, Springer Science + Business Media, (2007).

[67] M. Santori, *IEEE Spectrum*, **27**(8), (1990) 36.

[68] D P Blair, P H Sydenham, *J. Phys. E: Sci. Instrum.*, **8** (1975) 621.

[69] "*GPIB 101 - a Tutorial about the GPIB Bus*", Application Bulletin AB48-11, ICS ELECTRONICS-IEEE 488, (2006).

[70] V. A. Kheraj, P. K. Patel, C. J. Panchal, T. K. Sharma, *Proc. of Sixth DAE-BRNS National Laser Symposium (NLS-6)*, Indore, India, (2006) 70.

[71] Yangang Xi ,Thomas Gassmann: "Junction temperature in UV LED", *Jpn. J. Appl. Phys.*, **44**(10), (2005) 7260.

[72] Leszek Ornoch, Emil Kowalczyk, *optical applicata*, **XXXV** (3), (2005) 591.

[73] R. D. Dupuis, *IEEE J. Quantum Electron*., **23** (1987) 651.

[74] D. Bimberg, M. Grundmann, N. N. Ledentsov, "*Quantum Dot Heterostructures*", John Wiley & Sons, New York, (1999).

[75] Tarun Kumar Sharma, PhD Thesis, "*Metal organic vapour phase epitaxial growth of III-V semiconductors*", Devi Ahilya Vishwa Vidyalaya, Indore, (2002).

[76] J. J. Coleman, *Proc. of IEEE*, **85** (1997) 1715.

[77] H. M. Manasevit, *Appl. Phys. Lett.*, **12** (1968) 165.

[78] R.D. Dupius, P.D. Dapkus, N. Holonyak, E.A. Rezek, R.Chin, *Appl. Phys. Lett.*, **32** (1978) 295.

[79] S.D. Hersee, M. Krakowski, R. Blondeau, M. Baldy, B. De Créoux, J. P. Duchemin, *J. Cryst. Growth*, **68** (1984) 383.

[80] S.J. Bass, *J. Cryst. Growth*, **31** (1975) 172.

[81] Markus Weyers, Arnab Bhattacharya, Frank Bugge, Arne Knauer, "*Epitaxy of High-Power Diode Laser Structures*", High Power Diode Lasers, Ed.: R. Diehl, *Topics Appl. Phys.*, **78**, Springer-Verlag Berlin Heidelberg, (2000)

[82] Sadao Adachi, "Properties of Semiconductor Alloys: Group-IV, III–V and II–VI Semiconductors", John Wiley & Sons, Ltd., West Sussex, United Kingdom, (2009).

[83] I.Vurgaftman, J.R. Meyer, L.R. Ram Mohan, *J. Appl. Phys.*, **89** (2001) 5815.

[84] http://www.tf.uni-kiel.de/matwis/amat/semi_en/index.html

[85] Y. Suematsu, A.R. Adams, "*Handbook of Semiconductor Lasers and Photonic Integrated Circuits*", Chapman and Hall, London (1994).

[86] T. Katsuyama, I. Yoshida, J. Shinkai, J. Hashimoto, H. Hayashi, *Electronic Letters*, **26** (1990) 1375.

[87] "*Lift-off processes*", http://snf.stanford.edu/Process/Lithography/liftoff.html

[88] G.E. Chaika, R.V. Konakova, V.G. Lyapin, V.V. Milenin, E.A. Soloviev, D.I. Voitsikhovskyi, N.S. Boltovets, V.N. Ivanov, *IEEE Proc. International Semiconductor Conference (CAS-2000)*, **1** (2000) 167.

[89] M.R. Krames, A.D. Minervini, N. Holonyak, Jr., *Appl. Phys. Lett.*, **67** (1995) 73.

[90] M.R. Krames, E.I. Chen, N. Holonyak, Jr., *Appl. Phys. Lett.*, **65** (1994) 3221.

[91] Sukhdev S. Gill, Mark A. Crouch, and John R. Dawsey, "*Ni-Ge-Au ohmic contacts for GaAs and GaAlAs*", United States Patent, **5309022** (1994).

[92] J. A. Caballero, C. He, and S. Djavani-Tabrizi, T. Yin, R. Mallard, S. R. Das, *J. Vac. Sci. Technol.*, A **22** (3), (2004) 865.

[93] R. D. Dupuis, R. L. Hartman, F. R. Nash, *IEEE Electron. Device Lett.*, **EDL-4**(8), (1983) 286.

[94] V. Kummler, A. Lell, V. Harle, U. T. Schwarz, T. Schoedl, W. Wegscheider, *Appl. Phy. Lett.*, **84**(16) (2004) 2989.

[95] T. Guhne, V. Gottschalch, G. Leibiger, H. Herrnberger, J. Kovac, J. Kovác, Jr., R. Schmidt-Grund, B. Rheinländer, D. Pudis, *Laser Physics*, **16**(3) (2006) 441.

[96] J. Sacher, W. Elsasser, E. O. Gobel, H. Jung, *Electronic Letters*, **27**(16), (1991) 1463.

[97] Shi-Yun Cho, Baik-Hyung Han, Jong-In Shim, Jun-Sang Yu and Tae-I Kim, *J. Korean Phys. Soc*, **32** (1998) 132.

[98] Jaskorzynska Bozena, Nilsson Johan, Thyirn Lars. *J. Opt. Soc. Am. B*, **8**(2), (1991) 484.

[99] Y. Yamamoto, "*Coherence, Amplification and Quantum Effects in Semiconductor Lasers*", John Wiley & Sons, New York, (1990).

[100] http://www.instrument.com.cn/show/literature/c117306.pdf

[101] J.E. Ungar, N.S.K. Kwong, S.W. Oh, J.S. Chen, N. Bar Chaim, *Electron. Lett.*, **30** (1994) 1766.

[102] M. Matsumoto, K. Sasaki, M. Kondo, T. Ishizumi, S. Yamamoto et al., *Jpn. J. Appl. Phys.*, **32** (1993) L665.

[103] O. S. Heavens, "Thin Film Physics", pp. 78, Methuen & Co. Ltd, London, (1970)

[104] Eisenstein G., Stulz L. W., *Appl. Opt.*, **23** (1984) 161.

[105] M. Passlack, C. G. Bethea, W.S.Hobson, John Lopata, E.F. Schubert, G.J.Zydzik, D. T. Nichols, J.F. de Jong, U. K. Chakrabarti, N. K. Dutta, *IEEE J. Select. Topics Quant. Electron.*, **1**(2) (1995) 110.

[106] S. Guha, E. Cartier, N.A. Bozarczuk, J. Bruley, L. Gignac, J. Karasinski, *J. Appl. Phy.*, **90** (2001) 512.

[107] Jun-ichi Hashimoto, Nobuyuki Ikoma, Michio Murata, *E*, and Tsukuru Katsuyama, IEEE Journal of Quantum Electronics, **36** (8), (2000) 971.

[108] M. Bugajski, B. Mroziewicz, K. Reginski, J. Muszalski, K. Kosiel, M. Zbroszczyk, T. Ochalski, T. Piwonski, D. Wawer, A. Szerling, E. Kowalczyk, H. Wrzesinska, and M. Górska, Bulletin of the Polish Academy of Sciences Technical Sciences, **53** (2), (2005) 113.

[109] Mingju Nie, Deming Liu, and Bichun Hu, Proc. of SPIE, **6149**, (2006) 61492O1-5.

[110] K. J. Patel, M. S. Desai and C. J. Panchal, *Adv.Mat.Lett.*, **3** (5), (2012) 410.

[111] Marvin J.Weber, "*Handbook of Optical Materials*", CRC Press, (2003).

[112] CERAC Coating Materials News, **20** (**1**), (2010).

[113] Shin-ichi Nagahama, Yasunobu Sugimoto, Tokuya Kozaki and Takashi Mukai, Proc. of SPIE, **5738**, (1995) 57.

[114] Donald M. Mattox, "*Handbook of Physical Vapor Deposition (PVD) Processing*"., Noyes Publications, Westwood, New Jersey, U.S.A., (1998).

[115] K. L. Chopra, P. D. Paulson and V. Dutta, *Progress in Photovoltaics: Research and Applications*, **12** (2004) 69.

[116] S. M. Rossnagel, *J. Vac. Sci. Technol. A*, **21**(5), (2003) S74.

[117] G. Eisenstein, L. W. Stulz, L. G. Van Uitert, J. Lightwave Tech., **LT-4**, (1986) 1373.

[118] A. Chambers, R. K. Fitch, B. S. Halliday, "*Basic Vacuum Technology*", 2nd Edn., CRC Press, (1998).

[119] V. A. Kheraj, C. J. Panchal, M. S. Desai, V. Potbhare, Paamana - Journal of Physics, Vol. **72**(06), (2009) 1011.

[120] E. Hecht, "*Thin film optical filters*", 2nd ed., Adam Hilger Ltd, Bristol, (1986).

[121] V.A. Kheraj, C.J. Panchal, P.K. Patel, B.M. Arora, T.K. Sharma, *Optics & Laser Technology*, **39** (**7**), (2007) 1395.

[122] R. Overend and D. R. Gibson, *Vacuum*, **43** (1992) 71.

[123] A. Paradisi, A. de Campos Sachs, A. Gobbi, J. R. Filho and R. B. Martins, *IEEE Photon. Technol. Lett.*, **8**, (1996) 605.

[124] M. Sagawa, K. Hiramoto, T. Toyonaka, T. Kikawa, S. Fujisaki and K. Uomi, *Electron. Lett.,* **32**, (1996) 2277.

[125] A. Shima, H. Kizuki, A. Takemoto, S. Karakida, M. Miyashita, Y. Nagai, T. Kamizato, K. shigihara, A. Adachi, E. Omura and M. Otsubo, *IEEE J. Quantum Electron.*, **1**, (1995) 102.

[126] Maria Isabel Anastacio Faria, Manoel Damião Sousa-Neto, Aline Evangelista Souza-Gabriel, Edson Alfredo, Umberto Romeo, Yara Teresinha Correa Silva-Sousa, *Lasers in Medical Science*, **28** (1), (2013) 275.

[127] R. I. Laming, M. C. Farries, P. R. Morkel, L. Reekie, D. N. Payne, P. L. Scrivener, F. Fontana, and A. Righetti, *Electron. Lett*., **25**, (1989) 12.

[128] Tapas Ganguli, Tarun Sharma, V.K.Dixit, S.Pal, S.D.Singh, R.Jangir, Shailesh Khamari, S.Porwal, Ravi Kumar, Alexander Khakha, S.M.Oak, C.Mukherjee, Pragya Tiwari, Dr. G. Sai Saravanan, Mr. Sangam Bhalke and Dr. R. Muralidharan, *KIRAN*, **19** (3), (2008) 64.

[129] J.W. Ronnie Teo, G.Y. Li, M.S. Ling, Z.F. Wang, X.Q. Shi, *Thin Solid Films*, **515**(10), (2006) 4340

[130] Ajit R. Dhamdhere, Ajay P. Malshe, William F. Schmidta, William D. Brown, *Microelectronics Reliability*, **43**(2), (2003) 287.

[131] Lisa M. Kirby, "*Solvent-free floor covering adhesive and method of producing same*", United States Patent, **5258425**, (1993).

[132] Sammy Kayali, George Ponchak, Roland Shaw, "*GaAs MMIC Reliability Assurance Guideline for Space Applications*", JPL Publication, **96-25**, (1996)

[133] http://www.ami.ac.uk/courses/topics/0203_dbm/index.html#5

[134] William W. So and Chin C. Lee, *IEEE Trans. Comp. Packag. Technol*, **23**(2), (2000) 377.

[135] Xingsheng Liu, Ronald W. Davis, Lawrence C. Hughes, Michael H. Rasmussen, Rajaram Bhat, Chung-En Zah, Jim Stradling, *J. Appl. Phy.*, **100** (2006) 013104

[136] Qu, Y.; Yuan S.; Liu, C.Y.; Bo, B.X.; Liu, G.J. & Jiang,H.L., *IEEE Photon. Technol. Lett.* **16** (2), (2004) 389.

[137] W. S. Capinski, H. G. Maris, T. Ruf, M. Cardona, K. Ploog, and D. S. Katzer, *Phys. Rev. B*, **59**(12), (1999) 8105.

[138] O. J. F. Martin, G.L. Bona, P. Wolf, *IEEE J. Quantum Electron.*, **28** (1992) 2582.

[139] X. Liu, M. H. Hu, H. K. Nguyen, C. G. Caneau, M. H. Rasmussen, R. W. Davis Jr., C.E. Zah, *IEEE Trans. Adv. Packag.*, **27** (2004) 640.

[140] X Liu, M. H. Hu, C. G. Caneau, R. Bhat, C.E. Zah, *IEEE Trans. Compon. Packag. Technol.*, **29** (2006) 268.

[141] E. C. C. Yeh, W. J. Choi, K. N. Tu, P. Elenius, H. Balkan, *Appl. Phys. Lett.*, **80** (2002) 580.

[142] Chin C. Lee, David H. Chien, *Proc. Ninth IEEE SEMI-THERM Symposium*, (1993) 75.

[143] V. A. Kheraj, C. J. Panchal, T. K. Sharma, *Proc. of Seventh DAE-BRNS National Laser Symposium (NLS-7)*, (2007) 105.

[144] J. R. Davis, "*Metals Handbook*", 2nd Ed., Materials Park, OH: ASM International, (1998).

[145] Zonghe Lai and Johan Liu, Chapter A: Wire Bonding, http://extra.ivf.se/ngl/awirebonding/chaptera.htm

[146] Teo Jin Wah Ronnie, "Ch. 17 – Advances in High-Power Laser Diode Packaging, Semiconductor Laser Diode Technology and Applications", Dr. D. S. Patil (Ed.), ISBN: 978-953-51-0549-7, InTech (2012).

[147] J. R. Ray, "*High Efficiency Copper Indium Gallium Diselenide (CIGS) Thin Film Solar Cells*", Ph.D. Thesis, The M. S. University of Baroda, Vadodara (India), Ch. 2, (2013) 24.

[148] L. A. Johnson, "Laser Diode Burn-in and Reliability Testing", http://www.ilxlightwave.com.

[149] James L. Spencer, *Proceedings of the SPIE - Fiber Optics Reliability: Benign and Adverse Environments*, **842** (1987) 63.

[150] M. Fukuda, *Microelectron. Reliab.*, **42** (2002) 679 and **46** (2006) 263.

[151] O. Ueda, "*Reliability and Degradation of III-V Optical Devices*", Artech House, Norwood, MA (1996).

[152] F. R. Gfeller and D. J. Webb, *J. Appl. Phys*. **68** (1990) 14.

[153] S. Kishino, H. Nakashima, R. Ito, and O. Nakada, *Appl. Phys. Lett*., **27** (1975) 207.

[154] P. M. Petroff and R. L. Hartman, *Appl. Phys. Lett.* **23** (1973) 469.

[155] O. Ueda, H. Imai, T. Fujiwara, S. Yamakoshi, T. Sugawara, and T. Yamaoka, *J. Appl. Phys*., **51** (1980) 5316.

[156] P. M. Petroff, *Semicond. Insul*., **5** (1983) 307.

[157] K. Kondo, O. Ueda, S. Isozumi, S. Yamakoshi, K. Akita, T. Kotani, *IEEE Trans. Elect. Device*, **ED-30** (1983) 321.

[158] T. Uji, T. Suzuki and T. Kamejima, *Appl. Phys. Lett.* **36** (1980) 655.

[159] S. Todoroki, M. Sawai, and K. Aiki, *J. Appl. Phys*. **58** (1985) 1124.

[160] H. Brugger and P. W. Epperlein, *Appl. Phys. Lett*. **56** (1990) 1049.

[161] R. G. Waters, *Prog. Quant. Electron*. **15** (1991) 153.

[162] W. C. Tsang, H. J. Rosen, P. Vettiger, D. J. Webb, *Appl. Phys. Lett*. **59**, (1991) 1005.

[163] M. Fukuda, "*Reliability and Degradation of Semiconductor Lasers and LED's",* Artech House, London (1991).

[164] Ulrich Martin, "*COMD behavior of semiconductor laser diodes*", Annual Report, Dept. of Optoelectronics, University of Ulm, (1999) 39.

[165] L. W. Tu, E. F. Schubert, M. Hong, G. J. Zydik Meyer, *J. Appl. Phys*. **80** (1996) 6448.

[166] M. Ohkubo, T. Ijichi, A. Iketani, T. Kikuta, Electron. Lett. **28** (1992) 1149.

[167] J.H. Marsh, IEEE Photonics Society Newsletter **24** (2010) 4.

[168] L.J. Mawst, A. Bhattacharya, J. Lopez, D. Botez, D.Z. Garbuzov, L. DeMarco, J.C. Connolly, M. Jansen, F. Fang, R.F. Nabiev, *Appl. Phys. Lett*. **69** (1996), 1532.

[169] J.H. Marsh, *Laser Technik Journal*, **4** (2007) 32.

[170] V. A. Kheraj, C. J. Panchal, "*Laser and Bose-Einstein Condensation Physics*", Ed. Man Mohan, Anil Kumar, Aranya B. Bhattacherjee, Anil Kumar Razdan, Narosa Publishing House, (2010).

[171] P.V. Bhorea, A.P. Shah, M.R. Gokhale, S. Ghosh, A. Bhat-tacharya, B.M. Arora, *Indian J Eng Mate S*, **11** (2004) 438.

[172] C.J. Panchal, V.A. Kheraj, K.M. Patel, P.K. Patel, B.M. Arora, T.K. Sharma, *Proc. of SPIE-ICO20: Lasers and Laser Technologies*, **6028** (2005) 35.

[173] K. Itaya, M. Ishikawa, H. Okuda, Y. Watanabe, K. Nitta, H. Shiozawa, Y. Uematsu, *App. Phy. Lett*. **53** (1988) 1363.

[174] ISO-11254-1/2:2001(E), International Organization for Standardization

[175] T.W. Walker, A.H. Guenther, P.E. Nielsen, *IEEE J. Quan-tum Elect*. **17** (1981) 2041.

[176] A. V. Kuanr, S. K. Bansal, G. P. Srivastava, *Opt. Laser. Technol*. **28** (1996) 25.

[177] Yajun Li, *Optics & Laser Technology*, **40** (2008) 92.

[178] B. Sumpf, J. Fricke, P. Ressel, M. Zorn, G. Erbert, G. Tränkle, Proc. SPIE **8277** (2012) 827711.

[179] Kevin K. Smith, *Thin Solid Films*. **84** (1981) 171.

[180] V. K. Dixit, S. D. Singh, S. Porwal, Ravi Kumar, Tapas Ganguli, A. K. Srivastava and S. M. Oak, *J Appl Phy*, **109** (2011) 083702.

* * *

❖ List of Symbols

ν	laser frequency
λ	laser wavelength
φ	incident angle
τ	lifetime
Ω	ohm
σ	conductivity
ρ	density
λ_0	center wavelength of the laser
θ_0	angles of incidence in the incident medium
η_d	differential efficiency
ΔE	energy separation between quasi fermi levels
Γg	modal gain
α_i	absorption coefficient
η_i	internal efficiency
ΔI	change in operating current
ΔP	change in output power
Γ-point	center of the brillouin zone
θ_s	angles of incidence in the substrate
η_{slope} or dP/dI	slope efficiency
μ	mobility
μm	micrometer
μ_n	mobility of electron
μ_p	mobility of hole
A	group III constituent species
c	velocity of light in vacuum
D	group V constituent species
d	thickness
E_0	ground state energy level
E_1	excited state energy level
E_a	activation energy
E_c	energy of the conduction band edge
E_F	Fermi level
$E_{Fc, Fv}$	quasi Fermi levels
E_g	band-gap energy
$E_{g,cl}$	energy difference of cladding layers
E_v	energy of the valance band edge
eV	electron volt
g	optical gain
gm	gram
g_{th}	threshold gain
h	Plank's constant
$h\nu$	energy of photon
hr	hour
I_0	initial intensity
I_{op}	operating current
I_{rt}	intensity after a round trip
I_{th}	threshold current
J_{th}	threshold current density
k_b	Boltzmann's constant
k	momentum
K	kelvin
kT	kinetic energy of an atom
L	laser cavity length
M	characteristic matrix
m	meter
N_0	number of atoms in ground state
n_0'	effective refractive indices of the incident medium
N_1	number of atoms in excited state

n_a	refractive index of the air
n_{cl}	refractive index of cladding layer
n_{eff}	effective refractive index
n_f	refractive index of core layer
n_H	high refractive index
n_L	low refractive index
nm	nanometer
n_s	refractive index of semiconductor
n_s'	effective refractive indices of the substrate
P	reactor pressure
P_0	initial power
P_{COMD}	power level at COMD
P_{max}	maximum power
P_{out}	optical output power
q	electronic charge
R	reflectivity at normal incident
r	molecular diameter
$R_{1,2}$	facet mirror reflectivity
r_g	growth rate
R_n	lower order organic radical
R_{nr}	non-radiative recombination rate
R_{rr}	radiative recombination rate
R_s	dynamic series resistance
R_{SP}	spontaneous emission rate
R_{th}	thermal resistance
s	second
T	temperature
t	time
T_0	characteristic temperature
T_j	junction temperature
V	gas velocity
V_0	turn-on voltage
V_b	bias voltage
V_f	forward voltage
W	watt

* * *

❖ Abbreviations

3D	Three-Dimensional
ACC	Automatic Current Control
Ag	Silver
Al_2O_3	Aluminum Oxide
AlGaAs	Aluminum Gallium Arsenide
AlGaInP	Aluminum Gallium Indium Phosphide
AlGaN	Aluminum Gallium Nitride
APC	Automatic Power Control
AR	Anti Reflection
AsH_3	Arsine
AuGe	Gold-Germanium
Ausn	Gold-tin
BHF	Buffer Hydro-Fluoric Acid
CEERI	Central Electronics Engineering Research Institute
CH_3OH	Methanol
COD	Catastrophic Optical Damage
COMD	Catastrophic Optical Mirror Damage
CTE	Coefficient of Thermal Expansion
Cu	Copper
CuW	Copper-Tungsten
CVD	Chemical Vapor Deposition
CW	Continuous Wave
DAQ	Data Acquisition
DFB	Distributed Feed-Back
DH	Double Heterostructure
DI	De-Ionized
DLD	Dark Line Defect
DMZn	Dimethyl Zinc
DSD	Dark-Spot Defects
DUT	Device Under Test
ECDL	External Cavity Diode Laser
EL	Electro-Luminescence
FWHM	Full Width at Half Maxima
GaAs	Gallium Arsenide
GaN	Gallium Nitride
GaP	Gallium Phosphide
GPIB	General Purpose Interface Bus
GUI	Graphical User Interface
H_2O_2	Hydrogen Peroxide
H_3PO_4	Phosphoric Acid
HPLD	High-Power Laser Diode
HR	High Reflection
HVPE	Hydride Vapor Phase Epitaxy
In	Indium
InAs	Indium Arsenide
InGaAs	Indium Gallium Arsenide
InGaP	Indium Gallium Phosphide
InP	Indium Phosphide
LabVIEW	Laboratory Virtual Instrument Engineering Workbench
LASER	Light Amplification by the Stimulated Emission of Radiation
LIDT	Laser Induced Damage Threshold
LOR	Lift-off Resist
LPE	Liquid Phase Epitaxy
MBE	Molecular-Beam Epitaxy
mfp	Mean Free Path
MgF_2	Magnesium Fluoride
MOVPE	Metalorganic Vapor Phase Epitaxy
MQW	Multiple Quantum Well
Nd:YAG	Neodymium Yttrium Aluminum Garnet
NH_4F	Ammonium Fluoride
NPR	Negative Photoresist

PbSn	Lead-Tin
PH_3	Phosphine
PL	Photo-Luminescence
ppm	Parts Per Million
PPR	Positive Photoresist
PVD	Physical Vapor Deposition
QCW	quasi-CW
QD	Quantum Dot
QW	Quantum Well
QWOT	Quarter-Wave Optical Thick
QWR	Quantum Wire
REDC	Recombination Enhanced Dislocation Climb
REDG	Recombination Enhanced Dislocation Glide
RF	Radio Frequency
rpm	Rotation Per Minute
RRCAT	Raja Ramanna Centre for Advanced Technology
RTA	Rapid Thermal Annealing
SAMEER	Society for Applied Microwave Electronics Engineering and Research
SEM	Scanning Electron Microscope
SH	Single Heterostructure
SiO_2	Silicon Dioxide
SSPL	Solid State Physics Laboratory
T/C	Thermo-Compression
T/S	Thermosonic
TEC	Thermo Electric Cooler
TEGa	Triethyl Gallium
TIFR	Tata Institute of Fundamental Research
TiO_2	Titanium dioxide
TMAl	Trimethyl Aluminum
TMGa	Trimethyl Gallium
TMIn	Trimethyl Indium
U/S	Ultrasonic
USB	Universal Serial Bus
VECSEL	Vertical External Cavity Surface Emitting Laser
VI	Virtual Instrumentation
VPE	Vapor Phase Epitaxy
ZrO_2	Zirconium Oxide

* * *

❖ List of Publications

➢ International Journals

1. **The optimization of optical thin films deposition using In-situ reflectivity measurements and simulation**
   G.G. Bhatt, Vipul Kheraj, M. S. Desai, C. J. Panchal
   Journal of nano- and electron Physics, **3** (2011) 721

2. **Laser induced damage studies on Al_2O_3, SiO_2, and MgF_2 thin films for anti-reflection coating application in high power laser diode**
   G.G. Bhatt, A. L. Patel, M. S. Desai, C. J. Panchal
   Journal of nano- and electron Physics, **5** (2013) 02016

➢ International Conference Proceedings

1. **Estimation of the reliability and junction temperature of the InGaP 650 nm quantum well laser diode**
   G.G. Bhatt, C. J. Panchal, M. S. Desai, V. A. Kheraj, T. K. Sharma
   Proceedings of XV International Workshop on the Physics of Semiconductor Devices (IWPSD-09)
   Jamia Millia Islamia, NewDelhi, December 2009

➢ National Conference Proceedings

1. **Automated Lifetime Measurement Facility for Laser Diodes**
   G.G. Bhatt, C. J. Panchal, M. S. Desai, V. A. Kheraj, T. K. Sharma
   Proceedings of National Laser Symposium-08 (NLS-08)
   LASTEC, DRDO, New Delhi, December 2008

2. **Optimization of thin films of Al_2O_3 AR and pairs of Al_2O_3-TiO_2 HR coatings for facets of 808 nm laser diode**
   G.G. Bhatt, Vipul Kheraj, M. S. Desai, C. J. Panchal
   Proceedings of National Laser Symposium-19 (NLS-19)

RRCAT, Indore, December 2010

3. **Effect of die bonding on the performance of high power semiconductor laser diode**
   G.G. Bhatt, M. Shrivastava, A. Marathe, S. K. Khamari, A. Khakha, S. Porwal, V. Agnihotri, S. Pal, C. J. Panchal, V. K. Dixit, T. K. Sharma, S. M. Oak
   Proceedings of National Laser Symposium-22 (NLS-22)
   Manipal University, Manipal, Karnataka, January 2014

4. **Facet coating and its effect on the characteristics of 980nm quantum well laser diode**
   Archana Marathe, **Gopal Bhatt**, S.K Khamari, S.Pal, K.Rajiv, C. Mukharjee, C.J Panchal, V.K Dixit, T.K Sharma,, S.M Oak
   Proceedings of National Laser Symposium-22 (NLS-22)
   Manipal University, Manipal, Karnataka, January 2014

* * *